Durham E-Theses

Next-to-Next-to-Leading Order QCD Corrections to Higgs Boson Production in Association with two Jets in Vector Boson Fusion

CRUZ-MARTINEZ, JUAN,MANUEL

How to cite:

CRUZ-MARTINEZ, JUAN,MANUEL (2018) *Next-to-Next-to-Leading Order QCD Corrections to Higgs Boson Production in Association with two Jets in Vector Boson Fusion*, Durham theses, Durham University. Available at Durham E-Theses Online: http://etheses.dur.ac.uk/12806/

Use policy

The full-text may be used and/or reproduced, and given to third parties in any format or medium, without prior permission or charge, for personal research or study, educational, or not-for-profit purposes provided that:

- a full bibliographic reference is made to the original source
- a link is made to the metadata record in Durham E-Theses
- the full-text is not changed in any way

The full-text must not be sold in any format or medium without the formal permission of the copyright holders.

Please consult the full Durham E-Theses policy for further details.

Academic Support Office, Durham University, University Office, Old Elvet, Durham DH1 3HP
e-mail: e-theses.admin@dur.ac.uk Tel: +44 0191 334 6107
http://etheses.dur.ac.uk

Next-to-Next-to-Leading Order QCD Corrections to Higgs Boson Production in Association with two Jets in Vector Boson Fusion

Juan Manuel Cruz-Martinez

A Thesis presented for the degree of
Doctor of Philosophy

Institute for Particle Physics Phenomenology
Department of Physics
Durham University
United Kingdom

August 2018

Next-to-Next-to-Leading Order QCD Corrections to Higgs Boson Production in Association with two Jets in Vector Boson Fusion

Juan Manuel Cruz-Martinez

Submitted for the degree of Doctor of Philosophy

August 2018

Abstract: In this thesis the second-order QCD corrections to electroweak production of a Higgs boson in association with two jets through vector boson fusion are considered. This calculation is fully differential in the kinematics of the Higgs boson and of the final state jets. Infrared divergences are regulated using the antenna subtraction method. We detail the implementation of the process in the parton-level Monte Carlo integrator NNLOjet and present inclusive calculations as well as differential distributions for a wide range of observables at different center-of-mass energies.

Dedicated to

the memory of my father.

Declaration

The work in this thesis is based on research carried out in the Department of Physics at Durham University. No part of this thesis has been submitted elsewhere for any degree or qualification. All work is my own in collaboration with my supervisor Professor E.W.N. Glover, unless referenced to otherwise within the text. Chapters 4 and 5 are based upon research done in collaboration with T. Gehrmann and A. Huss and presented in the following publications and conferences,

J. Cruz-Martinez (Durham U., IPPP), T. Gehrmann (Zurich U.), E.W.N. Glover (Durham U., IPPP), A. Huss (CERN), "Second-order QCD effects in Higgs boson production through vector boson fusion". *Phys. Lett. B* vol. 781 (2018) p.672-677. arXiv:1802.02445 [hep-ph]

J. Cruz-Martinez (Durham U., IPPP), T. Gehrmann (Zurich U.), E.W.N. Glover (Durham U., IPPP), A. Huss (CERN), "NNLO corrections to VBF Higgs boson production". *Loops and Legs in Quantum Field Theory (LL2018) St. Goar, Germany.* arXiv:1807.07908 [hep-ph]

Copyright © 2018 Juan Manuel Cruz-Martinez.

The copyright of this thesis rests with the author. No quotation from it should be published without the author's prior written consent and information derived from it should be acknowledged.

Acknowledgements

A PhD is made of mixed experiences, full of lights and shadows. During these the course of this work I have learned many things and grown as a person, but this thesis has also been witness of some of the most distressing times of my life. The loss of my father, José Manuel, was a terrible blow, even today, more than one year after it happened, it is hard to find words to describe how I feel. He was the person who made me into who I am today, all I can say is Thanks. Thank you for everything you did, I miss you every day.
Thanks to my mother Ondina, my brother Josean and my sister Carmen. Their care, love and company have been key for me to get through these very difficult times. I also want to thank Fran, Luis, Ana, López, Aure, Bea, Javi, Valeria, little Valentina and the many friends that were there with me when I most needed them. I cannot thank you enough.

I would like to thank my supervisor, Nigel, for his help, support, patience and guidance during these last four years. For his leadership as a commander-in-chief of the Higgstools Initial Training Network and for making my PhD a successful one, which was not a simple task. Thanks also to Thomas Gehrmann for his kind hospitality and guidance during my time in Zurich; to the OC325 crew, Duncan and James, for their help on destroying the environment via intensive NNLOJET runs; and to the rest of the NNLOJET team, past and present, Xuan Chen, James Currie, Rhorry Gauld, Aude Gehrmann-De Ridder, Marius Höfer, Alexander Huss, Imre Majer, Jonathan Mo, Tom Morgan, Jan Niehues and Joao Pires. It is a pleasure collaborating with all of you.

I also want to acknowledge here some of the people who provided invaluable assistance, Davide Napoletano and Robin Linten on getting Sherpa to produce seemingly meaningful answers, Jonas Lindert on generating the necessary OpenLoops amplitudes and, all members of the department on leaving two cores of their machines free for me to use. I want to thank the members of the Computing Club, from whom I have learned a whole lot. Andreas' lessons on *making makefiles*, David's on mixing Fortran and C and Daniel's ideas for parallelising code have been key on getting NNLO integrations done in human timescales.

During the past few years I have had the opportunity to travel across Europe, meeting myriads of people and making as many friends: the people from Durham, Shell, Zurich and, of course, the whole of the Higgstools brigade (P&L!). A special mention to the *Primera Promoción de Grado* of Physics in Seville. Being the guinea pigs of the Bologna Process in Spain nine years ago was more than worthwhile if only for the fun we had with the Frank-Einstein awards. I feel lucky to have many more friends than pages of this thesis I could fill. To all of you, thanks.

Finally, I want to give a special thanks to all members of the IPPP; from OC118 and C.S. Mann to the top office, OC325. It has been a pleasure enduring the hardships of the PhD together with all of you; the code that would not compile, the singularities that did not cancel and the sandwiches from Yum with way too much bread. Thank you very much and I hope the spirit of camaraderie of the IPPP never disappears.

Muchas gracias y buena suerte.

Contents

Contents **vii**

List of Figures **xi**

List of Tables **xix**

1 Introduction **1**

1.1 The Standard Model 2

1.1.1 The electroweak sector 3

1.1.2 Broken symmetries 7

1.1.3 The QCD sector 11

1.1.4 The cross section: from theory to experiment 11

1.1.5 Regularisation, renormalisation and ultraviolet divergences . 14

1.2 Higgs boson phenomenology 16

1.2.1 Higgs boson production at hadron colliders 16

1.2.2 Higgs boson decay at hadron colliders 18

1.2.3 The discovery of the Higgs boson 20

2 Higher-Order QCD Corrections **22**

2.1 The improved parton model 22

2.2 Infrared divergences 25

2.2.1 Colour ordered matrix elements 27

2.2.2 Virtual corrections 29

2.2.3 Real radiation, implicit divergences 30

2.2.4 Infrared cancellation . . . 33
2.2.5 Jet cross sections . . . 36
2.3 Antenna Subtraction method . . . 39
2.3.1 Azimuthal rotations . . . 42
2.4 Scale dependence of the cross section at NNLO in QCD . . . 43

3 Vector Boson Fusion Higgs Production 47
3.1 Higgs production in Vector Boson Fusion . . . 48
3.1.1 Topology of the process . . . 49
3.1.2 VBF cuts . . . 50
3.2 The DIS approach . . . 52
3.2.1 Comparison between ggF, VBF, VH . . . 55
3.3 Matrix elements . . . 60
3.3.1 Notation . . . 61
3.3.2 Leading Order: Born contribution . . . 63
3.3.3 Next to Leading Order: Real radiation . . . 65
3.3.4 Next to Leading Order: Virtual contribution . . . 67
3.3.5 Next to Next to Leading Order: Double Real contribution . 68
3.3.6 Next to Next to Leading Order: Real Virtual contribution . 72
3.3.7 Next to Next to Leading Order: Double Virtual contribution 74

4 NNLOjet Implementation 77
4.1 NNLOjet . . . 78
4.1.1 Technical description . . . 78
4.1.2 Features . . . 80
4.1.3 Code autogeneration . . . 82
4.2 Numerical integration . . . 86
4.2.1 Monte Carlo methods . . . 86
4.2.2 Importance sampling . . . 88
4.2.3 NNLOjet Vegas implementation . . . 89

4.2.4 Parallel computing and benchmarking 93
4.3 Phase space generator 96
4.3.1 Naive phase space 98
4.3.2 The VBF phase space 104
4.3.3 Wedges 106
4.3.4 Rotations 110
4.3.5 Comparison between the naive sequential and VBF phase space generators 112
4.3.6 Phase space validation 113
4.4 Validation 122
4.4.1 Matrix elements 123
4.4.2 Pole testing 125
4.4.3 Layer tests 127
4.4.4 Technical cut dependence 127
4.4.5 Scale evolution 130
4.4.6 Inclusive cross section 130
4.4.7 Differential cross section 132

5 Phenomenological Results 134
5.1 NNLO corrections to VBF-2j 135
5.1.1 Inclusive calculation 135
5.1.2 Fiducial result and differential cross sections 136
5.2 NNLO corrections to VBF-3j 141
5.3 Jet dependence of VBF cross section 142
5.4 Phenomenology of VBF at NNLO in the HE-LHC 146
5.4.1 High Energy LHC, 27 TeV 147

6 Conclusions 155

Appendices 157

A Maple input file **158**

B Relevant Antennae **162**

B.1 $X_3^0(i_1, i_2, i_3)$ antennae 162

B.2 $X_4^0(i_1, i_2, i_3, i_4)$ antennae 163

B.3 $X_3^1(i_1, i_2, i_3)$ antennae 164

B.4 $\mathcal{X}_3^0(i_1, i_2)$ antennae 164

B.5 $\mathcal{X}_3^1(i_1, i_2)$ antennae 165

B.6 $\mathcal{X}_4^0(i_1, i_2)$ antennae 165

B.7 Mass factorisation terms, $\Gamma_{ab}^n(z)$ 166

B.8 J_2^1 antennae 166

B.9 The integrated NLO J-dipoles 167

C Subtraction terms **169**

C.1 NLO: R 169

C.2 NLO: V 174

C.3 NNLO: RR 176

C.4 NNLO: RV 190

C.5 NNLO: VV 201

D pyHepGrid **216**

Bibliography **219**

List of Figures

1.1 Graphical example of the potential $V(|\Phi|^2)$, of Eq. (1.19) for Φ a complex field such as $\Phi = \phi_1 + i\phi_2$. 8

1.2 Examples of Higgs boson production processes in hadron collisions. 16

1.3 Higgs production rate for different subprocess at a center of mass energy of $\sqrt{s} = 7$ TeV. Plots by the Higgs cross section working group [13]. 17

1.4 Vector Boson Fusion Higgs boson production or VBF. 17

1.5 Higgs boson branching ratios as a function of the mass of the boson. Plot by the Higgs cross section working group [13]. 19

1.6 Examples of Higgs boson decay modes. 19

1.7 Experimental limits from LEP, Tevatron and LHC on the Higgs boson mass on the $100 - 600$ GeV mass range by the year 2011. The dashed limit show the expected limit in the absence of the Higgs boson. Plot from Ref. [18]. 20

1.8 Best fit value for the Higgs boson cross section for each decay mode relative to the expected Standard Model value: $\mu = \frac{\sigma}{\sigma_{SM}}$. Plots from Ref. [19]. 21

2.1 Example of higher-order corrections for a scattering process. The incoming arrows represent the i.s. particles, the outgoing arrow one of the f.s. particles. The shaded blob in the middle represents the rest of the hard-scattering process. 25

2.2 Diagrams corresponding to a quark current from which two gluons are radiated. 27

3.1 Schematic representation of a VBF-type process in a proton-proton collision in which the radiated vector bosons fuse to form a Higgs boson. The generated particle then decays into measurable products (represented as photons in this case). 48

3.2 Example of Higgs boson production processes in association with two jets. 49

3.3 Born-level vector boson fusion process. 50

3.4 Examples of neglected diagrams appearing in the VV layer for VBF Higgs boson production. The first of these diagrams vanishes due to colour algebra while the other two are neglected. 53

3.5 Example of neglected VBF contributions for the Born, RR and RV layers. 54

3.6 Examples of second order QCD corrections (RR, RV, VV) to the quark currents. 54

3.7 Comparison between ggF and VBF for the differential distributions on the transverse momentum of the leading jet (left) and the Higgs boson (right). 57

3.8 Comparison between ggF and VBF for the differential distributions on the invariant mass of the dijet system formed by the two tagging jets and the corresponding rapidity gap. 58

3.9 Comparison between electroweak Higgs boson plus 2 jets production for the invariant mass of the dijet system and the corresponding rapidity gap. VBF$^{u/t}$ corresponds to the inclusion of the u and t-channel interferences whereas Full EW H+2j correspond to the the sum of VH, VBF$^{u/t}$ and interferences thereof. 59

3.10 Comparison between ggF, the Full H2j Electroweak production and VBF for the differential distributions on the invariant mass of the dijet system formed by the two tagging jets and the corresponding rapidity gap. 61

3.11 Comparison between ggF, the Full H2j Electroweak Production and VBF for the differential distributions on the transverse momentum of the leading jet and the Higgs. 62

3.12 Only diagram contributing to the Born level VBF amplitude. . . . 63

3.13 Quark current with one gluon being radiated. 65

3.14 Example of quark current with two emissions of gluons. For the full current see Fig. 2.2. 68

3.15 Example of quark current with a $q\ \bar{q}$ pair splitting of the radiated gluon. 69

3.16 Example of one loop one radiation diagrams contributing to the $\mathbf{J}^{(1)}_{\mu}(1,k,i)$ current. 73

4.1 Flow chart for the implementation of new processes in NNLOJET. . 84

4.2 Example of the evolution of the subdivisions generated by Vegas for two of the random variables. The coloured lines correspond to the edges of the Δx_i grid. 92

4.3 Study of the performance evolution of Vegas as a function of the number of threads for a VBF Real integration with minimal cuts. Default corresponds to the typical implementation of Vegas based on OpenMP. Experimental removes some restriction on the capacity of OpenMP for parallelisation. Tested in Intel(R) Xeon(R) Gold G6130, 64 physical cores. 94

4.4 Schematic view of a sequential phase space generator. 99

4.5 Sequential phase space generator with a detachment of a colourless state represented by s_H. 99

4.6 Schematic representation of the Born level VBF phase space. . . . 104

4.7 2 to 3 phase space for a VBF-like topology. 105

4.8 Example of phase space divided in three regions through a condition on s_{ij}. If the integration wedge corresponds to the phase space point $(1,2,3) \to \{p_1, p_2, p_3\}$ then full coverage is restored through the permutations $(1,2,3) \to (1,3,2)$ and $(1,2,3) \to (3,2,1)$. Note that $s_{ij} = s_{ji}$. 106

4.9 Possible $2 \to 4$ phase space configurations for a VBF-like topology . 107

4.10 Possible 2 to 5 phase space configurations for a VBF-like process. The two configuration correspond to different singularity structures. . . 108

4.11 Schematic representation of the VBF phase space, region A. 109

4.12 Schematic representation of the VBF phase space, region B. 109

4.13 Comparison between a sequential phase space of Fig. 4.5 (naive, dashed red) and our optimised VBF phase space (VBF, green) showing the necessary number of Monte Carlo shots (left) and the corresponding integration time (right) to reach similar levels of precision. In blue we include the expected Monte Carlo relation between the error and the number of shots, we observe the sequential phase space to have a slightly worse than $\frac{1}{\sqrt{N}}$ growth while the VBF phase space improves in the expected MC error. 113

4.14 Study of the y_0 behaviour for $M = \frac{1}{s_{ij}}$ with i and j both f.s. particles, $\sqrt{s} = 8$ TeV. 116

4.15 Study of the y_0 behaviour for $M = \frac{1}{s_{aj}}$ with a i.s. parton and j f.s. particle, $\sqrt{s} = 8$ TeV. 116

4.16 Study of the y_0 behaviour for $M = \frac{1}{s_{ij}}$ with i and j both f.s. particles, $\sqrt{s} = 8$ TeV. 118

4.17 Study of the y_0 behaviour for $M = \frac{1}{s_{aj}}$ with a i.s. parton and j f.s. particle, $\sqrt{s} = 8$ TeV. 119

4.18 Study of the y_0 behaviour for $M = \frac{1}{s_{ij}}$ with i and j both f.s. particles, $\sqrt{s} = 8$ TeV. 120

4.19 Study of the y_0 behaviour for $M = \frac{1}{s_{aj}}$ with a i.s. parton and j f.s. particle, $\sqrt{s} = 8$ TeV. 121

4.20 "Spike plots" generated for two different singular limits. As we lower the technical cut on our invariants ($y_0 = \frac{s_{ij}}{\hat{s}}$) the cancellation becomes more exact as we move closer to the actual limit. 125

4.21 Output of the pole check for NNLOJET. Left is an analytical comparison between the matrix elements and the Catani pole structure while right show a numerical comparison between the matrix elements and the subtraction terms. 126

4.22 Output of the layer test for one of the antenna substructures. . . . 127

4.23 Bin by bin comparison for the Δy_{jj} and p_T^H distributions for different values of the technical cut y_0 for a NNLO VBF calculation The shaded regions correspond solely to scale variations while the errorbars correspond to statistical uncertainty. 129

4.24 Scale evolution of the total VBF cross section. We select $\mu_{\rm F} = \mu_{\rm R} =$ 125 GeV as the reference scale and numerically integrate for different values of $\mu_{\rm R}$. 130

4.25 Bin by bin comparison ratio between [1] and the corrected results of [95]. The red errors correspond to the statistical error from NNLOJET, the blue errors the statistical error of proVBF and the yellow bars the combination of both. NLO and NNLO correspond to the NLO and NNLO coefficients only respectively. 133

5.1 Transverse momentum distribution of VBF-2j. In red we plot the LO distribution. Both the NLO (green) and NNLO (blue) corrections reduce noticeably the scale uncertainty bands. Beyond $p_T^H \sim 150$ GeV the NNLO corrections become negligible and well within the LO and NLO uncertainty bands. 137

5.2 Transverse momentum distribution of leading and subleading jet for VBF-2j. Both the NLO and NNLO corrections change the shape of the observables. Note that the NLO scale uncertainty bands are much bigger than those seen in Fig. 5.1, this suggest the scale choice of Eq. (5.2) might be suboptimal for these two observables. At NNLO, however, the dependence with the scale is well reduced, which proves the convergence of the perturbative series. 138

5.3 Study of the rapidity separation and angular decorrelation of the two leading jets in the VBF process. The scale uncertainties in both distributions were well under control already at NLO. The NNLO corrections further reduce the scale dependence making it almost negligible as the statistical error of the Monte Carlo integration becomes dominant. 139

5.4 Distribution on the invariant mass of the system formed by the two tagging jets of the VBF process. Both the NLO and NNLO corrections are quite uniform across the accessible range of the observable. The scale dependence at NNLO is negligible at low and moderate values of m_{jj}, where the statistical error dominates. 140

5.5 Differential distributions on Δy_{jj} and z_3, Eq. (5.6). We observe a reduction of the scale uncertainty going from LO to NLO, with a dominance of the statistical error with respect to the scale dependence for certain values of the observables. The NNLO corrections are very large, amounting to up to $\sim 30\%$ with noticeable scale uncertainty bands. 142

5.6 Total cross section as a function of R for LO (red), NLO (green) and NNLO (blue). Here the independence of the LO cross section with respect to the choice of R is seen explicitly. The NNLO cross section is well within the NLO scale uncertainty bands for $R > 0.4$. . . . 144

5.7 Variation of the NNLO cross section as a function of R for different values of the dijet invariant mass cut m_{jj}. We choose $R = 1.0$ to normalise the results as the effect of the higher order corrections are the smallest. In general we find the results for different values of the m_{jj} to be compatible within statistical errors. The main feature discussed in the main text can still be observed, i.e., a bigger dependence on the cross section on the jet radius R as the cut on m_{jj} becomes more restrictive. 145

5.8 Differential distribution on the rapidity gap (Δy_{jj}) between the tagging jet for several values of the jet radius R. The computed values of the differential cross section are compatible within statistical errors beyond $\Delta y_{jj} > 5$. All other parameters are set equal to those of Section 5.1, crucially $m_{jj} > 600$ GeV and $|y_j| < 4.5$. 145

5.9 Two-dimensional plots on the rapidity gap between the two tagging jets (Δy_{jj}) and the invariant mass of the dijet system formed by those two tagging jets (m_{jj}) for two different choices of the transverse momentum cut. We observe the bulk of the cross section to be concentrated in $m_{jj} > 200$ GeV, $\Delta y_{jj} > 2.5$. These two plots have been obtained with proVBF [95] and provided by A. Karlberg. . . 148

5.10 Fraction of events lost as a function of the acceptance in rapidity of the detector. Non-tagging jets can have any value of the rapidity. Only **minimal** VBF cuts are applied in this case, we observe the acceptance to be less punishing for a bigger cut on the transverse momentum. 149

5.11 Fraction of events lost as a function of the acceptance in rapidity of the detector. Non-tagging jets can have any value of the rapidity. In contrast to Fig. 5.10, **tight** VBF cuts are applied in this case. The effect of the tighter VBF cuts is to move a bigger (relative to minimal cuts) fraction of event outside of the detector limits. 149

5.12 Differential distributions for the transverse momentum (left) and absolute rapidity (right) of the Higgs boson at $\sqrt{s} = 27$ TeV. Error-bars correspond exclusively to statistical errors. We find the NNLO to considerably reduce the scale uncertainties at larger values of p_T^H. . 151

5.13 Differential distributions for the transverse momentum (left) and absolute rapidity (right) of the two tagging jets. The top row corresponds to the leading (ordered in p_T^j) jet while the bottom row corresponds to the subleading jet. NLO scale uncertainties are moderate for most the rapidity spectrum and large at high p_T^j, NNLO corrections greatly reduce scale uncertainties. 153

5.14 Differential distributions for the spatial distribution of the two tagging jets as well as the invariant mass of the dijet system. NLO and NNLO corrections noticeably reduce the scale uncertainties for both observables over the entire range considered. 154

C.1 Real emission matrix element squared `sC1g0ZFH` $= sC_{1g}^0$, which is a sum over the gluon being emitted from the upper and lower currents. 169

C.2 Subtraction term of Eq. (C.1) where we show the reduced matrix element graphically for clarity. 170

C.3 Virtual amplitude corresponding to the matrix element squared `C0g1ZFH` $= C_{0g}^1$ upon interference with the tree level amplitude. 174

List of Tables

1.1 Fermionic content of the Standard Model with their respective $\mathrm{SU}(2)_L$ and $\mathrm{U}(1)_Y$ charges. The electromagnetic charge Q is related to the electroweak charges through Eq. (1.12). 6

3.1 Subprocesses that contribute to VBF-$2j$ up to NNLO in NNLOJET. 54

3.2 Comparison between different Higgs boson plus 2 jets production modes. In this calculation we use the NNPDF30_nnlo_as_0118 [75] PDF set as included in the LHAPDF [76] library with $\mu_\mathrm{F} = \mu_\mathrm{R} = m_H$. Errors are statistical. 56

3.3 Comparison between different Higgs boson plus 2 jets production modes using VBF cuts. In this calculation we use the NNPDF30_nnlo_as_0118 [75] PDF set as included in the LHAPDF [76] library with $\mu_\mathrm{F} = \mu_\mathrm{R} = m_H$. Cut efficiency compares the % of events that go through the extra cuts imposed in Eq. (3.6). 60

4.1 Values for the unit phase space for $\sqrt{s} = 8$ TeV. In this comparison no selection cuts are imposed and the PDFs are assumed to be identically one for any initial state. 114

4.2 NNLOJET values for the VBF phase space volume for $n = 4$ with different combinations of $s_{ij}^{-1/2}$ for $\sqrt{s} = 8$ TeV, no selection cuts imposed and PDFs are assumed to be identically one for any initial state. 115

4.3 Comparison of the phase space volume for $\frac{1}{s_{ij}}$ for different values of y_0 between the ggF H+2jets phase space and the VBF phase space for a center of mass energy $\sqrt{s} = 8$ TeV, no selection cuts imposed and PDFs are assumed to be identically one for any initial state. . 117

4.4 Values for the phase space volume for $n = 5$ for different combinations of $s_{ij}^{-1/2}$ for $\sqrt{s} = 8$ TeV, no selection cuts imposed and PDFs are assumed to be identically one for any initial state. 117

4.5 Values for the phase space volume for $n = 5$ for different combinations of s_{ij}^{-1} for $\sqrt{s} = 8$ TeV and $y_0 = 10^{-7}$, no selection cuts imposed and PDFs are assumed to be identically one for any initial state. . . . 118

4.6 Values for the different combinations of $s_{ij}^{-1/2}$ with i, j final particles for $\sqrt{s} = 8$ TeV, no selection cuts imposed and PDFs are assumed to be identically one for any initial state. 119

4.7 Values for the different combinations of $s_{ij}^{-1/2}$ with i initial and j final for $\sqrt{s} = 8$ TeV, no selection cuts imposed and PDFs are assumed to be identically one for any initial state. 120

4.8 Values for the phase space volume for $n = 6$ for different combinations of s_{ij}^{-1} for $\sqrt{s} = 8$ TeV and $y_0 = 10^{-7}$. No PDFs or cuts. 120

4.9 Validation test suite for the VBF process in NNLOJET. Red ticks refer to tests against external tools, green ticks are internal NNLOJET tests. Non-applicable tests are marked with an hyphen. 123

4.10 Example of pointwise comparison against and OpenLoops for a selection of RR and RV matrix elements. Tests have been performed for all colour levels and possible configurations of initial and final states allowed in the DIS approach described in Section 3.2. 123

4.11 Comparison of the different levels of the cross section for different values of the technical cut. LO refers to the Born cross section, NLO to the sum of R and V and NNLO to the sum of RR, RV and VV. . 128

4.12 Fully inclusive VBF cross section. The uncertainty corresponds to a scale variation of $\mu_F = \mu_R = \left\{\frac{1}{2}, 1, 2\right\} \times \mu_0$. μ_0 is given in (5.2). Reference results are taken from [95]. 131

4.13 Fully inclusive VBF NNLO coefficient (RR+RV+VV) broken down by initial state. The scale choice is $\mu_{\rm F} = \mu_{\rm R} = m_H$. The results were obtained with a privately modified version of proVBFH and Hoppet. 132

5.1 Fully inclusive VBF-2j cross section for a center of mass energy of $\sqrt{s} = 13$ TeV. We find a factor of about a -3% at NLO and -4% at NNLO with respect to LO. 135

5.2 Total VBF-2j cross section after VBF cuts are applied for a center of mass of $\sqrt{s} = 13$ TeV. The NLO corrections is three times bigger than in the fully inclusive case, amounting to a $\sim -9\%$. A further -3% correction is obtained when we add the NNLO coefficient. As an effect of the tight VBF cuts of Eq. (5.3), a 78% of the total cross section at NNLO is lost. 136

5.3 Total VBF-2j cross section at NNLO for a center of mass energy of $\sqrt{s} = 27$ TeV for three different choices of cuts. Inclusive imposes no cuts at all while minimal corresponds to the cuts of Eq. (5.12) and tight to the cuts of Eq. (5.13). Inclusive results obtained with proVBFH, all others with NNLOJET. 150

B.1 The correspondence between the real radiation matrix elements, M^0_{n+3} and the integrated NLO dipoles $J^{(1)}_2$ and reduced matrix elements, M^0_{n+2} for various particle assignments and colour structures for the final-final configuration. 167

B.2 The correspondence between the real radiation matrix elements, M^0_{n+3} and the integrated NLO dipoles $J^{(1)}_2$ and reduced matrix elements, M^0_{n+2} for various particle assignments and colour structures for the initial-final configuration. For brevity $\delta(1 - z_i) = \delta_i$ for $i = 1, 2$. . . 167

B.3 The correspondence between the real radiation matrix elements, M^0_{n+3} and the integrated NLO dipoles $J^{(1)}_2$ and reduced matrix elements, M^0_{n+2} for various particle assignments and colour structures for the initial-initial configuration. For brevity $\delta(1-z_1)=\delta_1$, $\delta(1-z_2)=\delta_2$. 168

Chapter 1

Introduction

The research described in this thesis focuses on the production of Higgs bosons in hadron colliders through Vector Boson Fusion (VBF) and its implementation in the parton-level fixed-order Monte Carlo NNLOJET.

In the first chapter we introduce the Standard Model, outlining its Lagrangian density and motivating the phenomenological necessity for higher-order corrections in the strong coupling α_s. We also briefly review the phenomenological properties of the Higgs boson.

In the second chapter we describe the theoretical and technical problems introduced by higher-order calculations, focusing on infrared singularities and their cancellation through the antenna subtraction formalism.

In the third chapter we motivate the study of the Vector Boson Fusion production mode as a way of precisely studying the properties of the Higgs boson. We define our implementation of the Vector Boson Fusion Higgs production process in the so-called DIS approach and demonstrate its validity by comparing the Higgs production rate in this mode with other competing channels.

The fourth chapter describes the numerical implementation of the process up to second order in α_s in the parton-level Monte Carlo NNLOJET. We also summarise our extensive and successful suite of tests and checks we perform to ensure the correctness of our results. This suite of tests led to the discovery of several errors

in previous calculations for this process which propagated to other codes and went unnoticed for years.

Having established our implementation of the VBF Higgs production mode and once all numerical tools are presented, we dedicate chapter five to the phenomenological impact of our calculation. Sections 5.1 and 5.2 contains work published in Ref. [1] whereas Section 5.4 contains ongoing work in collaboration with Alexander Karlberg to be published as part of the High Energy/High Luminosity Working Group report.

1.1 The Standard Model

The Standard Model of particle physics has been able to survive experimental challenges for many years. Among its many successes are the discovery of the W and Z bosons in 1983, the top quark in 1995 and, more recently, the discovery of the Higgs boson in 2012, nearly 50 years after its proposal. Its many predictive successes, and the lack of specific evidence for any competing theory, have consolidated the Standard Model as the *de facto* theory of fundamental physics.

Although the theory describes our current knowledge of the quantum world, it is known to be incomplete. For instance, in its current form, the Standard Model lacks a suitable candidate for the Dark Matter content of the universe. It also lacks a mass term for the neutrinos, which are known today to be massive. Other problems include the strong CP problem, the absence of axions and a quantum description of gravity. The wider high energy physics community, from cosmology to string theory, dedicates a lot of effort to the resolution of many of these issues.

This work is dedicated to the precise study and stress-testing of the Standard Model through particle collisions. We calculate the higher orders of the perturbative series in α_s for electroweak Higgs boson production in association with two jets. In this section we describe the relevant pieces of the strong, electroweak and Higgs sectors of the Lagrangian which are necessary to introduce our calculation.

The governing principles of the Standard Model are the renormalisability and gauge invariance of the theory. These constraints define the terms allowed to be included in the Lagrangian density of the Standard Model ($\mathcal{L}_{\rm SM}$). The gauge symmetry group $\mathrm{SU}(3)_c \times \mathrm{SU}(2)_L \times \mathrm{U}(1)_Y$ is at the core of the Standard Model.

In Section 1.1.1 we detail the electroweak sector, corresponding to the $\mathrm{SU}(2)_L \times \mathrm{U}(1)_Y$ content of the Lagrangian. In Section 1.1.2 we introduce the concept of spontaneous symmetry breaking, which is central to the problem of the vector boson masses and is responsible for the generation of the Higgs boson. In Section 1.1.3 we complete our study of the Lagrangian of the Standard Model with the introduction of the QCD $\mathrm{SU}(3)_c$ sector. In Section 1.1.4 we introduce the core concept of particle physics phenomenology: the cross section. In Section 1.1.5 we briefly consider the concept of ultraviolet divergences and introduce regularisation and renormalisation.

1.1.1 The electroweak sector

The electroweak sector of the Standard Model unifies electromagnetism and weak interactions. It is described by the Glashow-Weinberg-Salam Lagrangian, governed by the $\mathrm{SU}(2)_L \times \mathrm{U}(1)_Y$ symmetry. When the symmetry is spontaneously broken, a $\mathrm{U}(1)_{\rm EM}$ symmetry remains which corresponds to the description of electromagnetism.

The $\mathrm{U}(N)$ group corresponds to the unitary $N \times N$ matrices while $\mathrm{SU}(N)$ is the group of unitary $N \times N$ matrices of determinant equal 1. In other words, the matrices M of $\mathrm{SU}(N)$ must fulfil the following two properties,

$$MM^\dagger = 1, \qquad \det\{M\} = 1. \tag{1.1}$$

Any matrix M can be generated via infinite small transformations from the identity matrix I. Let us then consider a matrix M infinitely close to the identity,

$$M = I + iT, \tag{1.2}$$

where T is an infinitesimal transformation. Since M must fulfil the relations of Eq. (1.1),

T must be a traceless hermitian matrix, i.e.,

$$T = T^\dagger, \qquad \mathrm{Tr}\{T\} = 0, \tag{1.3}$$

the basis of these infinitesimal transformations, formed by $N^2 - 1$ matrices, are the generators of the group and are a core concept for the study of the Standard Model.

Quantum Electrodynamics (QED)

In order to introduce relevant concepts for the discussion of the Standard Model, let us begin with the Dirac Lagrangian which describes the dynamical properties of a free fermion $\psi(x)$ of mass m,

$$\mathcal{L}_D(\psi) = \overline{\psi}(x)(i\partial\!\!\!/ - m)\psi(x), \tag{1.4}$$

where $\partial\!\!\!/ = \partial_\mu \gamma^\mu$ and $\overline{\psi}(x) = \psi^\dagger(x)\gamma_0$. ψ has four components and correspondingly the matrices γ^μ with $\mu = 0, \ldots, 3$ are the four 4×4 dirac matrices.

The Lagrangian of Eq. (1.4), albeit symmetric under global U(1) transformations, does not respect local U(1) symmetry. This can be explicitly seen by applying a transformation $\psi(x) \to \psi'(x) = e^{-iQ\theta(x)}\psi(x)$,

$$\mathcal{L}'_D(\psi') = \overline{\psi}(x)(i\partial\!\!\!/ - m)\psi(x) + iQ\overline{\psi}(x)\psi(x)\partial\!\!\!/\theta(x) \neq \mathcal{L}_D(\psi). \tag{1.5}$$

In order to restore gauge invariance we can postulate a generalisation of the partial derivative D_μ which transforms with the field $\psi(x)$ such that,

$$D_\mu\psi(x) \to D'_\mu\psi'(x) = U(x)D_\mu\psi(x), \tag{1.6}$$

this is called the *covariant derivative* and for U(1) takes the following form,

$$D_\mu = \partial_\mu + iQeA_\mu(x), \tag{1.7}$$

where interactions of the new gauge vector field A_μ are characterised by the constant e (the electric charge). Q is the charge operator taking ψ as an electron, $Q\psi = -\psi$. The field A_μ transforms under local transformations of the $\mathrm{U(1)_{EM}}$ symmetry group

as

$$A_\mu \to A'_\mu = A_\mu + \frac{1}{e}\partial_\mu \theta(x). \tag{1.8}$$

In the context of QED, the vector field A_μ corresponds to the photon. The description is only complete once we add a gauge invariant kinetic term to the Lagrangian,

$$\mathcal{L}_{\gamma,kin} = -\frac{1}{4}F_{\mu\nu}F^{\mu\nu}, \tag{1.9}$$

where $F_{\mu\nu}$ is the field strength tensor $F_{\mu\nu} = -\frac{i}{e}[D_\mu, D_\nu] = \partial_\mu A_\nu - \partial_\nu A_\mu$.

It is important to note that a mass term for the photon ($m^2 A_\mu A^\mu$) would immediately break gauge invariance, therefore the photon in this theory is massless. This is consistent with our observations of nature. After all these considerations, the QED Lagrangian for the description of electromagnetism reads,

$$\mathcal{L}_{\text{EM}} = \overline{\psi}(x)(i\not{D} - m)\psi(x) - \frac{1}{4}F_{\mu\nu}F^{\mu\nu}. \tag{1.10}$$

The electroweak sector

We can extend the same ideas in order to discuss the $\text{SU}(2)_L \times \text{U}(1)_Y$ gauge symmetry of the electroweak sector of the Standard Model. Let us begin by setting up the covariant derivative, necessary for the preservation of gauge invariance,

$$D_\mu = \partial_\mu + ig_1\frac{Y}{2}B_\mu + ig_2\tau^a W^a_\mu, \tag{1.11}$$

which introduces the vector fields B_μ and W^a_μ with $a = 1, 2, 3$. The matrices τ^a are the generators of $\text{SU}(2)_L$ and are proportional to the three 2×2 Pauli matrices [2] $\tau^a = \frac{\sigma^a}{2}$. The charges of $\text{SU}(2)_L$ and $\text{U}(1)_Y$ are known respectively as weak isospin and hypercharge and are related to the classical electromagnetic charge of QED through:

$$Q = T_3 + \frac{Y}{2}. \tag{1.12}$$

The electroweak theory distinguishes between fermions in which the spin is antiparallel to the direction of motion (left-handed particles) and fermions in which the spin is instead parallel (right-handed particles). Right-handed particles are not

charged under $\mathrm{SU}(2)_L$. A theory that distinguishes between right and left-handed particles is a chiral theory.

ψ	T_3	Y	Q
$\begin{pmatrix} u_L \\ d_L \end{pmatrix}$	$\begin{matrix} 1/2 \\ -1/2 \end{matrix}$	$1/3$	$\begin{matrix} 2/3 \\ -1/3 \end{matrix}$
u_R	0	$4/3$	$2/3$
d_R	0	$-2/3$	$-1/3$
$\begin{pmatrix} \nu_L \\ l_L \end{pmatrix}$	$\begin{matrix} 1/2 \\ -1/2 \end{matrix}$	-1	$\begin{matrix} 0 \\ -1 \end{matrix}$
l_R	0	-2	-1

Table 1.1: Fermionic content of the Standard Model with their respective $\mathrm{SU}(2)_L$ and $\mathrm{U}(1)_Y$ charges. The electromagnetic charge Q is related to the electroweak charges through Eq. (1.12).

In Table 1.1 we present the full fermionic content of the Standard Model. We can decompose Dirac fermions into chiral ones through the use of the right and left-handed operators P_R and P_L,

$$P_R = \frac{1+\gamma_5}{2}, \qquad P_L = \frac{1-\gamma_5}{2}, \tag{1.13}$$

with $\Psi = (P_R + P_L)\,\Psi = \psi_R + \psi_L$.

Note that left-handed particles (ψ_L) are $\mathrm{SU}(2)_L$ doublets whereas right-handed particles (ψ_R) are $\mathrm{SU}(2)_L$ singlets. Note the absence of the partner of the lepton as a right-handed particle. A right-handed neutrino had not been observed in nature and is thus omitted in the original formulation of the Standard Model.

The complete gauge invariant electroweak Lagrangian yields then,

$$\mathcal{L}_{EW} = i\overline{\psi}_L \not{D} \psi_L + i\overline{\psi}_R \not{D} \psi_R - \frac{1}{4} B_{\mu\nu} B^{\mu\nu} - \frac{1}{4} W^a_{\mu\nu} W^{\mu\nu}_a, \tag{1.14}$$

where $B_{\mu\nu}$ and $W^a_{\mu\nu}$ are the field strength tensors analogous to $F_{\mu\nu}$ for the fields B_μ

and W^a_μ respectively:

$$B_{\mu\nu} = \partial_\mu B_\nu - \partial_\nu B_\mu, \tag{1.15}$$

$$W^a_{\mu\nu} = \partial_\mu W^a_\nu - \partial_\nu W^a_\mu - g_2 \epsilon^{abc} W^b_\mu W^c_\nu, \tag{1.16}$$

where ϵ^{abc} is the fully antisymmetric tensor. In the $\mathrm{SU}(2)_L$ we find for the first time interactions between the gauge bosons of the theory. This is due to the commutation relations of the generators of SU(2): $[\tau^a, \tau^b] = i\epsilon^{abc}\tau^k$.

It must be noted that in $\mathcal{L}_{EW}$ no mass term is present for the fermions nor the gauge bosons. However, we know experimentally that massive bosons and fermions do exist. This apparent paradox is solved by the symmetry breaking mechanism which we introduce in the next section.

1.1.2 Broken symmetries

A symmetry is broken when a physical system does not realise all governing symmetries present in the Lagrangian. If it is possible to find a solution to the system which does not respect a given symmetry, we say that the symmetry is spontaneously broken. The spontaneous symmetry breaking mechanism gives masses to gauge bosons and fermions in an elegant and consistent manner. In this section we introduce the Higgs-Englert-Brout mechanism [3–5] as the symmetry breaking mechanism of the Standard Model. In Section 1.2 we will expand on the phenomenological properties of this particle.

Let us begin by considering a complex scalar field Φ of hypercharge $Y = 1$ and weak isospin $T_3 = \pm\frac{1}{2}$,

$$\Phi = \begin{pmatrix} \phi_1 + i\phi_2 \\ \phi_3 + i\phi_4 \end{pmatrix}, \tag{1.17}$$

where ϕ_i are real fields. The dynamics of the field are described by the Lagrangian [2],

$$\mathcal{L}_\Phi = |D_\mu \Phi|^2 - V\left(|\Phi|^2\right), \tag{1.18}$$

with D_μ given by Eq. (1.11) and where the potential term of Eq. (1.18) can be expanded as,

$$V\left(|\Phi|^2\right) = -\mu^2|\Phi|^2 + \lambda|\Phi|^4, \tag{1.19}$$

where we fix $\lambda > 0$ in order to guarantee the potential is bounded from below.

We must consider two possible scenarios for the potential of Eq. (1.19): $\mu^2 < 0$ and $\mu^2 > 0$. We are interested in the case $\mu^2 > 0$ as in this case the minimum for the potential ($V(|\Phi_0|^2)$), occurs for non-trivial solutions of Φ,

$$|\Phi_0|^2 = \frac{\mu^2}{2\lambda} = \frac{v^2}{2} \tag{1.20}$$

where we have noted the expectation value of the vacuum, $\langle 0|\Phi|0\rangle$, as $v = \frac{\mu}{\sqrt{\lambda}}$.

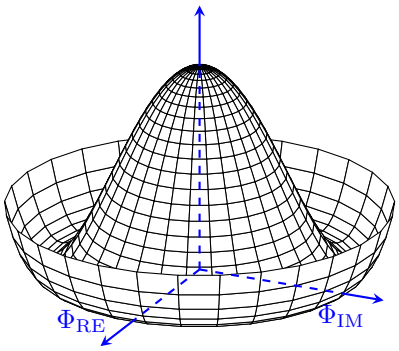

Figure 1.1: Graphical example of the potential $V(|\Phi|^2)$, of Eq. (1.19) for Φ a complex field such as $\Phi = \phi_1 + i\phi_2$.

We can expand the field around the minimum, where the perturbation $h(x)$ corresponds to the Higgs field whose physical realisation is the Higgs boson. In full generality we can write, for a system close to the bottom of the potential,

$$\Phi = \frac{e^{i\tau^a\xi^a(x)}}{\sqrt{2}}\begin{pmatrix} 0 \\ v + h(x) \end{pmatrix}, \tag{1.21}$$

where the v.e.v. of the field $h(x)$ is equal to 0. It is clear from Eq. (1.21) that there are infinitely many choices that would lead to the same solution for the potential. A graphical example is shown in Fig. 1.1. The Goldstone theorem states that there must exist a massless particle (called Goldstone boson) for every spontaneously broken continuous symmetry [6]. For the broken SU(2) symmetry this corresponds

to the three fields $\xi(x)$. Substituting Eq. (1.21) into the potential of Eq. (1.19) it reads,

$$V\left(|\Phi|^2\right) = -\frac{\mu^2}{2}(v+h(x))^2 + \frac{\lambda}{4}(v+h(x))^4, \tag{1.22}$$

which generates self-interactions for the Higgs field ($h(x)$) as well as a mass term for the scalar boson. Dropping constant terms and defining the Higgs boson mass as $m_H = v\sqrt{2\lambda}$ we can reformulate Eq. (1.22) as,

$$V\left(|\Phi|^2\right) = \frac{1}{2}m_H^2 h^2(x) + \frac{m_H^2}{2v}h^3(x) + \frac{m_H^2}{8v^2}h^4(x), \tag{1.23}$$

where, together with a mass term for the Higgs field, we find the trilinear and quartic self-couplings of the Higgs boson.

Through a gauge transformation, we can eliminate the (explicit appearance of) fields $\xi(x)$. As a result of this transformation the weak gauge bosons obtain one extra degree of freedom, becoming massive. This is known as the unitary gauge, in which the field Φ reads,

$$\Phi = \frac{1}{\sqrt{2}}\begin{pmatrix} 0 \\ v+h(x) \end{pmatrix}. \tag{1.24}$$

We now study how Eq. (1.24) affects the electroweak gauge bosons by substituting Eq. (1.24) into the kinetic term of Eq. (1.18) and keeping only the terms quadratic in the gauge fields containing no derivatives,

$$|D_\mu \Phi|^2 = \frac{1}{8}(v+h(x))^2\left\{(g_1 B_\mu - g_2 W_\mu^3)^2 + g_2^2((W_\mu^1)^2 + (W_\mu^2)^2)\right\}, \tag{1.25}$$

where we have used $\tau^a = \frac{\sigma^a}{2}$. These terms generate masses for the gauge bosons as well as interactions between the Higgs boson and the massive electroweak gauge bosons. It is possible to identify in Eq. (1.25) three massive bosons corresponding to the $W^{\pm}$ and Z bosons,

$$|D_\mu \Phi|^2 = \left(1 + \frac{h(x)}{v}\right)^2 \left(\frac{1}{2}m_Z^2 Z^\mu Z_\mu + m_W^2 W^{+\mu} W_\mu^-\right), \tag{1.26}$$

where we have applied the following transformations,

$$\mathrm{W}^{\pm}_{\mu} = \frac{1}{\sqrt{2}}\left(W^1_{\mu} \pm iW^2_{\mu}\right), \qquad m_W = \frac{v}{2}g_2, \tag{1.27}$$

$$\mathrm{Z}^0_{\mu} = \frac{1}{\sqrt{g_1^2+g_2^2}}\left(g_2 W^3_{\mu} - g_1 B_{\mu}\right), \qquad m_Z = \frac{v}{2}\sqrt{g_1^2+g_2^2}, \tag{1.28}$$

$$A^0_{\mu} = \frac{1}{\sqrt{g_1^2+g_2^2}}\left(g_2 W^3_{\mu} + g_1 B_{\mu}\right), \qquad m_A = 0. \tag{1.29}$$

The fourth boson (A^0_{μ}), massless and orthogonal to Z^0_{μ}, corresponds to the photon of the theory of electromagnetism and does not interact directly with the Higgs field.

Spontaneous symmetry breaking can also be used to give mass to the fermions in a gauge invariant way. Let us first see what would happen if we tried to generate masses for a fermion Ψ_f; such a mass term would have the following structure:

$$\mathcal{L}_f = m_f \overline{\Psi}_f \Psi_f = m_f \overline{\psi}_{f,L}(x)\psi_{fR}(x), \tag{1.30}$$

Such a term violates the gauge symmetry $\mathrm{SU}(2)_L \times \mathrm{U}(1)_Y$ and is thus not allowed. It is however possible to generate a mass term for the fermions through the use of the scalar field Φ adding the following gauge invariant Yukawa term,

$$\mathcal{L}_Y = -\sum_f \lambda_f \overline{\Psi}_f(x)\Phi(x)\Psi_f(x), \tag{1.31}$$

Expanding $\mathcal{L}_Y$ we obtain a mass term for the fermions as well as a Higgs-fermion interaction proportional to the mass of the fermion,

$$\mathcal{L}_Y = -\sum_f m_f \left(1 + \frac{h(x)}{v}\right)\overline{\psi}_{f,L}(x)\psi_{f,R}(x), \tag{1.32}$$

with $m_f = \frac{1}{\sqrt{2}} v\lambda_f$ and where the sum is over the entire fermionic content of the Standard Model (Table 1.1).

In general the coupling λ_f is a non-diagonal matrix, $(\lambda_f)_{ij}$, which can introduce a mixing between different generations of fermions (only of quarks for massless neutrinos) if we wish to work in the mass basis. The mixing is parameterised by the Cabbibo-Kobayashi-Maskawa (CKM) matrix. In the work presented in this thesis we take the following two approximations: the CKM matrix is diagonal, i.e., no

mixing is considered, and all quarks save the top are massless particles.

1.1.3 The QCD sector

The remaining gauge group, $\mathrm{SU}(3)_c$, corresponds to the theory of Quantum Chromodynamics, QCD, which describes strong interactions and is characterised by the following Lagrangian,

$$\mathcal{L}_{\mathrm{QCD}} = -\frac{1}{4} F^a_{\mu\nu} F^{\mu\nu}_a + \sum_f \overline{\Psi}_f (i \not{D} - m_f) \Psi_f, \tag{1.33}$$

where the quarks are the only colour-charged fermions, $f \equiv q$, behaving as a triplet under $\mathrm{SU}(3)_c$ transformations. The covariant derivative in this case is given by:

$$D_\mu = \partial_\mu + i g_s t^a A^a_\mu, \tag{1.34}$$

where we have introduced the vector field A^a_μ, corresponding to the gluons, and the matrices t^a which are the eight generators of SU(3). The coupling constant for the strong interactions is g_s and it is usually written in terms of $\alpha_s = \frac{g_s^2}{4\pi}$.

SU(3) is a non-abelian group and thus the gauge bosons of this theory, the gluons, interact with themselves. This self-interaction of the gluon arises from a quadratic term in the field strength tensor $F^a_{\mu\nu}$ analogous to Eq. (1.16),

$$F^a_{\mu\nu} = \partial_\mu A^a_\nu - \partial_\nu A^a_\mu - g_s f^{abc} A^b_\mu A^c_\nu, \tag{1.35}$$

where f^{abc} are the structure constants of $SU(3)$ defined by, $\left[t^a, t^b\right] = i f^{abc} t^c$.

1.1.4 The cross section: from theory to experiment

The experimental study of the Standard Model is performed through the collision of fundamental particles at high speeds. Due to the quantum nature of the theory, the outcome of a collision is not deterministic but probabilistic. In analogy with classical mechanics, we can define a "cross section" from a state $|i\rangle$ to a state $|f\rangle$ as

a measure of the probability of such a transition to occur,

$$\sigma_{i\to f} = \frac{N_f}{N_A N_B}, \tag{1.36}$$

where N_f is the number of outgoing particles and N_A and N_B the number of incoming particles from beams A and B per unit area.

The cross section is related to the Lagrangian through the scattering matrix S, which gives the probability of transition between states,

$$P_{if} = |\langle f|S|i\rangle|^2 = |\mathrm{M}_{i\to f}|^2, \tag{1.37}$$

the matrix elements $\mathrm{M}_{i\to f}$ are usually computed following the diagrammatic notation introduced by Feynman [7]. Calculations in this thesis follow closely the techniques of Ref. [8].

The matrix elements are a function of the momenta of the incoming (p_a and p_b) and outgoing ($\{p_n\}$) particles involved in the collision. In order to obtain a prediction for the cross section it is necessary to integrate over all possible configurations of the momenta of the final state particles. This is known as the phase space. The formula for the cross section from ab to f is then,

$$\sigma_{ab\to f}(p_a, p_b; \{p_n\}) = \frac{1}{2s}\int \mathrm{d}\Phi_n \left|\mathrm{M}_{ab\to f}\left(p_a, p_b; \{p_n\}\right)\right|^2, \tag{1.38}$$

where $\sqrt{s}$ is the center of mass energy such that $s = (p_a + p_b)^2$, the particles a and b are coming respectively from beams A and B. $\mathrm{d}\Phi_n$ is the short-hand notation for the phase space,

$$\mathrm{d}\Phi_n = \prod_{i=1}^{n}\left(\frac{\mathrm{d}^3 p_i}{2E_i(2\pi)^3}\right)(2\pi)^4\,\delta^4\left(p_a + p_b - \sum p_i\right). \tag{1.39}$$

Hadronic collisions and the partonic cross section

In the previous discussion it is assumed that the particles incoming into the scattering event are fundamental. However, this does not need to be the case. In hadron collisions, complex objects made of partons (quarks and gluons) interact. The strong dynamics of the partons within the hadrons cannot be described in terms of the scat-

tering of free particles but, at the high energies that collisions occur it is possible to factorise Eq. (1.38) into a partonic cross section ($\mathrm{d}\hat{\sigma}_{ab\to f}$) and a function describing the probability density of the partons within the hadrons, a parton distribution function or PDF [9],

$$\sigma_{h_A,h_B\to f} = \sum_{a,b} \int \frac{\mathrm{d}x_a}{x_a}\frac{\mathrm{d}x_b}{x_b} f_a^A(x_a) f_b^B(x_b)\, \mathrm{d}\hat{\sigma}_{ab\to f}\left(p_a, p_b; \{p_n\}\right), \tag{1.40}$$

where h_A and h_B are the hadrons coming from beams A and B and $f_a^A(x_a)$ is the PDF for finding parton a inside hadron h_A with a fraction of the momentum of the hadron carried by the parton x_a. The validity of Eq. (1.40) will be challenged in Section 2.1.

Perturbative expansion of the cross section

The experimental study of particle collisions at colliders corresponds to very energetic situations in which the particles interact for a very short amount of time. In this situation the matrix element squared, $M = |\mathrm{M}|^2$, can be expanded in terms of powers of the coupling α_s. If there are n QCD interactions at the lowest order we can break the matrix element squared as,

$$M = \left(\frac{\alpha_s}{2\pi}\right)^n M^{LO} + \left(\frac{\alpha_s}{2\pi}\right)^{n+1} M^{NLO} + \left(\frac{\alpha_s}{2\pi}\right)^{n+2} M^{NNLO} + \mathcal{O}\left(\alpha_s^{n+3}\right), \tag{1.41}$$

and accordingly the differential partonic cross section as,

$$\mathrm{d}\hat{\sigma} = \left(\frac{\alpha_s}{2\pi}\right)^n \mathrm{d}\hat{\sigma}^{\mathrm{LO}} + \left(\frac{\alpha_s}{2\pi}\right)^{n+1} \mathrm{d}\hat{\sigma}^{\mathrm{NLO}} + \left(\frac{\alpha_s}{2\pi}\right)^{n+2} \mathrm{d}\hat{\sigma}^{\mathrm{NNLO}} + \mathcal{O}\left(\alpha_s^{n+3}\right), \tag{1.42}$$

Each new term in Eqs. (1.41) and (1.42) introduce new QCD interactions in the form of closed loops or radiation of particles both suppressed by factors of α_s, despite this suppression they are known to be of importance for an accurate description of the theory. The terms LO, NLO and NNLO refer to the order in the expansion on α_s being leading order, next-to-leading order and next-to-next-to-leading order corrections respectively. Chapter 2 is dedicated to the computation of higher-order QCD corrections.

1.1.5 Regularisation, renormalisation and ultraviolet divergences

The calculation of quantum corrections to scattering rates requires loop integrals over the momenta of the virtual particles contained within the loop. The momentum of a virtual particle can grow arbitrarily large, giving rise to ultraviolet (UV) divergences.

UV divergences can be controlled by dimensional regularisation (DR)[10]. In DR the integral is calculated as an analytic function of the continuous space-time dimension $D = 4 - 2\epsilon$ such that divergences are expressed as poles in $\frac{1}{\epsilon}$. In the limit $\epsilon \to 0$ we recover the usual 4-dimensional space.

UV poles always appear in the form [11]:

$$\frac{\Gamma(1+\epsilon)}{\epsilon} = \frac{1}{\epsilon} + \log(4\pi) - \gamma_E + \mathcal{O}(\epsilon), \tag{1.43}$$

and can be removed through a redefinition of the quantities in the Lagrangian, for QCD this means a reformulation of the quark and gluon fields as well as the couplings and the masses.

$$\Psi_{\text{bare}} = Z_2^{1/2}\Psi(x) \qquad A^\mu_{\text{bare}}(x) = Z_3^{\frac{1}{2}} A^\mu(x), \tag{1.44}$$

$$g^2_{s,\text{bare}} = Z_g g_s^2, \qquad m_{\text{bare}} = Z_m m. \tag{1.45}$$

In performing this redefinition, the Lagrangian has lost predictive power as masses and couplings have become inputs of the theory. Counterterms absorb all UV divergences order by order. By taking the perturbative expansion of the $Z_i = 1 + \delta Z_i$ we can define a counterterm Lagrangian ($\mathcal{L}_{\text{c.t.}}$) relating the renormalised Lagrangian ($\mathcal{L}_{\text{ren}}$) and the original bare Lagrangian ($\mathcal{L}_{\text{bare}}$),

$$\mathcal{L}_{\text{bare}} = \mathcal{L}_{\text{ren}} + \mathcal{L}_{\text{c.t.}}, \tag{1.46}$$

so that all UV divergences live in $\mathcal{L}_{\text{c.t.}}$.

The choice of the pole-subtracting counterterm is not unique. In the minimal-

subtraction scheme (MS) the counterterms are chosen such that only the $\frac{1}{\epsilon}$ pole is removed. In the calculations presented in this thesis, all quantities are renormalised using the $\overline{\text{MS}}$ scheme in which the whole of Eq. (1.43) is subtracted, which corresponds to a re-scaling of the $\frac{1}{\epsilon}$ poles, $\frac{1}{\bar{\epsilon}} = \overline{C}(\epsilon)\frac{1}{\epsilon}$,

$$\overline{C}(\epsilon) = (4\pi)^{\epsilon} e^{-\epsilon\gamma_E}. \tag{1.47}$$

After the regularisation procedure, the coupling constant α_s is promoted to a massive quantity $\alpha_s \to \mu_{\text{R}}^{2\epsilon}\alpha_s$. The scale at which we renormalise the theory, μ_{R}, is an unphysical parameter on which physical predictions must not depend. When computing fixed-order corrections in perturbative theory a residual dependence of order $\mathcal{O}(\alpha_s^{n+1})$ is kept as we truncate the series at order n.

Imposing μ-independence leads to the renormalisation group equation (RGE), which for the coupling α_s takes the form:

$$\mu_{\text{R}}^2 \frac{\partial \alpha_s(\mu_{\text{R}}^2)}{\partial \mu_{\text{R}}^2} = \beta(\alpha_s(\mu_{\text{R}}^2)), \tag{1.48}$$

requiring a boundary condition, $\alpha_s(Q_0^2) = \alpha_s^{\text{reference}}$ (usually chosen to be $Q_0 = m_Z$), determined experimentally.

The function $\beta(\alpha_s)$, known to 5-loops [12], characterises the behaviour of $\alpha_s(Q^2)$ which at leading order reads,

$$\alpha_s(Q^2) = \frac{\alpha_s(\mu_{\text{R}}^2)}{1 + \beta_0 \left(\frac{\alpha_s(\mu_{\text{R}}^2)}{4\pi}\right) \log\left(\frac{Q^2}{\mu_{\text{R}}^2}\right)}. \tag{1.49}$$

The positive sign for the value of β_0 for QCD means the evolution equation for $\alpha_s(Q^2)$ gives rise to a phenomenon known as asymptotic freedom, i.e., $\alpha_s(Q^2)$ decreases as the energy transfer increases. Asymptotic freedom allow us to compute predictions for high energy collisions making use of perturbative tools where the expansion is on the small parameter α_s. In contrast, as the energy decreases $\alpha_s(Q^2)$ will increase, and so the low energy strong dynamics cannot be computed perturbatively. In Section 2.4 we detail the higher-order evolution of the strong coupling up to NNLO as well as the dependence on μ_{R} of arbitrary observables computed at fixed-order in perturbation

theory.

1.2 Higgs boson phenomenology

The electroweak symmetry breaking mechanism (Section 1.1.2) as proposed by P. Higgs [3, 4] and F. Englert and R. Brout [5] has, as a consequence, the existence of an additional massive particle as the physical manifestation of the scalar field. These massive modes were realised as scalar bosons and would later be referred to as the Higgs bosons.

Shortly after its inception, the Higgs boson became part of the Standard Model and alongside the discovery of the third generation of quarks and the gauge vector bosons, is another proof of the immense predictive success of the Standard Model of particle physics.

In this section we outline the production modes for the Higgs boson at hadron colliders (Section 1.2.1) and its decay modes (Section 1.2.2) and we finish with a review of its discovery in 2012.

1.2.1 Higgs boson production at hadron colliders

Higgs boson production at hadron colliders can occur through four different channels: in **gluon fusion** and $\mathbf{t\bar{t}H}$ the Higgs boson is produced via its Yukawa coupling to massive quarks whereas in **Vector Boson Fusion** and **associated production VH** it is produced via its VVH vertex. Some examples are depicted in Fig. 1.2.

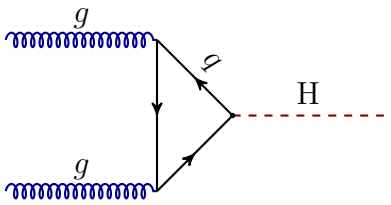

(a) Gluon fusion Higgs boson production or ggF.

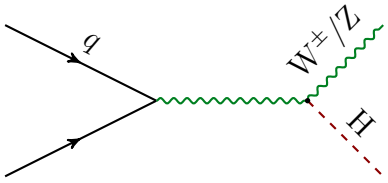

(b) Associated Higgs and gauge boson production or VH.

Figure 1.2: Examples of Higgs boson production processes in hadron collisions.

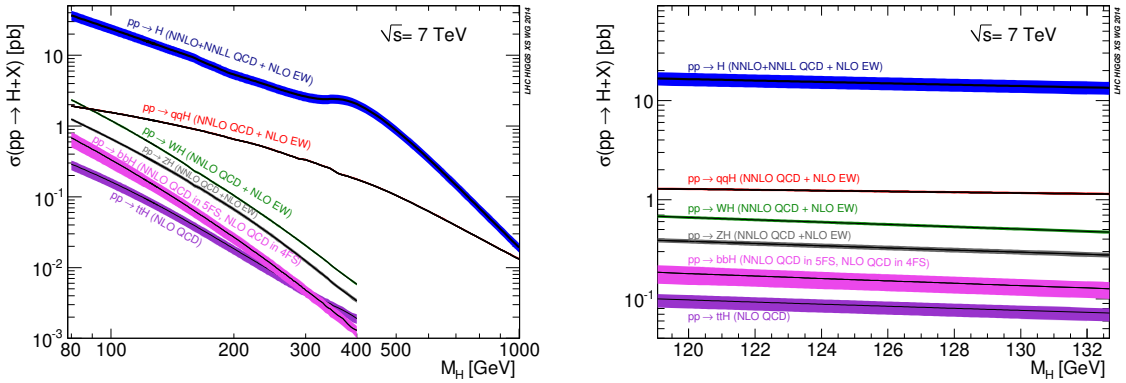

Figure 1.3: Higgs production rate for different subprocess at a center of mass energy of $\sqrt{s} = 7$ TeV. Plots by the Higgs cross section working group [13].

Of all production modes, the most important in the LHC is the gluon fusion or ggF mode. The Higgs boson does not couple directly to gluons, but indirectly through a massive quark loop. Fig. 1.3 shows the production rate for the Standard Model Higgs boson at the LHC as a function of its mass. The ggF mode is the dominant production mode in the entire range of the Higgs boson masses available to the LHC. Today we know the Higgs boson mass sits around $m_H \sim 125$ GeV, where the ggF channel is an order of magnitude greater than any other.

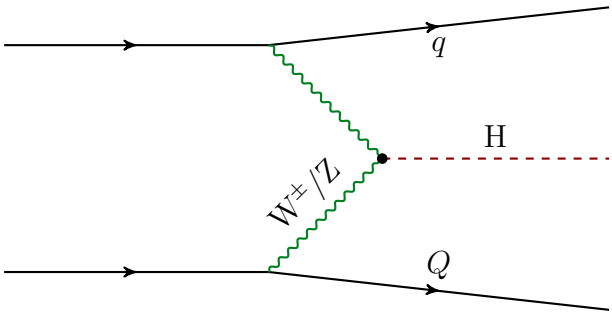

Figure 1.4: Vector Boson Fusion Higgs boson production or VBF.

The second most important channel is the Vector Boson Fusion Higgs boson production or VBF mode, to which this thesis is dedicated, depicted in Fig. 1.4. In this mode each of the incoming protons radiates a gauge vector boson which then fuse to produce a Higgs boson. This channel is the most important among processes in which the Higgs boson is produced via a VVH vertex. It is also second overall in the inclusive production rate of the boson, amounting to an approximately 10% of the dominant ggF mode.

Third in importance is associated production with a vector boson or VH mode. In this channel a quark and an antiquark annihilate to produce a vector boson which then radiates a Higgs boson. Note that this channel would gain importance with respect to VBF in a proton-antiproton collider, where both annihilating quarks are valence quarks.

The last of the production channels is associated production alongside a $t\bar{t}$ pair. All of them have been observed at the LHC [14].

1.2.2 Higgs boson decay at hadron colliders

For a Higgs boson of mass $m_H \simeq 125$ GeV, compatible with the current experimental figures [15] the decay width of the particle is $\Gamma \simeq 4$ MeV [13]. This narrow value of Γ_H makes the Higgs boson a very short-lived boson which almost immediately decays into longer-lived particles. Experimentally, the current bound for the Higgs boson width is $\Gamma_H < 13$ MeV [16]. The branching ratio (BR) for the decay of a particle to a particular final state is the ratio between the decay rate for that process and the total decay rate integrating over every possible final state. In Fig. 1.5 the branching ratio of the Higgs boson to different final states is plotted as a function of the mass of the resonance.

For $m_H \simeq 125$ GeV, the dominant production channels are the Higgs boson decays to b-quarks and to gauge vector bosons which can suffer from important backgrounds coming from other production modes and are thus experimentally challenging. Experimentally it is preferred to use decay modes in which the final products are composed only of photons ($\mathrm{H} \to \gamma\gamma$) or leptons and missing energy ($\mathrm{H} \to \mathrm{ZZ}^* \to 4l$ or $\mathrm{H} \to \mathrm{WW}^* \to 2l2\nu$). Although they might have a smaller branching ratio, these decay channels are much easier to isolate. In Fig. 1.6 we show examples of diagrams for the Higgs boson decay into two photons (like ggF, this mode is mediated by a heavy gauge boson and quark loops) and Higgs boson decay into two gauge bosons which decay themselves into a pair of fermions each.

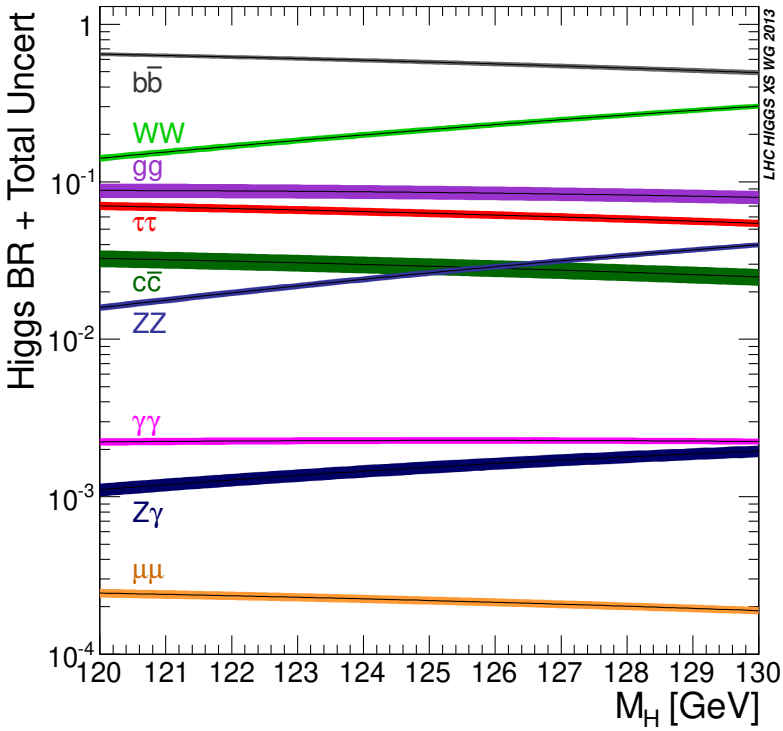

Figure 1.5: Higgs boson branching ratios as a function of the mass of the boson. Plot by the Higgs cross section working group [13].

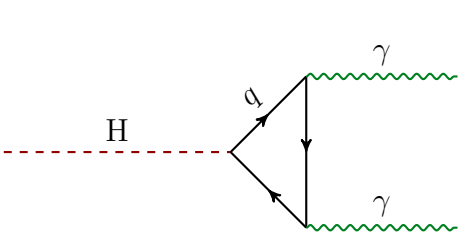

(a) Higgs boson decay into two photons via a heavy quark loop.

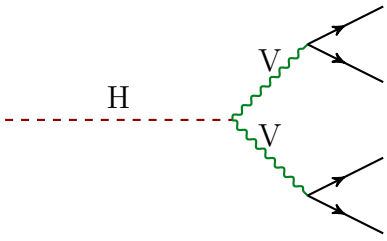

(b) Decay of the Higgs boson to four fermions.

Figure 1.6: Examples of Higgs boson decay modes.

1.2.3 The discovery of the Higgs boson

The Higgs boson has been part of the experimental agenda for many years. Direct searches were performed in the LEP and Tevatron colliders with no success. The LEP collider was able to set a lower limit for the resonance, finding $m_H > 114$ GeV. The Tevatron collider conducted searches for the Higgs boson in the range $100 - 200$ GeV and was able to exclude a resonance at the very start of the range ($100 - 103$ GeV) as well as near the upper end ($m_H < 147$ GeV). Events were found in the range in which the Higgs boson was later confirmed by the LHC, but with no statistical significance [17, 18].

The ATLAS and CMS experiments of the LHC, prior to the announcement of the discovery, were able to confirm and extend the exclusion ranges from previous colliders. The 2011 exclusion range can be seen in Fig. 1.7.

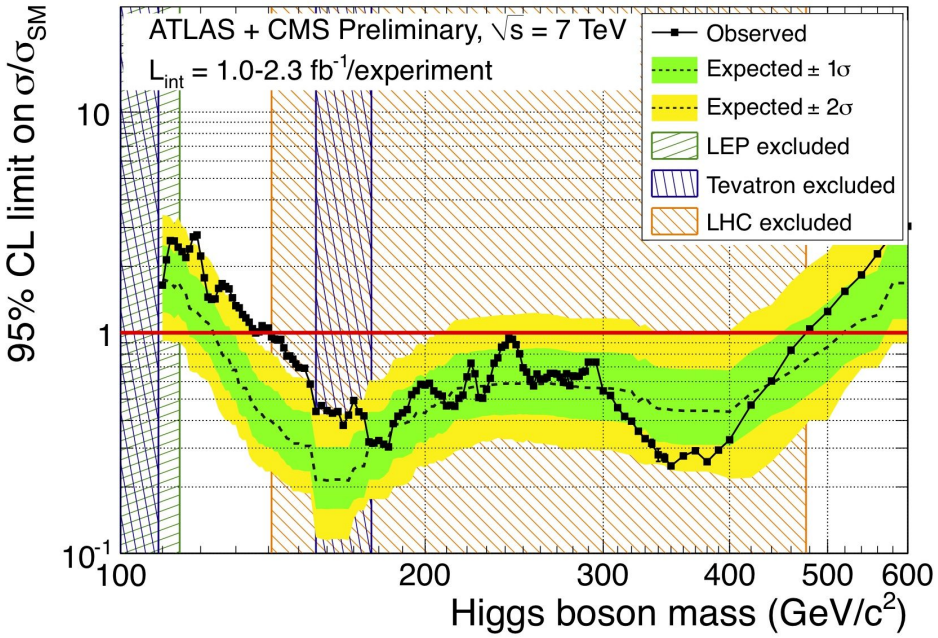

Figure 1.7: Experimental limits from LEP, Tevatron and LHC on the Higgs boson mass on the $100 - 600$ GeV mass range by the year 2011. The dashed limit show the expected limit in the absence of the Higgs boson. Plot from Ref. [18].

The discovery of the Higgs boson was announced in the summer of 2012, both the ATLAS and CMS experiments were able to independently identify a resonance at a mass of around 125 GeV which was compatible with the Standard Model Higgs

boson. The signal strength of the different Higgs boson decay modes at the time of the discovery of the particle are shown in Fig. 1.8.

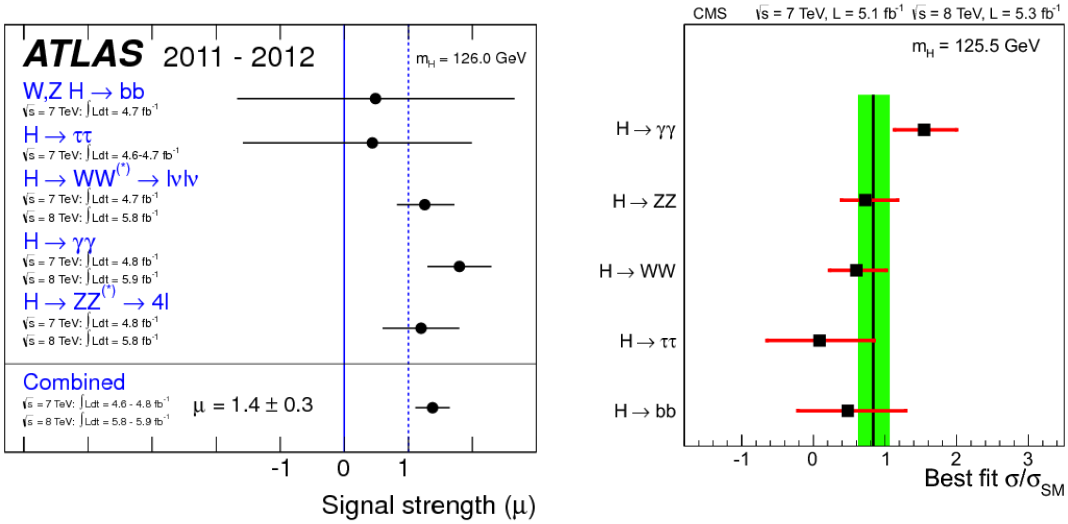

Figure 1.8: Best fit value for the Higgs boson cross section for each decay mode relative to the expected Standard Model value: $\mu = \frac{\sigma}{\sigma_{SM}}$. Plots from Ref. [19].

After the discovery of the boson, some key questions remain: is this the Standard Model Higgs boson? Or does it correspond to one of the many supersymmetric Higgs-like particles which *just happens* to be compatible with the Standard Model? Do the couplings of the Higgs boson correspond to the Standard Model couplings in all cases? These questions and many more motivate the precise study of the Higgs boson production modes at hadron colliders in order to stress test the Standard Model and find evidence of new physics.

Chapter 2

Higher-Order QCD Corrections

This chapter is dedicated to the challenges of cross-section calculations beyond leading order in perturbative QCD. Let us begin by recalling the formula for the perturbative cross section of Eq. (1.42),

$$\mathrm{d}\hat{\sigma} = \left(\frac{\alpha_s}{2\pi}\right)^n \mathrm{d}\hat{\sigma}^{\mathrm{LO}} + \left(\frac{\alpha_s}{2\pi}\right)^{n+1} \mathrm{d}\hat{\sigma}^{\mathrm{NLO}} + \left(\frac{\alpha_s}{2\pi}\right)^{n+1} \mathrm{d}\hat{\sigma}^{\mathrm{NNLO}} + \mathcal{O}\left(\alpha_s^{n+3}\right), \qquad (2.1)$$

where the NLO and NNLO pieces are the first and second order QCD corrections respectively.

Firstly, in Section 2.1 we challenge the validity of the naive factorisation between partonic and physical cross sections. In Section 2.2 we review the different types of infrared divergences appearing in NLO and NNLO calculations and in Section 2.3 we introduce a method to remove them: the antenna formalism. The chapter concludes with the application of the RGE to arbitrary observables in order to study their scale-dependent terms.

2.1 The improved parton model

In Eq. (1.40) we naively factorised the physical cross section into a partonic cross section and a PDF. In the partonic cross section the momenta of the initial-state (i.s.) partons are fixed and the integration is performed over the final-state (f.s.) particles. The PDF encodes the parton dynamics within the hadron depending only

on a variable x, the fraction of the hadron momentum carried by the parton.

The i.s. partons can themselves radiate other particles before entering the scattering process. Two scenarios can be distinguished: if the radiated partons are unresolved with respect to the incoming parton (which acts as the radiator) then the momentum fraction it carries will be modified. On the other hand, if the transverse momenta of the emissions are large enough, the radiated particles will be identified as external particles and must be computed as part of the scattering matrix element. This distinction between short and long distance physics is parameterised by the introduction of a cut-off factorisation scale μ_{F}.

We can relate the "bare PDF" of Eq. (1.40) to the physical PDF by convolution with a factorisation kernel of inverse $\boldsymbol{\Gamma}^{-1}$ [20]. In symbolic notation*,

$$\boldsymbol{f}^b(x) = \boldsymbol{f}(\mu_F) \otimes \boldsymbol{\Gamma}^{-1}(\mu_{\mathrm{F}}), \tag{2.2}$$

where the elements Γ_{ij} of the (n_{partons} x n_{partons}) $\boldsymbol{\Gamma}$ matrix can also be perturbatively expanded in α_s corresponding to the number of emissions:

$$\boldsymbol{\Gamma}_{ij}(z,\mu_{\mathrm{F}}) = \boldsymbol{\delta}_{ij}\delta(1-z) + \left(\frac{\alpha_s(\mu_{\mathrm{F}})}{2\pi}\right)\boldsymbol{\Gamma}^1_{ij}(z) + \left(\frac{\alpha_s(\mu_{\mathrm{F}})}{2\pi}\right)^2\boldsymbol{\Gamma}^2_{ij}(z) + \mathcal{O}\big(\alpha_s(\mu_{\mathrm{F}})^3\big). \tag{2.3}$$

The notation $\boldsymbol{\Gamma}_{ij}$ indicates that they contain all colour information from the splitting vertex, as opposed to the colour striped Γ_{ij}. In the $\overline{\mathrm{MS}}$ scheme they read [20, 21],

$$\boldsymbol{\Gamma}^1_{ij}(z) = -\frac{1}{\epsilon}\boldsymbol{P}^0_{ij}(z), \tag{2.4}$$

$$\boldsymbol{\Gamma}^2_{ij}(z) = \frac{1}{2\epsilon^2}\left[(\boldsymbol{P}^0_{jk}\otimes\boldsymbol{P}^0_{ki})(z) + 2\beta_0\boldsymbol{P}^0_{ij}(z)\right] - \frac{1}{2\epsilon}\boldsymbol{P}^1_{ij}(z), \tag{2.5}$$

where for simplicity $\boldsymbol{\Gamma}^2_{ij}(z)$ can be decomposed as,

$$\boldsymbol{\Gamma}^2_{ij}(z) = \overline{\boldsymbol{\Gamma}}^2_{ij}(z) - \frac{\beta_0}{\epsilon}\boldsymbol{\Gamma}^1_{ij}(z) + \frac{1}{2}\left(\boldsymbol{\Gamma}^1_{ik}\otimes\boldsymbol{\Gamma}^1_{kj}\right), \tag{2.6}$$

$$\overline{\boldsymbol{\Gamma}}^2_{ij}(z) = -\frac{1}{2\epsilon}\left(\boldsymbol{P}^1_{ij}(z) + \frac{\beta_0}{\epsilon}\boldsymbol{P}^0_{ij}(z)\right). \tag{2.7}$$

These functions are defined in terms of the DGLAP [22] kernels ($\boldsymbol{P}_{ij}(z)$), which

*Defining $(f\otimes g)(x) = \int_0^1 \mathrm{d}y\,\mathrm{d}z\,\delta(x-yz)f(y)g(z)$.

can be understood as the probability for a parton j emitting a collinear parton i with momentum fraction of the original parton z. The splitting functions are definite positive for $z < 1$ and at the lowest order they read [11],

$$\boldsymbol{P}^0_{qq}(z) = \frac{N^2-1}{2N}\left(\frac{1+z^2}{(1-z)_+} + \frac{3}{2}\delta(1-z)\right), \tag{2.8}$$

$$\boldsymbol{P}^0_{qg}(z) = \frac{1}{2}\left(z^2 + (1-z)^2\right), \tag{2.9}$$

$$\boldsymbol{P}^0_{gq}(z) = \frac{N^2-1}{2N}\left(\frac{1+(1-z)^2}{z}\right), \tag{2.10}$$

$$\boldsymbol{P}^0_{gg}(z) = 2N\left(\frac{z}{(1-z)_+} + \frac{1-z}{z} + z(1-z)\right) + \delta(1-z)\frac{11N-2N_f}{6}, \tag{2.11}$$

with the plus distribution defined as,

$$\int_0^1 \mathrm{d}z\, g(z) f_+(z) = \int_0^1 f(z)\left(g(z) - g(1)\right). \tag{2.12}$$

We can now replace the bare PDF we used in Eq. (1.40) with the physical PDF of Eq. (2.2), dropping the x-dependence for simplicity,

$$\begin{aligned}\mathrm{d}\boldsymbol{\sigma} &= \boldsymbol{f}^b \cdot \mathrm{d}\hat{\boldsymbol{\sigma}} \cdot \boldsymbol{f}^b \\ &= \boldsymbol{f} \otimes \boldsymbol{\Gamma}^{-1} \cdot \mathrm{d}\hat{\boldsymbol{\sigma}} \cdot \boldsymbol{\Gamma}^{-1} \otimes \boldsymbol{f} = \boldsymbol{f} \otimes \mathrm{d}\hat{\boldsymbol{\sigma}}' \otimes \boldsymbol{f},\end{aligned} \tag{2.13}$$

where after mass factorisation the partonic cross section is,

$$\mathrm{d}\hat{\boldsymbol{\sigma}}' = \boldsymbol{\Gamma}^{-1} \cdot \mathrm{d}\hat{\boldsymbol{\sigma}} \cdot \boldsymbol{\Gamma}^{-1}. \tag{2.14}$$

Using Eq. (2.3) it is possible to define LO, NLO and NNLO contributions akin to Eq. (2.1) depending on the order in α_s at which they enter the calculation [21],

$$\mathrm{d}\hat{\sigma}_{ij}^{\mathrm{MF,\ NLO}}(p_a, p_b) = -\int \frac{dz_1}{z_1}\frac{dz_2}{z_2}\boldsymbol{\Gamma}^1_{ij;kl}(z_1, z_2)\,\mathrm{d}\hat{\sigma}_{kl}^{\mathrm{LO}}(z_1 p_a, z_2 p_b), \tag{2.15}$$

$$\begin{aligned}\mathrm{d}\hat{\sigma}_{ij}^{\mathrm{MF,\ NNLO}}(p_a, p_b) = -\int \frac{dz_1}{z_1}\frac{dz_2}{z_2}\Bigg\{&\overline{\boldsymbol{\Gamma}}^2_{ij;kl}(z_1, z_2)\,\mathrm{d}\hat{\sigma}_{kl}^{\mathrm{LO}}(z_1 p_a, z_2 p_b) \\ &+ \boldsymbol{\Gamma}^1_{ij;kl}(z_1, z_2)\left(\mathrm{d}\hat{\sigma}_{kl}^{\mathrm{NLO}}(z_1 p_a, z_2 p_b) - \left(\frac{\alpha_s}{2\pi}\right)\frac{\beta_0}{\epsilon}\,\mathrm{d}\hat{\sigma}_{kl}^{\mathrm{LO}}(z_1 p_a, z_2 p_b)\right) \\ &+ \frac{1}{2}\left[\boldsymbol{\Gamma}^1_{ij;ab} \otimes \boldsymbol{\Gamma}^1_{ab;kl}\right](z_1, z_2)\,\mathrm{d}\hat{\sigma}_{kl}^{\mathrm{LO}}(z_1 p_a, z_2 p_b)\Bigg\}\end{aligned} \tag{2.16}$$

where we make use of the short-hand notation,

$$\mathbf{\Gamma}^{l}_{ij;kl}(z_1, z_2) = \bar{C}^{l}(\epsilon)\left(\frac{\alpha_s}{2\pi}\right)^{l}\left(\mathbf{\Gamma}^{l}_{ki}(z_1)\delta_{jl}\delta(1-z_2) + \mathbf{\Gamma}^{l}_{lj}(z_2)\delta_{ik}\delta(1-z_1)\right). \tag{2.17}$$

The form of the mass factorisation or MF terms is completely general and its inclusion is of vital importance for the regulation of initial-state collinear singularities which will be introduced in the next section.

2.2 Infrared divergences

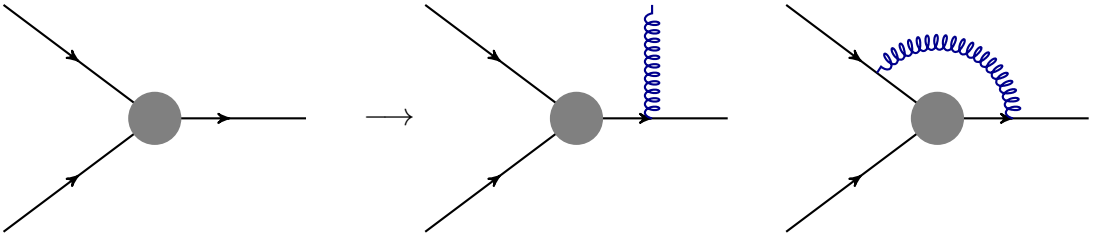

(a) Born level diagram. (b) Real radiation diagram. (c) Virtual diagram.

Figure 2.1: Example of higher-order corrections for a scattering process. The incoming arrows represent the i.s. particles, the outgoing arrow one of the f.s. particles. The shaded blob in the middle represents the rest of the hard-scattering process.

In Section 1.1.5 the integration over all possible momentum configurations in the loop integral gave rise to UV divergences when the momenta of the particles were large. Similarly, when the momenta of massless particles in the loop become very small we may encounter infrared (IR) divergences.

Physical observables are required to be IR-safe. An observable is said to be infrared safe or IR-safe when it is insensitive to radiation in the infrared limit. These can take the form of soft or collinear limits, a differentiation which will be further explored within this section. For soft limits this condition can be formulated for a given observable O which depends on a set of momentum $\{p_1, \ldots, p_i, \ldots, p_n\}$ as

$$\lim_{p_i \to 0} O\left(p_1, \ldots, p_{i-1}, p_i, p_{i+1}, \ldots, p_n\right) = O\left(p_1, \ldots, p_{i-1}, p_{i+1}, \ldots, p_n\right), \tag{2.18}$$

while for collinear limits it takes the form

$$\lim_{p_i||p_{i+1}} O\left(p_1,\ldots,p_i,p_{i+1},\ldots,p_n\right) = O\left(p_1,\ldots,p_i+p_{i+1},\ldots,p_n\right). \tag{2.19}$$

A good example of an IR-unsafe observable would be the number of particles in a collision. In contrast, observables such as the number of jets in an event (which we study later in this chapter) can be defined to be IR-safe.

The calculation of scattering amplitudes, however, can bring about IR singularities. In dimensional regularisation these appear as poles on the parameter ϵ. When the dependency on ϵ is explicit the singularities are known as "explicit singularities". These can appear in virtual (V) amplitudes, i.e., diagrams with loops.

On the other hand, if the ϵ-dependency is not explicit, the singularities are said to be "implicit". This is the case of real radiation amplitudes (R) where the momenta of the radiated partons can go arbitrarily small or collinear*. When this happen we say the radiator and radiated partons are "unresolved", i.e., they can no longer be resolved as separate objects.

Naively, one could think these considerations make the calculation of higher order cross sections (which include both R and V contributions) IR-unsafe. For instance, at NLO we could write,

$$\hat{\sigma}_{ij}^{\mathrm{HO}} = \hat{\sigma}_{ij}^{\mathrm{V}} + \hat{\sigma}_{ij}^{\mathrm{R}}. \tag{2.20}$$

As there should be no infrared singularities the expectation is that they should cancel. Indeed, the work of Bloch and Nordsieck [23] for QED and more generally by Kinoshita [24], Lee and Nauenberg [25] shows this is the case, infrared singularities cancel between R and V contributions when all unresolved or mass-degenerated states are summed together. This is known as the **KLN theorem**.

Note that this result does not apply to i.s. collinear singularities as they are a fixed input to the scattering. These are however eliminated by the MF terms introduced in Section 2.1. We can reformulate Eq. (2.20) for hadronic initial states

*Note we consider massless QCD, i.e., a pair of collinear quark and antiquark is massless and generates a singularity. This will be seen more clearly later in this chapter when we review the different types of singularities.

to include these mass factorisation terms in order to make the cross section IR-safe,

$$\hat{\sigma}_{ij}^{\mathrm{HO}} = \hat{\sigma}_{ij}^{\mathrm{V}} + \hat{\sigma}_{ij}^{\mathrm{R}} + \hat{\sigma}_{ij}^{\mathrm{MF}}. \tag{2.21}$$

2.2.1 Colour ordered matrix elements

QCD amplitudes can be decomposed into colour stripped subamplitudes such that colour and kinematics can be separated [8, 26]. The full matrix element M is obtained upon summing over all possible gluon permutations of the partial amplitude $\mathcal{M}$,

$$\mathrm{M} = \sum_{\text{perm.}} \lambda(a, b, \ldots)\mathcal{M}(a, b, \ldots), \tag{2.22}$$

where $\mathcal{M}$ depends only on the helicity and phase space configurations and all colour content is encoded in the function λ. In this picture singularities, be they real or virtual, only occur between colour-neighbouring partons. In our notation, this is represented as adjacent arguments in functions, for instance in the amplitude $\mathcal{M}$,

$$\mathcal{M}(\ldots, i, j, k, \ldots), \tag{2.23}$$

the two colour-neighbours of j are i and k.

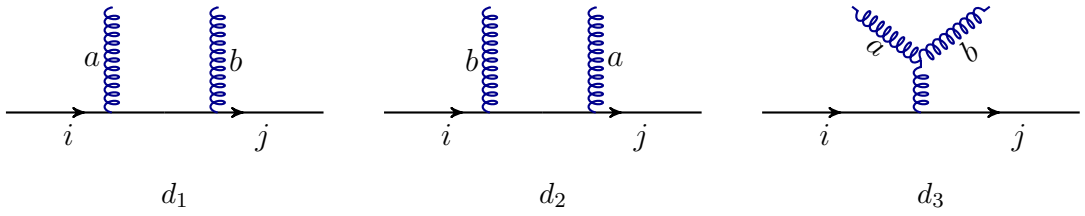

Figure 2.2: Diagrams corresponding to a quark current from which two gluons are radiated.

Let us see this explicitly using as an example the two-emission quark current of Fig. 2.2, made up of three diagrams. The complete current $\mathrm{J}_2^{(0)}$ in terms of the three partial amplitudes of Fig. 2.2 is,

$$\mathrm{J}_2^{(0)} = t^b_{jk} t^a_{ki}\, d_1 + t^a_{jk} t^b_{ki}\, d_2 + i f^{cab} t^c_{ji}\, d_3, \tag{2.24}$$

corresponding to the two permutations of gluons a and b. It will be useful for the

discussion of Section 2.2.3 to note that the first two diagrams present propagators proportional to $\frac{1}{s_{ia}}$ while only the three-gluon diagram presents a propagator proportional to $\frac{1}{s_{ab}}$.

The treatment of the colour content is performed extracting the colour coefficient of the QCD vertices, which are proportional either to the $\mathrm{SU}(3)_c$ generators t^a or to the structure constant f^{abc}, related to the t^a matrices through,

$$f^{abc} = 2i\left(\mathrm{Tr}\{t^a t^b t^c\} - \mathrm{Tr}\{t^a t^c t^b\}\right), \tag{2.25}$$

The traces can be removed through the Fierz relation:

$$t^a_{ij} t^b_{kl} = \frac{1}{2}\left(\delta_{il}\delta_{jk} - \frac{1}{N}\delta_{ij}\delta_{kl}\right). \tag{2.26}$$

Using these relations we can reformulate Eq. (2.24) as,

$$\mathrm{J}_2^{(0)} = t^b_{jk} t^a_{ki}\, J_2^{(0)}(i,a,b,j) + t^a_{jk} t^b_{ki}\, J_2^{(0)}(i,b,a,j) \tag{2.27}$$

with,

$$J_2^{(0)}(i,a,b,j) = d_1 + d_3, \tag{2.28}$$

$$J_2^{(0)}(i,b,a,j) = d_2 - d_3. \tag{2.29}$$

The square of the current can then be separated according to the different colour prefactors, summing over final and averaging over initial colours as,

$$\sum \left|\mathrm{J}_2^{(0)}\right| = \frac{N^2-1}{4}\left(M_{2g}^{(0)} - \frac{1}{N^2}\widetilde{M}_{2g}^{(0)}\right), \tag{2.30}$$

where here we have notated the colour leading and subleading squared matrix elements M and $\widetilde{M}$ as,

$$M_{2g}^{(0)} = \left|J_2^{(0)}(i,a,b,j)\right|^2 + \left|J_2^{(0)}(i,b,a,j)\right|^2, \tag{2.31}$$

$$\widetilde{M}_{2g}^{(0)} = \left|J_2^{(0)}(i,\widetilde{a},\widetilde{b},j)\right|^2 = \left|J_2^{(0)}(i,a,b,j) + J_2^{(0)}(i,b,a,j)\right|^2. \tag{2.32}$$

Note the absence of the three-gluon vertex from Eq. (2.32). Since we have removed the gluon self-interaction, they behave like a photon. We note these abelian-like

gluons as $\widetilde{a}$.

2.2.2 Virtual corrections

After UV poles in $\frac{1}{\epsilon}$ have been absorbed in the redefinition of the physical parameters of the system, the leftover $\frac{1}{\epsilon}$ poles correspond to the IR divergences of the loop calculation. The IR $\frac{1}{\epsilon}$ structure of the QCD virtual amplitudes is known up to two loops [27] and allows for the decomposition of virtual amplitudes such as the one depicted in Fig. 2.1c,

$$\mathcal{M}_n^{(l)}\left(\epsilon;\{p_n\}\right) = \mathcal{M}_{n,\text{finite}}^{(l)}(\{p_n\}) + \sum_{i=1}^{l} \boldsymbol{I}_n^{(i)}\left(\epsilon;\{p_n\}\right) \mathcal{M}_n^{(l-i)}\left(\epsilon;\{p_n\}\right), \tag{2.33}$$

where $\boldsymbol{I}_n^{(i)}\left(\epsilon;\{p_n\}\right)$ are the appropriate combinations of the Catani pole operators that can be found in Refs. [27, 28].

At NLO the virtual matrix element squared corresponds to the interference between the virtual amplitude and the tree level amplitude of the same multiplicity. Dropping $(\{p_n\})$ from the argument list we have,

$$M_n^{(1)}(\epsilon) \equiv \left\langle \mathcal{M}_n^{(1)}(\epsilon) \middle| \mathcal{M}_n^{(0)} \right\rangle + \left\langle \mathcal{M}_n^{(0)} \middle| \mathcal{M}_n^{(1)}(\epsilon) \right\rangle, \tag{2.34}$$

accordingly, the $\frac{1}{\epsilon}$ structure of the squared matrix elements, using Eq. (2.33), will be proportional to the tree level squared amplitude, $M_n^{(0)}$;

$$M_n^{(1)}(\epsilon) = \left(\boldsymbol{I}^{(1)}(\epsilon) + \boldsymbol{I}^{(1)\dagger}(\epsilon)\right) M_n^{(0)}. \tag{2.35}$$

At NNLO we can find one-loop one-emission matrix elements, which correspond to the same structure as Eq. (2.34) with $n \to n+1$,

$$M_{n+1}^{(1)}(\epsilon) \equiv \left\langle \mathcal{M}_{n+1}^{(1)}(\epsilon) \middle| \mathcal{M}_{n+1}^{(0)} \right\rangle + \left\langle \mathcal{M}_{n+1}^{(0)} \middle| \mathcal{M}_{n+1}^{(1)}(\epsilon) \right\rangle. \tag{2.36}$$

We also find at NNLO two-loop matrix elements which are different from Eq. (2.34) in that they also receive a contribution from the 1-loop amplitude squared,

$$M_n^{(2)}(\epsilon) \equiv \left\langle \mathcal{M}_n^{(1)}(\epsilon) \middle| \mathcal{M}_n^{(1)}(\epsilon) \right\rangle + \left\langle \mathcal{M}_n^{(2)}(\epsilon) \middle| \mathcal{M}_n^{(0)} \right\rangle + \left\langle \mathcal{M}_n^{(0)} \middle| \mathcal{M}_n^{(2)}(\epsilon) \right\rangle, \tag{2.37}$$

and thus the $\frac{1}{\epsilon}$ singular structure of the double virtual matrix element squared yields,

$$M_n^{(2)}(\epsilon) = \left(\boldsymbol{I}^{(1)}(\epsilon)\boldsymbol{I}^{(1)\dagger}(\epsilon)\right) M_n^{(0)} + \left(\boldsymbol{I}^{(1)}(\epsilon) + \boldsymbol{I}^{(1)\dagger}(\epsilon)\right) M_n^{(1)}(\epsilon) + \left(\boldsymbol{I}^{(2)}(\epsilon) + \boldsymbol{I}^{(2)\dagger}(\epsilon)\right) M_n^{(0)}. \tag{2.38}$$

2.2.3 Real radiation, implicit divergences

Consider a real emission diagram such as Fig. 2.1b. If the arrow represents a massless fermion the propagator is proportional to:

$$\frac{\not{p}_i + \not{p}_j}{s_{ij}} = \frac{\not{p}_i + \not{p}_j}{2E_iE_j(1-\cos(\theta_{ij}))}, \tag{2.39}$$

whereas if it were a gluon, we would find,

$$\frac{1}{s_{ij}} = \frac{1}{2E_iE_j(1-\cos(\theta_{ij}))}, \tag{2.40}$$

where in both equations i and j are the two outgoing particles, E_i and E_j are their energies, and θ_{ij} the angle between them.

When partons i and j can be independently measured, we say they are resolved. Otherwise the parton is said to be unresolved. The propagators of Eq. (2.39) and Eq. (2.40) develop singularities when any of their components becomes unresolved, which can occur in two different configurations:

- Soft limits, denoted as $p_i \to 0$: the momentum of a parton goes to 0. If both i and j are gluons, both E_i and E_j give rise to the singularities. If one of the particles is a quark, fermion number conservation will make the whole matrix element vanish in that limit.

- Collinear limit, denoted as $p_i||p_j$: the two partons become collinear and thus inseparable, it corresponds to $\cos(\theta_{ij}) \to 1$.

In both cases the invariant s_{ij} becomes much smaller than the rest of the scales of the scattering process. The phase space integral is over all possible physical configurations which include both the collinear and soft limits as well as combinations

of the two. In the singular limits, colour-stripped QCD amplitudes factorise into a singular function $f(i,j,k)$ and a reduced matrix element M' with the unresolved particle pinched out [29]. The singular function $f(i,j,k)$ depends only on the partons involved in the limit, where j is the unresolved parton and i and k are the two resolved hard radiators. M' is a function of a reduced momentum set corresponding to a mapping of the unresolved parton into its two hard radiators, $\{p_n\} \to \{\bar{p}_{n-1}\}$. At tree level we can write,

$$\lim_{p_j \to \text{unresolv.}} M_n(\ldots, p_i, p_j, p_k, \ldots) = f(p_i, p_j, p_k) \cdot M'_{n-1}(\ldots, \bar{p}_I, \bar{p}_K, \ldots). \tag{2.41}$$

The functional form of the function f depends on the type of limit we are considering: soft or collinear.

Soft limit

In the soft limits, the function f is a soft eikonal factor, $S_{ijk} = \frac{2s_{ik}}{s_{ij}s_{jk}}$, and depends only on the momentum of the particles involved in the limit. The momentum set of the reduced matrix element ($\{\bar{p}_{n-1}\}$) is such that, as the momentum of the unresolved parton vanishes, all other must remain the same. If we consider a soft limit in which the parton j goes soft between i and k we find,

$$\bar{p}_I \to p_i, \tag{2.42}$$

$$\bar{p}_K \to p_k, \tag{2.43}$$

which any $\{p_n\} \to \{\bar{p}_{n-1}\}$ mapping must fulfil.

The factorisation of a matrix element M for j going soft takes the form [29],

$$\lim_{p_j \to 0} M_n(\ldots, p_i, p_j, p_k, \ldots) = S_{ijk} \cdot M'_{n-1}(\ldots, \bar{p}_I, \bar{p}_K, \ldots). \tag{2.44}$$

In Eq. (2.44) it is clear that singularities occur only through the invariants s_{ij} and s_{jk}. This is in accordance with Section 2.2.1.

Collinear limit

In collinear limits the function f describing the singularity is one of the Altarelli-Parisi splitting functions [22]: $P^{\mu\nu}_{ij\to I}(x)$, where the spin dependence is made explicit through the indices $\mu\nu$. The variable x represents the fraction of momentum $\bar{p}_I = p_i + p_j$ carried by parton j. In the singular limit in which particle i is parallel to particle j the factorisation of M takes the form,

$$\lim_{p_i \| p_j} M_n(\ldots, p_i, p_j, \ldots) = \frac{P^{\mu\nu}_{ij\to I}}{s_{ij}} \cdot M'^{\mu\nu}_{n-1}(\ldots, \bar{p}_I, \ldots). \tag{2.45}$$

Contrary to soft functions, the form of the splitting functions depends on the identity of the partons involved in the limit and on their helicity configuration.

For simplicity, it is convenient to define and use the spin-averaged splitting functions instead,

$$\frac{P^{\mu\nu}_{ij\to I}}{s_{ij}} \cdot M'^{\mu\nu}_{n-1}(\ldots, \bar{p}_I, \ldots) = \frac{P_{ij\to I}}{s_{ij}} \cdot M'_{n-1}(\ldots, \bar{p}_I, \ldots) + \text{angular terms}, \tag{2.46}$$

where the angular terms are non-zero only when the splitting parton I is a gluon. These terms are not singular and they vanish after integration over the azimuthal variable [30]. They will be further explored in Section 2.3.1, as they introduce spurious local singularities beyond NLO in our subtraction prescription.

The mapping of the original momentum set to the reduced set merges the two collinear partons, i and j, into a parton I carrying the sum of both. The condition the mapping $\{p_n\} \to \{\bar{p}_{n-1}\}$ should fulfil is then,

$$\bar{p}_I = p_i + p_j. \tag{2.47}$$

The splitting functions also depend on whether the partons involved in the limit are final or initial-state particles. Since i.s. are always resolved, when one of the i.s. partons is involved in the limit it can only act as a hard radiator. However, it is not guaranteed for the i.s. parton to conserve its identity between the original matrix element M_n and the reduced matrix element M'_{n-1}. We call such cases "identity-changing" limits.

The previous discussion also applies beyond NLO, where two limits can appear together and more than one function (soft or splitting) must be applied. It is useful to highlight two special cases:

Triple collinear limit

In this case, analogous to the collinear limit, a third particle k goes collinear with i and j. This triple collinear singularity results in a new family of splitting functions [31, 32].

$$\lim_{p_i||p_j||p_k} M_n(\ldots, p_i, p_j, p_k, \ldots) = P_{ijk\to I} \cdot M'_{n-1}(\ldots, \bar{p}_I, \ldots). \tag{2.48}$$

One-loop one-radiation

The previous discussion can also be extended to the one-loop one-emission matrix element, with the exception that, since the one-loop matrix element squared is the result of the interference between a one-loop and a tree-level amplitude of the same multiplicity (Eq. (2.36)), the factorisation of Eq. (2.41) needs to be reformulated as

$$\begin{aligned}\lim_{p_j\to\text{unresolv.}} M_n^{(1)}(\ldots, p_i, p_j, p_k, \ldots) = f^{(1)}(p_i, p_j, p_k) \cdot M_{n-1}^{\prime(0)}(\ldots, \bar{p}_I, \bar{p}_K, \ldots) \\ + f^{(0)}(p_i, p_j, p_k) \cdot M_{n-1}^{\prime(1)}(\ldots, \bar{p}_I, \bar{p}_K, \ldots),\end{aligned} \tag{2.49}$$

where $f^{(1)}$ is the one-loop soft or splitting function [33].

2.2.4 Infrared cancellation

It has been previously stated that singularities introduced by the phase space integration of unresolved particles cancel against the virtual contributions at a given order in α_s as a result of the KLN theorem. However, by splitting the cross section into different pieces defined by the multiplicity of the phase space, the divergences are also split among different terms. Despite cancelling after integration, each component in Eq. (2.20) is divergent by itself. We recall here the relevant formulae making explicit the dimensionality of the phase space of each component (dropping

the indices for the i.s. partons i and j for simplicity),

$$\int \mathrm{d}\hat{\sigma}^{\mathrm{HO}} = \int \mathrm{d}\hat{\sigma}^{\mathrm{R}}_{n+1} + \int \mathrm{d}\hat{\sigma}^{\mathrm{V}}_{n}\,, \tag{2.50}$$

$$\mathrm{d}\hat{\sigma}^{\mathrm{R}}_{n+1} = \mathrm{d}\Phi_{n+1}\left(\{p_{n+1}\}\right) M^{(0)}_{n+1}, \tag{2.51}$$

$$\mathrm{d}\hat{\sigma}^{\mathrm{V}}_{n} = \mathrm{d}\Phi_{n}\left(\{p_{n}\}\right) M^{(1)}_{n} + \mathrm{d}\hat{\sigma}^{\mathrm{MF}}_{n}\,, \tag{2.52}$$

where for now we absorb the MF piece within the V contribution as they share the same final state kinematics. The singular part of the phase space in the R contribution can be analytically integrated in dimensional regularisation so that the poles in ϵ are made explicit, cancelling with the poles of the V contribution and making the integration finite. In general the analytical integration is not feasible and numerical methods for evaluating the cross section are used instead. These numerical methods require each integrand to be finite by itself and so Eq. (2.50) cannot be directly evaluated.

One method for rendering the different pieces of the cross section finite is to subtract divergences from the R-type contributions and make them explicit in the V-type contributions, thus cancelling the $\frac{1}{\epsilon}$ poles. Methods implementing this idea are called subtraction methods [34–37]. Two "counterterms" are then added to the cross section, S and T,

$$\int \mathrm{d}\hat{\sigma}^{\mathrm{HO}} = \int \left(\mathrm{d}\hat{\sigma}^{\mathrm{R}}_{n+1} - \mathrm{d}\hat{\sigma}^{\mathrm{S}}_{n+1}\right) + \int \left(\mathrm{d}\hat{\sigma}^{\mathrm{V}}_{n} - \mathrm{d}\hat{\sigma}^{\mathrm{T}}_{n}\right), \tag{2.53}$$

where each bracketed term is finite by itself and where the T and S terms are related through:

$$\int_{1} \mathrm{d}\hat{\sigma}^{\mathrm{S}}_{n+1} = -\,\mathrm{d}\hat{\sigma}^{\mathrm{T}}_{n}\,, \tag{2.54}$$

i.e., the subtraction term for the virtual level (T) must equal the integration over the phase space of the extra emissions (denoted as 1 in this case) of the real subtraction term (S). As a consequence, the total cross section is also left unchanged.

In order to transfer divergences from the real radiation matrix element to the virtual contributions it is necessary to be able to integrate the singular pieces by

themselves, keeping the reduced matrix element untouched. Therefore, the phase space must be factorisable:

$$\mathrm{d}\Phi_{n+1}\left(\{p_{n+1}\}\right) = \mathrm{d}\Phi_X\left(p_i, p_j, p_k; \bar{p}_I, \bar{p}_K\right) \mathrm{d}\Phi_n\left(\{\bar{p}_n\}\right), \tag{2.55}$$

where $\mathrm{d}\Phi_X$ is the phase space of the singular partons and $\mathrm{d}\Phi_n$ the phase space of the reduced momentum set $\{\bar{p}_n\}$ which corresponds to a mapping of the original set $\{p_{n+1}\}$ with the unresolved particle removed.

Beyond NLO

At NNLO each term in the full cross section of Eq. (2.1) needs to be broken down in terms of the multiplicity of the phase space,

$$\begin{aligned}\int \mathrm{d}\hat{\sigma} = &\left(\frac{\alpha_s}{2\pi}\right)^m \int \mathrm{d}\hat{\sigma}_n^{\mathrm{B}} \\ &+ \left(\frac{\alpha_s}{2\pi}\right)^{m+1} \int \left(\mathrm{d}\hat{\sigma}_{n+1}^{\mathrm{R}} + \mathrm{d}\hat{\sigma}_n^{\mathrm{V}}\right) \\ &+ \left(\frac{\alpha_s}{2\pi}\right)^{m+2} \int \left(\mathrm{d}\hat{\sigma}_{n+2}^{\mathrm{RR}} + \mathrm{d}\hat{\sigma}_{n+1}^{\mathrm{RV}} + \mathrm{d}\hat{\sigma}_n^{\mathrm{VV}}\right),\end{aligned} \tag{2.56}$$

where RR, RV and VV stand for double real, real virtual and double virtual respectively. MF terms at NNLO have been absorbed into the RV or VV layers depending on their multiplicity.

Since each term (other than the Born contribution) is singular when integrated by itself, it is necessary to add a counterterm for each higher-order contribution:

$$\begin{aligned}\int \mathrm{d}\hat{\sigma} = &\left(\frac{\alpha_s}{2\pi}\right)^m \int \mathrm{d}\hat{\sigma}_n^{\mathrm{B}} \\ &+ \left(\frac{\alpha_s}{2\pi}\right)^{m+1} \left[\int \left(\mathrm{d}\hat{\sigma}_{n+1}^{\mathrm{R}} - \mathrm{d}\hat{\sigma}_{n+1}^{\mathrm{S,\,NLO}}\right) + \int \left(\mathrm{d}\hat{\sigma}_n^{\mathrm{V}} - \mathrm{d}\hat{\sigma}_n^{\mathrm{T,\,NLO}}\right)\right] \\ &+ \left(\frac{\alpha_s}{2\pi}\right)^{m+2} \left[\int \left(\mathrm{d}\hat{\sigma}_{n+2}^{\mathrm{RR}} - \mathrm{d}\hat{\sigma}_{n+2}^{\mathrm{S}}\right) + \int \left(\mathrm{d}\hat{\sigma}_{n+1}^{\mathrm{RV}} - \mathrm{d}\hat{\sigma}_{n+1}^{\mathrm{T}}\right) + \int \left(\mathrm{d}\hat{\sigma}_n^{\mathrm{VV}} - \mathrm{d}\hat{\sigma}_n^{\mathrm{U}}\right)\right],\end{aligned} \tag{2.57}$$

S, T and U are the subtraction terms such that all integrals (each corresponding to a given multiplicity) are finite for any phase space point.

In order for the physical cross section to remain unchanged, upon their respective

integrations they must satisfy

$$\int \mathrm{d}\hat{\sigma}^{\mathrm{S}}_{n+2} + \int \mathrm{d}\hat{\sigma}^{\mathrm{T}}_{n+1} + \int \mathrm{d}\hat{\sigma}^{\mathrm{U}}_{n} = 0, \tag{2.58}$$

in analogy to Eq. (2.54), Eq. (2.58) must be valid at the differential level. While in Eq. (2.54) the relationship between the higher and lower multiplicity cross sections was clear, this is not the case at NNLO, where there are three different multiplicity configurations to consider. Let us first separate the RR subtraction term (S) and RV subtraction term (T) into two subcomponents (a) and (b),

$$\mathrm{d}\hat{\sigma}^{\mathrm{S}}_{n+2} = \mathrm{d}\hat{\sigma}^{\mathrm{S,(a)}}_{n+2} + \mathrm{d}\hat{\sigma}^{\mathrm{S,(b)}}_{n+2}\,, \tag{2.59}$$

$$\mathrm{d}\hat{\sigma}^{\mathrm{T}}_{n+1} = \mathrm{d}\hat{\sigma}^{\mathrm{T,(a)}}_{n+1} + \mathrm{d}\hat{\sigma}^{\mathrm{T,(b)}}_{n+1}\,, \tag{2.60}$$

where component (a) subtracts the NLO-like singularities (single emission in the RR case and explicit poles in the RV case) and the (b) component subtracts the rest. The integration over the phase space of the single unresolved configurations of the RR subtraction term S will correspond to the explicit poles of the RV subtraction term, denoted $\mathrm{d}\hat{\sigma}^{\mathrm{S,(a)}}_{n+2}$ and $\mathrm{d}\hat{\sigma}^{\mathrm{T,(a)}}_{n+1}$ respectively. Explicitly the different terms must be related by,

$$\int_1 \mathrm{d}\hat{\sigma}^{\mathrm{S,(a)}}_{n+2} + \mathrm{d}\hat{\sigma}^{\mathrm{T,(a)}}_{n+1} = 0, \tag{2.61}$$

$$\int_2 \mathrm{d}\hat{\sigma}^{\mathrm{S,(b)}}_{n+2} + \int_1 \mathrm{d}\hat{\sigma}^{\mathrm{T,(b)}}_{n+1} + \mathrm{d}\hat{\sigma}^{\mathrm{U}}_{n} = 0. \tag{2.62}$$

Through this work the subtraction terms will be constructed using the so-called antenna subtraction method, to be introduced in Section 2.3.

2.2.5 Jet cross sections

In Section 1.1.4 we dealt with the fact that the i.s. partons were actually parts of more complex objects called hadrons. Similarly, f.s. partons are not observed experimentally but rather a stream of collimated hadrons, known as a "jet", is measured instead. The non-perturbative process by which the products of the scattering cross

section become hadrons is known as hadronisation.

The connection between the perturbative regime (where partons can be isolated) with the non-perturbative physics of colour-confined hadrons is made through the notion of "parton-hadron duality" [38]. In our perturbative QCD predictions, this means taking the production rates for partons (which is what we compute) to be equivalent to the production rate of hadrons.

The use of jets allow us to compare predictions to experiment, the mapping between the f.s. particles and the colourless jets is done through the jet function $J_m^n(\{p_n\})$, defined as

$$J_m^n(\{p_n\}) = \begin{cases} 0 & \text{if } < m \text{ jets in the final state} \\ 1 & \text{if } \geq m \text{ jets in the final state,} \end{cases} \tag{2.63}$$

i.e., only events in which the n partons form m or more jets are accepted. It is commonly agreed that the function $J_m^n(\{p_n\})$ should fulfil a number of properties [39]:

1. To be simple to implement both in experimental and theoretical frameworks.

2. To be defined at any order of perturbation theory.

3. To be (relatively) insensitive to hadronisation effects.

4. To yield a finite cross section at any order.

The jet selector function also has a clear relation with the singularities of the system as real emission singularities can only be generated when the number of required jets and the number of final partons in the scattering process do not match. We can write the partonic cross section up to NNLO making the jet content explicit

and absorbing any constants into the factor $\mathcal{N}$,

$$\int \mathrm{d}\hat{\sigma}^{\mathrm{LO}} = \mathcal{N}^{\mathrm{B}} \int \mathrm{d}\Phi_n \left(\{p_n\}\right) M^{(0)}_{n+2} J^n_n \left(\{p_n\}\right), \tag{2.64}$$

$$\begin{aligned}\int \mathrm{d}\hat{\sigma}^{\mathrm{NLO}} = {} & \mathcal{N}^{\mathrm{R}} \int \mathrm{d}\Phi_{n+1} \left(\{p_{n+1}\}\right) M^{(0)}_{n+3} J^{n+1}_n \left(\{p_{n+1}\}\right) \\ & + \mathcal{N}^{\mathrm{V}} \int \mathrm{d}\Phi_n \left(\{p_n\}\right) M^{(1)}_{n+2} J^n_n \left(\{p_n\}\right),\end{aligned} \tag{2.65}$$

$$\begin{aligned}\int \mathrm{d}\hat{\sigma}^{\mathrm{NNLO}} = {} & \mathcal{N}^{\mathrm{RR}} \int \mathrm{d}\Phi_{n+2} \left(\{p_{n+2}\}\right) M^{(0)}_{n+4} J^{n+2}_n \left(\{p_{n+2}\}\right) \\ & + \mathcal{N}^{\mathrm{RV}} \int \mathrm{d}\Phi_{n+1} \left(\{p_{n+1}\}\right) M^{(1)}_{n+3} J^{n+1}_n \left(\{p_{n+1}\}\right) \\ & + \mathcal{N}^{\mathrm{VV}} \int \mathrm{d}\Phi_n \left(\{p_n\}\right) M^{(2)}_{n+2} J^n_n \left(\{p_n\}\right).\end{aligned} \tag{2.66}$$

At the LO or Born level there are only contributions from matrix elements with the same number of f.s. particles as jets are required. Since this implies that all particles are resolved, no singularities arise.

At NLO level we find two layers, real (R) and virtual (V). In the real contribution we find one extra particle with respect to the Born level, which can be unresolved while still fulfilling the jet selection. The virtual contribution has the same multiplicity as the Born and the singularities come exclusively from virtual loops in the form of $\frac{1}{\epsilon}$ poles.

At NNLO level three layers are found: double real (RR), real virtual (RV) and double virtual (VV). The RR contribution has two extra emissions with respect to Born, the RV has one extra emission (same multiplicity as R) and one loop, and in the VV contribution we find two extra loops with the same multiplicity as the Born and V level. The jet requirement of n jets in the final state means contributions with up to two unresolved particles can be found at the NNLO level.

Jet algorithms

Throughout this work we make use of the family of sequential recombination algorithms known as k_T algorithms, which build jets recursively from fundamental objects.

We begin by defining the spatial distribution of the particles through d_{ij}, the

distance between partons i and j and d_{iB}, the distance between parton i and the beam line [9],

$$d_{ij} = \min(p_{T_i}^{2p}, p_{T_j}^{2p}) \frac{(y_i - y_j)^2 + (\phi_i - \phi_j)^2}{R^2}, \tag{2.67}$$

$$d_{iB} = p_{T_i}^{2p}, \tag{2.68}$$

where p_{T_i}, y_i and ϕ_i are the transverse momentum, rapidity and azimuthal angle respectively of particle i. R is the jet radius and the power p defines the order in which the jets are clustered.

Through the power p, three classes of k_T algorithms are defined, $p = 1$ corresponds to the original version of the k_T algorithm [40], which clusters in increasing order of the partons transverse momentum. The Cambridge-Aachen algorithm [41], with $p = 0$, orders in $y - \phi$ space. Finally, $p = -1$ defines the anti-k_T algorithm [42] which we use in most of this work. One feature that makes the anti-k_T algorithm particularly desirable is that jets tend to have a regular shape, whereas other choices of p give a more irregular shape following the QCD radiation pattern. This makes the anti-k_T algorithm more attractive experimentally and, as a consequence, more commonly used for theoretical predictions.

Once a choice of R and p has been made, the algorithm computes Eq. (2.67) for all combinations of f.s. partons and clusters together the i and j particles for which d_{ij} is smaller, afterwards all distances are recalculated. If d_{iB} is the smallest distance the parton i (or cluster) is promoted to a jet. The algorithm terminates when no partons are left.

2.3 Antenna Subtraction method

When we introduced IR singularities we outlined the necessity of removing the divergences *at the level of the integrand* in order to perform the numerical integration. For that reason we introduce the antenna subtraction formalism where the solution to the problem of rendering the higher-order cross sections finite corresponds to

subtracting all explicit poles analytically and all implicit singularities numerically.

Without loss of generality let us recall the higher order cross section of Eq. (2.53), making explicit the MF term,

$$\int \mathrm{d}\hat{\sigma}^{\mathrm{HO}} = \int \left(\mathrm{d}\hat{\sigma}^{\mathrm{R}} - \mathrm{d}\hat{\sigma}^{\mathrm{S}}\right) + \int \left(\mathrm{d}\hat{\sigma}^{\mathrm{V}} - \mathrm{d}\hat{\sigma}^{\mathrm{T}} + \mathrm{d}\hat{\sigma}^{\mathrm{MF}}\right), \tag{2.69}$$

where the two bracketed terms correspond to different multiplicities and type of singularities.

We want to construct two functions, $\mathrm{d}\sigma^{\mathrm{S}}$ and $\mathrm{d}\sigma^{\mathrm{T}}$ such that they render each bracketed term finite without changing the final value of the cross section, i.e.,

$$\mathrm{d}\hat{\sigma}^{\mathrm{V}} - \mathrm{d}\hat{\sigma}^{\mathrm{T}} = \mathcal{O}\left(\epsilon^0\right), \tag{2.70}$$

$$\lim_{p_j \to \text{unresolved}} (\mathrm{d}\hat{\sigma}^{\mathrm{R}} - \mathrm{d}\hat{\sigma}^{\mathrm{S}}) = 0, \tag{2.71}$$

$$\int \left(\mathrm{d}\hat{\sigma}^{\mathrm{R}} + \mathrm{d}\hat{\sigma}^{\mathrm{V}} + \mathrm{d}\hat{\sigma}^{\mathrm{MF}}\right) = \int \left(\mathrm{d}\hat{\sigma}^{\mathrm{R}} + \mathrm{d}\hat{\sigma}^{\mathrm{V}} - \mathrm{d}\hat{\sigma}^{\mathrm{S}} - \mathrm{d}\hat{\sigma}^{\mathrm{T}} + \mathrm{d}\hat{\sigma}^{\mathrm{MF}}\right), \tag{2.72}$$

where $\mathrm{d}\hat{\sigma}^{\mathrm{S}}$ and $\mathrm{d}\hat{\sigma}^{\mathrm{T}}$ must also fulfil Eq. (2.54).

Real subtraction

The antenna subtraction method exploits the factorisation of singular limits studied in Section 2.2 in order to build a set of function taking as ingredient the ratio of a matrix element containing the singularity and their reduced counterpart. For instance, the antenna function X_3^0 for a parton j going unresolved and radiated between partons i and k is given by:

$$X_3^0(p_i, p_j, p_k) = \frac{M_3^0(p_i, p_j, p_k)}{M_2^{0\prime}(\bar{p}_I, \bar{p}_K)}. \tag{2.73}$$

The counterterm for the singular limit of j between i and k in a matrix element $M_n(\dots, p_i, p_j, p_k, \dots)$ is then given by,

$$\mathrm{d}\hat{\sigma}^{\mathrm{S}}\left(\{p_{n+1}\}\right) = \mathrm{d}\Phi_n\left(\{\bar{p}_n\}\right) \mathrm{d}\Phi_X\left(p_i, p_j, p_j; \bar{p}_I, \bar{p}_k\right) X_3^0(p_i, p_j, p_k) M'_{n-1}(\dots, \bar{p}_I, \bar{p}_K, \dots), \tag{2.74}$$

where the antenna function X_3^0 depends on the identity of the particles involved in the limit as well as on the limit we consider. The factor $\mathrm{d}\Phi_X$ is the phase space of the particles of the antenna. We dissect a R subtraction term in Appendix C.1 as an example.

The antenna formalism also requires the phase space to be factorisable (see Eq. (2.55)). The actual mappings required for the factorisation of the phase space are dependent on whether the partons involved in the limit are initial or final-state partons and its form has been derived in [43]. The NNLOJET implementation of the phase space mappings is detailed in Section 2.3 of Ref. [44].

For NNLO calculations the set of unintegrated antennae necessary for the subtraction of implicit IR singularities consist of the types $\{X_3^0, X_4^0, X_3^1\}$, those relevant to the calculations presented in this thesis are listed in Appendix B. X_4^0 and X_3^1 appear only at NNLO, where we find double unresolved limits as well as with radiation in loop amplitudes.

Virtual subtraction

Upon integration over the phase space of the unresolved particles these functions expose the $\frac{1}{\epsilon}$ poles necessary for the cancellation of IR explicit poles in virtual matrix elements,

$$\mathcal{X}_3^0(\bar{p}_I, \bar{p}_K; \epsilon) = \int \mathrm{d}\Phi_X \left(p_i, p_j, p_j; \bar{p}_I, \bar{p}_k\right) X_3^0(p_i, p_j, p_k), \tag{2.75}$$

The set of integrated antennae necessary for NNLO calculations corresponds to $\{\mathcal{X}_3^0, \mathcal{X}_3^1\}$, with the later appearing only at NNLO. They can also be found in Appendix B. The virtual subtraction form (of which we detail one example in Appendix C.2) have the general form

$$\mathrm{d}\hat{\sigma}^{\mathrm{T}}\left(\{p_n\}; \epsilon\right) = \mathrm{d}\Phi_n\left(\{p_n\}\right) \mathcal{X}_3^0(p_i, p_j; \epsilon) M_n^{(0)}(\{p_n\}). \tag{2.76}$$

The expression for all necessary antenna functions and their integrals have been derived in [21, 34, 43, 45–50]. In Appendix C we list all subtraction terms up to NNLO for the calculations presented in this thesis.

Since the form of the mass factorisation term is not process dependent (see Eqs. (2.15) and (2.16)), the same initial-state integrated antenna (i.e., antennae containing i.s. partons) will always be accompanied by the same factorisation kernel. It is thus convenient to define a set of functions J formed by the integrated antennae plus the corresponding mass factorisation terms mimicking the pole structure of the one loop virtual amplitudes. These functions are listed in Appendix B and are a combination of the integrated antennae $\mathcal{X}_3^0$ and the splitting kernels Γ_{ij}. For a initial state limit in which partons i, j have become partons I, K, the J-string is of the form,

$$J_2^1(I,K) = \delta_{kK}\Gamma_{iI}(x_I) + \delta_{iI}\Gamma_{kK}(x_K) + \mathcal{X}_3^0(I,K). \tag{2.77}$$

Effectively we are absorbing $\mathrm{d}\hat{\sigma}^{\mathrm{MF}}$ in the definition of $\mathrm{d}\hat{\sigma}^{\mathrm{T}}$.

2.3.1 Azimuthal rotations

Antenna functions subtracting collinear limits are proportional to spin-averaged splitting functions (Eq. (2.46)). Beyond NLO we can find angular terms multiplying singular functions which gives rise to spurious local divergences. These spurious terms are proportional to $\cos(2\phi + \alpha)$ [30] and thus cancel over the integral over the azimuthal variable ϕ.

Numerically, these angular terms produce locally divergent events which make the subtraction formalism non-local beyond NLO, posing a numerical challenge. The solution within NNLOJET is to rotate each phase space point by $\frac{\pi}{2}$ such that angular terms cancel out,

$$\mathrm{d}\hat{\sigma}^{\mathrm{R}}_{\mathrm{finite}} = \left(\mathrm{d}\hat{\sigma}^{\mathrm{R}} - \mathrm{d}\hat{\sigma}^{\mathrm{S}}\right)(\{p_n\}) + \left(\mathrm{d}\hat{\sigma}^{\mathrm{R}} - \mathrm{d}\hat{\sigma}^{\mathrm{S}}\right)(\{p'_n\}). \tag{2.78}$$

where p'_n is the rotated momentum set.

The technicalities of the implementation of the azimuthal rotations are given in Section 4.3.4.

2.4 Scale dependence of the cross section at NNLO in QCD

In order to compute a cross section to fixed order in perturbation theory, one must fix the renormalisation scale μ_R for the strong coupling constant $\alpha_s(\mu_R)$, and the mass factorisation scale μ_F for the parton distribution functions $f_i(x, \mu_F)$.

The behaviour of the coupling constant and parton distribution functions under scale variations is determined by evolution equations (Eq. (1.48)). For the strong coupling constant the evolution equation up to second order reads,

$$\mu_{\mathrm{R}}^2 \frac{\mathrm{d}\alpha_s(\mu_{\mathrm{R}})}{\mathrm{d}\mu_{\mathrm{R}}^2} = -\alpha_s(\mu_{\mathrm{R}}) \left[\beta_0 \left(\frac{\alpha_s(\mu_{\mathrm{R}})}{2\pi} \right) + \beta_1 \left(\frac{\alpha_s(\mu_{\mathrm{R}})}{2\pi} \right)^2 + \mathcal{O}\big(\alpha_s^3\big) \right], \tag{2.79}$$

where the coefficients for the QCD β function are [11],

$$\begin{aligned} \beta_0 =& \frac{11C_A - 4T_R N_f}{6}, \\ \beta_1 =& \frac{17C_A^2 - 10C_A T_R N_f - 6C_F T_R N_f}{6}, \end{aligned} \tag{2.80}$$

Solving Eq. (2.79), the coupling at any fixed scale μ_0 can be expressed in terms of the coupling at μ_{R},

$$\alpha_S(\mu_0) = \alpha_s(\mu_R) \left[1 + \beta_0 L_R \frac{\alpha_s(\mu_R)}{2\pi} + \left[\beta_0^2 L_R^2 + \beta_1 L_R \right] \left(\frac{\alpha_s(\mu_R)}{2\pi} \right)^2 + \mathcal{O}(\alpha_s^3) \right], \tag{2.81}$$

where we have introduced

$$L_R = \log \left(\frac{\mu_R^2}{\mu_0^2} \right). \tag{2.82}$$

The calculation of the higher-order corrections for an observable O requires evaluating the expansion coefficient at a given renormalisation scale ($O^{(i)}(\mu_{\mathrm{R}}) \equiv O^{(i)}$). For instance, the expansion to NNLO ($i = 2$) for the cross section reads:

$$\sigma(\mu_0, \alpha_s(\mu_0)) = \left(\frac{\alpha_s(\mu_0)}{2\pi} \right)^n \sigma^{(0)} + \left(\frac{\alpha_s(\mu_0)}{2\pi} \right)^{n+1} \sigma^{(1)} + \left(\frac{\alpha_s(\mu_0)}{2\pi} \right)^{n+2} \sigma^{(2)} + \mathcal{O}(\alpha_s^{n+3}), \tag{2.83}$$

The scale-dependence of the cross section can then be reconstructed by inserting

(2.81):

$$\begin{aligned}\sigma(\mu_R,\alpha_s(\mu_R),L_R) = &\left(\frac{\alpha_s(\mu_\mathrm{R})}{2\pi}\right)^n \sigma^{(0)} + \left(\frac{\alpha_s(\mu_\mathrm{R})}{2\pi}\right)^{n+1}\left(\sigma^{(1)} + n\beta_0 L_R\sigma^{(0)}\right)\\ &+\left(\frac{\alpha_s(\mu_\mathrm{R})}{2\pi}\right)^{n+2}\left(\sigma^{(2)} + (n+1)\beta_0 L_R\sigma^{(1)}\right.\\ &\left.+n\beta_1 L_R\sigma^{(0)} + \frac{n(n+1)}{2}\beta_0^2 L_R^2\sigma^{(0)}\right)\\ &+\mathcal{O}(\alpha_s^{n+3})\,. \end{aligned} \tag{2.84}$$

Note that for this formula to be valid, the ratio μ_R/μ_0 must be constant event-by-event. This means it is possible to re-scale from a dynamical scale $\mu_0 = p_T^H$ to $\mu_\mathrm{R} = \frac{1}{2}p_T^H$ but not to an arbitrary observable such as $\mu_\mathrm{R} = p_T^j$.

The evolution of PDFs is determined by the DGLAP evolution equations [22]. Omitting the dependence on the momentum fraction x we have,

$$\mu_F^2\frac{\mathrm{d}}{\mathrm{d}\mu_\mathrm{F}^2}f_i(\mu_F,\mu_R) = \sum_j P_{ij}(\alpha_s(\mu_R),\mu_\mathrm{F},\mu_\mathrm{R})\otimes f_j(\mu_\mathrm{F},\mu_\mathrm{R}), \tag{2.85}$$

The expansion to second order in α_s in terms of the splitting functions $P_{ij}^{(n)}$ computed at $\mu_\mathrm{R} = \mu_\mathrm{F}$ yields,

$$P_{ij}(\alpha_s(\mu_F),\mu_F) \;=\; \frac{\alpha_s(\mu_F)}{2\pi}P_{ij}^{(0)} + \left(\frac{\alpha_s(\mu_F)}{2\pi}\right)^2 P_{ij}^{(1)} + \mathcal{O}\big(\alpha_s^3\big). \tag{2.86}$$

The expansion in $\alpha_s(\mu_\mathrm{F})$ of the PDFs, giving the evolution of the PDFs between scales μ_0 and μ_F, can then be written as [51],

$$\begin{aligned} f_i(\mu_0) = f_i(\mu_F) &- \frac{\alpha_s(\mu_F)}{2\pi}P_{ij}^{(0)}\otimes f_j(\mu_F)L_F\\ &-\left(\frac{\alpha_s(\mu_F)}{2\pi}\right)^2\left[P_{ij}^{(1)}\otimes f_j(\mu_F)L_F - \frac{1}{2}P_{ij}^{(0)}\otimes P_{jk}^{(0)}\otimes f_k(\mu_F)L_F^2\right.\\ &\left.+\frac{1}{2}P_{ij}^{(0)}\otimes f_j(\mu_F)\beta_0 L_F^2\right] + \mathcal{O}(\alpha_s^3), \end{aligned} \tag{2.87}$$

where we introduce

$$L_F = \log\left(\frac{\mu_F^2}{\mu_0^2}\right). \tag{2.88}$$

Let us now consider the perturbative expansion of the cross section up to NNLO,

computed at a fixed scale, making explicit the α_s and partonic dependence,

$$\begin{aligned}\sigma(\mu_0,\mu_0,\alpha_s(\mu_0)) &= \left(\frac{\alpha_s(\mu_0)}{2\pi}\right)^n \hat{\sigma}_{ij}^{(0)} \otimes f_i(\mu_0) \otimes f_j(\mu_0) \\ &+ \left(\frac{\alpha_s(\mu_0)}{2\pi}\right)^{n+1} \hat{\sigma}_{ij}^{(1)} \otimes f_i(\mu_0) \otimes f_j(\mu_0) \\ &+ \left(\frac{\alpha_s(\mu_0)}{2\pi}\right)^{n+2} \hat{\sigma}_{ij}^{(2)} \otimes f_i(\mu_0) \otimes f_j(\mu_0) + \mathcal{O}(\alpha_s^{n+3})\,.\end{aligned} \tag{2.89}$$

We can restore the full scale dependence of the cross section by inserting Eq. (2.81) and Eq. (2.87) into the above, which allows us to compute the NNLO cross section at a fixed scale μ_0 and later generate the cross section (for the same parameters) at

any given scale $\mu_{\rm R}$,

$$
\begin{aligned}
&\sigma(\mu_R,\mu_F,\alpha_s(\mu_R),L_R,L_F) = \\
&\left(\frac{\alpha_s(\mu_{\rm R})}{2\pi}\right)^n \hat{\sigma}_{ij}^{(0)} \otimes f_i(\mu_{\rm F}) \otimes f_j(\mu_{\rm F}) \\
&+\left(\frac{\alpha_s(\mu_{\rm R})}{2\pi}\right)^{n+1} \Bigg\{ \left(\hat{\sigma}_{ij}^{(1)} + L_R(n\beta_0\hat{\sigma}_{ij}^{(0)})\right) \otimes f_i(\mu_{\rm F}) \otimes f_j(\mu_{\rm F}) \\
&\qquad - L_F\hat{\sigma}_{ij}^{(0)} \otimes \left[f_i(\mu_{\rm F}) \otimes \left(P_{jk}^{(0)} \otimes f_k(\mu_{\rm F})\right) + \left(P_{ik}^{(0)} \otimes f_k(\mu_{\rm F})\right) \otimes f_j(\mu_{\rm F}) \right] \Bigg\} \\
&+\left(\frac{\alpha_s(\mu_{\rm R})}{2\pi}\right)^{n+2} \Bigg\{ \Bigg[\left(\hat{\sigma}_{ij}^{(2)} + L_R((n+1)\beta_0\hat{\sigma}_{ij}^{(1)} + n\beta_1\hat{\sigma}_{ij}^{(0)})\right) \\
&\qquad\qquad + L_R^2\frac{n(n+1)}{2}\hat{\sigma}_{ij}^{(0)} \Bigg] \otimes f_i(\mu_{\rm F}) \otimes f_j(\mu_{\rm F}) \\
&\qquad - L_F \Bigg[\hat{\sigma}_{ij}^{(0)} \otimes \left[f_i(\mu_{\rm F}) \otimes \left(P_{jk}^{(1)} \otimes f_k(\mu_{\rm F})\right) + \left(P_{ik}^{(1)} \otimes f_k(\mu_{\rm F})\right) \otimes f_j(\mu_{\rm F}) \right] \\
&\qquad\quad + \hat{\sigma}_{ij}^{(1)} \otimes \left[f_i(\mu_{\rm F}) \otimes \left(P_{jk}^{(1)} \otimes f_k(\mu_{\rm F})\right) + \left(P_{ik}^{(1)} \otimes f_k(\mu_{\rm F})\right) \otimes f_j(\mu_{\rm F}) \right] \\
&\qquad\quad + \left(L_R(n+1) + \frac{1}{2}L_F\beta_0\right)\hat{\sigma}_{ij}^{(0)} \otimes \Big[\\
&\qquad\qquad f_i(\mu_{\rm F}) \otimes \left(P_{jk}^{(0)} \otimes f_k(\mu_{\rm F})\right) + \left(P_{ik}^{(0)} \otimes f_k(\mu_{\rm F})\right) \otimes f_j(\mu_{\rm F}) \Big] \Bigg] \\
&\qquad + L_F^2\hat{\sigma}_{ij}^{(0)} \otimes \Bigg[\left(P_{ik}^{(0)} \otimes f_k\mu_{\rm F}\right) \otimes \left(P_{jl}^{(0)} \otimes f_l(\mu_{\rm F})\right) \\
&\qquad\qquad + \frac{1}{2} f_i(\mu_{\rm F}) \otimes \left(P_{jk}^{(0)} \otimes P_{kl}^{(0)} \otimes f_l(\mu_{\rm F})\right) \\
&\qquad\qquad + \frac{1}{2}\left(P_{ik}^{(0)} \otimes P_{kl}^{(0)} \otimes f_l(\mu_{\rm F})\right) \otimes f_j(\mu_{\rm F}) \Bigg] \Bigg\}. \qquad (2.90)
\end{aligned}
$$

Chapter 3

Vector Boson Fusion Higgs Production

The detailed experimental study of the Higgs boson coupling to electroweak gauge bosons requires to discriminate between the Yukawa and VVH categories and thus the reduction of the ggF background is crucial. The VBF production mode is particularly relevant for the study of the VVH vertex due to a very clean experimental signature that greatly facilitates the reduction of the important ggF background through a series of cuts known as VBF cuts. These cuts not only reduce the ggF background, but also reduce the background from other VVH production channels such as associated production (which become background to the VBF process when the gauge vector boson decays to two quarks) and interferences between different production modes, crucially ggF$\times$VBF.

In Section 3.1 we introduce the VBF cuts and motivate them by inspecting the Born-level topology of the process. In Section 3.2 we define the "structure function" or DIS approach, according to which we neglect contributions deemed irrelevant for the study of Higgs boson production in VBF. We then prove that these removed contributions are indeed negligible and that our approach is well justified when VBF cuts are applied. We finish this chapter by explicitly listing all amplitudes contributing to this process in our implementation in NNLOjet.

3.1 Higgs production in Vector Boson Fusion

In the context of hadron collisions, the Vector Boson Fusion process refers to the production of a Higgs boson via the fusion of two Z or W bosons, each radiated from one of the two hadrons that participate in the collision as shown in Fig. 3.1.

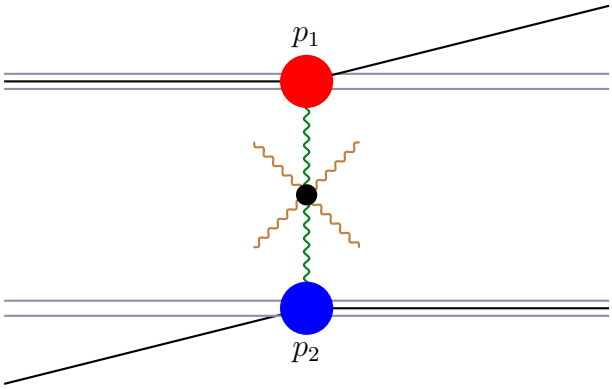

Figure 3.1: Schematic representation of a VBF-type process in a proton-proton collision in which the radiated vector bosons fuse to form a Higgs boson. The generated particle then decays into measurable products (represented as photons in this case).

However, a meticulous study of Higgs boson production in VBF must not ignore other competing modes for the same final state: one Higgs boson produced in association with two partonic jets. We recall here some of those competing Higgs plus two jets (H2j) processes:

- **Gluon fusion** in association with two jets or ggF, shown in Fig. 3.2a. Since the Higgs boson does not couple to gluons, the Higgs boson is generated through a quark loop at lowest order. Nonetheless, due to the abundance of gluons at the LHC, this is the dominant H2j production channel.

- Associated production or **Higgs-strahlung**, in which the Higgs boson is radiated from a vector boson which then decays into a quark-antiquark pair forming jets, depicted in Fig. 3.2b. Also referred to as VH.

- **Vector Boson Fusion** or VBF, shown in Fig. 3.2c. This corresponds to a crossing of the VH process and, strictly speaking, they are indeed the same

process. The reason for distinguishing between these two production modes will become clear in this chapter.

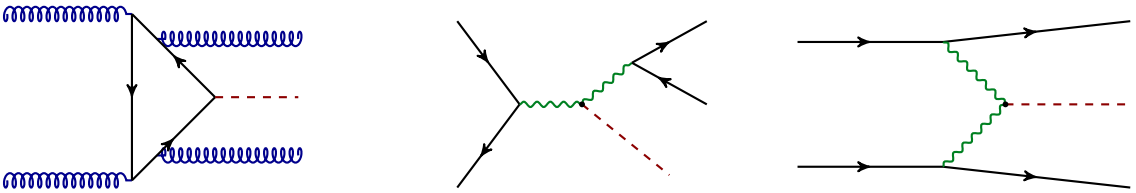

(a) ggF (b) VH (V→ $q\bar{q}$) (c) VBF

Figure 3.2: Example of Higgs boson production processes in association with two jets.

Uniquely amongst these three processes, the VBF mode offers both a very distinct and clear experimental signature as well as direct access to the Higgs boson couplings to electroweak gauge bosons. Its production rate is greater than any other purely electroweak production mode and its unique topology, with two very forward jets of opposite rapidity, allows for a good discrimination against the dominant ggF process [52–54]. The spatial distribution of the outgoing Higgs boson is also exploited in experimental searches as both the boson and its decay products tend to be much more central than in other Higgs boson production modes [55–60].

The VBF production mode also offers a good opportunity for the detailed study of the properties of the Higgs boson. One example is the CPT properties of the boson, which can be probed through the azimuthal distribution of the two tagging jets [1, 61–63]. Another example is the self-coupling of the Higgs boson through di-Higgs and tri-Higgs production which will be accessible at 100 TeV [64–66].

3.1.1 Topology of the process

At the lowest order, the Higgs production process via the VBF mechanism consists of two quark currents scattering off two electroweak gauge bosons. These two vector bosons, exchanged in a t-type channel, fuse into a Higgs boson through a VVH vertex while the two quark currents go on to form two jets. This is depicted in Fig. 3.3 in terms of the constituent currents.

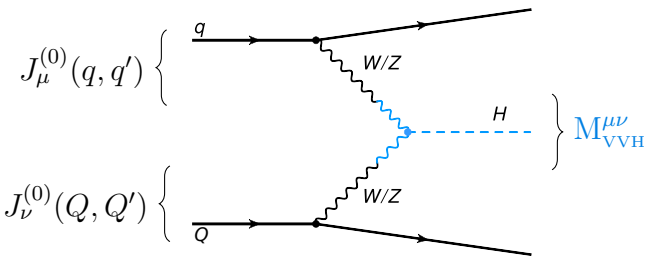

Figure 3.3: Born-level vector boson fusion process.

The lack of colour exchange between the two currents implies colour coherence between the initial and final state, in our case, between the two colliding protons and their corresponding outgoing jets. These two jets are called "tagging jets" and they are the main signature of the VBF process. The vector bosons, which recoil against the jet and couple to the Higgs boson, tend to carry a low fraction of the incoming energy. As a consequence the tagging jets tend to be quite energetic with a small transverse momentum and well separated in rapidity.

The Higgs boson, on the other hand, tends to be produced in the central region (i.e., between the two tagging jets in rapidity space) with moderate p_T and its decay products are also produced centrally.

These features are in contrast with the ggF and VH production modes. In these two cases there is a flux of colour between the two final state particles during the process, which tend to produce jets closer in rapidity space. In the VH case, where the vector boson is exchanged in the s-channel, the two outgoing jets also have lower energy than in the VBF case.

All these considerations are crucial elements on the selection cuts that allow the experimentalist to discriminate between VBF-like events and other production modes.

3.1.2 VBF cuts

The separation of the two tagging jets in rapidity space suggest the usage of a cut on the rapidity gap generated between the two leading jets, noted Δy_{jj}. Furthermore, we can choose to only select events in which only the Higgs boson is found within

the rapidity gap, with no other QCD emission between both leading jets. These cuts on the spatial distribution of the particles works as a discriminator of VBF against VH and ggF.

Separating VH and VBF is straightforward, in a VH-like process the vector boson is generated in the s-channel. This vector boson then radiates a Higgs boson and goes on to finally decay into two jets. As such, these two jets are preferably generated with an invariant mass close to the resonance of the vector boson itself, i.e., much lower values than in the VBF case. We can thus use the invariant mass of the dijet system formed by the two tagging jets (noted m_{jj}) as a discriminator between VH and VBF-like events.

Following these considerations we can define certain parameters which will enable us to preferentially select VBF-like events in a collision with a Higgs boson and two jets in the final state. These selection cuts form what is known as "VBF cuts" and they sit at the core of VBF phenomenology. As an example, the ATLAS template cross section defines VBF events as those in which the two tagging jets are separated in rapidity by more than $\Delta y_{jj} = 2.8$ and have an invariant mass of $m_{jj} > 400$ GeV. Furthermore, **neither** of the two tagging jets can have a transverse momentum of more than 200 GeV (or less than 30 GeV). They impose a further cut on the rapidity of the Higgs boson of $|y_H| < 2.5$ in order to capture the decay products of the particle inside the detector. In summary,

$$\begin{aligned} m_{jj} > 400 \text{ GeV} \qquad & \Delta y_{jj} > 2.8, \\ 30 \text{ GeV} < p_T^{j_{1,2}} < 200 \text{ GeV} \qquad & |y_H| < 2.5. \end{aligned} \tag{3.1}$$

In cases in which there are more than two jets in the final state, the two tagging jets are those with the greatest transverse momentum.

3.2 The DIS approach

The VBF Higgs boson production is a $2 \to 3$ scattering process at the lowest order and due to the complexity of the higher order corrections it is helpful to simplify the calculation by imposing certain approximations. We will work in a framework usually known as the structure function or DIS approach. In this framework the two currents forming the VBF process are treated as completely independent objects as if they corresponded to identical but not interacting copies of QCD. In other words, gluons radiated from one current do not interact with gluons from the other current.

This approach is obtained by considering the VBF production mode as two independent Deep Inelastic Scattering (DIS) processes where the two off-shell vector bosons fuse through a VVH vertex, as depicted in Fig. 3.3. In this picture, the VBF process is formed by two quark currents, $J_\mu^{(l)}(q, q', \ldots)$ and $J_\nu^{(l)}(Q, Q', \ldots)$, connected through a weak boson-Higgs vertex, $\mathrm{M}_{\mathrm{VVH}}^{\mu\nu}(Q_1^2, Q_2^2)$, which includes the vector boson propagator: $\Delta_{V_i}(Q_i^2)$.

In the classical picture of the DIS approach, the cross section can be expressed in terms of the hadronic tensors $\mathcal{W}_{\mu\nu}^{\mathrm{V}}(x, Q^2)$, which are a combination of the neutral and charge-current hadronic structure functions [67],

$$\mathrm{d}\sigma = \mathcal{C}\ \mathcal{W}_{\mu\nu}^{\mathrm{V}}(x_1, Q_1^2)\ \mathrm{M}_{\mathrm{VVH}}^{\mu\rho}(Q_1^2, Q_2^2)\ \mathrm{M}_{\mathrm{VVH}}^{\nu\sigma}(Q_1^2, Q_2^2)\ \mathcal{W}_{\rho\sigma}^{\mathrm{V}}(x_2, Q_2^2)\ \mathrm{d}\Phi\,, \tag{3.2}$$

where $\mathcal{C}$ accounts for all couplings and flux factors, $Q^2 = -q^2$ is energy transfer of the vector boson and x is the Bjorken variable. In the hadronic tensor $\mathcal{W}_{\mu\nu}^{\mathrm{V}}(x, Q^2)$ an integration is implicit over extra emissions and loops. As a trade-off, only inclusive calculations can be obtained directly from Eq. (3.2) [68–70].

In order to obtain differential distributions, the cross section can also be constructed in terms of matrix elements squared. These can be written in terms of the currents $J_\mu^{(l)}(q, q')$. Explicitly, the Born-level amplitude is written,

$$\mathcal{M}_{0g}^{(0)}(q, Q, Q', q') = J_\mu^{(0)}(q, q')\ \mathrm{M}_{\mathrm{VVH}}^{\mu\nu}\ J_\nu^{(0)}(Q, Q'), \tag{3.3}$$

where the labels q and Q refer to a massless quark or antiquark of any flavour (we

consider five massless flavours: u, d, c, s, b).

At LO level, the only matrix element that enters the calculation is the square of Eq. (3.3):

$$C_{0g}^{(0)} = |\mathcal{M}_{0g}^{(0)}(q, Q, Q', q')|^2, \tag{3.4}$$

i.e., we neglect interference effects from the special case in which the flavours of the two quark currents, q and Q, coincide and the two final state quarks are indistinguishable:

$$D_{0g}^{(0)} = \frac{2}{N} \mathrm{Re}\left\{\mathcal{M}_{0g}^{(0)}(q, Q, Q', q')\, \mathcal{M}_{0g}^{(0)}(q, Q, q', Q')^*\right\}. \tag{3.5}$$

These matrix elements account for interference effects between the two currents and are suppressed kinematically in the regions of the phase space defined by the VBF cuts (see Section 3.2.1) and also by a factor of $\frac{1}{N}$. The notation chosen for the definition of the matrix elements, C and D, will be further detailed in Section 3.3.1.

Similarly, we neglect the colour and kinematically suppressed contributions due to the interference of gluons radiated from different currents [69, 71, 72] at higher orders. This approximation is exact at NLO but not NNLO. In summary, all contributions with colour exchange between the two currents are neglected at all orders.

In Fig. 3.4 we show examples of neglected diagrams appearing at two loops. These VV diagrams have corresponding contributions from RR and RV layers, which for consistency must be removed as well. Examples of neglected Born, RR and RV contributions are shown in Fig. 3.5.

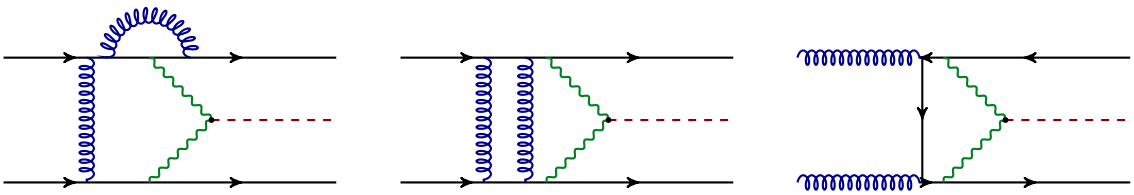

Figure 3.4: Examples of neglected diagrams appearing in the VV layer for VBF Higgs boson production. The first of these diagrams vanishes due to colour algebra while the other two are neglected.

We also neglect contributions in which the two final state quarks are identical

Layer	Processes
Born, V, VV	$q\ Q \to q\ Q\ \mathrm{H}$
R, RV	$q\ Q \to q\ Q\ g\ \mathrm{H}$; $q\ g \to q\ Q\ \bar{Q}\ \mathrm{H}$
RR	$q\ Q \to q\ Q\ g\ g\ \mathrm{H}$; $q\ Q \to q\ Q\ q'\ \bar{q}'\ \mathrm{H}$ $q\ g \to q\ Q\ \bar{Q}\ g\ \mathrm{H}$; $g\ g \to q\ \bar{q}\ Q\ \bar{Q}\ \mathrm{H}$

Table 3.1: Subprocesses that contribute to VBF-2j up to NNLO in NNLOJET.

which leads to interferences between t and u channel type diagrams. One example is shown in Fig. 3.5a.

The reason for removing all these contributions is twofold: first, they are suppressed by a factor of $\frac{1}{N}$ in the identical quark case and a factor of $\frac{1}{N^2}$ for the gluon interference, and second, they are kinematically suppressed in the phase space regions allowed by typical of VBF cuts as proven in Section 3.2.1.

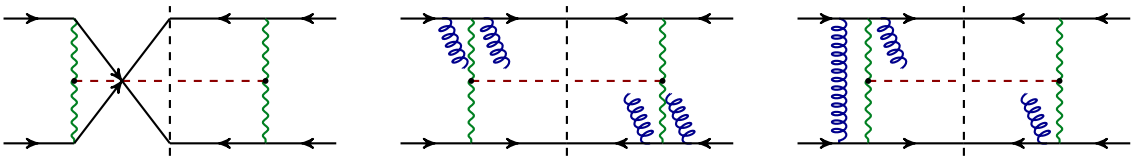

(a) Born (b) RR (c) RV

Figure 3.5: Example of neglected VBF contributions for the Born, RR and RV layers.

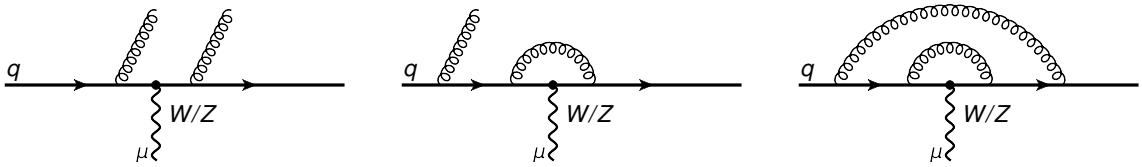

Figure 3.6: Examples of second order QCD corrections (RR, RV, VV) to the quark currents.

Therefore the subset of diagrams we keep is equivalent to the DIS approach as defined in Ref. [67], as we are effectively considering QCD corrections to each current separately (Fig. 3.6).

Table 3.1 lists all Higgs boson production subprocesses contributing up to $\mathcal{O}(\alpha_s^2)$ for VBF-2j, VBF-3j and VBF-4j. The labels q' and $\bar{q}'$ in this table refer to the quarks produced when a gluon radiated from either of the currents subsequently

splits into a quark-antiquark pair.

In the previous discussion we have not taken into consideration other production modes which share the same final state (a Higgs boson and two jets) and thus interfere with the VBF process. Interferences with gluon fusion have been studied in the literature and its effect is found to be negligible [73]. On the other hand, the VH production mode corresponds to the same set of diagrams up to a crossing of initial and final states and the removal of this process and interferences thereof must be well justified. In the next section we will prove that taking this approximation has a reduced impact with respect to the full calculation in the phenomenologically relevant regions of the phase space.

3.2.1 Comparison between ggF, VBF, VH

We finish this section by studying the phenomenological impact of the DIS approach and how it can be minimised by appropriate selection cuts.

In the following comparisons we use the VBF, ggF and VH ($V \to q\bar{q}$) processes as implemented in the NNLOJET code. The ggF plus two jets process is implemented in the HEFT framework [51, 74] up to NLO in QCD. The VBF process is implemented in the DIS approach as discussed in this section at NNLO in QCD, for consistency the VBF process is only calculated at NLO QCD in this section. The implementation of VH ($V\to q\bar{q}$) at NLO QCD that we use is implemented as an add-on to the VBF process, with the possibility of including interference terms between VBF and VH ($V \to q\bar{q}$). Equally, u/t-channel interferences are implemented at LO in the VBF process and can be turned on and off.

In this section VBF refers always to the VBF process in the DIS approach whereas $\text{VBF}^{u/t}$ also considers u/t-channel interferences. We use "Full H2j EW" to denote the sum of VH, $\text{VBF}^{u/t}$ and interferences thereof.

Inclusive comparison

Although we have already argued in favour of the usage of certain selection criteria in Section 3.1.2, we will start by comparing the inclusive production rate of the different production mechanisms as well as differential distributions making no assumptions about the cuts. It is necessary, however to include a technical cut of $p_T^j > 25$ GeV in order to define two jets and render the cross section finite due to the inclusion of the ggF channel in the comparison. Jets are defined through the anti-k_T algorithm (Section 2.2.5) with jet radius parameter $R = 0.4$

In Table 3.2 we present the production rates for the various H2j production modes for proton collisions at 13 TeV. As anticipated, the gluon fusion channel is the dominant mode with more than 58% of the total cross section. VBF follows, with a rate of about 32% of the total cross section and the smallest is VH with a contribution of less than a 10% of the total.

Production mode	Total cross section (fb)	% of Total
ggF	4889.1 +/- 0.6	58.464 +/- 0.010
VBF	2722.8 +/- 0.4	32.559 +/- 0.006
VBF$^{u/t}$	2717.7 +/- 0.4	32.499 +/- 0.006
VH	750.7 +/- 0.9	8.98 +/- 0.01
Total	8362.6 +/- 1.0	100

Table 3.2: Comparison between different Higgs boson plus 2 jets production modes. In this calculation we use the NNPDF30_nnlo_as_0118 [75] PDF set as included in the LHAPDF [76] library with $\mu_{\mathrm{F}} = \mu_{\mathrm{R}} = m_H$. Errors are statistical.

The dominance of the ggF production channel is also apparent in differential distributions, such as the transverse momentum of the Higgs boson or the jets as can be seen in Fig. 3.7 although the ratio of the production via the ggF channel over the VBF channel is not constant over the entirety of the phase space.

Attending to the argument made in Section 3.1.2, it should be possible to find a better discrimination between different production modes by looking at the spatial distribution of the tagging jets (Δy_{jj}) or the invariant mass (m_{jj}). In Fig. 3.8 we see for $\Delta y_{jj} > 3.0$ or $m_{jj} > 400$ GeV the VBF production channel actually takes

over the ggF mode. This is in agreement with the previous discussion; in the ggF channel the two jets tend to be produced closer in rapidity space whereas in VBF the peak production rate occurs with the jets well separated in rapidity.

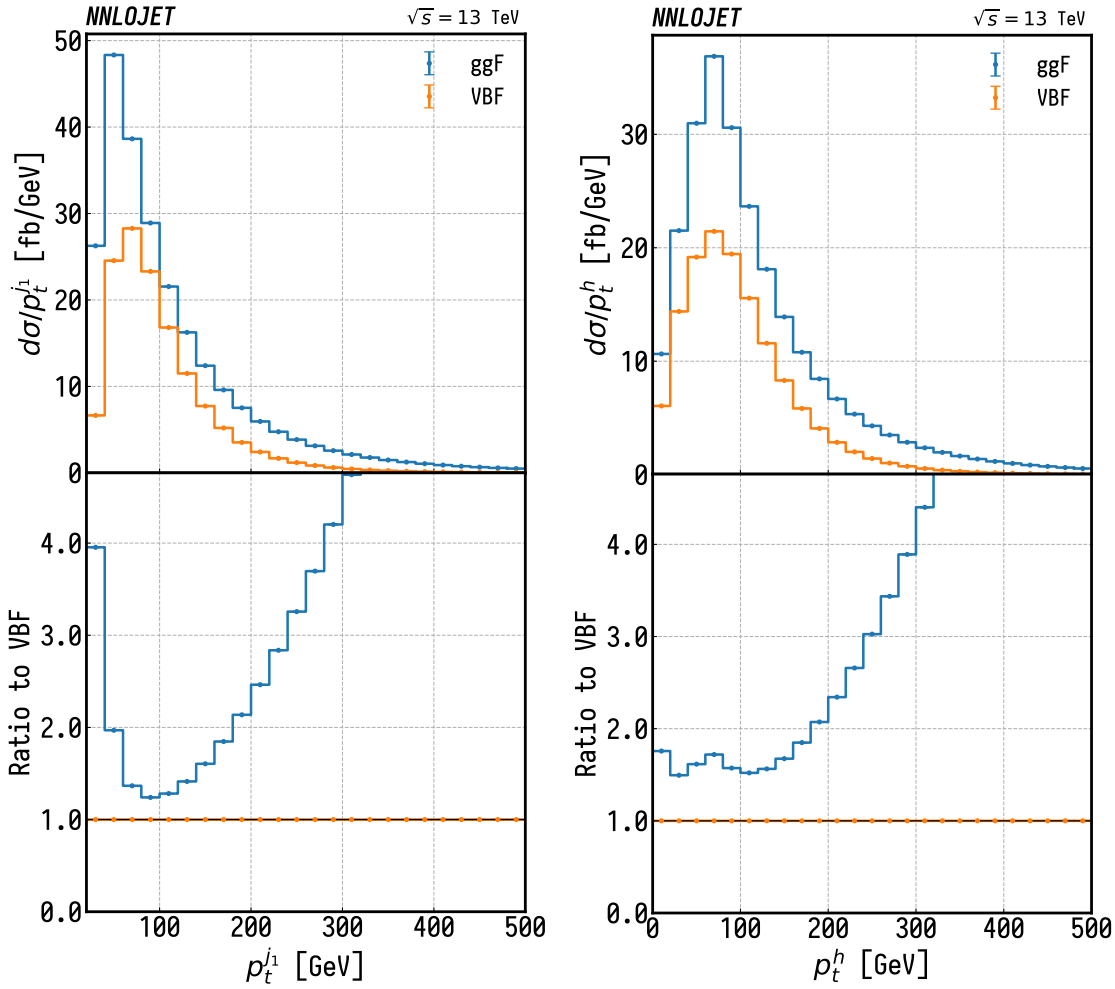

Figure 3.7: Comparison between ggF and VBF for the differential distributions on the transverse momentum of the leading jet (left) and the Higgs boson (right).

Very similar features are observed in the electroweak production processes. We show a comparison between VH, VBF, VBF$^{u/t}$ and the sum of them all in Fig. 3.9. We observe that the u/t-channels interferences are suppressed in the entire range of all observables. Only for very small values of Δy_{jj} and m_{jj} can an effect be observed.

The discrimination between the VH and VBF contribution is most obvious in the m_{jj} distribution of Fig. 3.9, as the bulk of the VH cross section occurs in the phase space region in which the two jets are produced around the resonance mass of the vector boson (i.e., $m_{jj} \sim 100$ GeV). Similarly, in the rapidity gap distribution

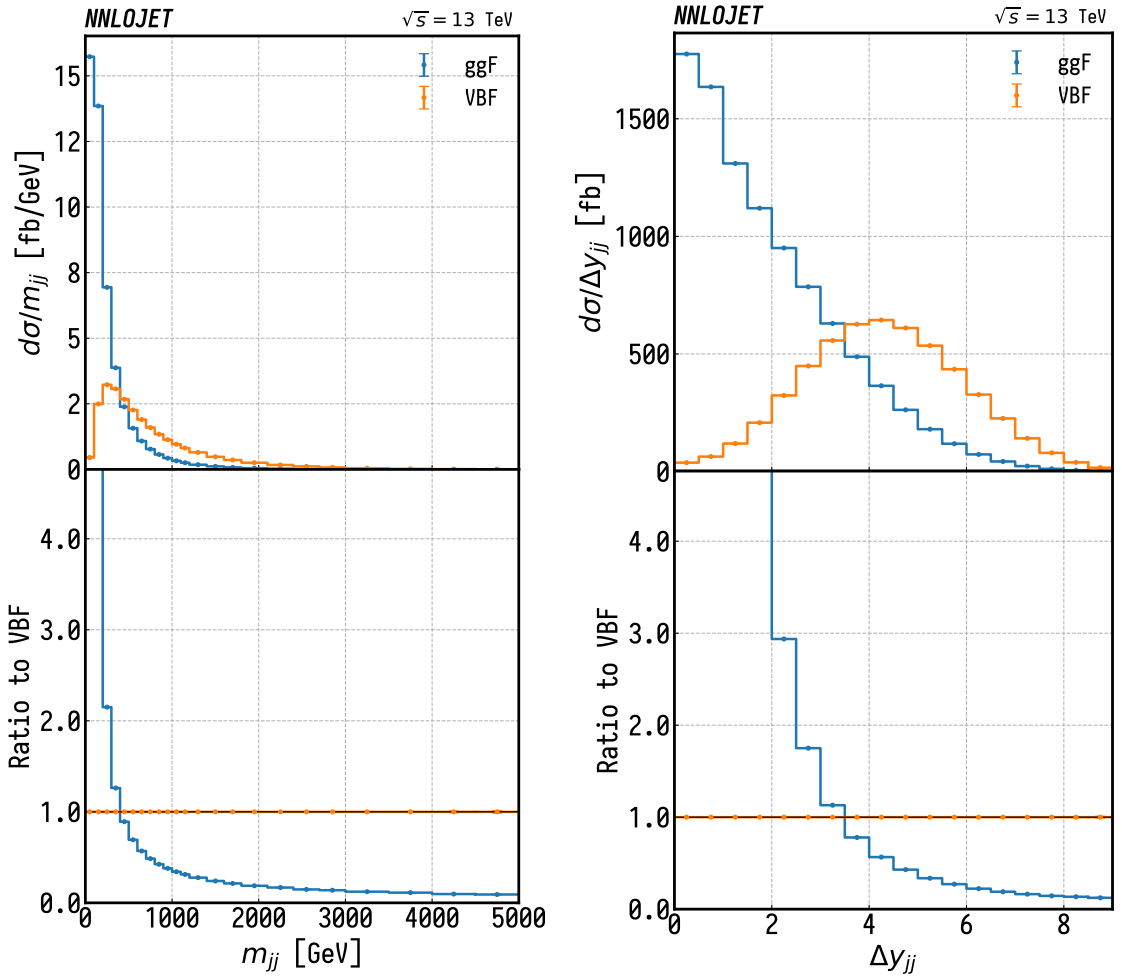

Figure 3.8: Comparison between ggF and VBF for the differential distributions on the invariant mass of the dijet system formed by the two tagging jets and the corresponding rapidity gap.

Δy_{jj} we find a clear separation between the VBF and VH production modes, with a clear suppression of VH for higher values of Δy_{jj}.

It is clear VBF cuts such as Eq. (3.1) suppress both VH contributions and u/t-channel interferences as well as softening the dominance of the ggF channel.

Impact of the VBF cuts

Let us now consider an example set of VBF cuts in order to study their impact on the relative contributions of the different H2j processes to differential distributions and fiducial cross sections.

Results shown in this section use the same parameters and implementations

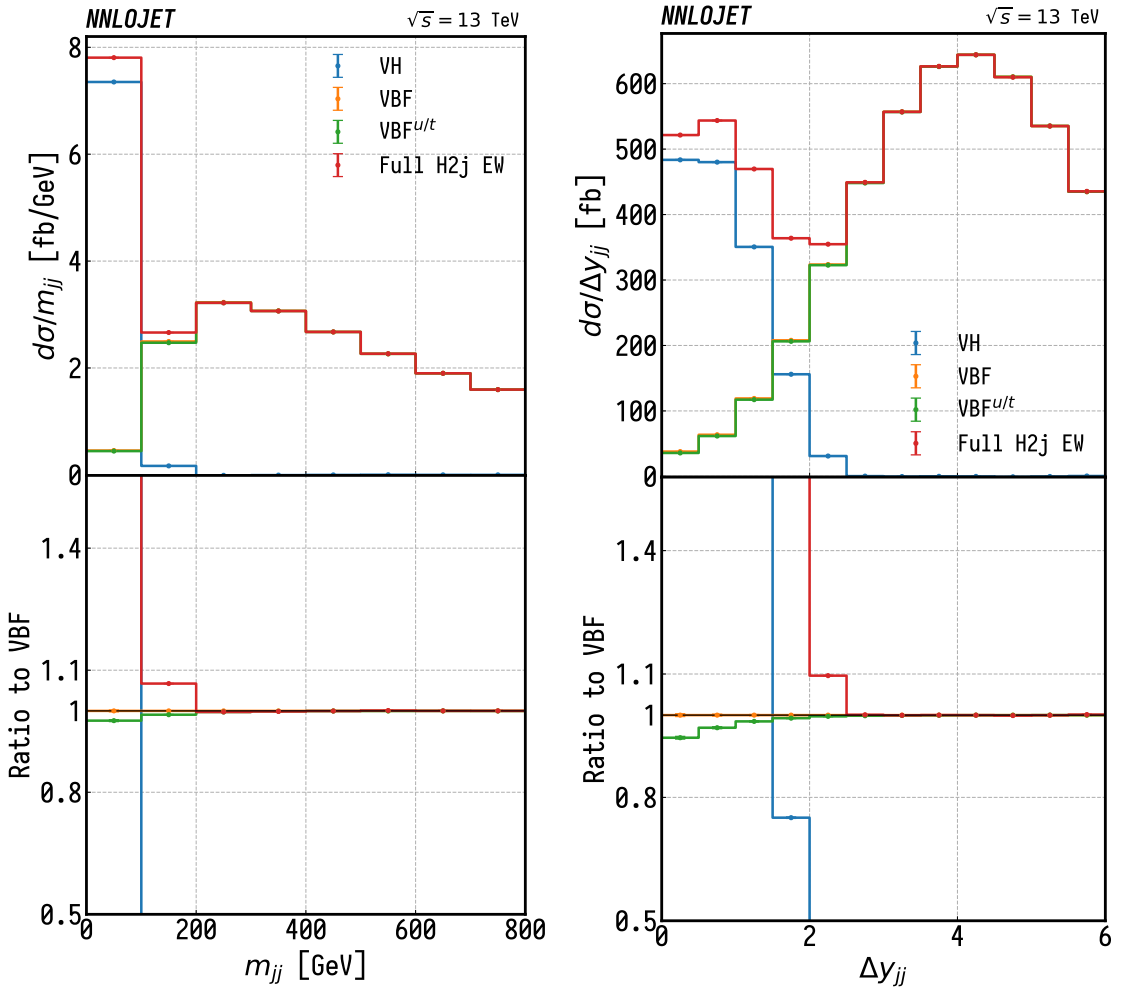

Figure 3.9: Comparison between electroweak Higgs boson plus 2 jets production for the invariant mass of the dijet system and the corresponding rapidity gap. VBF$^{u/t}$ corresponds to the inclusion of the u and t-channel interferences whereas Full EW H+2j correspond to the the sum of VH, VBF$^{u/t}$ and interferences thereof.

as the previous inclusive comparison with only two additional selection cuts as a minimal representation of VBF cuts:

$$m_{jj} > 400 \text{ GeV} \qquad \Delta y_{jj} > 3.0. \tag{3.6}$$

In Table 3.3 we see that the situation has drastically changed compared to Table 3.2. The dominant contribution on H2j production is no longer ggF and VBF dominates claiming almost a 75% of the total Higgs boson production rate. The VH contribution has been completely suppressed, with a production rate compatible with 0.

The dominance of the VBF production mode over gluon fusion is observed in

Production mode	Total cross section (fb)	% of Total	Cut efficiency
ggF	637.20 +/- 0.08	26.969 +/- 0.006	13.03 %
VBF	1725.69 +/- 0.24	73.04 +/- 0.02	63.38 %
VH	-0.18 +/- 0.35	-0.01 +/- 0.01	0 %
Total	2362.7 +/- 0.4	100	

Table 3.3: Comparison between different Higgs boson plus 2 jets production modes using VBF cuts. In this calculation we use the NNPDF30_nnlo_as_0118 [75] PDF set as included in the LHAPDF [76] library with $\mu_{\mathrm{F}} = \mu_{\mathrm{R}} = m_H$. Cut efficiency compares the % of events that go through the extra cuts imposed in Eq. (3.6).

the entire range of the differential distributions for m_{jj} and Δy_{jj} Fig. 3.10.

In Fig. 3.11, we show the transverse momentum of the leading jet and the Higgs boson, we find dominance of VBF only for low and moderate values of the transverse momentum while ggF regains importance for very high values of the transverse momentum.* This is in accordance with our discussion in Section 3.1.2 where we state that the two tagging jets of the VBF process are preferentially produced with lower transverse momentum. This is taken into account by the experiments by imposing an extra cut on the maximum value of the transverse momentum of the objects of the system (e.g., Eq. (3.1)).

We also observe in Fig. 3.10 and Fig. 3.11 that the full calculation (Full H2j EW) and the DIS approach (VBF) are indistinguishable, proving that these cuts have not introduced any spurious dependence in the interferences but rather have eliminated their already small effect.

3.3 Matrix elements

In this chapter we have studied the validity of the approximation under which we have implemented the VBF production process in the NNLOJET code as well as justified some of the necessary approximations we have made.

We conclude by explicitly listing all matrix elements included in our implemen-

*For high p_T^H the HEFT approximation in which we compute ggF is not reliable anymore, as the heavy quark loop becomes relevant and a full calculation of the ggF should be used instead for a more rigorous calculation [77].

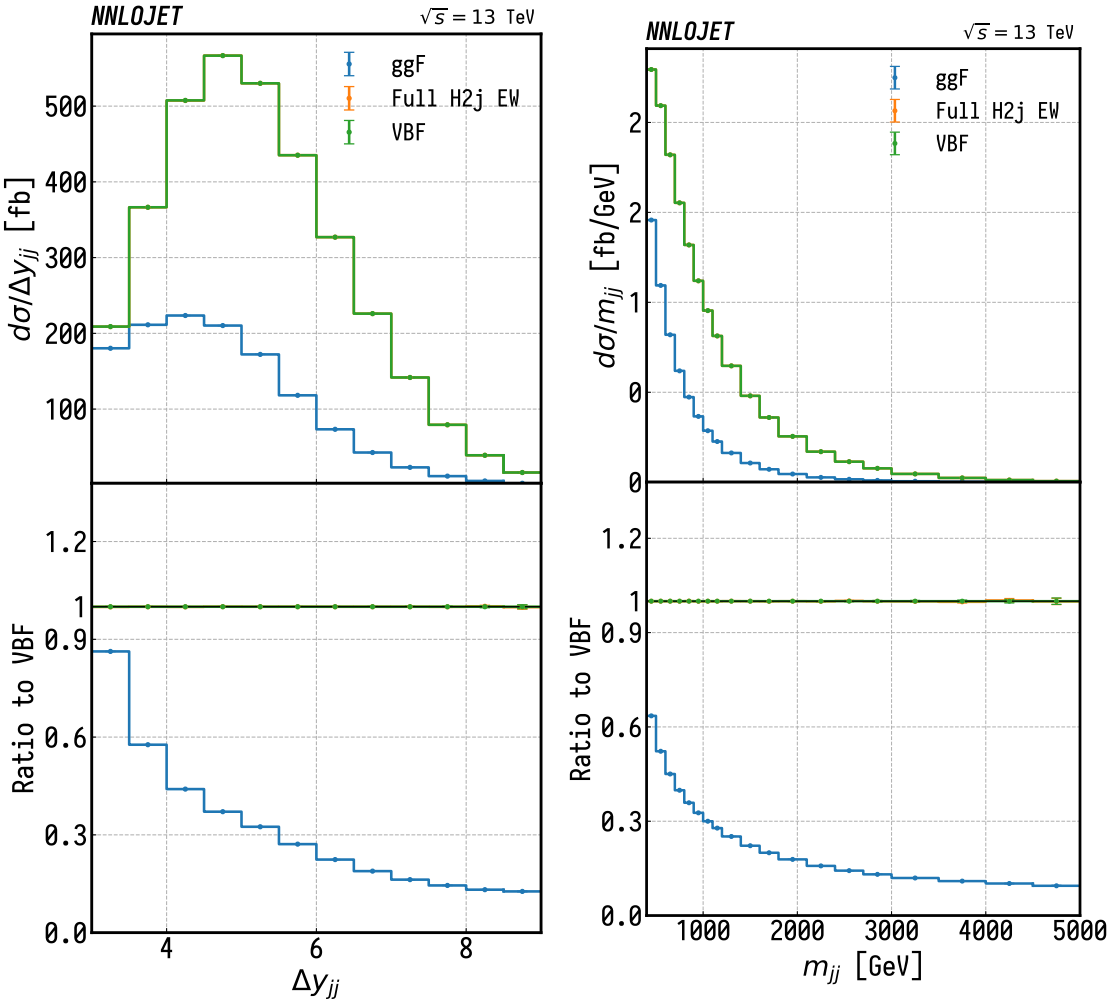

Figure 3.10: Comparison between ggF, the Full H2j Electroweak production and VBF for the differential distributions on the invariant mass of the dijet system formed by the two tagging jets and the corresponding rapidity gap.

tation together with the notation and conventions we use in NNLOJET.

3.3.1 Notation

All matrix elements squared are named in the form $X_{ng}^{(l)}$, where (l) stands for the number of loops while n defines the number of gluons in the matrix element. The character X defines the number of quark pairs in the matrix elements as per the following notation:

$$X \to \begin{cases} C, D & 2 \text{ quark pairs}, \\ E, F & 3 \text{ quark pairs}, \end{cases} \tag{3.7}$$

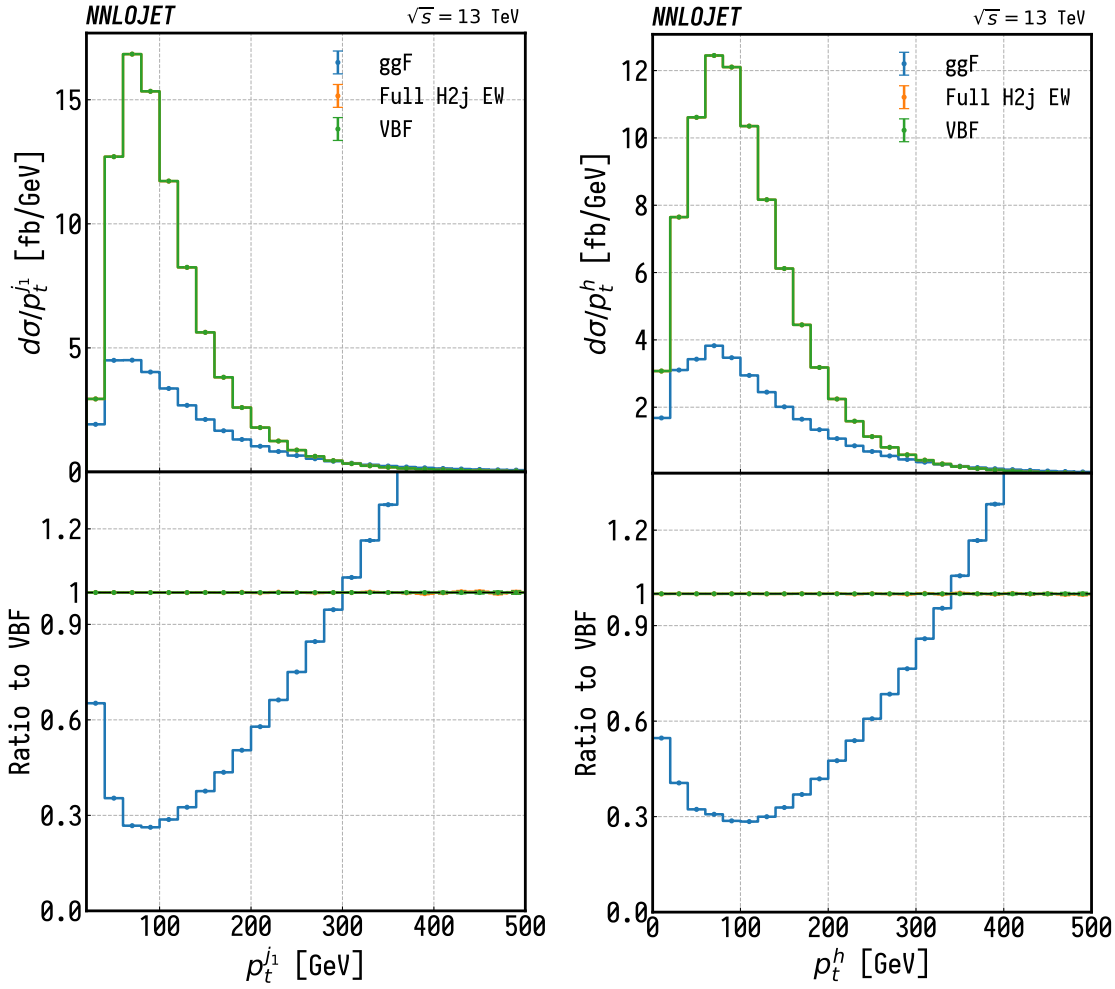

Figure 3.11: Comparison between ggF, the Full H2j Electroweak Production and VBF for the differential distributions on the transverse momentum of the leading jet and the Higgs.

where D and F correspond to interferences between four identical quarks. In the DIS approach no D contribution is allowed since it always corresponds to interferences between different DIS currents. F contributions are allowed when the interference is contained within just one of the currents.

Since we use the colour decomposition defined in Section 2.2.1, we also break each type of matrix element down according to the colour prefactors of the matrix element squared. In our notation we adopt the following convention which dresses the notation of Eq. (3.7),

- $\widetilde{X}$: Abelian-like gluons, does not contain collinear limits between gluons. A subleading colour contribution with a prefactor of $\frac{1}{N_c^2}$.

- $\hat{X}$: Matrix elements with quark loops, comes with a prefactor of $\frac{N_f}{N}$.

In VBF these terms appear only at NNLO.

3.3.2 Leading Order: Born contribution

We begin by explicitly computing the LO contribution in the helicity amplitude formalism with the following bracket notation:

$$\left\langle i^+ \right| \equiv \bar{u}_+(p_i) \equiv [i| \qquad \left| i^+ \right\rangle \equiv u_+(p_i) \equiv |i\rangle\,, \tag{3.8}$$

$$\left\langle i^- \right| \equiv \bar{u}_-(p_i) \equiv \langle i| \qquad \left| i^- \right\rangle \equiv u_-(p_i) \equiv |i]\,. \tag{3.9}$$

We can compute the amplitudes considering the VBF process as two quark currents as depicted in Fig. 3.12:

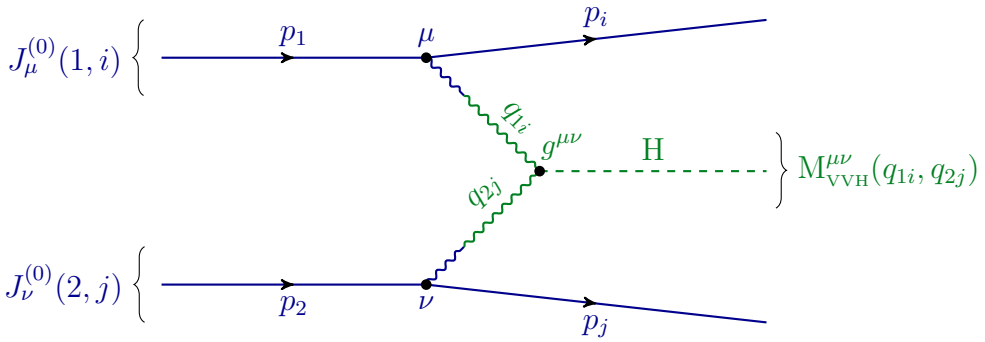

Figure 3.12: Only diagram contributing to the Born level VBF amplitude.

$$J_\mu^{(0)}(1,i)^\pm = \left\langle i^\pm \right| \gamma_\mu \mathcal{C}_V^f \left| 1^\pm \right\rangle, \qquad J_\mu^{(0)}(2,j)^\pm = \left\langle j^\pm \right| \gamma_\mu \mathcal{C}_V^f \left| 2^\pm \right\rangle,$$
$$\mathrm{M}_{\mathrm{VVH}}^{\mu\nu}(q_{1i}, q_{2j}) = \left(i g_W \frac{m_V^2}{m_W} \right) \frac{g^{\mu\nu}}{(q_{1i}^2 - m_V^2 - i\Gamma_V m_V)(q_{2j}^2 - m_V^2 - i\Gamma_V m_V)}, \tag{3.10}$$

where m_V and Γ_V are the masses and width of the vector bosons and $q_{1i} = (p_1 - p_i)$. $\mathcal{C}_V^\pm$ is the coupling of the electroweak gauge boson to the quark current, which depends on the gauge boson being considered (W or Z), and on the flavour (f) of

the quarks [9],

$$\mathcal{C}_Z^f = \frac{2g_W}{\cos(\theta_W)}\left(P_R Q_f \sin^2(\theta_W) + P_L(T_3^f - Q^f \sin^2(\theta_W))\right), \tag{3.11}$$

$$\mathcal{C}_W^f = 2P_L g_W, \tag{3.12}$$

where $\cos(\theta_W) = \frac{m_W}{m_Z}$ and P_R and P_L are the right and left-handed projector operators defined in Eq. (1.13).

The colour stripped born level amplitude for the diagram shown in Fig. 3.12 can thus be written as:

$$\mathcal{M}_{0g}^{(0)}(1i^{\pm}; 2j^{\pm}) = J_{\mu}^{(0)}(1,i)^{\pm} \mathrm{M}_{\mathrm{VVH}}^{\mu\nu}(q_{1i}, q_{2j}) J_{\nu}^{(0)}(2,j)^{\pm} \tag{3.13}$$

Recovering colour factors we can write for the Born level VBF amplitude (a sum over helicity configurations is implied),

$$\mathrm{M}_0^{(0)}(1,j,2,i) = \delta_{1i}^c \delta_{2j}^c \mathcal{M}_{0g}^{(0)}(1i;2j). \tag{3.14}$$

For Z boson exchange we can encounter situations in which the final state quarks (i and j) are indistinguishable from each other. These contributions are dropped as per the DIS approach but in order to be explicit let us write, in full generality, for Z fusion,

$$\mathrm{M}_{0,\mathrm{Z}}^{(0)}(1,j,2,i) = \frac{1}{\sqrt{2}}\left(\delta_{1i}^f \delta_{1i}^c \delta_{2j}^c \mathcal{M}_{0g}^{(0)}(1i;2j) - \delta_{1j}^f \delta_{1i}^c \delta_{2j}^c \mathcal{M}_{0g}^{(0)}(1j;2i)\right), \tag{3.15}$$

where δ_f signals the identical quark configuration,

Squared matrix elements

In W fusion the squared amplitude of (3.14) corresponds only to a C-type matrix element such that,

$$\sum^{N_c} \left|\mathrm{M}_{0,\mathrm{W}}^{(0)}(1,j,2,i)\right|^2 = N_c^2 C_{0g}^{(0)}(1,j,2,i). \tag{3.16}$$

In Z fusion, however, we need to consider the case in which the quark flavours are the same so that upon taking the square of Eq. (3.15) we generate both a C-type

and D-type contributions at different colour levels (with different colour factors),

$$\sum^{N_c} \left|\mathrm{M}^{(0)}_{0,\mathrm{Z}}(1,j,2,i)\right|^2 = N_c^2 \left(C^{(0)}_{0g}(1,j,2,i) - \frac{1}{N_c}\delta^{ij}_f D^{(0)}_{0g}(1,j,2,i) + i \leftrightarrow j \right), \quad (3.17)$$

where,

$$C^{(0)}_{0g}(1,j,2,i) = \left|\mathcal{M}^{(0)}_{0g}(1i;2j)\right|^2, \quad (3.18)$$

$$D^{(0)}_{0g}(1,j,2,i) = \mathrm{Re}\Big\{ \mathcal{M}^{(0)}_{0g}(1i;2j) \left(\mathcal{M}^{(0)}_{0g}(1j;2i)\right)^* \Big\}. \quad (3.19)$$

In the DIS approximation, however, we do not consider contributions in which there are interference terms between the two currents. This is equivalent to dropping all D-type matrix elements at every order.

The amplitudes are implemented in NNLOJET at the level of the colour stripped amplitudes of Eq. (3.14) so that matrix elements outside the VBF approximation can be easily constructed from their constituent parts.

3.3.3 Next to Leading Order: Real radiation

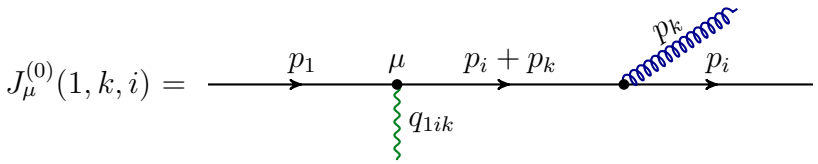

Figure 3.13: Quark current with one gluon being radiated.

The computation of the amplitude of the R layer follows the same rules as the Born level, with the inclusion of one external gluon. The quark current now takes the form shown in Fig. 3.13 and the base amplitude implemented in NNLOJET can be written in term of currents as:

$$\mathcal{M}^{(0)}_{1g}(1ki;2j) = J^{(0)}_\mu(1,k,i)\mathrm{M}^{\mu\nu}_{\mathrm{VVH}}(q_{1ki},q_{2j})J^{(0)}_\nu(2,j) \quad (3.20)$$

Since the gluon can be radiated from both currents, the full amplitude is given by a sum over the possible radiations:

$$\mathrm{M}^{(0)}_1(1,k,j,2,i) = T^k_{1i}\delta^c_{2j}\mathcal{M}^{(0)}_{1g}(1ki;2j) + T^k_{2j}\delta^c_{1i}\mathcal{M}^{(0)}_{1g}(1i;2kj), \quad (3.21)$$

where we have dropped terms corresponding to identical quark configurations so that M has the same functional form for W and Z fusion. We make use of $T^k_{1i} = \sqrt{2}t^k_{1i}$ in order to avoid a proliferation of factors of 2 in the final colour factors.

Squared matrix elements

With no identical quarks, the square of (3.21) is equivalent for Z and W boson fusion,

$$\begin{aligned}\sum^{N_c} |\mathrm{M}^{(0)}_{1g}(1,k,j,2,i)|^2 = \sum^{N_c} &(\delta^{2j}_c)^2 \left(T^a_{1i}T^a_{i1}\right) |\mathcal{M}^{(0)}_{1g}(1ki;2j)|^2 + (\delta^{1i}_c)^2 \left(T^b_{2j}T^b_{j2}\right) |\mathcal{M}^{(0)}_{1g}(1ki;2j)|^2 \\ &+ 2\delta^{1i}_c\delta^{2j}_c T^a_{1i}T^b_{2j} \left(\mathcal{M}^{(0)}_{1g}(1ki;2j)\mathcal{M}(1i;2kj)^*\right) \\ &= N_c(N_c^2-1)\left(C^{(0)}_{1g}(1,k,j,2,i)\right). \end{aligned} \tag{3.22}$$

so that the matrix element $C^{(0)}_{1g}$ is defined,

$$C^{(0)}_{1g}(1,k,j,2,i) = |\mathcal{M}^{(0)}_{1g}(1ki;2j)|^2 + |\mathcal{M}^{(0)}_{1g}(1i;2kj)|^2 \tag{3.23}$$

Two points must be highlighted from Eq. (3.22). Firstly, due to colour conservation the DIS approach is exact at NLO (up to D-type matrix elements). It is not necessary to artificially drop any terms in order to prohibit interferences between gluons since they do not appear in the final answer. Secondly, in Eq. (3.22) the matrix element $C^{(0)}_{1g}$ implies a sum over the possible configurations for the radiation of the gluon (denoted by k). However, when constructing the subtraction terms, it is useful to access the matrix element squared in which the gluon is only radiated from one of the two currents. This is notated adding s^0 to the name,

$$C^{(0)}_{1g}\mathrm{s}^0(1,k,j,2,i) = |\mathcal{M}^{(0)}_{1g}(1ki;2j)|^2. \tag{3.24}$$

These more basic matrix elements are included in the repository and are extensively used in the computation of the subtraction terms at the RR and RV levels listed in Appendix C.

In order to simplify the construction of the subtraction terms we also define a flavour averaged matrix element for gluon-initiated configurations in which we sum

over the final state quarks coming from the splitting of the gluon,

$$\mathrm{s}C_{1g}^{(0)}(k,1,j,2,i) \equiv \frac{1}{2}\left(C_{1g}^{(0)}(k,1,j,2,i) + C_{1g}^{(0)}(i,1,j,2,k)\right), \tag{3.25}$$

when the matrix element is quark-initiated the matrix element is defined to be the same,

$$\mathrm{s}C_{1g}^{(0)}(1,k,j,2,i) \equiv C_{1g}^{(0)}(1,k,j,2,i). \tag{3.26}$$

3.3.4 Next to Leading Order: Virtual contribution

Since we have dropped D-type contributions, as we saw in Section 3.3.3, and the gluon exchange is forbidden between different currents due to colour considerations, it follows that the virtual amplitude for the VBF process corresponds to the form factor of each current.

In other words, the one loop current $\boldsymbol{J}_{\mu}^{(1)}(q_1,q_2)$ reads:

$$\boldsymbol{J}_{\mu}^{(1)}(1,i)^{\pm} = \boldsymbol{F}_{q}^{1}(q_{1i})\delta_{1i}^{c}J_{\mu}^{(0)}(1,i)^{\pm}, \tag{3.27}$$

where we use the form factors $\boldsymbol{F}_{q}^{1} = \frac{N_c^2-1}{N_c}F_{q}^{1}$ as computed in Ref. [78]. Both the one loop quark current and the virtual matrix element are proportional to their Born level counterparts.

$$\begin{aligned}\boldsymbol{\mathcal{M}}_{0g}^{(1)}(1i;2j) &= \boldsymbol{J}_{\mu}^{(1)}(1,i)\mathrm{M}_{\mathrm{VVH}}^{\mu\nu}(q_{1i},q_{2j})J_{\nu}^{(0)}(2,j) + J_{\mu}^{(0)}(1,i)\mathrm{M}_{\mathrm{VVH}}^{\mu\nu}(q_{1i},q_{2j})\boldsymbol{J}_{\nu}^{(1)}(2,j)\\ &= \left(\boldsymbol{F}_{q}^{1}(q_{1i}) + \boldsymbol{F}_{q}^{1}(q_{2j})\right)\mathcal{M}_{0g}^{(0)}(1i;2j)\end{aligned} \tag{3.28}$$

The full matrix element, accounting for the fact that the loop can appear in both currents and making colour factors explicit, is given by,

$$\mathrm{M}_{0}^{(1)}(1,j,2,i) = \frac{N_c^2-1}{N_c}\delta_{1i}^{c}\delta_{2j}^{c}\left(F_{q}^{1}(q_{1i}) + F_{q}^{1}(q_{2j})\right)\mathcal{M}_{0g}^{(0)}(1i;2j), \tag{3.29}$$

Squared matrix element

In Eq. (3.29) the virtual amplitude is a form factor depending only on the momentum transfer q_{1j} times the born amplitude. Taking the interference between the one-loop

and Born amplitudes the one-loop matrix element squared, $C_{0g}^{(1)}$, yields,

$$\sum^{N_c} \mathrm{Re}\{\mathrm{M}_0^{(1)}(1,j,2,i)\mathrm{M}_0^{(0)}(1,j,2,i)^*\} = N_c(N_c^2-1)C_{0g}^{(1)}(1,j,2,i), \tag{3.30}$$

which is proportional to the Born contribution $C_{0g}^{(0)}$,

$$C_{0g}^{(1)}(1,j,2,i) = \left(F_q^1(q_{1i}) + F_q^1(q_{2j})\right) C_{0g}^{(0)}(1,j,2,i). \tag{3.31}$$

3.3.5 Next to Next to Leading Order: Double Real contribution

The RR amplitude introduces three different scenarios:

a) One gluon emitted from each of the currents.

b) Two gluons emitted from the same current.

c) One gluon emitted from one of the currents which subsequentially splits into a $q\ \bar{q}$ pair.

We already have the current for case a), as it corresponds to the same structure as the real radiation studied in Section 3.3.3 where we compute the real corrections to the process. In this case both currents have a gluon emission.

Cases b) and c) appear for the first time at NNLO and their respective currents are shown in Fig. 3.14 and Fig. 3.15.

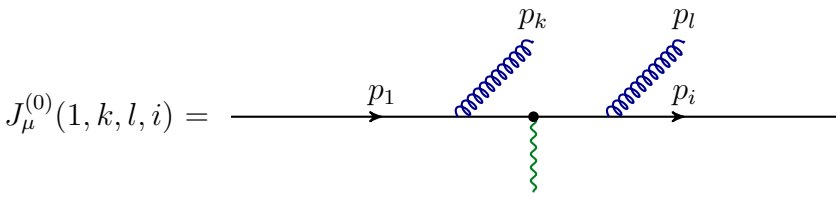

Figure 3.14: Example of quark current with two emissions of gluons. For the full current see Fig. 2.2.

As per the DIS approximation, we drop any contributions in which interferences between the two currents appear (be it due to gluon exchange or identical flavour

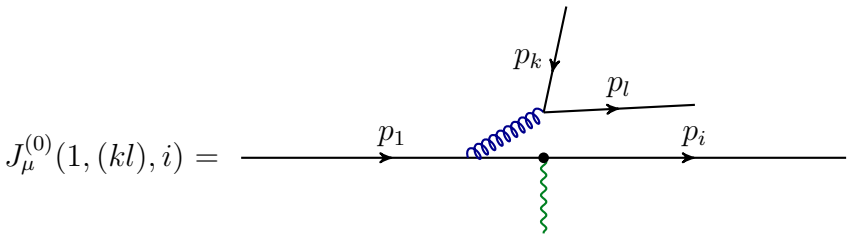

Figure 3.15: Example of quark current with a $q\,\bar{q}$ pair splitting of the radiated gluon.

quarks). We can split the RR contribution into three separated matrix elements with no interference between themselves corresponding to cases a), b) and c).

Two gluons non adjacent amplitude

The amplitude in scenario a) is similar to the real amplitude at NLO and can be written as:

$$\mathcal{M}_{2g}^{(0)}(1ki;2lj) = J_\mu^{(0)}(1,k,i)\mathrm{M}_{\mathrm{VVH}}^{\mu\nu}(q_{1ki},q_{2lj})J_\nu^{(0)}(2,l,j), \tag{3.32}$$

$$\mathrm{M}_{2g}^{(0)}(1,k,j,2,l,i) = T_{1i}^k T_{2j}^l \mathcal{M}_{2g}^{(0)}(1ki;2lj) + T_{1i}^l T_{2j}^k \mathcal{M}_{2g}^{(0)}(1li;2kj), \tag{3.33}$$

where we sum over the exchange $k \leftrightarrow l$.

Upon taking the square and dropping any interferences between gluons coming from different currents we find:

$$\sum^{N_c} \left|\mathrm{M}_2^{(0)}(1,k,j,2,l,i)\right|^2 = (N_c^2-1)^2 \left(C_{2g,\mathrm{nadj}}^{(0)}(1,k,j,2,l,i) + C_{2g,\mathrm{nadj}}^{(0)}(1,l,j,2,k,i)\right) \tag{3.34}$$

where $C_{2g,\mathrm{nadj}}^{(0)}$ is defined as,

$$C_{2g,\mathrm{nadj}}^{(0)}(1,k,j,2,l,i) = |\mathcal{M}_{2g}^{(0)}(1ki;2lj)|^2. \tag{3.35}$$

Two gluons adjacent amplitude

In case b), where two gluons are radiated from the same current, we find a more complicated colour structure. In this case terms subleading in colour (with two colour disconnected gluons) appear for the first time. For simplicity, let us write the

situation in which the two gluons are radiated only from the $(1,i)$ line,

$$\mathcal{M}_{2g}^{(0)}(1,k,l,i;2j) = J_{\mu}^{(0)}(1,k,l,i)\mathrm{M}_{\mathrm{VVH}}^{\mu\nu}(q_{1kli},q_{2j})J_{\nu}^{(0)}(2,j) + J_{\mu}^{(0)}(1,(k-l),i)\mathrm{M}_{\mathrm{VVH}}^{\mu\nu}(q_{1kli},q_{2j})J_{\nu}^{(0)}(2,j), \tag{3.36}$$

$$\mathcal{M}_{2g}^{(0)}(1,l,k,i;2j) = J_{\mu}^{(0)}(1,l,k,i)\mathrm{M}_{\mathrm{VVH}}^{\mu\nu}(q_{1kli},q_{2j})J_{\nu}^{(0)}(2,j) - J_{\mu}^{(0)}(1,(k-l),i)\mathrm{M}_{\mathrm{VVH}}^{\mu\nu}(q_{1kli},q_{2j})J_{\nu}^{(0)}(2,j), \tag{3.37}$$

where we have notated the current for the three-gluon vertex as $(k-l)$, analogous to Eq. (2.27) we can write for the full amplitude for gluons k and l radiated from the $(1,i)$ current as,

$$\mathrm{M}_{2}^{(0)}(1,k,l,j,2,i) = \delta_{2j}^{c}\left(T_{1b}^{k}T_{bi}^{l}\mathcal{M}_{2g}^{(0)}(1,k,l,i;2j) + T_{1b}^{l}T_{bi}^{k}\mathcal{M}_{2g}^{(0)}(1,l,k,i;2j)\right). \tag{3.38}$$

The case in which the gluons come from the $(2,j)$ line is obtained by the substitution $(1i) \leftrightarrow (2j)$. For the $(1,i)$ radiation the squared matrix elements yields,

$$\sum^{N_c}\left|\mathrm{M}_{2}^{(0)}(1,k,l,j,2,i)\right|^2 = N_c^2(N_c^2-1)\left\{C_{2g,\mathrm{adj}}^{(0)}(1,k,l,j,2,i) - \frac{1}{N_c^2}\widetilde{C}_{2g,\mathrm{adj}}^{(0)}(1,\widetilde{k},\widetilde{l},j,2,i) + C_{2g,\mathrm{adj}}^{(0)}(1,l,k,j,2,i)\right\}. \tag{3.39}$$

where the squared matrix elements, leading and subleading in colour, are defined as,

$$C_{2g,\mathrm{adj}}^{(0)}(1,k,l,j,2,i) = |\mathcal{M}_{2g}^{(0)}(1,k,l,i;2j)|^2 \tag{3.40}$$

$$\widetilde{C}_{2g,\mathrm{adj}}^{(0)}(1,\widetilde{k},\widetilde{l},j,2,i) = |\mathcal{M}_{2g}^{(0)}(1,k,l,i;2j) + \mathcal{M}_{2g}^{(0)}(1,l,k,i;2j)|^2 \tag{3.41}$$

Since both cases a) and b) can be made to share the same colour global factor, they are included in NNLOJET as matrix elements squared combining both case. The

resulting combination matrix elements are $C_{2g}^{(0)}$ and $\widetilde{C}_{2g}^{(0)}$,

$$\begin{aligned} C_{2g}^{(0)}(1,k,l,j,2,i) &= C_{2g,\mathrm{nadj}}^{(0)}(1,k,j,2,l,i) + C_{2g,\mathrm{adj}}^{(0)}(1,k,l,j,2,i) \\ &\quad + C_{2g,\mathrm{adj}}^{(0)}(2,k,i,1,l,j), \end{aligned} \tag{3.42}$$

$$\begin{aligned} \widetilde{C}_{2g}^{(0)}(1,\widetilde{k},\widetilde{l},j,2,i) &= C_{2g,\mathrm{nadj}}^{(0)}(1,k,j,2,l,i) + \widetilde{C}_{2g,\mathrm{adj}}^{(0)}(1,\widetilde{k},\widetilde{l},j,2,i) \\ &\quad + C_{2g,\mathrm{nadj}}^{(0)}(1,l,j,2,k,i) + \widetilde{C}_{2g,\mathrm{adj}}^{(0)}(2,\widetilde{k},\widetilde{l},i,1,j). \end{aligned} \tag{3.43}$$

Six quarks amplitude

The four quark current shown in Fig. 3.15 gives raise to a six quarks contribution upon contraction with a born level current. The amplitude for six quarks yields,

$$\mathcal{M}_{0g}^{(0)}(1,(kl)i;2j) = J_{\mu}^{(0)}(1(kl),i)\mathrm{M}_{\mathrm{VVH}}^{\mu\nu}(q_{1ikl},q_{2j})J_{\nu}^{(0)}(2,j), \tag{3.44}$$

where (kl) are the two quarks which are not associated with a vector boson. In order to obtain the full amplitude it is necessary to consider the coupling of the vector boson to the initial state current ($J(1,(kl),i)$) and to the final state current ($J(k,(1i),l)$).

$$\begin{aligned} M_0^{(0)}(1,k,l,j,2,i) = \delta_{2j}^{c} \Big\{ & T_{1i}^{a}T_{kl}^{a}\left(\delta_{\bar{k}\bar{l}}^{f}\mathcal{M}_{0g}^{(0)}(1(kl)i;2j) + \delta_{1i}^{f}\mathcal{M}_{0g}^{(0)}(k(1i)l;2j)\right) \\ & + T_{1l}^{a}T_{ki}^{a}\left(\delta_{1\bar{l}}^{f}\mathcal{M}_{0g}^{(0)}(k(1l)i;2j) + \delta_{\bar{k}i}^{f}\mathcal{M}_{0g}^{(0)}(1(ki)l;2j)\right)\Big\} \\ & + (1,i) \leftrightarrow (2,j), \end{aligned} \tag{3.45}$$

where δ_{ij}^{f} indicates that i and j need to share the same flavour. This will remove certain contributions, crucially W-fusion interferences.

Note that in this case identical quark interferences can arise upon taking the square in which the interfering lines all correspond to the same current. These are included in our calculation with the letter F,

$$\begin{aligned} \sum^{N_c} |M_0^{(0)}(1,k,l,j,2,i)|^2 = (N_c^2-1)\Big(& N_c E_{0g}^{(0)}(1,k,l,j,2,i) + N_c E_{0g}^{(0)}(1,k,i,j,2,l) \\ & - F_{0g}^{(0)}(1,k,l,j,2,i) - F_{0g}^{(0)}(k,1,i,j,2,l)\Big). \end{aligned} \tag{3.46}$$

with,

$$E_{0g}^{(0)}(1,k,l,j,2,i) = \left|\delta_{\bar{k}l}^{f}\mathcal{M}_{0g}^{(0)}(1(kl)i;2j) + \delta_{1i}^{f}\mathcal{M}_{0g}^{(0)}(k(1i)l;2j)\right|^2 + (1,i)\leftrightarrow(2,j). \tag{3.47}$$

$$F_{0g}^{(0)}(1,k,l,j,2,i) = 2\delta_{1\bar{k}}^{f}\,\mathrm{Re}\left\{\mathcal{M}_{0g}^{(0)}(1(kl)i;2j)(\mathcal{M}_{0g}^{(0)}(k(1l)i;2j)^*) + \mathcal{M}_{0g}^{(0)}(k(1i)l;2j)(\mathcal{M}_{0g}^{(0)}(1(ki)l;2j)^*)\right\} + (1,i)\leftrightarrow(2,j). \tag{3.48}$$

3.3.6 Next to Next to Leading Order: Real Virtual contribution

Since gluons are not exchanged between upper and lower currents in the DIS approach, we only need to consider two cases:

A) One loop correction to the Born level current $J_{\mu}^{(1)}(1,i)$ where the emission occurs in the other current $J_{\mu}^{(0)}(2,k,j)$. This can be compared to the "non-adjacent" scenario in the previous section.

B) One loop correction to a R current, notated as $J_{\mu}^{(1)}(1,k,i)$, while the second current is a born level current $J_{\mu}^{(0)}(2,j)$. This situation is comparable to the two gluons adjacent amplitude from the previous section.

Non adjacent amplitude

In the RR case we could treat the non-adjacent amplitude as two single R currents, similarly we can substitute one of the real radiation currents for a one-loop no-radiation current so that the amplitude is a form factor times the real radiation amplitude.

$$\mathcal{M}_{1g}^{(1)}(1ki;2j) = J_{\mu}^{(0)}(1,k,i)\mathrm{M}_{\mathrm{VVH}}^{\mu\nu}(q_{1ki},q_{2j})J_{\nu}^{(1)}(2,j) \tag{3.49}$$

$$= F_q^1(q_{2j})J_{\mu}^{(0)}(1,k,i)\mathrm{M}_{\mathrm{VVH}}^{\mu\nu}(q_{1ki},q_{2j})J_{\nu}^{(0)}(2,j) \tag{3.50}$$

Taking the interference with the R amplitude and summing over loop and radiation from both legs we find a familiar structure,

$$\sum^{N_c} \mathrm{Re}\{\mathrm{M}_1^{(1)}(1,k,j,2,i)\mathrm{M}_1^{(0)}(1,k,j,2,i)^*\} = \tag{3.51}$$
$$= (N_c^2-1)^2(F_q^1(q_{2j})C_{1g}^{(0)}\mathrm{s}^0(1,k,j,2,i) + F_q^1(q_{1i})C_{1g}^{(0)}\mathrm{s}^0(1,j,2,k,i))$$
$$= (N_c^2-1)^2(C_{1g,\mathrm{nadj}}^{(1)}(1,k,j,2,i) + C_{1g,\mathrm{nadj}}^{(1)}(1,j,2,k,i)),$$

from which we can define $C_{1g,\mathrm{nadj}}^{(1)}$ in terms of the real matrix element squared defined in Eq. (3.24).

$$C_{1g,\mathrm{nadj}}^{(1)}(1,j,2,k,i) = F_q^1(q_{1i})C_{1g}^{(0)}\mathrm{s}^0(1,j,2,k,i). \tag{3.52}$$

Adjacent amplitude

The one loop one radiation current, shown for reference in Fig. 3.16, is much more involved and presents a complicated colour structure already at the level of the currents. We implement the method and formulae of [79] in a Form program in order to assemble a one-loop one-radiation current in terms of colour stripped currents

$$\mathbf{J}_\mu^{(1)}(1,k,i) = T_{1i}^k\left(N_c J_\mu^{(1)}(1,k,i) + N_f \hat{J}_\mu^{(1)}(1,k,i) - \frac{1}{N_c}\widetilde{J}_\mu^{(1)}(1,k,i)\right). \tag{3.53}$$

Figure 3.16: Example of one loop one radiation diagrams contributing to the $\mathbf{J}_\mu^{(1)}(1,k,i)$ current.

From Eq. (3.53) we can define three different amplitudes attending to the colour prefactors upon contraction with the Born-level $(2,j)$ current,

$$\mathcal{M}_{1g}^{(1)}(1ki;2j) = J_\mu^{(1)}(1,k,i)\mathrm{M}_{\mathrm{VVH}}^{\mu\nu}(q_{1ki},q_{2j})J_\nu^{(0)}(2,j), \tag{3.54}$$
$$\widetilde{\mathcal{M}}_{1g}^{(1)}(1ki;2j) = \widetilde{J}_\mu^{(1)}(1,k,i)\mathrm{M}_{\mathrm{VVH}}^{\mu\nu}(q_{1ki},q_{2j})J_\nu^{(0)}(2,j), \tag{3.55}$$
$$\hat{\mathcal{M}}_{1g}^{(1)}(1ki;2j) = \hat{J}_\mu^{(1)}(1,k,i)\mathrm{M}_{\mathrm{VVH}}^{\mu\nu}(q_{1ki},q_{2j})J_\nu^{(0)}(2,j). \tag{3.56}$$

Which in turn will give rise to three different matrix element squared when we take the interference with the 0-loop 1-gluon real amplitude:

$$\sum^{N_c} \mathrm{Re}\Big\{\mathrm{M}_1^{(1)}(1,k,j,2,i)\mathrm{M}_1^{(0)}(1,k,j,2,i)^*\Big\} = (N_c^2-1)\Big\{N_c^2 C^{(1)}_{1g,\mathrm{adj}}(1,k,j,2,i) + N_c N_f \hat{C}^{(1)}_{1g,\mathrm{adj}}(1,k,j,2,i) - \widetilde{C}^{(1)}_{1g,\mathrm{adj}}(1,k,j,2,i)\Big\}, \tag{3.57}$$

respectively,

$$C^{(1)}_{1g,\mathrm{adj}}(1,k,j,2,i) = \mathrm{Re}\Big\{\mathcal{M}^{(1)}_{1g}(1ki;2j)\mathcal{M}^{(0)}_{1g}(1ki;2j)^*\Big\}, \tag{3.58}$$

$$\widetilde{C}^{(1)}_{1g,\mathrm{adj}}(1,k,j,2,i) = \mathrm{Re}\Big\{\widetilde{\mathcal{M}}^{(1)}_{1g}(1ki;2j)\mathcal{M}^{(0)}_{1g}(1ki;2j)^*\Big\}, \tag{3.59}$$

$$\hat{C}^{(1)}_{1g,\mathrm{adj}}(1,k,j,2,i) = \mathrm{Re}\Big\{\hat{\mathcal{M}}^{(1)}_{1g}(1ki;2j)\mathcal{M}^{(0)}_{1g}(1ki;2j)^*\Big\}. \tag{3.60}$$

In the same fashion as Section 3.3.5 we can organise both adjacent and non-adjacent matrix elements together attending to their colour factors:

$$C^{(1)}_{1g}(1,k,j,2,i) = C^{(1)}_{1g,\mathrm{adj}}(1,k,j,2,i) + C^{(1)}_{1g,\mathrm{nadj}}(1,k,j,2,i) + \{(1,i)\to(2,j)\}, \tag{3.61}$$

$$\widetilde{C}^{(1)}_{1g}(1,k,j,2,i) = \widetilde{C}^{(1)}_{1g,\mathrm{adj}}(1,k,j,2,i) + C^{(1)}_{1g,\mathrm{nadj}}(1,k,j,2,i) + \{(1,i)\to(2,j)\}, \tag{3.62}$$

$$\hat{C}^{(1)}_{1g}(1,k,j,2,i) = \hat{C}^{(1)}_{1g,\mathrm{adj}}(1,k,j,2,i) + \hat{C}^{(1)}_{1g,\mathrm{adj}}(2,k,i,1,j), \tag{3.63}$$

which are the matrix element squared that can be found in the NNLOJET codebase.

3.3.7 Next to Next to Leading Order: Double Virtual contribution

The final ingredient of our implementation is the VV matrix element. Contrary to other higher order calculations and thanks to the DIS approach, the two loop matrix elements appear in only two configurations corresponding to vertex corrections to the quark currents, each with a structure similar to the V amplitude:

a) Two loops in the same current and no loops in the other. A F_q^2 form factor.

b) One loop in each current. Two F_q^1 form factors.

Both configurations are proportional to the Born level current. The form factors computed in Ref. [78] can be broken down attending to their colour prefactors

$$\mathbf{F_q^2}(q_{1i}) = \frac{(N_c^2-1)}{N_c}\left(N_c F_q^2(q_{1i}) + N_f \hat{F}_q^2(q_{1i}) - \frac{1}{N_c}\widetilde{F}_q^2(q_{1i})\right), \tag{3.64}$$

which allow us to expand the two loops quark current and the VV amplitude

$$\mathbf{J}_\mu^{(2)}(1,i) = \delta_{1i}^c \frac{(N_c^2-1)}{N_c}\left(N_c J_\mu^{(2)}(1,i) + N_f \hat{J}_\mu^{(2)}(1,i) - \frac{1}{N_c}\widetilde{J}_\mu^{(2)}(1,i)\right), \tag{3.65}$$

in analogy with Section 3.3.6 we can define,

$$\begin{aligned}
\mathcal{M}_{0g}^{(2)}(1i;2j) &= J_\mu^{(2)}(1,i)\mathrm{M}_{\mathrm{VVH}}^{\mu\nu}(q_{1i},q_{2j})J_\nu^{(0)}(2,j) + J_\mu^{(1)}(1,i)\mathrm{M}_{\mathrm{VVH}}^{\mu\nu}(q_{1i},q_{2j})J_\nu^{(1)}(2,j) \\
&\quad + J_\mu^{(0)}(1,i)\mathrm{M}_{\mathrm{VVH}}^{\mu\nu}(q_{1i},q_{2j})J_\nu^{(2)}(2,j), \qquad (3.66)\\
\widetilde{\mathcal{M}}_{0g}^{(2)}(1i;2j) &= \widetilde{J}_\mu^{(2)}(1,i)\mathrm{M}_{\mathrm{VVH}}^{\mu\nu}(q_{1i},q_{2j})J_\nu^{(0)}(2,j) + J_\mu^{(1)}(1,i)\mathrm{M}_{\mathrm{VVH}}^{\mu\nu}(q_{1i},q_{2j})J_\nu^{(1)}(2,j) \\
&\quad + J_\mu^{(0)}(1,i)\mathrm{M}_{\mathrm{VVH}}^{\mu\nu}(q_{1i},q_{2j})\widetilde{J}_\nu^{(2)}(2,j), \qquad (3.67)\\
\hat{\mathcal{M}}_{0g}^{(2)}(1i;2j) &= \hat{J}_\mu^{(2)}(1,i)\mathrm{M}_{\mathrm{VVH}}^{\mu\nu}(q_{1i},q_{2j})J_\nu^{(0)}(2,j). \qquad (3.68)
\end{aligned}$$

Squared matrix element

Upon taking the square of the V amplitude and the interference of the VV amplitude with the Born level we find the same colour structure as in Eq. (3.57), which we implement as independent matrix elements squared in our codebase.

$$\begin{aligned}
&\sum^{N_c}\mathrm{Re}\Big\{\mathrm{M}_0^{(2)}(1,j,2,i)\mathrm{M}_0^{(0)}(1,j,2,i)^*\Big\} + \Big|\mathrm{M}_0^{(1)}(1,j,2,i)\Big|^2 = \\
&(N_c^2-1)\Big\{N_c^2 C_{0g}^{(2)}(1,j,2,i) + N_c N_f \hat{C}_{0g}^{(2)}(1,j,2,i) - \widetilde{C}_{0g}^{(2)}(1,j,2,i)\Big\},
\end{aligned} \tag{3.69}$$

with,

$$C^{(2)}_{0g}(1,j,2,i) = \mathrm{Re}\Big\{\mathcal{M}^{(2)}_{0g}(1ki;2j)\mathcal{M}^{(0)}_{0g}(1ki;2j)^*\Big\}, \tag{3.70}$$

$$\widetilde{C}^{(2)}_{0g}(1,j,2,i) = \mathrm{Re}\Big\{\widetilde{\mathcal{M}}^{(2)}_{0g}(1ki;2j)\mathcal{M}^{(0)}_{0g}(1ki;2j)^*\Big\}, \tag{3.71}$$

$$\hat{C}^{(2)}_{0g}(1,j,2,i) = \mathrm{Re}\Big\{\hat{\mathcal{M}}^{(2)}_{0g}(1ki;2j)\mathcal{M}^{(0)}_{0g}(1ki;2j)^*\Big\}. \tag{3.72}$$

Chapter 4

NNLOjet Implementation

In previous chapters we have outlined all of the ingredients that are required to obtain predictions for physical observables in a Higgs plus two jets production process via VBF. The final step is the combination of all previous elements and the numerical integration of the cross section as defined in Eq. (2.57), to which this chapter is dedicated.

Section 4.1 will be focused on the fixed order parton-level Monte Carlo generator NNLOjet. We present an overview of important features included in the code which are used in the calculations presented in this thesis.

In Section 4.2 we review Monte Carlo techniques and detail our implementation of Vegas and in Section 4.3 the construction of the VBF phase space generator in the NNLOjet framework. Both the numerical integrator and the phase space generator have an important effect on the numerical efficiency of the computation of scattering rates. Finally, in Section 4.4 we list and detail all tests included in the NNLOjet framework and their application to the VBF NNLO calculation. We argue that such an extensive collection of validation checks should become a standard requirement for higher order calculations published in the literature.

4.1 NNLOjet

All calculations in this thesis, unless stated otherwise, have been made with the software NNLOJET, the product of an extensive collaboration between different groups around the world [80]. NNLOJET is a fixed order parton-level event generator for inclusive or jet processes at higher orders in QCD, primarily using the antenna subtraction method for the subtraction of the IR divergences. It provides a standard framework for the calculation of scattering processes as well as analysis and histograming tools for producing single and multi differential distributions.

Section 4.1.1 presents a technical description of the NNLOJET code and Section 4.1.2 lists the most relevant features for the work presented in this thesis while Section 4.1.3 describes the necessary steps and prerequisites for the implementation of new processes in the NNLOJET codebase.

At the time of writing, the processes available in NNLOJET at NNLO accuracy include: Higgs production in association with one jet [51, 74, 81–83], Higgs production in association with two jets in VBF [1], vector boson plus jet production [84–88], di-jet production in hadron-hadron collisions [89, 90] and in lepton-hadron collisions [91–93] and three-jet production in e^+e^- annihilation [94]. Recently, a combined implementation of the antenna subtraction method and the Projection to Born method [95] has also been included in the NNLOJET framework, presenting the first N3LO differential results for single jet production in hadron-lepton deep inelastic scattering [96].

4.1.1 Technical description

At the core of NNLOJET is the Monte Carlo algorithm Vegas, first presented in Ref. [97]. We have implemented our own version of the algorithm in order to take advantage of the technological advances in computing since the publication of [98], specifically CPU parallelisation and grid computing. We detail our implementation of Vegas and discuss some of its advantages in Section 4.2.3.

The majority of the NNLOJET codebase is written in Fortran and is compatible with the Fortran 95 standard [99] and thus compilable with all modern versions of the compiler `gfortran` included in the GNU Compiler Collection [100] as well as the Intel Fortran Compiler commonly known as `ifort` [101].

Our version of the Vegas algorithm uses the methods and subroutines specificed in the version 4.0 of the OpenMP Standard [102] for CPU parallelisation. This standard was first implemented in version 4.9.1 of `gfortran` and version 15.0 of `ifort`, which are necessary in order to use the parallelisation capabilities of NNLOJET. Note that NNLOJET can be compiled with no OpenMP support with the compiler flag `useomp=False` for backwards compatibility.

NNLOJET can also be interfaced to external tools such as FastJet [103] or APPLGRID [104] and requires LHAPDF version 6 [76]. Tools have been built around the NNLOJET framework which are not exclusive to this code and can be generalised to other applications. Two examples are the Vegas implementation for grid computing detailed in Section 4.2.3 and the pyHepGrid tool documented in Appendix D.

Accompanying the NNLOJET code is a suite of autogeneration routines written in the symbolic manipulation software FORM [105] and the mathematical software Maple [106] which provide a way of writing pseudocode and standardise most of the Fortran codebase. The usage of these autogeneration tools allows us to propagate any changes to the entire codebase in a fully systematic and automatic way. Autogeneration and standardisation of the code is also crucial for testing and validation when looking for bugs or adding new features. This will be further explored in Section 4.4.

4.1.2 Features

Numerical stability and technical cuts

Subtraction methods require numerical cancellation of soft and collinear singularities in real emission configurations at integration time. This leads to a sum of two large* equal numbers with opposite sign that cancel to 0. Since computer memory is a finite resource not all digits of a number are significant.† When all significant numbers cancel out, the leftover are just random numbers. It is thus more appropriate to set a technical cut from which we assume cancellation before the two numbers actually reach infinity (without performing the sum). Schematically, we apply the Heaviside step function Θ to the calculation, such that:

$$\sigma = \int \Theta\left(y - y_0\right) \mathrm{d}\sigma \,, \tag{4.1}$$

where $y = \min(\frac{s_{ij}}{\hat{s}})$ for any i, j and $s_{ij} = (p_i + p_j)^2$.

The technical cut y_0 is an unphysical parameter and there must be no dependence of the cross section on it as $y_0 \to 0$. Values below $y_0 = 10^{-7}$ are often found to be a good compromise between convergence and y_0 independence. The independence of the integration result on the technical cut is a crucial check on the validity of the subtraction term and will be discussed and tested in Section 4.4.4.

The step function is implemented at the level of the phase space generator, before the evaluation of the matrix element is performed; if for a phase space point any invariant is found with a value y below the cut y_0, then the event is discarded.

Even with the use of a technical cut the stochastic nature of Monte Carlo integration can introduce "jokers", events that produce awkward numbers orders of magnitude greater. This can be problematic as their addition to any other number effectively means losing all significant figures below a certain (computer precision dependent) threshold.

The core NNLOjet code implements the summation technique known as Kahan

*Infinite, in the singular limit

†Only the 15 first in double precision arithmetics.

summation [107] in order to minimise the effect of numerical instabilities introduced by floating point arithmetics. The effect of "jokers" is also minimised by softening the peaks of the integration through the techniques detailed in Sections 4.2.3 and 4.3.

Statistical treatment of results

For a large enough number of events, the results from individual runs of the program are distributed around the true value of the cross section (σ) following a Gaussian distribution:

$$\bar{\sigma} = \frac{\sum \sigma_i s_i^{-2}}{\sum s_i^{-2}} \qquad \bar{s}^2 = \frac{1}{\sum s^{-2}} \tag{4.2}$$

where σ_i are the individual cross section computed by independent NNLOjet iterations and s_i is the associated statistical error.

However, the number of events per iteration N is often kept small in order reduce the integration time which allows for a more efficient parallelisation of the code. As a consequence independent iterations are not necessarily statistically compatible. This is particularly true for higher dimensional phase spaces where errors are larger for a given number of events. One solution to this problem is to combine k iterations into one pseudorun with:

$$\sigma^{\text{pseudo}} = \frac{1}{k}\sum_i^k \sigma^i \qquad s^2 = \frac{1}{kN}\left(\frac{1}{kN}\sum^{k,N}\sigma_i^2 - \left(\frac{1}{k}\sum^k \sigma^i\right)\right) \tag{4.3}$$

which is equivalent to one iteration of $k \times N$ events.

The value of k depends on both the process considered and the integration parameters so a scan over different values of k is in general required. The stop point for the scan occurs when independent pseudoruns become statistically compatible.

A python code is included alongside NNLOjet which implements these statistical techniques in a consistent way for NNLOjet calculations and the production of histograms [108].

4.1.3 Code autogeneration

One of the key features of NNLOjet is the autogeneration the process dependent Fortran code. With a large library of processes and of their associated matrix elements and subtraction terms, making the code both maintainable and easily extensible is a highly non-trivial task. The NNLOjet code can be divided between "core software", shared between all processes, and process dependent code, mainly autogenerated by Maple and FORM routines.

The NNLOjet core software includes the integration algorithm, analysis routines and the whole set of antennae, integrated and unintegrated, necessary for the computation, up to NNLO in QCD, of scattering rates at hadron colliders assuming massless quarks.

On the other hand, the implementation of new processes into the NNLOjet framework can be divided into three main steps:

- Calculation and code implementation of the matrix elements.
- Construction of the subtraction terms as pseudocode in Maple scripting language.
- Addition of the new process to the driver.

Implementation of the matrix elements

The NNLOjet framework exposes a derived type `Kin`. The `Kin` type contains arrays providing spinors, momenta and invariants for all particles of the system as generated by the phase space generator. The indices of the `Kin` array are the labels of the particles where 1 and 2 are always the initial particles.

The matrix element should then be a Fortran compatible function taking as input the labels of the particles as `integer` values and returning a `double precision` type with the value of the square of the amplitude. This step is completely manual and is left to the developer, although currently an effort to interface NNLOjet with external matrix element providers such as OpenLoops [109] is underway.

Construction of the subtraction terms

The implementation of the subtraction terms for NNLO calculation can be a very involved task for complex processes. The number of possible singular configurations, combined with parton orderings, phase space mappings and colour levels introduces a level of complexity that would make coding the subtraction terms a very complicated and bug-prone task were it to be done manually.

The subtraction terms are written as pseudocode and only in terms of the antenna functions and reduced matrix elements. The Maple autogeneration scripts are able to take this pseudocode as input and output Fortran code which includes the required calls to the antenna functions and performs the mapping to the reduced momentum set required by the matrix elements.

For virtual corrections, a preprocessing step using a set of FORM routines precedes the creation of the Fortran file. The FORM code ensures all explicit $\frac{1}{\epsilon}$ poles cancel by comparing the subtraction terms with the Catani structure for infrared poles.

Adding new processes to the library

Once matrix elements are provided following the notation in Section 3.3.1, a new maple generation card needs to be created in the `driver/maple` directory. This `.map` card includes process dependent parameters such as the particles to be considered for each matrix element and colour level, the number of flavours or the LO prefactor as well as identification of the different layers (LO, R, V ...) and the corresponding matrix elements. The generation card for the VBF process is given in Appendix A.

A set of maple scripts will then generate, using the `.map` file as input, all Fortran routines necessary to integrate the process. Crucially, it will generate all calls to the Parton Distribution Functions (PDFs) for the different partonic initial state configurations that enter the process as well as for all possible combinations of the ordering of the final states.

Afterwards, the python script `autoAddFortran.py` will register (or update if it

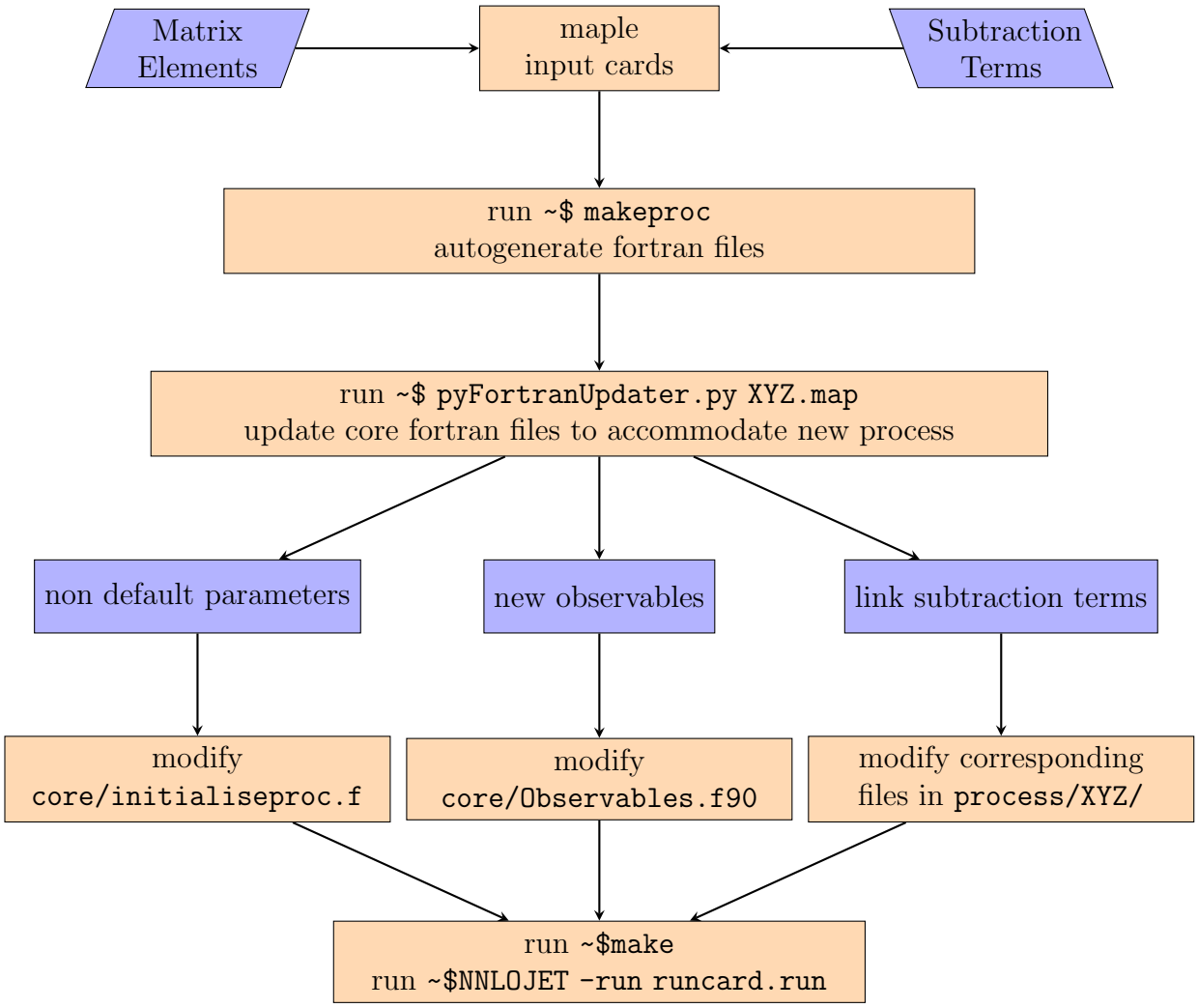

Figure 4.1: Flow chart for the implementation of new processes in NNLOjet.

already exists) the new process into the NNLOJET core code. This script ensures that all files are available for compilation and initialises all subtraction term calls. At this stage only the linking of the subtraction terms is left to the user. By default all subtraction terms are initialised to 0. The user must set each of the subtraction terms for each of the matrix elements to the correct Fortran functions autogenerated from the Maple pseudocode. A schematic workflow for the implementation of a new process in NNLOJET is depicted in Fig. 4.1.

Non-default initialisation parameters and analysis routines can also be used by modifying the appropriate files. We list here some of the modules where default parameters can often be a suboptimal choice:

- `initialiseproc.f`: After following implementation as in Fig. 4.1 a working default template for the initialisation of the process will be already included in this file which in general needs to be modified. The modifications required include the number of jets of the Born process and initialisation of common blocks.

- `Observables.f90`: The definitions of all observables that NNLOJET can compute are found in the Observables module. In this file a number of observables which are automatically registered for all processes are declared, for instance observables referring to jets kinematics. The addition of new observables, be they generic or process specific, is also done in this module, where the user has access to the same `Kin` object accessible by the matrix elements.

- `genphase.f` and `sig.f`: NNLOJET includes default phase space generators for different topologies of processes. Selecting the phase space generator to be used by the new process is done in these files.

4.2 Numerical integration

Monte Carlo integration methods are particularly well suited for phase space integration in high energy physics applications as they offer several advantages with respect to other methods:

- The first and main advantage of Monte Carlo algorithm is that the error decreases as $\sqrt{\frac{1}{N}}$ regardless of the dimensionality of the integral, where N is the number of events or Monte Carlo shots. This is crucial for phase space integration in multiparticle collisions as it implies a high dimensionality integral.

- In contrast to other integration methods, the integrand is not required to be analytic or continuous. If the volume of integration Φ_d has a particularly difficult shape, the Monte Carlo solution to this issue is to integrate over a larger volume V_d fully containing Φ_d and set the integrand to 0 for any points that happens to fall outside Φ_d.

- The evaluation of the integral of a function f via Monte Carlo methods requires evaluating f for many different points in the integration space. These points can be used not only to estimate the integral of f over Φ_d but also to simultaneously fill in differential histograms $\frac{\mathrm{d}f(x)}{\mathrm{d}\mathcal{O}(x)}$.

- Due to the stochastic nature of the method, events are treated in a similar way as they appear in actual particle collisions. In this sense colliders like the LHC are, essentially, a very expensive Monte Carlo integrator.

4.2.1 Monte Carlo methods

The underlying problem is the numerical calculation of a multidimensional integral for which we do not know the analytical form:

$$I^t = \int \mathrm{d}^m x \, f(\vec{x}), \tag{4.4}$$

where $\vec{x} = \{x_i\}, x_i \in [0,1]$ and I^t is the "true" result of the integral.

The integration algorithm must provide, in a finite amount of time, an estimation I of Eq. (4.4) as well as an estimation of the error with respect to the true value I^t. The Monte Carlo estimate for Eq. (4.4) is obtained by evaluating the function $f(\vec{x})$ for N random points uniformly distributed in the region of integration $V = [0,1]^d$. Let us define the Monte Carlo estimator of the integral as:

$$I = \frac{1}{N}\sum_{i=1}^{N} f(\vec{x}_i) = \langle f \rangle. \tag{4.5}$$

The estimated error with respect to the true value (I^t) is given by the variance* which we denote by s^2 and which is given by:

$$s^2 = \frac{1}{N}\left(\frac{1}{N}\sum_{i=1}^{N} f(\vec{x}_i)^2 - I^2\right), \tag{4.6}$$

where it is clear that the Monte Carlo error is reduced as $\frac{1}{\sqrt{N}}$, independently of the number of dimensions.

We write the Monte Carlo estimation of a function f over N points distributed over the unit volume as:

$$I = \int \mathrm{d}^m x\, f(\vec{x}) \approx \langle f \rangle \pm \sqrt{\frac{\langle f^2 \rangle - \langle f \rangle^2}{N}}. \tag{4.7}$$

Note that a reduction of the error of $\frac{1}{\sqrt{N}}$ is relatively slow, specially when compared to other integration methods. For comparison, the error using the extended Simpson's rule scale as $\frac{1}{N^{4/d}}$, i.e., it converges faster than Monte Carlo for any $d < 8$. In other words, only when the number of dimensions is large do Monte Carlo methods become competitive in terms of convergence. The next section will introduce importance sampling as way of reducing the Monte Carlo error by appropriate changes of variables.

*Often the Greek letter σ is used for the variance. We use s here instead to avoid any confusion with the cross section.

4.2.2 Importance sampling

Instead of uniformly distributing N random points with which we sample the integrand, we can generate points according to a probability density function $\rho(\vec{x})$ which is positive for all $\vec{x}$ and normalised to unity:

$$\int \mathrm{d}^m x\, \rho(\vec{x}) = 1. \tag{4.8}$$

When sampling over $\rho(\vec{x})$, I becomes:

$$I = \int \rho(\vec{x})\, \mathrm{d}^m x\, \frac{f(\vec{x})}{\rho(\vec{x})} \approx \left\langle \frac{f}{\rho} \right\rangle \pm \sqrt{\frac{\langle f^2/\rho^2\rangle - \langle f/\rho\rangle^2}{N}}, \tag{4.9}$$

and our goal is to find a function $\rho(\vec{x})$ that minimises the variance s^2 of the estimator

$$s^2 = \int \mathrm{d}^m x\, \rho(\vec{x}) \left(\frac{f(\vec{x})}{\rho(\vec{x})}\right)^2 - \left(\int \mathrm{d}^m x\, \rho(\vec{x}) \frac{f(\vec{x})}{\rho(\vec{x})}\right)^2. \tag{4.10}$$

Intuitively, any $\rho(\vec{x}) \propto f(\vec{x})$ will result in a reduction of the minimal value of s. We minimise the variance Eq. (4.10) using the method of Lagrange multipliers which allow us to ensure the solution still fulfils Eq. (4.8) through the multiplier λ. In the following we set $\rho(\vec{x}) \equiv \rho$, $f(\vec{x}) \equiv f$ and $\vec{x} \equiv x$ for brevity.

$$\begin{aligned}\frac{\delta s}{\delta \rho} &= \frac{\delta}{\delta \rho}\left(\int \rho\, \mathrm{d}x\, \frac{f^2}{\rho^2} + \left(\int \rho\, \mathrm{d}x\, \frac{f}{\rho}\right)^2 + \lambda\left(\int \mathrm{d}x\, \rho - 1\right)\right) \\ &= \int \mathrm{d}x \left(\frac{-f^2}{\rho^2} + \lambda\right) = 0,\end{aligned} \tag{4.11}$$

from which we can set:

$$\rho = \frac{|f|}{\int \mathrm{d}x\, |f|}. \tag{4.12}$$

The optimal choice of $\rho(\vec{x})$ is proportional to $f(\vec{x})$ but requires knowledge of the value of the integral of $|f(\vec{x})|$ which we lack prior to integration. We can circumvent this limitation through the use of adaptive Monte Carlo techniques which iteratively build a distribution function $\rho(\vec{x})$ able to capture the general features of the integrated function. One example of an adaptive Monte Carlo algorithm is Vegas, which

we consider here.

4.2.3 NNLOjet Vegas implementation

The Vegas algorithm has been part of the toolkit of the wider physics community since its inception by Lepage [97] in 1977. The original implementation was written in Fortran [98] and primarily based on the concept of importance sampling. Newer versions of the algorithm have been published in multiple languages* as well as modified versions [110, 111] aiming to provide improvements for specific applications.

We have implemented a modified version of the algorithm as presented in Ref. [110] using the random number generator proposed by Marsaglia and Zaman [112, 113] and extended with extra features which we briefly describe at the end of this section.

Let us first review the Vegas algorithm by considering a separable probability density distribution $\rho(\vec{x})$. If we are in a m-dimensional volume where $\vec{x} = (x_1, x_2, \ldots, x_m)$, separability allows us to write:

$$\rho(\vec{x}) = \prod^{m} \rho_i(x_i). \tag{4.13}$$

For the rest of this description we consider a one-dimensional probability density function $\rho(x)$. This is akin to how the algorithm is implemented, where each dimension is treated separately.

The algorithm breaks the integration region $x \in [x^-, x^+]$ into k subdivisions of different sizes Δx_i. Random points are then generated according to a stepwise distribution function:

$$\rho(x) = \frac{1}{k\Delta x_i} \qquad \text{for } x \in [x_{i-1}, x_i], \tag{4.14}$$

with $x_0 = x^-$, $x_i = x_{i-1} + \Delta x_{i-1}$, and $x_k = x^+$. An estimation of the integral is then computed within each of these subdivisions which are not changed until the iteration (meaning, obtaining one estimation for a number N of points) is completed.

*See for instance https://github.com/gplepage/vegas

The transformation between the random uniformly generated points (noted $z \in (0,1)$) and the distribution Eq. (4.14) is given by:

$$x(z = \frac{i}{k}) = x_i, \tag{4.15}$$

where $i = 1, \ldots, k$ are the edges of the Δx_i grid. For $z \neq \frac{i}{k}$ the value of x is obtained by a linear interpolation between the x_i. The Jacobian of this transformation is then

$$J\left(\frac{i-1}{k} < z < \frac{i}{k}\right) = k\Delta x_i = J_i. \tag{4.16}$$

We can rewrite now the Monte Carlo estimator of the integral and the variance as a sum over the Vegas subregions Δx_i:

$$I = \sum_{i=1}^{k} I_i = \sum_{i=1}^{k} J_i \int_{x_{i-1}}^{x_i} \mathrm{d}x\, f(x) \tag{4.17}$$

$$s^2 = \frac{1}{N}\left(\sum_{i=1}^{k} J_i \int_{x_{i-1}}^{x_i} \mathrm{d}x\, f^2(x) - I^2\right), \tag{4.18}$$

where the variance is minimised when, for any i, the following condition is fulfilled:

$$J_i \int_{x_{i-1}}^{x_i} \mathrm{d}x\, f^2(x) = \text{const.} \tag{4.19}$$

At the end of every iteration the increments Δx_i are reshaped aiming for the product $\Delta x_i \int_{x_{i-1}}^{x_i} \mathrm{d}x\, f^2(x)$ to remain constant for any i. The net effect is to produce bigger increments where the integrand $f(x)$ is smaller, and smaller increments where the integrand is bigger. The outcome is better resolution (smaller errors) in the regions that contribute the most to the integral.

Programmatically this is achieved by defining a reweighing variable r_w for each subdivision such that:

$$r_w^i = \left(\left(1 - \frac{\langle f_i^2\rangle}{\sum_j \langle f_j^2\rangle}\right)\left(\log\left(\sum_j \langle f_j^2\rangle\right) - \log\big(\langle f_i^2\rangle\big)\right)^{-1}\right)^{\alpha}, \tag{4.20}$$

where α is a damping parameter in order to avoid rapid and destabilising changes between iterations. Note that with $\alpha = 0$ the grid is frozen as all weights are the

Input: Vector $\langle f_i^2 \rangle$, previous Δx_i
Result: Reweighed increments Δx_i
for $i \in (1, k)$ **do**
  Compute the reweighting vector r_w^i as per Eq. (4.20) ;
end
Compute the total of the vector r_w as an auxiliary variable $t = \frac{1}{k} \sum r_w^i$;
Set $j = 0$, $dr = 0$;
for $i \in (1, k)$ **do**
  while $t > dr$ **do**
    $j = j + 1$;
    $dr = dr + r_w^j$;
  end
  $dr = dr - t$;
  Compute the new value of $\Delta x_i = x_i - (x_i - x_{x-1}) \frac{dr}{r_w^j}$;
end

Algorithm 1: Bin refining algorithm in the NNLOJET Vegas implementation.

same. The technical details of the implementation of the reshaping of the grid are given in Algorithm 1.

In Fig. 4.2 we integrate the LO cross section for the VBF process with a simple cut of $p_t^j > 25$ GeV for ten iterations with a value $k = 25$ and $\alpha = 1.5$. We choose two of the random variables: x_6 and x_9.

The x_6 variable (at the top) is mapped to the invariant mass of the system formed by one of the partons and the Higgs mass. The mapping between the invariant and the variable is not direct so the physical meaning is obscured but we can see that regions in which x_6 takes maximal values (either close to 0 or close to 1) are preferred, the increments in these regions are smaller. The x_9 variable, on the other hand, is directly mapped to the momentum fraction of the incoming partons. A very clear physical meaning can be deduced in this case: very low values of the momentum fraction (the phase space points don't pass the selection cuts) and very high values (suppressed by the PDFs) contribute very little to the total cross section and thus the increments Δx_i in this regions are much larger. Note that for this example by the fifth iteration the grid is stabilised and the increments Δx_i remain of the same size.

Integrating the total cross section with Vegas effectively means adapting to the

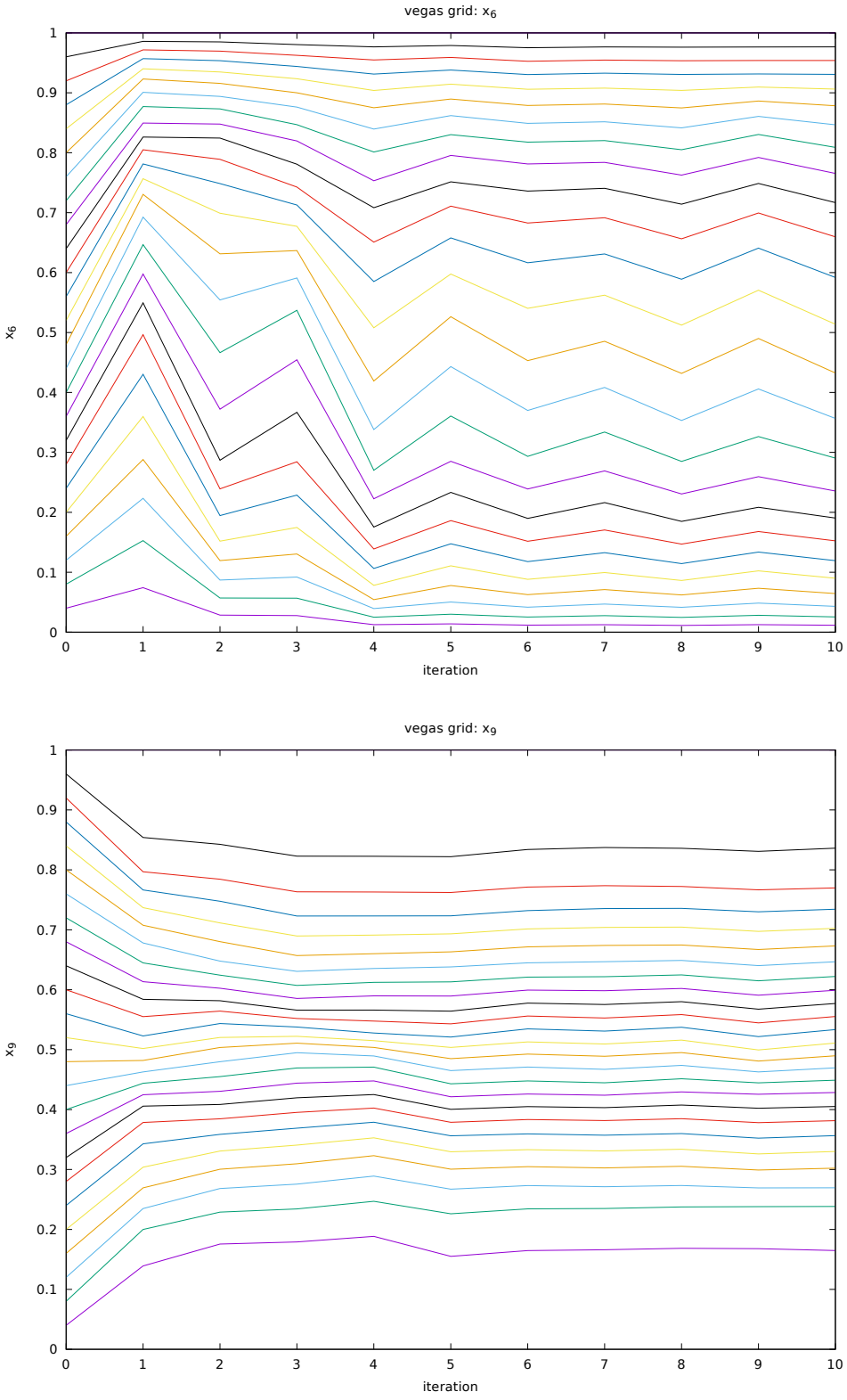

Figure 4.2: Example of the evolution of the subdivisions generated by Vegas for two of the random variables. The coloured lines correspond to the edges of the Δx_i grid.

shape of the total cross section as a function of the Vegas variables. However this is often not the optimal approach as we might be interested in regions of the phase space which might not greatly contribute to the cross section but are phenomenologically relevant in differential distributions for particular observables.

Our solution is to distort the Δx_i grid by multiplying the integrand f by a reweighting function which depends on the relevant kinematics. In this way we can artificially give more weight to regions of integration with little contribution to the cross section. The reweighting function is a free parameter in the NNLOJET runcard in the form of a polynomial of any observables.

4.2.4 Parallel computing and benchmarking

It is often useful to separate a Vegas integration into two phases: warmup and production. During the warmup phase we construct a grid that adapts to the shape of the integral without storing any results and during the production phase we freeze the grid and generate the desired output. Breaking down the integration in these two phases allows for a number of optimisations to be carried over and to exclude statistical distortions from unoptimised grids.

During the **production** phase, we are only interested on generating final output from as many statistically independent iterations as possible, using the same grid. The number of points (N) required in order to produce statistically sound results, however, might be too large for a computer to handle in one go*. Thanks to the techniques introduced in Section 4.1.2 we can break an N-point iteration into k sub-iterations of N/k points which will afterwards be fused into one pseudorun.

Due to the fact that no information needs to be shared between different production iterations, we are able to run multiple replicas of NNLOJET on different CPUs, machines or clusters and combine the results afterwards. In that respect, the production phase is a solved issue where getting more precise results and histograms simply requires consuming more resources. The technicalities of running

*The main limitation being the 48 hours "wall time" restriction of the Dirac system [114].

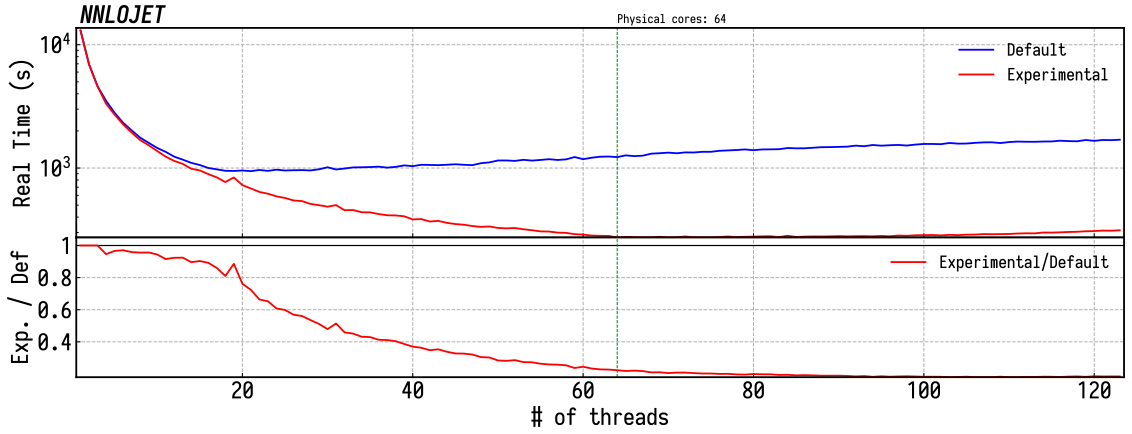

Figure 4.3: Study of the performance evolution of Vegas as a function of the number of threads for a VBF Real integration with minimal cuts. Default corresponds to the typical implementation of Vegas based on OpenMP. Experimental removes some restriction on the capacity of OpenMP for parallelisation. Tested in Intel(R) Xeon(R) Gold G6130, 64 physical cores.

production in a grid system are further detailed in the documentation of pyHepGrid in Appendix D.

The **warmup** phase, on the other hand, introduces some restrictions with respect to the production phase, most notably, each iteration needs information on the previous one in order to adapt the grid: they need to share memory. Several solutions to the problem of multithreaded programming exist. As a first step we implement the OpenMP standard so that the main task of the event generator is shared between a given number of threads. The number of threads to be used can be selected by the user through the environmental flag `OMP_NUM_THREADS`, each one reserving `OMP_STACKSIZE` Mb of memory. At the end of each warmup iteration all threads are synchronised and the adaptation of the grid is performed using the total combined set of information.

In Fig. 4.3 we study the performance gain when using OpenMP for a warmup run. We compare the real time (this is, human time between the start and end of the process) of a naive implementation of the OpenMP standard with a more aggressive implementation (still experimental) which requires some changes to the NNLOJET code. The naive implementation is akin to the implementation found in extensively used programs such as MCFM [115].

It can be seen that for the default (naive) implementation the performance gain saturates after a certain number of threads, beyond 16 threads almost no gain is observed and the performance is actually punished after ~ 25 cores are used. For the experimental implementation, on the other hand, we observe gains for any number of CPUs and we find a penalty only when we are using almost twice as many threads as physical cores the machine has. Once we enable as many threads as physical cores the machine has, we enter in the hyperthreading region. In this region the performance gain is much more modest (even negative when too many threads are active and the program competes with the operative system for resources).

The difference between the default and experimental implementations of Vegas is mainly due to the use of "critical" blocks, regions of code that are forced to run sequentially. The "experimental" implementation bypasses all these blocks of sequential code for a better threads-performance relation. The only trade-off for the experimental implementation of Vegas with respect to the default one is a greater memory usage of a $\sim +10\%$ in the benchmarks. NNLOJET can be compiled with these experimental features with the use of the compile flag `critical=off`.

Another drawback of OpenMP is that parallelisation is limited to one single memory-sharing node or CPU. For processes with many particles in the final state, this is often insufficient to warm up a grid to stability in a reasonable amount of time. As in the production phase, we would ideally be able to run our warmup across different independent nodes, synchronising the results at the end of every iteration before the grid is adapted.

Since the adaptation process only requires the knowledge of the value of the integral in each subvolume *after the iteration finishes*, it follows that we only need a way to share this information (an array of numbers) at the end of every iteration between different NNLOJET instances in order to use multiple nodes and speed up

runtime.*

In the Vegas implementation of NNLOJET, we share the information between the independent instances using tcp sockets. At the end of every iteration all separate instances of NNLOJET pause and synchronise information with a central server by data transfer through tcp sockets. We use standard unix libraries so the only requirement is for the target system to have a network connection able to communicate with the central server. This solution allows us to parallelise NNLOJET within a single node (via OpenMP) and among independent resources at the same time and the usage of unix standard libraries guarantees that does work in any target system.

NNLOJET is compiled with socket support with the use of the compile flag `sockets=true`.

4.3 Phase space generator

The partonic cross section is a function of the particle momenta such that we can in general write (for n particles in the final state) as seen in Eq. (1.38) where we defined the integration variable $\mathrm{d}\Phi_n$ representing the phase space for n particles in the final state,

$$\mathrm{d}\Phi_n = \prod_{i=1}^{n} \left(\frac{\mathrm{d}^3 p_i}{2E_i (2\pi)^3} \right) (2\pi)^4 \delta^4 \left(p_{ini} - \sum p_i \right). \tag{4.21}$$

In other words, the computation of rates of scattering processes requires the integration of the differential cross section over the final state phase space of the particles involved. The limits of the integration (neglecting selection cuts) are such that all physically possible configurations are to be considered: i.e., the whole phase space volume is covered.

In order to integrate the cross section we use the Monte Carlo method introduced

*There are several libraries in the market addressing the problem of sharing information over a network between resources with no shared memory, one of the best known solutions being MPI. For our purposes, however, the MPI protocol is often not the best solution since it requires a number of tools and libraries to be installed in all systems and is more disruptive to the codebase.

in Section 4.2.3 to sample random phase space points. The integration algorithm itself, however, only provides random numbers $x_i \in (0,1)$ with no physical meaning. We need to map the set of random points ($\{x_i\}$) to a set of momenta ($\{p_i\}$) to evaluate the cross section, a transformation $\rho(\vec{x}) \to \Phi(\{p_i\})$.

In practice, this phase space generator is an independent layer outside Vegas and takes a vector of numbers $\vec{x}$ of dimension $d = 4n-3$, returning an array of $(n+2)$ four-vectors $\{p_i\}$. This transformation corresponds to a mapping of the integration variables x_i to the physical quantities that define the kinematics of the event. The usual choice is the set of invariants $s_{ij} = (p_i + p_j)^2$.

The mapping $\{x_i\} \to \{p_i\}$ is, in principle, fully arbitrary besides trivial constraints such as covering the whole integration range or being momentum and energy-conserving. We take advantage of this arbitrariness in order to improve the integration efficiency by mapping the Vegas random numbers to relevant quantities of the scattering system. The goal is to soften the peaks of the integration which results in a much better Vegas adaptation and a reduction of the appearance of jokers.

In Section 4.3.1 we first study a naive phase space generator which does not take into account the topology of the VBF process. This phase space generator has, however, the advantage of being completely general for hadron collisions and serves as a stepping stone to introduce the fundamental ingredients for the construction of a much more complex phase space generator. Subsequently we study a phase space generator optimised for the VBF integration, adapted to the kinematics of the system and forcing singular invariants to be integration variables through the use of wedges.

The introduction of phase space wedges is also necessary for the required rotations for the pointwise subtraction of the antenna formalism. We conclude this section with a validation of the VBF phase space studying the integration of dummy matrix elements with a calculable analytical solution.

4.3.1 Naive phase space

As a first approximation, and ignoring any issues related to the initial state particles, we can start by generating an isotropic phase space where we populate the phase space homogeneously from the random vector input from Vegas. A well known algorithm implementing this approach is known as RAMBO [116] (RAndom Momenta Beautifully Organised).

In a VBF-type process, however, there exists a clear hierarchy between the particles involved in the collision which is not represented by such a democratic phase space.

Furthermore, at high orders in perturbation theory, singularities of the form $\frac{1}{s_{ij}}$ or $\frac{1}{s_{ijk}}$ appear (see Section 2.2) in the matrix elements. The adaptation of the phase space to the singular structure of the process smooths the peaks of the integration, greatly improving the stability of the calculation.

Taking into account the decay of the Higgs boson, the Vector Boson Fusion Higgs boson production process is a $2 \to 4(6)$ particles process at LO QCD (2/4 of which are particles coming from the decay of the Higgs boson and do not effect the singular structure of the process). The highest multiplicity phase space is found at the double real level, with two extra emissions it can be up to a $2 \to 8$ particles phase space. Our default configuration is the decay of the Higgs boson to two photons.

Iterative sequential phase space

Let us consider a state of mass $\hat{s}$ from which we detach, one by one, all particles participating in the collision using as integration variables the invariants $s_{ijk\ldots}$ of the subsequent states plus the solid angle that defines the motion of the detached particle (Ω). This is depicted in Fig. 4.4 where we split the entire body of the phase space into a series of factorising two body phase spaces such that, if 1 to 6 are the final partons, we perform a sequential splitting: $(123456) \to 1 + (23456) \to 1 + 2 + (3456) \to \cdots \to 1 + 2 + 3 + 4 + 5 + 6$.

The phase space generator of Fig. 4.4 treats all particles equally. It is however

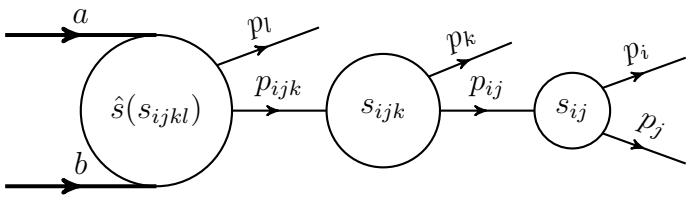

Figure 4.4: Schematic view of a sequential phase space generator.

useful to separate the phase space into partons, the only particles involving singular limits, and colourless particles (in this case the Higgs boson). This minimally modified version of the sequential generator is implemented in NNLOJET and shown in Fig. 4.5. It does not have a limit on the number of particles in the final state, which allows for quick testing of new processes before building a more optimal phase space for the specific application at hand.

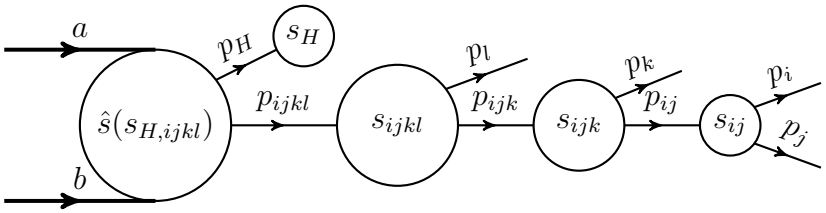

Figure 4.5: Sequential phase space generator with a detachment of a colourless state represented by s_H.

$\mathbf{1 \to 2}$

The basic ingredient of the phase space generator is the $1 \to 2$ reaction $a \to 1 + 2$ where the kinematics of the incoming particle p_a are fully known:

$$\Phi_2 = \int \frac{\mathrm{d}^4 p_1}{(2\pi)^4} \frac{\mathrm{d}^4 p_2}{(2\pi)^4} (2\pi)\delta(p_1^2 - m_1^2)(2\pi)\delta(p_2^2 - m_2^2)(2\pi)^4 \delta^4(p_a - p_1 - p_2), \quad (4.22)$$

where the δ functions enforce momentum conservation and on-shell external particles. We can make use of the δ functions in order to simplify the formula giving:

$$\Phi_2 = \frac{1}{4\pi^2} \int \frac{\mathrm{d}^3 p_1}{2E_1} \delta((p_a - p_1)^2 - m_2^2). \quad (4.23)$$

Working in the center of mass frame of the decaying particle p_a we can write $p_a = (\sqrt{s}, \vec{0})$ and the remaining δ function of Eq. (4.23) can promptly be rewritten as:

$$\delta((p_a - p_1)^2 - m_2^2) = \frac{1}{2\sqrt{s}}\delta\left(E_1 - \frac{1}{2\sqrt{s}}(s + m_1^2 - m_2^2)\right). \tag{4.24}$$

Recalling the relation between the energy and the momentum: $E^2 = m^2 + |\vec{p}|^2$ it is possible to also extract the value of $|\vec{p}|$ from Eq. (4.24):

$$\begin{aligned} |\vec{p}_1|^2 =& \frac{1}{4s}(s^2 + m_1^2 + m_2^2 - 2sm_1^2 - 2sm_2^2 - 2m_1^2 m_2^2) \\ =& \frac{1}{4s}\lambda(s, m_1^2, m_2^2) \qquad (4.25) \\ |\vec{p}_1| =& \frac{1}{2\sqrt{s}}\lambda^{1/2}(s, m_1^2, m_2^2) = |\vec{p}_2|, \qquad (4.26) \end{aligned}$$

where we have defined the function $\lambda^{1/2}$ which will be appearing in several occasions during phase space calculations. Note that the value of $|\vec{p}|$ depends only on the invariants of the system.

We are now ready to write the final form of the phase space for a $1 \to 2$ particles system:

$$\Phi_2 = \frac{\lambda^{1/2}(s, m_1^2, m_2^2)}{32\pi^2 s}\int \mathrm{d}\Omega \tag{4.27}$$

It is possible to factorise any n-particle phase space into a series of sequential $1 \to 2$ phase spaces where the incoming particle is one of the outgoing members of the previous step.

This technique allow us to build a completely general phase space such as Fig. 4.4 or Fig. 4.5 by iteratively applying Eq. (4.27) and the following equality:

$$1 = \int \frac{\mathrm{d}^3 p_{12}}{2E_{12}}\,\mathrm{d}s\,\delta^4(p_{12} - p_1 - p_2) \tag{4.28}$$

which introduces the dependence on the invariant mass of the decaying particle ($p_{12} = p_a$). Each of these $1 \to 2$ systems have then three free variables which in our implementation are chosen to be the invariant mass of the system ($\mathrm{d}s = \mathrm{d}s_{12}$) and

the solid angle $\mathrm{d}\cos(\theta)\,\mathrm{d}\phi$.

The Vegas sampling is then mapped onto these integration variables through a change of variables which for Fig. 4.5 take the following form:

$$\begin{aligned} s(x) &= s^{min} + x(s^{max} - s^{min}), \\ \phi(x) &= 0 + x(2\pi - 0), \\ \cos\theta &= -1 + x(1 - (-1)), \end{aligned} \tag{4.29}$$

where each x is a random number generated by Vegas.

$2 \to 2$

The first step in the generators of Fig. 4.4 and Fig. 4.5 is slightly different as it corresponds to a $2 \to 2$ system in which the initial state is known. The final state, however, is no different from the $1 \to 2$ system previously studied:

$$\Phi_2 = \int \frac{\mathrm{d}^4 p_1}{(2\pi)^3} \frac{\mathrm{d}^4 p_2}{(2\pi)^3} \delta(p_1^2 - m_1^2)\delta(p_2^2 - m_2^2)(2\pi)^4 \delta^4(p_{\mathrm{ini}} - p_1 - p_2), \tag{4.30}$$

where $p_{\mathrm{ini}} = p_a + p_b$. We work in the center of mass system of p_{ini}, with $\vec{p}_a = -\vec{p}_b$ and $(p_a + p_b)^2 = s$.

As in the previous section, only two variables are necessary in order to describe the system. We can choose, for instance, the scattering angle of one of the outgoing particles with respect to one of the incoming particles in the center of mass system (θ) as well as the azimuthal angle around the beam (ϕ). However, rotational symmetry around the beam axis allows us to integrate out the azimuthal variable ϕ, reducing the number of variables to 1.

Description on invariants

A crucial step when building a phase space generator is the correct choice of sampling variables as this can have a large impact on the stability and convergence of the

integral. Typically we want to sample invariants mapping directly to the topology of the system. For example, in a $2 \to 2$ situation, the three Mandelstam invariants define the whole system:

$$\begin{aligned} s &= (p_a + p_b)^2, \\ t &= (p_a - p_1)^2, \\ u &= (p_a - p_2)^2, \end{aligned} \tag{4.31}$$

which are related through $s+t+u = \sum_i^{a,\ldots,2} m_i^2$. Since the value of s (i.e., the incoming energy) and the outgoing masses are known, only one independent variable is left.

We can choose, for instance, the variable $t = t_{a1}$ as one of the sampling variables,

$$\begin{aligned} t_{a1} &= (p_a - p_1)^2 \\ &= m_a^2 + m_1^2 - 2E_aE_1 + 2p_ap_1\cos\theta_{a1}, \end{aligned} \tag{4.32}$$

where the integration limits are given by the values $\cos\left(\theta_{a1}^{\pm}\right) = \pm 1$. We can rewrite Eq. (4.32) in terms of the invariants of the system using Eq. (4.26), which gives the limits of integration $t_{a1}^{\pm}$ as:

$$\begin{aligned} t_{a1}^{\pm} = m_a^2 + m_1^2 - \frac{1}{2s}\Big\{&(s + m_a^2 + m_b^2)(s + m_1^2 + m_2^2) \\ &\mp \lambda^{1/2}(s, m_a^2, m_b^2)\lambda^{1/2}(s, m_1^2, m_2^2)\Big\} \end{aligned} \tag{4.33}$$

In a VBF type collision the t_{a1} variable represents the energy carried by the scattered gauge bosons and can take any value between t_{a1}^+ and t_{a1}^-. The mappings of Eq. (4.29) are, however, a suboptimal way of sampling t_{a1}. We know the VBF topology favour smaller energy transfers (closer to t_{a1}^+, as $t_{a1} < 0$), so we can write instead:

$$t_{a1} = t_{a1}^- \left(\frac{t_{a1}^+}{t_{a1}^-}\right)^x, \tag{4.34}$$

where x is again a Vegas random number.

The change of Eq. (4.34) favours regions of the phase space in which t_{a1} is smaller.

The outcome is a better resolution on the most important regions of the phase space while still covering the entire integration range.

Ahead of the derivation of the $2 \to 3$ phase space generator it will prove useful to derive the integration limits for t_{a1} (Eq. (4.33)) in terms of Gram determinants,

$$\Delta_n = |p_1 \wedge p_2 \wedge \ldots \wedge p_n|^2. \tag{4.35}$$

The Gram determinant offers the advantage that they correspond to the λ and G functions [117, 118] which are defined in terms of the invariants of the system. For a three particles phase space we have,

$$\Delta_2(p_a, p_b) = -\frac{1}{4}\lambda(s, m_a^2, m_b^2), \tag{4.36}$$

while for a four particles phase space we find the 3-particle Gram determinant,

$$\Delta_3(p_a, p_b, p_1) = -\frac{1}{4}G(s, t, m_2^2, m_a^2, m_b^2, m_1^2). \tag{4.37}$$

In both equations $s = (p_a + p_b)^2$, $t = (p_a - p_1)^2 = (p_b - p_2)^2$ and $m_i^2 = p_i^2$. A useful formulation for the four particles kinematic function G is,

$$G(x, y, z, u, v, w) = x\left[\left(y - u - w + \frac{1}{2x}(x + u - v)\right)^2 - \frac{1}{4x^2}\lambda(x, u, v)\lambda(x, w, z)\right]. \tag{4.38}$$

The Gram determinant of the system is related to the limits on t_{a1} through the angle θ_{a1}.

$$\sin^2\theta_{a1} = \frac{1}{s p_a p_1}\Delta_3(p_a, p_b, p_1), \tag{4.39}$$

where we transform the condition $\cos(\theta_{a1}) = \pm 1$ into $\sin^2(\theta_{a1}) \geq 0$. Rewriting Eq. (4.39) exclusively in terms of invariants we obtain:

$$\sin^2\theta_{a1} = -4s\frac{G(s, t, m_2^2, m_a^2, m_b^2, m_1^2)}{\lambda(s, m_a^2, m_b^2)\lambda(s, m_1^2, m_2^2)}, \tag{4.40}$$

where the functions $\lambda \geq 0$. The condition $\sin^2\theta_{a1} \geq 0$ is then equivalent to:

$$G(s, t, m_2^2, m_a^2, m_b^2, m_1^2) \leq 0. \tag{4.41}$$

The use of Gram determinants allows us, by changing any argument by a linear combination of them, to select the most appropriate integration variables for each scenario.

4.3.2 The VBF phase space

The VBF process is a $2 \to 3$ process at the Born level, where the most important variables to consider are the invariants between the particles that form each of the currents.

The Higgs boson and its decay products do not participate on any singular limit, and their phase space can be safely factored out into $1 \to X$ phase space where the decaying Higgs boson is the dashed red line in Fig. 4.6.

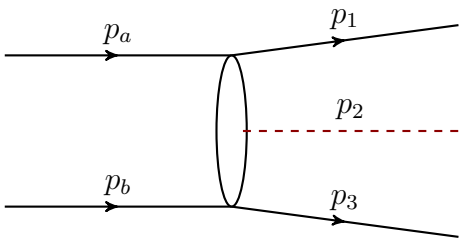

Figure 4.6: Schematic representation of the Born level VBF phase space.

Higher order corrections arise in two distinct configurations at NNLO as partons can be radiated from each current:

- Adjacent: two radiated partons from only one of the currents.
- Non-adjacent: one radiated parton from each of the current.

These two situations are factored out as a $1 \to 3$ phase space (adjacent) or two $1 \to 2$ phase spaces (non-adjacent) with two different phase space generators.

$2 \to 3$

The starting point for the VBF phase space is a completely general two to three phase space $\mathrm{d}\Phi_3$:

$$\Phi_3 = \int \frac{\mathrm{d}^3 p_1}{(2\pi)^3 2E_1} \frac{\mathrm{d}^3 p_2}{(2\pi)^3 2E_2} \frac{\mathrm{d}^3 p_3}{(2\pi)^3 2E_3} (2\pi)^4 \delta^4 \left(p_{ini} - \sum_i^3 p_i \right), \tag{4.42}$$

where we find 5 degrees of freedom which can once again be reduced to four by applying rotational symmetry about the beam axis.

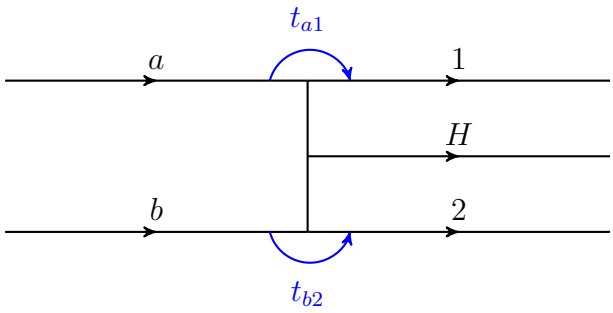

Figure 4.7: 2 to 3 phase space for a VBF-like topology.

In a VBF-type collision, situations in which the outgoing particles 1 and 2 carry a large fraction of the incoming energy are preferred. To improve our results in these configurations we artificially drive the integrator towards these regions so that they are preferentially chosen, which reduces their relative weights and improves stability. It also allows Vegas to perform a finer and more efficient adaptation to this region. The two relevant variables for this are the momentum transfers t_{a1} and t_{b2} in blue in Fig. 4.7.

For a description in four invariants we also include in our description s_{1H} and s_{2H} (or, equivalently, the angles between the Higgs boson and outgoing partons 1 and 2). With the appropriate change of variables the integral becomes

$$\Phi_3 = \frac{1}{16\lambda^{1/2}(\hat{s}, s_a, s_b)} \int \frac{\mathrm{d}t_{1a}\, \mathrm{d}t_{2b}\, \mathrm{d}s_{1H}\, \mathrm{d}s_{2H}}{(-\Delta_4)^{1/2}}, \tag{4.43}$$

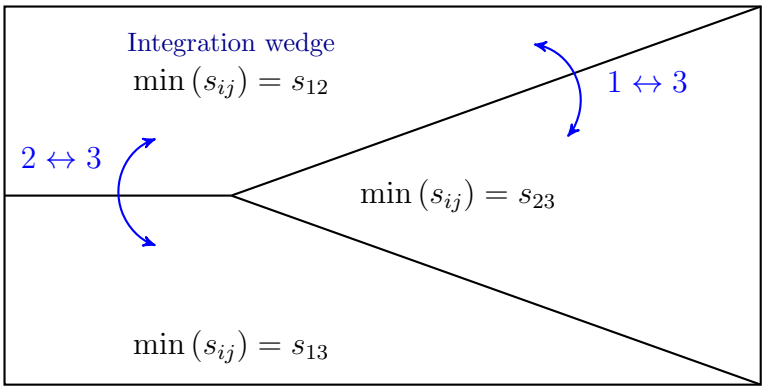

Figure 4.8: Example of phase space divided in three regions through a condition on s_{ij}. If the integration wedge corresponds to the phase space point $(1,2,3) \rightarrow \{p_1, p_2, p_3\}$ then full coverage is restored through the permutations $(1,2,3) \rightarrow (1,3,2)$ and $(1,2,3) \rightarrow (3,2,1)$. Note that $s_{ij} = s_{ji}$.

where Δ_4 is the Gram determinant of any four independent vectors in the space of p_a, p_b, p_1, p_2, p_H. We set the physical integration region for the four chosen variables through the condition $\Delta_4 \in \mathbb{R} < 0$, which can be expanded in terms of the 4-particle kinematic functions [117].

An optimal choice of variables not only improves stability by reducing the relative weight of the most ill-behaved terms of the matrix element in the integrand, it also plays an important role in the adaptation of Vegas and the cancellation of singularities via antenna subtraction. In the next section we study the particularities of the higher order VBF phase spaces and introduce the concept of wedges.

4.3.3 Wedges

For configurations including more than two partons in the final state it is necessary to introduce the concept of phase space wedges: regions of the phase space to which we restrict the integration.

We supplement our phase space generator with a system of wedges so that any phase space point we generate is restricted to a defined region. Appropriate permutations of the final states restore the full coverage of the phase space. This is depicted schematically in Fig. 4.8.

Each phase space point is then evaluated once per wedge, effectively multiplying

the number of Vegas shots by the number of wedges. Since we restrict the integration region to just one of the wedges at a time we also allow a much better Vegas adaptation of the grid, which improves the efficiency of the numerical integration.

Beyond numerical improvements, the system of wedges is required for the full cancellation of singularities in antenna subtraction. By restricting particular singularities to certain wedges and invariants, we can perform the required azimuthal rotations to achieve pointwise cancellation (see Section 2.3.1) in a systematic and consistent way. The implementation details are further explored in Section 4.3.4.

$2 \to 4$

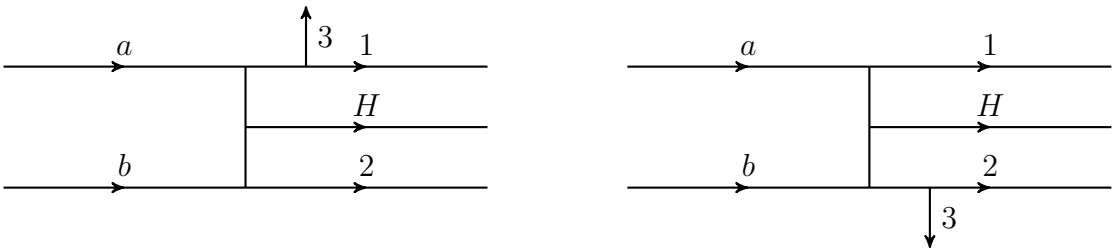

Figure 4.9: Possible $2 \to 4$ phase space configurations for a VBF-like topology

The R and RV layers both correspond to configurations with three jets in the final state. Here, two symmetric configurations are possible: one extra particle radiated from the $(a, 1)$ line or from the $(b, 2)$ line as depicted in Fig. 4.9. We can exploit this symmetry to improve the efficiency of the integration. Only one of the two configurations needs to be allowed in the integration wedge, covering the full phase space after swapping a and b. We also apply a hierarchy criteria so that in the integration wedge any singularity would always be generated in the current that radiates parton 3.

The integration region is chosen by the following stepwise function:

$$\Theta_4 = \begin{cases} 1 & \text{if} \quad s_{\min} = s_{ij} \quad \text{and} \quad s_{aij} < s_{bij}, \\ 1 & \text{if} \quad s_{\min} = s_{ai} \quad \text{and} \quad s_{ij} < s_{2i}, \\ 0 & \quad \text{otherwise}, \end{cases} \tag{4.44}$$

where $\{i, j\} = \{1, 3\}$. We cover the entire phase space with the permutations $(a \leftrightarrow b)$ and the three cyclic permutations of the final partons $(1, 2, 3)$.

$2 \to 5$

At the double real level we find two extra emissions with respect to the Born level. These possess the same symmetry as the $2 \to 4$ scenario with respect to being radiated from the $(a, 1)$ or $(b, 2)$ lines. However we also find two very distinct configurations which need to be considered separately from both programmatic and theoretical points of view. These two configurations are shown in Fig. 4.10.

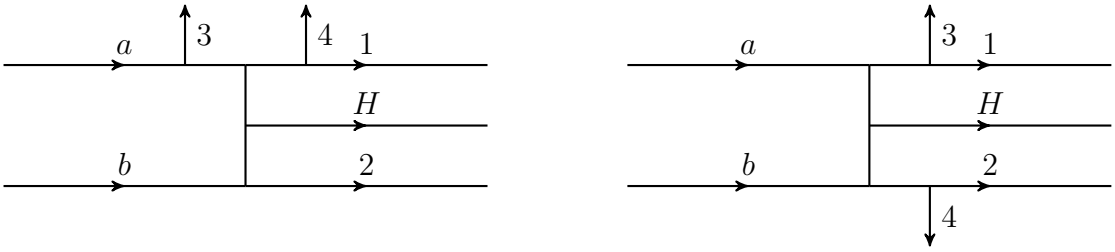

Figure 4.10: Possible 2 to 5 phase space configurations for a VBF-like process. The two configuration correspond to different singularity structures.

These two configurations correspond to the topologies in which 2 particles are emitted from the same line (left), adjacent to each other, so they can generate singularities by going collinear, and the topology in which each extra radiation is emitted from one line (right), non adjacent particles, where the only possible collinear singularities are situations in which the two emitted particles cannot go collinear with each other.

These two configurations are not only separated by a wedge selection as it was the case with the different configurations of Fig. 4.9, but also by the factorisation order of the phase space. In the first scenario (which we dub region A, shown in Fig. 4.11) we factorise a $1 \to 2 \to 3$ phase space onto one of the outgoing particles of the $2 \to 3$ core phase space. In the second scenario (region B, shown in Fig. 4.12) we factorise a $1 \to 2$ phase space onto each of the outgoing partonic lines.

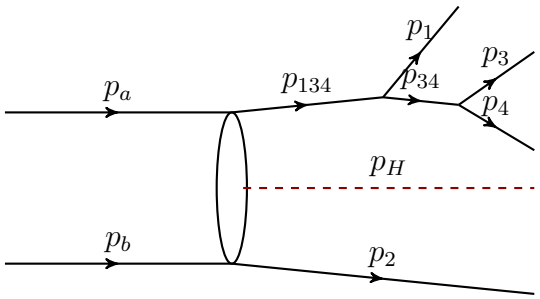

Figure 4.11: Schematic representation of the VBF phase space, region A.

Our choice of wedges for region A is as follows:

$$\Theta_{5A} = \begin{cases} 1 & \text{if} \quad s_{\min 1} = s_{34} \quad \text{and} \quad s_{\min 2} \in \{s_{13}, s_{14}\} \quad \text{and} \quad s_{a134} < s_{b134} \\ 1 & \text{if} \quad s_{\min 1}, s_{\min 2} \in \{s_{a3}, s_{a4}, s_{34}\} \quad \text{and} \quad s_{a1} < s_{a2} \\ 0 & \text{otherwise} \end{cases} \tag{4.45}$$

In order to cover the entire phase space, permutations are required over the initial partons a and b, particle 1 with (2,3,4) and, for each choice of particle 1, particle 2 with (3,4). The total number of permutations generated by region A is $N = 24$.

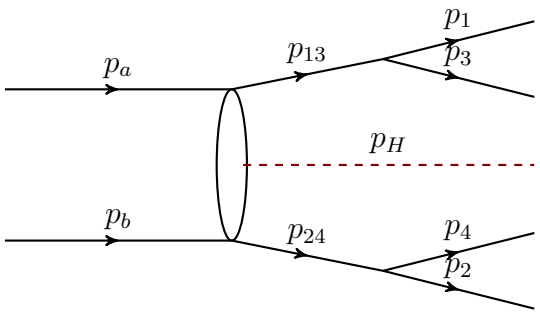

Figure 4.12: Schematic representation of the VBF phase space, region B.

In region B both the 1 and 2 lines are promoted to massive states, becoming the 13 and 24 lines respectively in Fig. 4.12. These two massive states each represent a $1 \to 2$ independent phase space.

The choice of wedges for region B reads as

$$\Theta_{5B} = \begin{cases} 1 \quad \text{if} \quad s_{\min 1} = s_{ik} \quad \text{and} \quad s_{\min 2} = s_{jl} \quad \text{and} \quad s_{ai} + s_{ak} < s_{bi} + s_{bk} \\ 1 \quad \text{if} \quad s_{\min 1} = s_{jl} \quad \text{and} \quad s_{\min 2} = s_{ik} \quad \text{and} \quad s_{bj} + s_{bl} < s_{aj} + s_{al} \\ 1 \quad \text{if} \quad s_{\min 1} = s_{ai} \quad \text{and} \quad s_{\min 2} = s_{bj} \quad \text{and} \quad s_{ik} < s_{il} \\ 1 \quad \text{if} \quad s_{\min 1} = s_{bj} \quad \text{and} \quad s_{\min 2} = s_{ai} \quad \text{and} \quad s_{jl} < s_{jk} \\ 0 \qquad \text{otherwise} \end{cases} \tag{4.46}$$

for all possible choices of $\{i, j, k, l\}$ such that i and k are the particles related to the initial parton a through t_{a1} in the 2→3 phase space (see Section 4.3.2) and likewise particles j and l are related to initial parton b through t_{b2}. i.e., $\{i, k\} = \{1, 3\}$ and $\{j, l\} = \{2, 4\}$.

The full phase space is covered after permutations of initial partons a and b and parton 3 with 2 and 4. The total number of permutations for region B is $N = 6$.

4.3.4 Rotations

As explained in Section 2.3.1, the subtraction of some collinear limits is only achieved after a rotation about the axis of the particles going collinear is performed to cancel azimuthal correlations.

In a democratic phase space generator, such as RAMBO, the Jacobian of the transformation $\{\vec{x}\} \to \{p_i\}$ is a constant: all points have the same weight. We can thus systematically rotate the system about the smallest invariant achieving perfect pointwise cancellation in all limits. Since all phase space points have the same weight, any new rotated point is guaranteed to be fully equivalent to any other rotation. In our VBF phase space generator, however, the phase space point obtained after rotation is not guaranteed to have the same weight or even fall within the same wedge. It is thus necessary to restrict rotations to situations which leave both weight and wedge invariant.

The wedge system is a powerful tool to discriminate between singularities of

the system. For instance, for $2 \to 5$ configurations, region A captures all triple limits while region B captures single and double collinear limits stemming from the splitting of a gluon into two quarks. Furthermore, it also defines which invariants are involved in the singularity in the integration wedge.

In order to guarantee the rotation does not affect the weight of the phase space (i.e., that the original point and its rotated counterpart are equivalent) we force the rotation to be performed through one of the integration variables, using the transformation:

$$\phi' = \phi + \frac{\pi}{2} \qquad\qquad \mathrm{d}\phi' = \mathrm{d}\phi\,. \tag{4.47}$$

Let us consider first the $(a, 13)$ line of region B (Fig. 4.12). In this line we can encounter the following collinear singularities: $a||1$, $1||3$, $3||a$ so we need to rotate about $\vec{p}_{a1}$, $\vec{p}_{13}$ and $\vec{p}_{a3}$.

The rotation about $\vec{p}_{13}$ is trivial, as the $p_{13} \to p_1 + p_3$ is the last step in the phase space generation and the angle ϕ_{1z} in the center of mass system of p_{13} is one of the integration variables: the transformation of Eq. (4.47) only affects p_1 and p_3 and the weight is clearly constant.

The rotations about the $\vec{p}_{a1}$ or $\vec{p}_{a3}$ are much more involved however, as any transformation requires that $\vec{p}_a$ remains in the beam line. As rotations are only required for the collinear limits (in this case $a||1$ or $3||a$) we can instead rotate the system about the $\vec{p}_a$ axis, which is equivalent to the $\vec{p}_{a1}$ or $\vec{p}_{a3}$ axes in the singular limit. In order to make the angle ϕ_{a1} an integration variable we boost the $\vec{p}_a$ to the center of mass frame of the $\vec{p}_{13}$ system and require it to lie in the z axis. This ensures $\phi_{z1} = \phi_{a'1}$ and we can then perform the rotation. We note this rotation $(1, 3; a)$, a rotation of the 13 system about axis a.

When rotations are active in a NNLOJET run, 4 points are generated per phase space, each with a relative weight of $\frac{1}{4}$. For region B of the $2 \to 5$ VBF phase space this means we generate the following sets: unrotated, $(1, 3; a)$, $(2, 4; b)$ and

$(1,3;a)+(2,4;b)$.

In the integration wedge of region A singularities only arise in the $(a,134)$ line. We follow the same strategy as in region B and boost the initial momenta $\vec{p}_a$ to the $1 \to 2$ system corresponding to the decay $p_{134} \to p_1 + p_{34}$ such that it lies on the z axis. This rotation captures all relevant singularities between initial and final partons. We further rotate the system about the $\vec{p}_{34}$ axis in order to capture singularities between the two final partons, this rotation is trivial and can be done directly on the ϕ_{3z} variable. The final output of region A of the phase space consists of: unrotated, $(1,34;a)$, $(3,4;34)$ and $(1,34;a)+(3,4;34')$.

4.3.5 Comparison between the naive sequential and VBF phase space generators

With the implementation of two different phase space generators in NNLOJET capable of integrating the VBF process, a useful exercise is a comparison in order to establish the differences in terms of efficiency and numerical stability.

In order to keep the integration time manageable while still accessing some features of the divergences, we integrate the real phase space for VBF + 2j with representative cuts. This is a $2 \to 5$ particle phase space (three partons and two photons) with six different wedges.

In Fig. 4.13 we show the number of Monte Carlo shots (i.e., events generated by Vegas) and CPU time required to achieve a given degree of accuracy (measured as the error relative to the total cross section). From these figures it is clear the VBF phase space offers a demonstrable advantage in terms of calculation efficiency. Note that the difference in the number of MC shots required is much bigger than the difference in CPU time due to the fact that the VBF phase space uses each shot six times (one per wedge), while the naive phase space only uses them once. Naively one would assume that only one in every six points goes through the wedge cuts, which would be true for iterations with an uniform non-adaptive grid. However, as the grid adapts, the Vegas random points are biased towards the non-0 wedge.

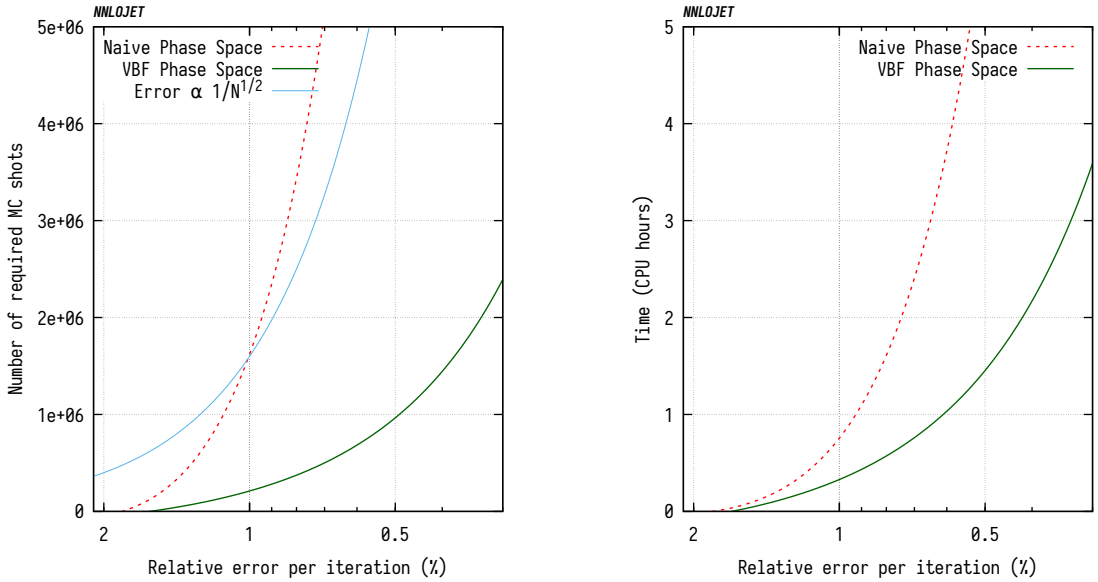

Figure 4.13: Comparison between a sequential phase space of Fig. 4.5 (naive, dashed red) and our optimised VBF phase space (VBF, green) showing the necessary number of Monte Carlo shots (left) and the corresponding integration time (right) to reach similar levels of precision. In blue we include the expected Monte Carlo relation between the error and the number of shots, we observe the sequential phase space to have a slightly worse than $\frac{1}{\sqrt{N}}$ growth while the VBF phase space improves in the expected MC error.

4.3.6 Phase space validation

We can perform multiple tests on the phase space routines in order to check the full coverage of the phase space as well as technical cut implementation. This can be done by independently integrating several different dummy matrix elements squared:

- $M = 1$, where after integration we expect to retrieve the phase space volume. This is a well-defined test also used as a nightly regression test for NNLOJET.
- $M = \frac{1}{\sqrt{s_{ij}}}$, which checks that all different permutations of i and j give the same result. We can also check its compatibility with the analytic result. $s_{ij}^{1/2}$ introduces a non-trivial dependence on the phase space variables with respect to $M = 1$.
- $M = \frac{1}{s_{ij}}$. This integration is divergent so it is necessary to regulate it through the introduction of a technical cut y_0 on the limits of integration, which allows us to test that the phase space presents the correct y_0 behaviour.

Unit phase space

We begin with the simplest scenario, $M = 1$. For a center of mass energy s, the volume of an n-particle phase space is given by

$$V_n = \frac{1}{2(4\pi)^{2n-3}} \frac{s^{\frac{2n-4}{2}}}{\Gamma(n)\Gamma(n-1)}, \tag{4.48}$$

where all particles are assumed to be massless.

In Table 4.1 we compare the analytical value (V_n) for different final state multiplicities with the results obtained with the sequential and VBF implementations of the phase space generators. For completeness, we also compare the results where possible with the Higgs plus jet phase space generator also implemented in NNLOJET. We find all results to be compatible.

n	V_n	NNLOJET H ps	NNLOJET seq ps	NNLOJET VBF ps	Units
4	5.44627	5.4458 ± 0.0006	5.44628 ± 0.00003	5.44625 ± 0.00002	10^8 GeV^4
5	1.83940	1.8389 ± 0.0006	1.83941 ± 0.00014	1.8391 ± 0.0004	10^{13} GeV^6
6	3.72742	NA	3.7274 ± 0.0004	3.7281 ± 0.0006	10^{17} GeV^8

Table 4.1: Values for the unit phase space for $\sqrt{s} = 8$ TeV. In this comparison no selection cuts are imposed and the PDFs are assumed to be identically one for any initial state.

Dummy matrix elements: general formulae

The phase space volume for a dummy matrix element of the form $M = \frac{1}{\sqrt{s_{ij}}}$, where i and j are both final state particles is given by

$$V_n = \frac{1}{2(4\pi)^{2n-3}} s^{\frac{2n-5}{2}} \prod_{i=3}^{n} \frac{4}{(2n-3)(2n-5)}. \tag{4.49}$$

For the case in which either i or j are one of the initial states the result is

$$V_n = \frac{1}{(4\pi)^{2n-3}} s^{\frac{2n-5}{2}} \left(\frac{2}{3}\right)^{n-3} \frac{a_n}{5}, \tag{4.50}$$

with $a_4 = 1$ and $a_5 = a_6 = \frac{1}{7}$.

For a dummy matrix element of the form $M = \frac{1}{s_{ij}}$ the integration is divergent. In order to control these divergences we introduce a dependence on a technical cut

y_0 such that the ration $\frac{s_{ij}}{s}$ is always greater than y_0 for any i, j.

For final state i and j, the y_0 dependent volume is:

$$V_n = \frac{1}{2(4\pi)^{2n-3}} \frac{s^{\frac{2n-6}{2}}}{\Gamma(n-2)\Gamma(n-1)} \left(\log\left(\frac{1}{y_0}\right) - a_n + \mathcal{O}\left(y_0 \log(y_0)\right) \right), \tag{4.51}$$

with $a_4 = \frac{5}{2}$, $a_5 = \frac{10}{3}$, $a_6 = \frac{47}{12}$.

On the other hand, when either i or j are in the initial state, we find:

$$V_n = \frac{1}{2(4\pi)^{2n-3}} \frac{s^{\frac{2n-6}{2}}}{\Gamma(n-1)^2} \left(\log\left(\frac{1}{y_0}\right) - a_n + \mathcal{O}\left(y_0 \log(y_0)\right) \right), \tag{4.52}$$

with $a_4 = \frac{3}{2}$, $a_5 = \frac{11}{6}$, $a_6 = \frac{25}{12}$.

The importance of the test for y_0 technical cut dependence is not only to find a result compatible with V_n but also to test the evolution of the result for different values of y_0.

VBF Born level, n=4

Since, by default, we consider the decay of the Higgs boson to two photons, the Born level configuration for the VBF phase space is a $2 \to 4$ process. In the results of this section we use the NNLOJET notation for parton ordering: particles 1 and 2 are the two incoming partons and the last two partons (5 and 6 for $n = 4$) are the two photons.

i, j final [GeV^3]		i initial, j final [GeV^3]	
s_{34}	290440 ±35	s_{13}	217847 ±24
s_{35}	290391 ±81	s_{14}	217842 ±11
s_{45}	290363 ±49	s_{23}	217840 ±11
s_{36}	290498 ±88	s_{24}	217837 ±11
s_{46}	290488 ±65		
Analytic result:	290467.879382523	Analytic result:	217850.909536892

Table 4.2: NNLOJET values for the VBF phase space volume for $n = 4$ with different combinations of $s_{ij}^{-1/2}$ for $\sqrt{s} = 8$ TeV, no selection cuts imposed and PDFs are assumed to be identically one for any initial state.

In Table 4.2 we show the value of the NNLOJET VBF phase space volumes for the integration of a $\frac{1}{\sqrt{s_{ij}}}$ dummy matrix element for different choices of i, j. We find

good agreement in all cases with the analytic result.

At the Born level there are no singularities in the actual matrix element. However, by introducing $M = \frac{1}{s_{ij}}$ we can force a singularity to occur. We integrate the phase space for a range of values of the technical cut y_0 and compare them to the theoretical values from Eq. (4.51) and Eq. (4.52). This is shown graphically in Fig. 4.14 and Fig. 4.15 for two final and one initial one final states respectively.

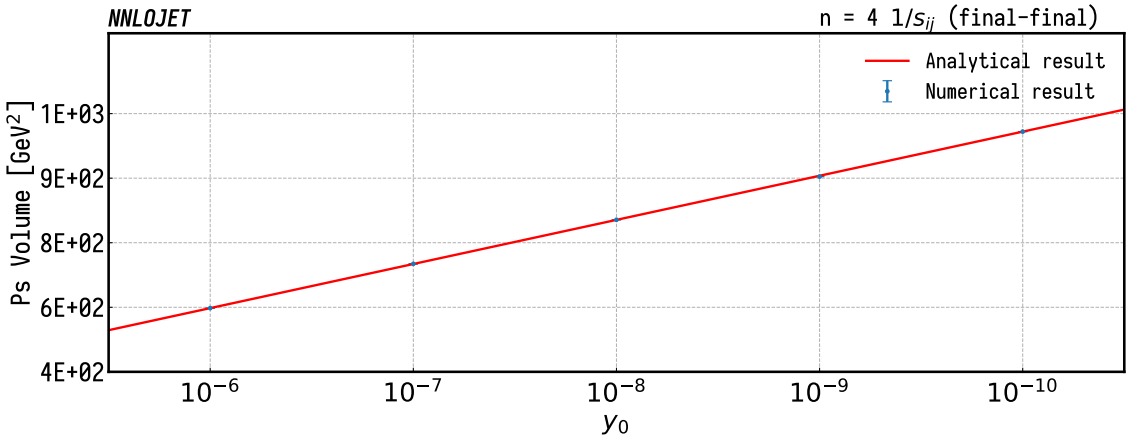

Figure 4.14: Study of the y_0 behaviour for $M = \frac{1}{s_{ij}}$ with i and j both f.s. particles, $\sqrt{s} = 8$ TeV.

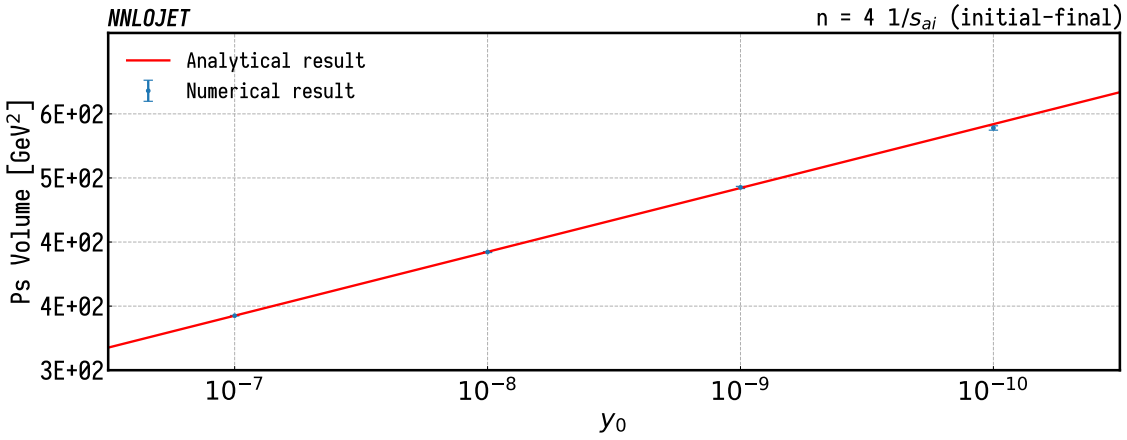

Figure 4.15: Study of the y_0 behaviour for $M = \frac{1}{s_{aj}}$ with a i.s. parton and j f.s. particle, $\sqrt{s} = 8$ TeV.

In Fig. 4.14 we also plot the results for the NNLOJET implementation of the ggF Higgs plus two jets phase space for a more complete test. Numerical results are shown in Table 4.3.

$(y_0 = 10^{-x})$	Theoretical	ggF H ps [GeV^2]	VFH ps [GeV^2]
6	577.7564	577.5 ±0.4	576.74 ±0.08
7	695.3237	695.1 ±0.6	695.8 ±0.7
8	812.8909	812.4 ±0.7	813.14 ±0.14
9	930.4582	929.9 ±0.8	928.3 ±0.14
10	1048.025	1047. ±1	1048.10 ±0.16

Table 4.3: Comparison of the phase space volume for $\frac{1}{s_{ij}}$ for different values of y_0 between the ggF H+2jets phase space and the VBF phase space for a center of mass energy $\sqrt{s} = 8$ TeV, no selection cuts imposed and PDFs are assumed to be identically one for any initial state.

One real emission, $n = 5$

i, j final [10^{10}GeV^5]		i initial, j final [10^9GeV^5]	
s_{34}	1.3455 ±0.0002	s_{13}	8.4081 ±0.0007
s_{35}	1.3455 ±0.0002	s_{14}	8.4081 ±0.0007
s_{45}	1.3455 ±0.0002	s_{15}	8.4081 ±0.0007
		s_{16}	8.4078 ±0.0010
An. result:	1.3453951954	An. result:	8.40872838546

Table 4.4: Values for the phase space volume for $n = 5$ for different combinations of $s_{ij}^{-1/2}$ for $\sqrt{s} = 8$ TeV, no selection cuts imposed and PDFs are assumed to be identically one for any initial state.

In Table 4.4 we show results for $\frac{1}{\sqrt{s_{ij}}}$ with different combinations of the i, j particles. In this case we consider only partons (particles 3,4,5) in the final state. As the wedge selection function is symmetric on 3, 4 and 5, the results are completely interchangeable, as expected. This effect is seen both in the initial state and the final state. When one of the photons is considered (particle 6) the result is no longer exactly equal but still compatible within errors.

We expect to find similar features when checking the technical cut dependence of a $\frac{1}{s_{ij}}$ dummy matrix element. In Table 4.5 the numerical results for the integration of $\frac{1}{s_{ij}}$ for a fixed value of y_0 for final-final and initial-final configurations are shown. We find results to be equal as we take different combinations of the final partons.

The evolution for a fixed invariant for a variable y_0 value is shown in Fig. 4.16 for a choice of final states i, j. In Fig. 4.17 the same study is performed, where we find a slight deviation from the theoretical result at very low y_0. This is due

to the fact that the analytic integration is performed by setting the limits of the integration of the s_{ij} invariant dependent of the technical cut whereas NNLOJET forces the smallest invariant to be able to pass the technical cut. For situations in which either i or j is an initial state, s_{ij} is not necessarily the smallest invariant for every phase space point.

i, j final $[10^7\text{GeV}^4]$		i initial, j final $[10^7\text{GeV}^4]$	
s_{34}	4.409 ±0.005	s_{13}	1.645 ±0.003
s_{35}	4.409 ±0.005	s_{14}	1.645 ±0.003
s_{45}	4.409 ±0.005	s_{25}	1.645 ±0.003
An. result:	4.40932709	An. result:	1.64222032

Table 4.5: Values for the phase space volume for $n = 5$ for different combinations of s_{ij}^{-1} for $\sqrt{s} = 8$ TeV and $y_0 = 10^{-7}$, no selection cuts imposed and PDFs are assumed to be identically one for any initial state.

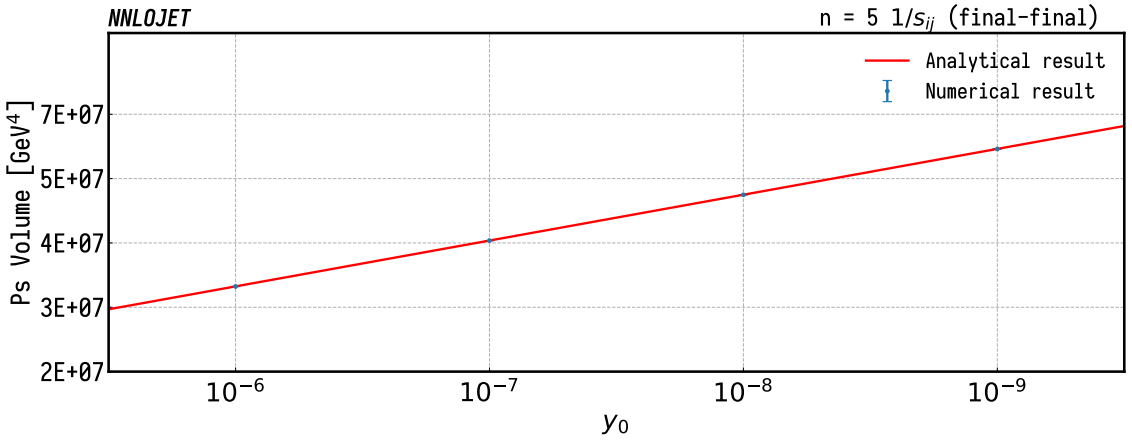

Figure 4.16: Study of the y_0 behaviour for $M = \frac{1}{s_{ij}}$ with i and j both f.s. particles, $\sqrt{s} = 8$ TeV.

Two real emissions, $n = 6$

With two extra emissions in the final state ($n = 6$, four partons and two photons) we need to integrate two separate regions of the phase space in order to achieve full coverage of the integration region.

Due to the system of wedges and permutations, we again expect all configurations to be equivalent in the A region but not in the B region where there is only (3,6) and (4,5) symmetry.

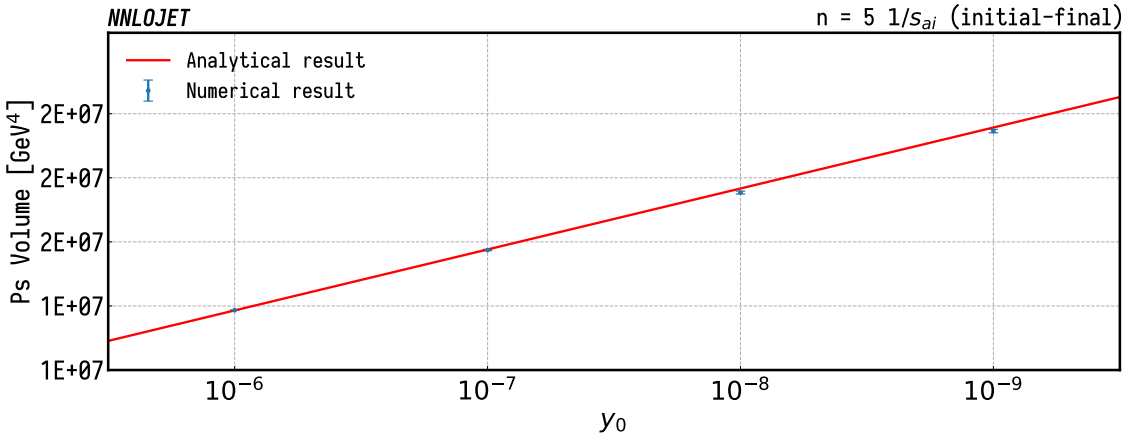

Figure 4.17: Study of the y_0 behaviour for $M = \frac{1}{s_{aj}}$ with a i.s. parton and j f.s. particle, $\sqrt{s} = 8$ TeV.

invariant	A region [10^{14}GeV^7]	B region [10^{14}GeV^7]	Total result [10^{14}GeV^7]
s_{34}	2.60164±0.00046	0.86074±0.00025	3.4624±0.0006
s_{35}	2.60164±0.00046	0.86067±0.00026	3.4623±0.0006
s_{45}	2.60164±0.00046	0.86082±0.00026	3.4625±0.0006
s_{36}	2.60164±0.00046	0.86082±0.00026	3.4625±0.0006
s_{46}	2.60164±0.00046	0.86059±0.00025	3.4622±0.0006
Analytic result: 3.46202336687517			

Table 4.6: Values for the different combinations of $s_{ij}^{-1/2}$ with i, j final particles for $\sqrt{s} = 8$ TeV, no selection cuts imposed and PDFs are assumed to be identically one for any initial state.

In Fig. 4.18 we show the evolution with y_0 for the integration of $\frac{1}{s_{ij}}$ for a choice of the final-final invariant. In Table 4.8 numerical values for different choices of i, j final and initial are shown. For similar CPU time, the convergence of the initial-final $\frac{1}{s_{ij}}$ matrix element is much slower than in the situation in which both particles i and j are chosen to be final state partons, this can be observed in Fig. 4.19 where the statistical errors for $y_0 < 10^{-6}$ are considerably bigger. We also see the feature first observed in $n = 5$ where there is a slight deviation in the initial-final phase space with respect to the analytical result due to extra cuts in invariants in the numerical computation.

invariant	A region [10^{14}GeV^7]	B region [10^{14}GeV^7]	Total result [10^{14}GeV^7]
s_{13}	1.33468±0.00027	0.55901±0.00016	1.8937±0.0003
s_{23}	1.33468±0.00027	0.55891±0.00016	1.8936±0.0003
Analytical result: 1.89329402875986			

Table 4.7: Values for the different combinations of $s_{ij}^{-1/2}$ with i initial and j final for $\sqrt{s} = 8$ TeV, no selection cuts imposed and PDFs are assumed to be identically one for any initial state.

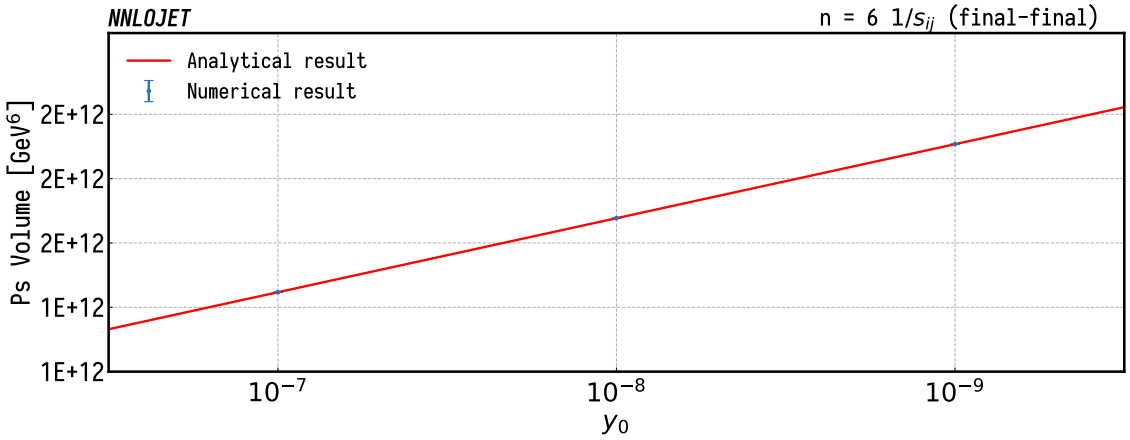

Figure 4.18: Study of the y_0 behaviour for $M = \frac{1}{s_{ij}}$ with i and j both f.s. particles, $\sqrt{s} = 8$ TeV.

i, j final [10^{12}GeV^6]		i initial, j final [10^{11}GeV^6]	
s_{35}	1.42140 ±0.00025	s_{14}	4.02 ±0.07
s_{36}	1.42140 ±0.00025	s_{13}	4.13 ±0.06
s_{45}	1.42140 ±0.00025	s_{23}	4.15 ±0.06
s_{46}	1.42138 ±0.00024		
An. result:	1.421246324426	An. result:	4.086991446617

Table 4.8: Values for the phase space volume for $n = 6$ for different combinations of s_{ij}^{-1} for $\sqrt{s} = 8$ TeV and $y_0 = 10^{-7}$. No PDFs or cuts.

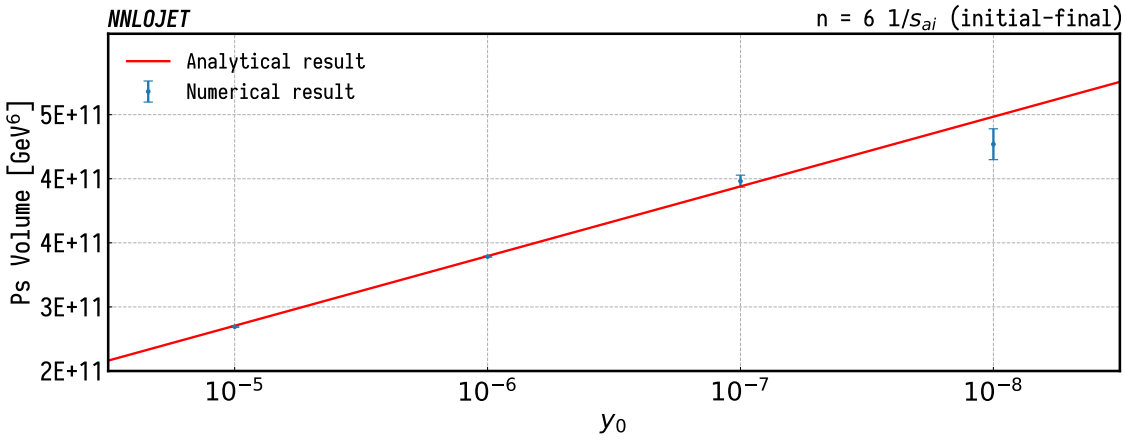

Figure 4.19: Study of the y_0 behaviour for $M = \frac{1}{s_{aj}}$ with a i.s. parton and j f.s. particle, $\sqrt{s} = 8$ TeV.

4.4 Validation

We conclude this chapter by summarising the validation tests performed on the implementation of the VBF Higgs boson production process at NNLO in NNLOJET to ensure the correctness of the integration.

Given the complexity of higher order calculations, extensive testing is required. In Table 4.9 we summarise the test suite for VBF Higgs boson production in NNLOJET. These include internal consistency checks within the NNLOJET framework as well as checks against well established external tools. Note the inclusion of the validation tests for the VBF phase space detailed in Section 4.3.6.

All internal tests, marked in green in Table 4.9, are generic to all other NNLOJET calculations whereas tests against external tools (in red) are not always available. For VBF Higgs boson production, matrix elements were available through automated tools such as Madgraph [119] and OpenLoops [109]. Inclusive calculations for LO, NLO and NNLO are also available with proVBFH [95]. For a more complete set of matrix element tests, real virtual matrix elements in the DIS approximation were privately made available from OpenLoops for testing purposes.

Fully differential calculations were available for NLO for Higgs boson plus two and three jets [72, 120, 121] and NNLO for Higgs boson plus two jets [95] prior to the publication of [1]. Some of these calculations however contain significant errors that were uncovered in the validation of this process in NNLOJET. Recently calculations were fixed both for Higgs boson production plus two jets at NNLO and for Higgs boson production plus three jets at NLO and their new versions are in agreement with the NNLOJET results published in [1]. See [122] for the erratum on [95].

The outline of this section is as follows: first, we validate the main ingredients of the calculation in a pointwise manner: the matrix elements and the subtraction terms. These tests are performed using RAMBO to generate phase space points which are then provided both to the reference code or subtraction term and to the NNLOJET matrix element and comparing the results. The layer test, which

	Level	ME	Spikes	$\frac{1}{\epsilon}$	Layer	Scale	Phase Space	Tech cut	Inclusive
LO	B	✓	-	-	-	-	✓	✓	✓
NLO	R	✓	✓	-	✓	✓	✓	✓	✓
	V	✓	-	✓	✓	✓	✓	✓	✓
NNLO	RR	✓	✓	-	✓	✓	✓	✓	✓
	RV	✓	✓	✓	✓	✓	✓	✓	✓
	VV	-	-	✓	✓	✓	✓	✓	✓

Table 4.9: Validation test suite for the VBF process in NNLOJET. Red ticks refer to tests against external tools, green ticks are internal NNLOJET tests. Non-applicable tests are marked with an hyphen.

checks Eq. (2.57), is performed by comparing autogenerated files and Maple input cards. All other tests are performed by integrating the cross section for various input parameters.

4.4.1 Matrix elements

The first test in Table 4.9, labelled ME, is a validation of our independent implementation of the matrix elements. This is arguably the most important test of the NNLOJET implementation as all other tests will fail if these are incorrect.

There exist several automated tools which provide tree and one loop matrix elements such as Madgraph [119] and OpenLoops [109]. Once we correct for differences in parameters and conventions between NNLOJET and the target programs, we find machine precision agreement for all parton-level configurations and colour levels for any given phase space point. Some examples are given in Table 4.10.

Process	NNLOJET	Madgraph/OpenLoops	Ratio
$qq \to qqgg$	5.1406085025982153E-014	5.1406085025982185E-014	1.0000000000000007
$gg \to qq\bar{q}\bar{q}$	4.0982703031871614E-017	4.0982703031871552E-017	1.0000000000000163
$qg \to qq\bar{q}$ (one loop)	-5.9293779081794126E-011	-5.9293779081799606E-011	0.99999999999990763

Table 4.10: Example of pointwise comparison against and OpenLoops for a selection of RR and RV matrix elements. Tests have been performed for all colour levels and possible configurations of initial and final states allowed in the DIS approach described in Section 3.2.

Technical discussion

Both Madgraph and OpenLoops include all possible diagrams for a given initial to final state at a fixed order in EW and QCD, i.e., they do not implement the DIS approach. This also includes same flavour interference. In order to make the matrix elements from NNLOJET and Madgraph (and Openloops) comparable it is necessary to introduce certain modifications.

In Madgraph we can manually alter the code to forbid some combinations of diagrams. This allows us to test all configurations for all possible flavours. However, it raises another issue: we are modifying the code we are testing against so it is no longer a truly external independent check anymore. A second method can also be used: the flavour of the incoming and outgoing quarks can be set such that we only generate configurations in which the diagrams appearing are exactly those allowed by the DIS approach. For instance, for uc scattering all possible diagrams fulfil the conditions of the DIS approach.

A combination of both methods allows us to check all possible configurations in a robust manner.

Another issue arises when comparing loop matrix elements due to differences of order $\mathcal{O}(\epsilon^2)$ in the choice of global factors. When we compare only unsubtracted matrix elements we find leftover $\frac{1}{\epsilon^2}$ poles which promote these differences to order $\mathcal{O}(1)$.

In Section 1.1.5 we chose a global factor for NNLOJET of $\bar{C}(\epsilon) = (4\pi^2)^\epsilon e^{\epsilon\gamma_E}$ whereas both Madgraph and OpenLoop take as a global factor,

$$C(\epsilon) = \frac{\Gamma(1-\epsilon)}{\Gamma(1-2\epsilon)}(4\pi^2)^\epsilon. \tag{4.53}$$

The difference between the two has to be taken into account in order to consistently test NNLOJET against Madgraph or Openloops.

$$\bar{C}(\epsilon) - C(\epsilon) = \epsilon^2 \frac{1}{4}\pi, \tag{4.54}$$

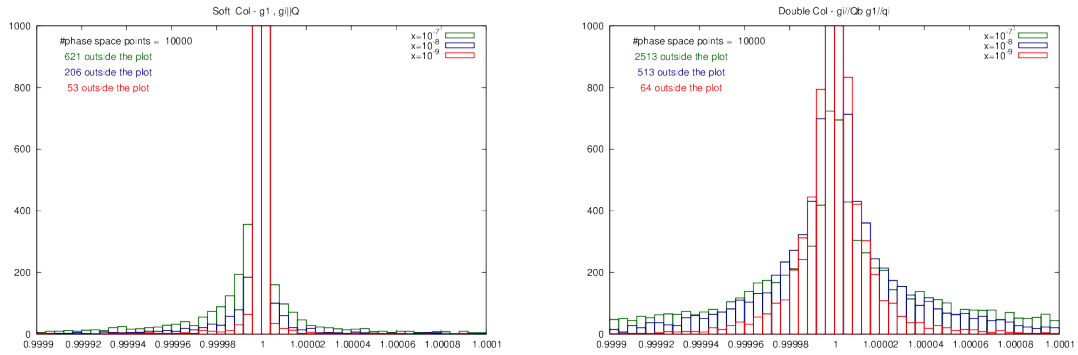

Figure 4.20: "Spike plots" generated for two different singular limits. As we lower the technical cut on our invariants ($y_0 = \frac{s_{ij}}{\hat{s}}$) the cancellation becomes more exact as we move closer to the actual limit.

or more explicitly,

$$M^{(1,f)}_{\text{Ref. Tool}} = M^{(1,f)}_{\text{NNLOJET}} - \frac{\pi}{4} M^{(1,2\epsilon)}_{\text{NNLOJET}}, \tag{4.55}$$

where $(1, f)$ corresponds to the finite piece of the 1-loop matrix element and $(1, 2\epsilon)$ to the $\frac{1}{\epsilon^2}$ coefficient of the 1-loop matrix element.

4.4.2 Pole testing

Implicit singularities

We confirm the (subtraction-matrix element) cancellation of the implicit singularities of the process by means of frequency histograms called "spike plot" of the ratio $\frac{\text{matrix element}}{\text{subtraction}}$ for phase space points chosen randomly around the unresolved limits such that $\frac{s_{ij}}{\hat{s}} \leq y_0$. As y_0 approach 0 we expect to find a δ function at 1, hence the name "spike".

The test is performed by a set of Fortran routines that loop over all possible parton orderings and colour levels testing each possible unresolved limit for different values of y_0 generating spike plots for each one. At the double real level of the VBF calculation this routine generates the order of $\mathcal{O}(10^3)$ spike plots. In Fig. 4.20 we show some examples.

In order to further automate this task, a threshold value is set so that we only consider the test as passed when less than a given percentage of points fall outside

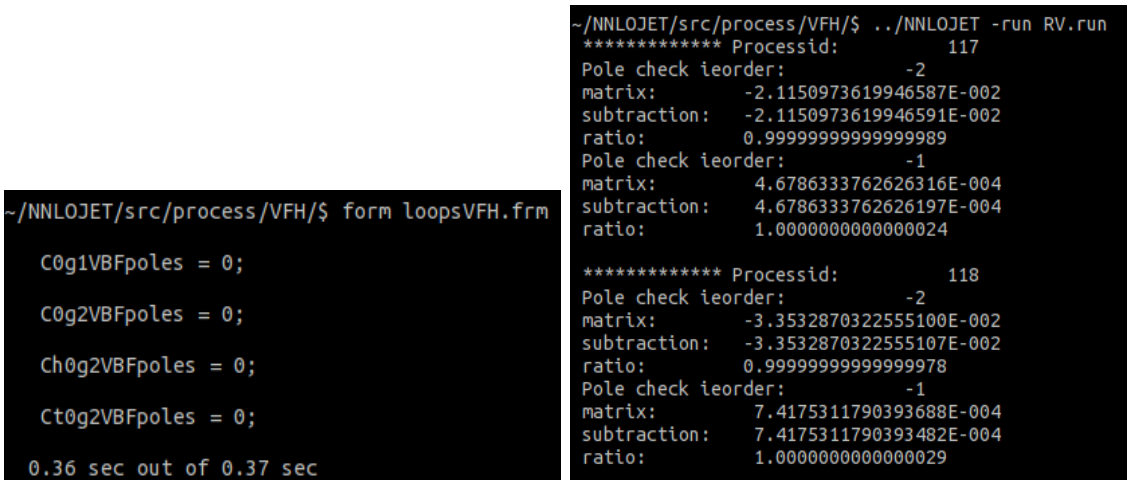

Figure 4.21: Output of the pole check for NNLOJET. Left is an analytical comparison between the matrix elements and the Catani pole structure while right show a numerical comparison between the matrix elements and the subtraction terms.

of the range $1-10^{-4} < \frac{\text{matrix element}}{\text{subtraction}} < 1+10^{-4}$. In the spike plots shown in Fig. 4.20 this value is set to 30% for the biggest value of y_0 and 5% for the smallest value.

Explicit $\frac{1}{\epsilon}$ poles

Virtual matrix elements, on the other hand, possess explicit infrared poles in $\frac{1}{\epsilon}$ coming from loop integrations which must be cancelled with the integrated counterterms. This cancellation can be checked numerically by randomly generating points in the whole range of the phase space. Since the cancellation must be exact for any phase space point we require, for the $(\frac{1}{\epsilon})^l$ coefficients,

$$\text{ME} - \text{Subtraction} = \mathcal{O}\big(10^{-8}\big). \tag{4.56}$$

An even more robust check is also implemented for 2-loops calculations where both the subtraction and the double virtual matrix elements can be tested against the Catani pole structure [27] using FORM routines available in NNLOJET . This check is done automatically for any 2-loop subtraction term upon generation from the respective Maple input files. In order to perform the same check for matrix elements they need to be implemented in FORM format. Two examples of these methods for checking $\frac{1}{\epsilon}$ poles are given in Fig. 4.21.

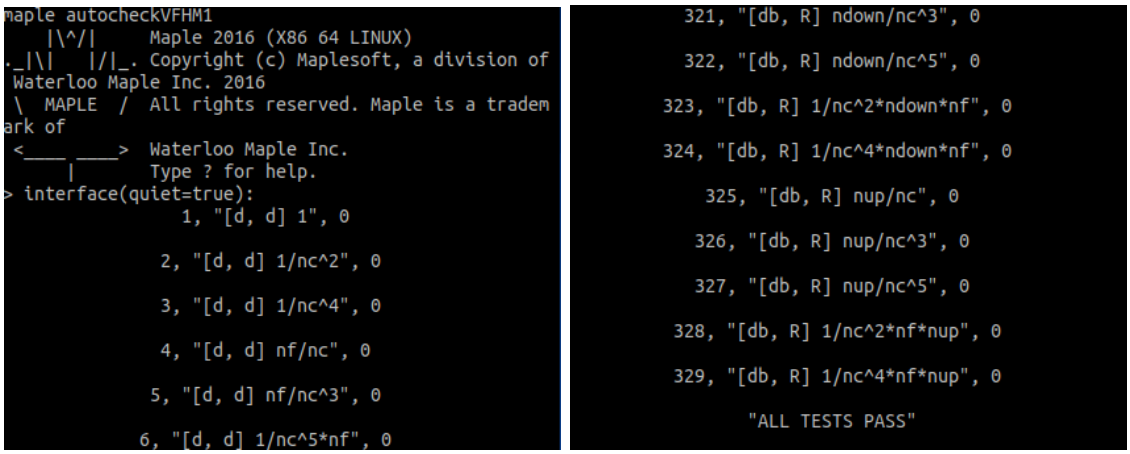

Figure 4.22: Output of the layer test for one of the antenna substructures.

4.4.3 Layer tests

Once matrix elements and subtraction terms are properly validated, the last step before integration is checking that Eq. (2.58) holds. This is equivalent to verifying the subtraction terms fulfil the equality:

$$\sigma^{\mathrm{S}} + \sigma^{\mathrm{T}} + \sigma^{\mathrm{U}} = 0, \tag{4.57}$$

In other words, all unintegrated antenna counterterms subtracted in σ^{S} and σ^{T} (cancelling the implicit singularities of the RR and RV contributions) are exactly reintroduced as integrated antennae in σ^{T} and σ^{U} (cancelling the $\frac{1}{\epsilon}$ poles). The complex structure of the different layers of the subtraction terms using the antenna formalism is shown graphically in Fig. 3 of Ref. [21].

We can exploit the autogenerated nature of the NNLOJET framework by reading in the Maple files that are used to autogenerate the Fortran code. A suite of Maple scripts and Unix tools then verifies Eq. (4.57) analytically for every colour level for every incoming parton channel. See Fig. 4.22.

4.4.4 Technical cut dependence

The technical cut (y_0) is an unphysical quantity introduced due to the limitations of the computational hardware we use and regulates how small the physical invariants

Level	10^6	10^7	10^8
LO	$957.46^{+66.12}_{-59.16} \pm 0.25$	$957.51^{+66.12}_{-59.17} \pm 0.24$	$957.53^{+66.12}_{-59.17} \pm 0.24$
NLO	$-80.59^{+66.60}_{-83.39} \pm 0.31$	$-80.39^{+66.57}_{-83.34} \pm 0.49$	$-80.04^{+66.54}_{-83.31} \pm 0.79$
NNLO	$-30.13^{+7.75}_{-1.23} \pm 0.62$	$-29.22^{+7.92}_{-1.27} \pm 0.86$	$-30.80^{+7.64}_{-1.29} \pm 0.67$

Table 4.11: Comparison of the different levels of the cross section for different values of the technical cut. LO refers to the Born cross section, NLO to the sum of R and V and NNLO to the sum of RR, RV and VV.

.

can go before the cross section is set to 0 for the event and the event skipped. This has the practical effect of avoiding divisions by zero and miscancellations of large numbers.

Its use is purely technical and should not have any effect on any physical quantity predicted by NNLOJET up to the statistical errors. The independence of the cross section with respect to the technical cut can be tested by integrating the cross section for decreasing values of y_0 until a plateau is reached, i.e., the effect of the technical cut is below the target statistical error. For the VBF calculation this plateau is found from values of $y_0 = 10^{-6}$.

In Table 4.11 we integrate the VBF cross section for different values of the technical cut. We choose $y_0 \in \{10^{-6}, 10^{-7}, 10^{-8}\}$, finding very good agreement within errors between the three choices. In Fig. 4.23 two differential distributions are also shown for the same choices of y_0. Both integrations include statistical uncertainties and scale variations so that for this comparison we stop the integration once the statistical uncertainty is below the scale variations across the range of the observables considered. It is also worthy of note that if the chosen technical cut is too small we risk a considerable increase in the number of jokers, which can be disastrous for the stability of the integration. It is usually better to choose the biggest possible y_0 once the plateau has been reached.

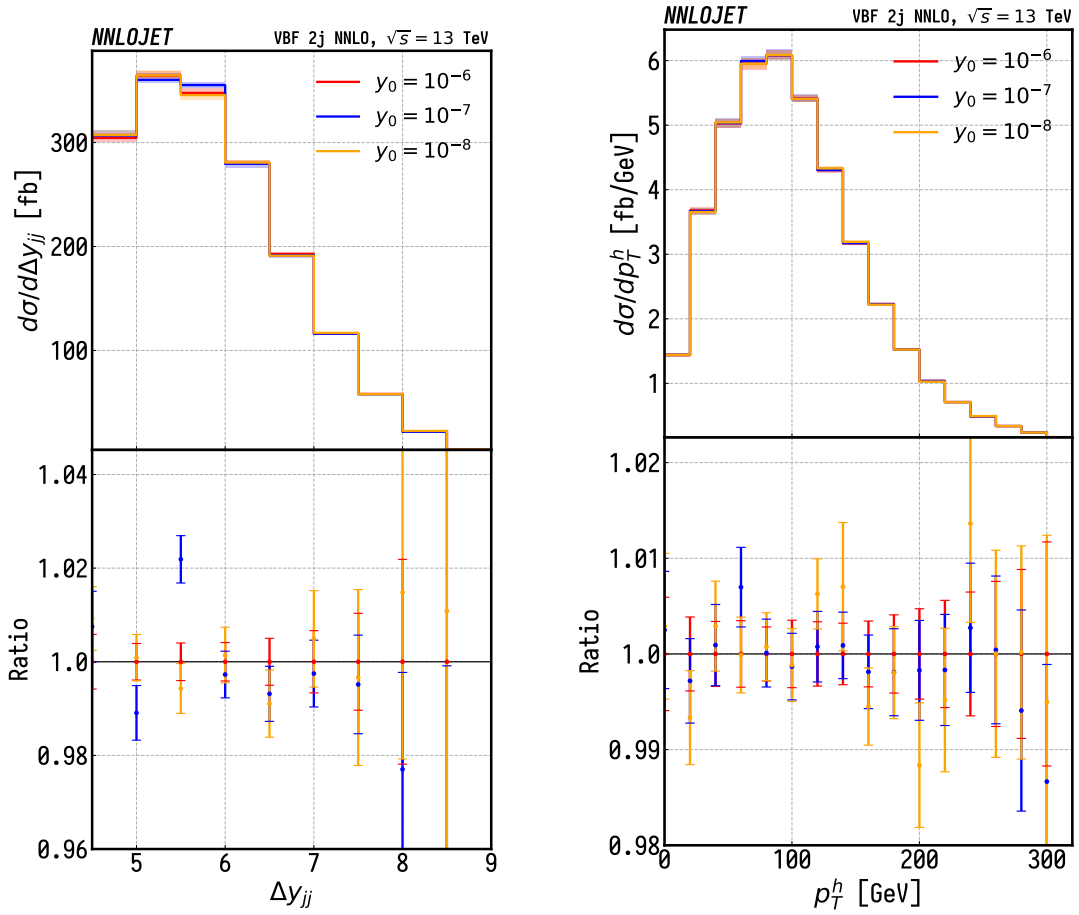

Figure 4.23: Bin by bin comparison for the Δy_{jj} and p_T^H distributions for different values of the technical cut y_0 for a NNLO VBF calculation The shaded regions correspond solely to scale variations while the error-bars correspond to statistical uncertainty.

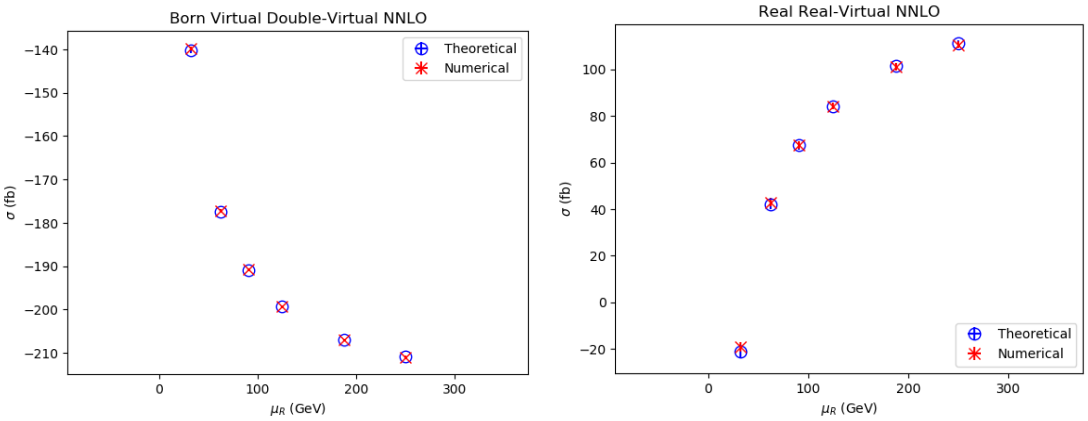

Figure 4.24: Scale evolution of the total VBF cross section. We select $\mu_{\mathrm{F}} = \mu_{\mathrm{R}} = 125$ GeV as the reference scale and numerically integrate for different values of μ_{R}.

4.4.5 Scale evolution

In Section 1.1.5 we derive a general formula for the evolution of the cross section from a reference scale μ_0 to an arbitrary scale μ_R which depends only on the relative value of the strong coupling between both scales $\frac{\alpha_s(\mu_{\mathrm{R}})}{\alpha_s(\mu_0)}$ and the lower order result at scale μ_{R}. Using the master formula of Eq. (2.90), it is possible to test whether the calculation exhibits the correct μ_{R} evolution. Furthermore, the scale evolution can be separated by multiplicity so that we can check the Born-type cross section (LO, V and VV) and real radiation-type cross section (R and RV) independently. This comparison is shown in Fig. 4.24 where we show the numerical result obtained with NNLOJET at NNLO compared to the analytic result using Eq. (2.90).

This test is limited in scope as only scale dependent terms can be check with this method. It is however an important closure test for the subtraction terms as they often introduce spurious scale dependence that only cancel once all subtraction terms are combined.

4.4.6 Inclusive cross section

The final validation test for the calculation is the integration of the total inclusive cross section. This test is unique to processes in which the Born level is integrable with no cuts applied. The inclusive VBF Higgs boson production calculation is

	$\sigma^{\text{reference}}$ (fb)	σ^{NNLOJET} (fb)
Total up to LO	4032^{+57}_{-69}	4032^{+56}_{-69}
Total up to NLO	3929^{+24}_{-23}	3927^{+25}_{-24}
Total up to NNLO	3888^{+16}_{-12}	3884^{+16}_{-12}

Table 4.12: Fully inclusive VBF cross section. The uncertainty corresponds to a scale variation of $\mu_F = \mu_R = \left\{\frac{1}{2}, 1, 2\right\} \times \mu_0$. μ_0 is given in (5.2). Reference results are taken from [95].

known in the DIS approach [68, 69] and is available in the form of a Fortran code named proVBFH [95] based on the structure functions provided by Hoppet [123]. The first test is made against the published results of Ref. [95], shown in Table 4.12 where we find very good agreement at LO, NLO and NNLO.

There is an important difference between the inclusive results of Refs. [68, 69, 95] and the inclusive calculation performed with NNLOJET. In the previous literature, the NNLO cross section is obtained directly from the DIS structure functions which combine together all parton-level subprocesses of different state multiplicity. In contrast, in NNLOJET, we evaluate all subprocesses separately using the antenna subtraction counterterms to regulate singularities, meaning we are computing a jet cross section lifting all cuts.

For completeness, in Table 4.13 we show a channel by channel comparison of the NNLO coefficient between NNLOJET and proVBFH. These results were obtained with a privately modified version of proVBFH and Hoppet in order to extract the VBF cross section for specific initial states. We find very good agreement in all channels between the reference code and our calculation.

Naively one can imagine this test to makes previous ones redundant, as it requires all of the previously validated components. However, in lifting all cuts we allow contributions in very unstable regions of the phase space, making the test very expensive in terms of computing power. Furthermore, regions with little contribution to the cross section can still hide erroneous contributions only realisable with specific cuts or differential distributions.

Initial state	σ^{proVBFH} (fb)	σ^{NNLOJET} (fb)
$q\ \ q$	36.67 ±0.07	36.3 ±0.5
$q\ \ \bar{q}$	19.52 ±0.07	19.6 ±0.4
$\bar{q}\ \ \bar{q}$	7.67 ±0.01	7.5 ±0.1
$q\ \ g$	-53.96 ±0.06	-54.2 ±0.4
$\bar{q}\ \ g$	-16.29 ±0.02	-16.4 ±0.1
$g\ \ g$	8.203 ±0.007	8.23 ±0.04

Table 4.13: Fully inclusive VBF NNLO coefficient (RR+RV+VV) broken down by initial state. The scale choice is $\mu_{\text{F}} = \mu_{\text{R}} = m_H$. The results were obtained with a privately modified version of proVBFH and Hoppet.

4.4.7 Differential cross section

Prior to the publication of [1], which makes uses of the work presented in this thesis, a differential calculation of VBF Higgs boson production was published in Ref. [95] using Projection to Born. A disagreement between our results and the results in the literature prompted us to extend our internal test suite in order to confirm our results. These results were shared with the authors of [95] and a bug in their implementation was found, leading to an update of their results as seen in Ref. [122].

We thank the authors of [95, 122] for sharing the raw data of their updated histograms (Ref. [122]) so a bin-by-bin comparison could be performed. This is shown in Fig. 4.25 where we find agreement between both calculations within statistical uncertainties. All parameters for the comparison match those in [1, 95].

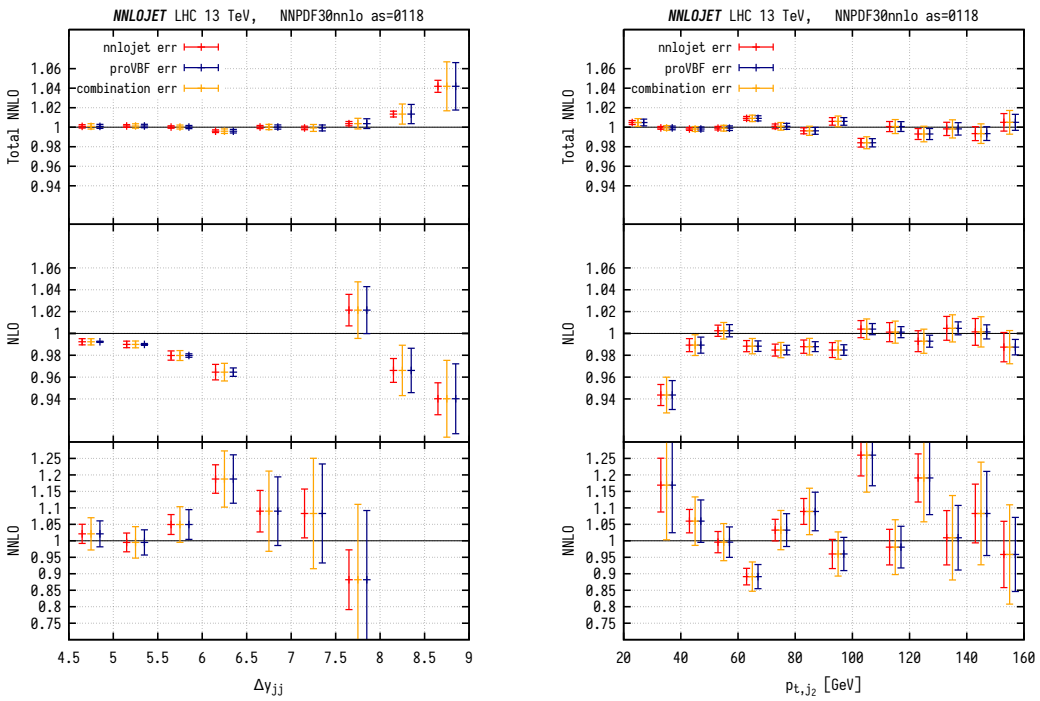

Figure 4.25: Bin by bin comparison ratio between [1] and the corrected results of [95]. The red errors correspond to the statistical error from NNLOJET, the blue errors the statistical error of proVBF and the yellow bars the combination of both. NLO and NNLO correspond to the NLO and NNLO coefficients only respectively.

Chapter 5

Phenomenological Results

This chapter presents the phenomenological study of electroweak Higgs boson production in association with two or more jets in VBF using the DIS approach.

In Section 5.1 we study the impact of the NNLO QCD corrections to Higgs boson production in association with two jets. Likewise in Section 5.2 the NLO QCD corrections for VBF Higgs boson plus three jets production is presented and we also motivate the study for higher-order corrections to this process. The results of Sections 5.1 and 5.2 have been published in Ref. [1]. In Section 5.3 we use our implementation of the process in NNLOjet in order to assess the effect of the jet algorithm on both the fiducial cross section and differential distributions. In Section 5.4 we present preliminary results for Higgs boson production in VBF in a future High Luminosity/High Energy LHC, at 27 TeV within the context of the HL/HE Working Group.*

Setup

For all numerical calculations presented in Sections 5.1 to 5.3 of this chapter we make use of the NNLO NNPDF3.0 parton distribution functions [75] with the value of $\alpha_s(M_Z) = 0.118$ as provided by LHAPDF [76]. We set the mass of the Higgs boson to $m_H = 125$ GeV, which is compatible with the combined results of ATLAS

*In collaboration with Alexander Karlberg.

and CMS [15]. Furthermore, we use the following electroweak parameters as input:

$$m_{\mathrm{W}} = 80.398 \text{ GeV}, \qquad \Gamma_{\mathrm{W}} = 2.141 \text{ GeV},$$
$$m_{\mathrm{Z}} = 91.188 \text{ GeV}, \qquad \Gamma_{\mathrm{Z}} = 2.495 \text{ GeV}. \tag{5.1}$$

Unless otherwise stated, jets are reconstructed using the anti-k_{T} algorithm [42] with a radius parameter $R = 0.4$, and are always ordered in transverse momentum.

Renormalisation and factorisation scales are chosen as suggested in [95]:

$$\mu_0^2(p_T^H) = \frac{m_H}{2}\sqrt{\left(\frac{m_H}{2}\right)^2 + (p_T^H)^2}. \tag{5.2}$$

Shaded error bands in plots always denote the scale uncertainty resulting of taking $\mu_{\mathrm{R}} = \mu_{\mathrm{F}} = \{\frac{1}{2}, 1, 2\} \times \mu_0$ whereas the error bars correspond exclusively to the statistical uncertainty of the numerical Monte Carlo integration.

5.1 NNLO corrections to Higgs boson plus 2 jet production in VBF

5.1.1 Inclusive calculation

We begin by computing the fully inclusive cross section for VBF Higgs boson production in association with two jets (VBF-2j) in Table 5.1. We observe an excellent perturbative convergence with very small NLO and NNLO corrections and a sizeable reduction of the scale uncertainty with each order.

	$\sigma^{\mathrm{NNLO_{JET}}}$ (fb)	K factor
LO	4032^{+56}_{-69}	1.000
NLO	3927^{+25}_{-24}	0.974
NNLO	3884^{+16}_{-12}	0.963

Table 5.1: Fully inclusive VBF-2j cross section for a center of mass energy of $\sqrt{s} =$ 13 TeV. We find a factor of about a -3% at NLO and -4% at NNLO with respect to LO.

The inclusive VBF cross section is, however, not a directly measurable quantity.

As discussed in Section 3.2 and demonstrated in Section 3.2.1, by not taking any selection cuts we are strongly dominated by ggF background. Moreover, the DIS approach is not well justified for the fully inclusive cross section as we are within the regions of phase space in which the competing VH production mode becomes important.

5.1.2 Fiducial result and differential cross sections

In order to single out the VBF contribution selections cuts are applied. Our choice of VBF cuts for the two leading jets are

$$\begin{aligned} p_{\mathrm{T}_j} > 25 \text{ GeV}, \qquad & |y_j| < 4.5, \\ m_{jj} > 600 \text{ GeV}, \qquad & \Delta y_{jj} = |y_{j_1} - y_{j_2}| > 4.5, \end{aligned} \tag{5.3}$$

these are identical to those used in Refs. [1] and [95]. A third or fourth jet can be present in the event at any rapidity, i.e. the cuts define a VBF-2j inclusive cross section. We note that the cut on Δy_{jj} and m_{jj} are more restrictive than the experimental template cross section of Eq. (3.1) which gets us deeper into the region in which the DIS approach is valid. Note as well that the cuts of Eq. (5.3) automatically imply that the jets are found in opposite hemispheres.

	$\sigma^{\mathrm{NNLO_{JET}}}$ (fb)	K factor
LO	957^{+66}_{-59}	1.000
NLO	877^{+7}_{-17}	0.916
NNLO	844^{+9}_{-9}	0.882

Table 5.2: Total VBF-2j cross section after VBF cuts are applied for a center of mass of $\sqrt{s} = 13$ TeV. The NLO corrections is three times bigger than in the fully inclusive case, amounting to a $\sim -9\%$. A further -3% correction is obtained when we add the NNLO coefficient. As an effect of the tight VBF cuts of Eq. (5.3), a 78% of the total cross section at NNLO is lost.

By application of these cuts, we obtain the fiducial VBF-2j cross sections as listed in Table 5.2. It is important to note the increase in magnitude of the higher order QCD corrections when VBF cuts are applied: we find a negative correction

factor at both NLO and NNLO which is three times larger in magnitude than what was found in the fully inclusive cross section reported in Table 5.1.

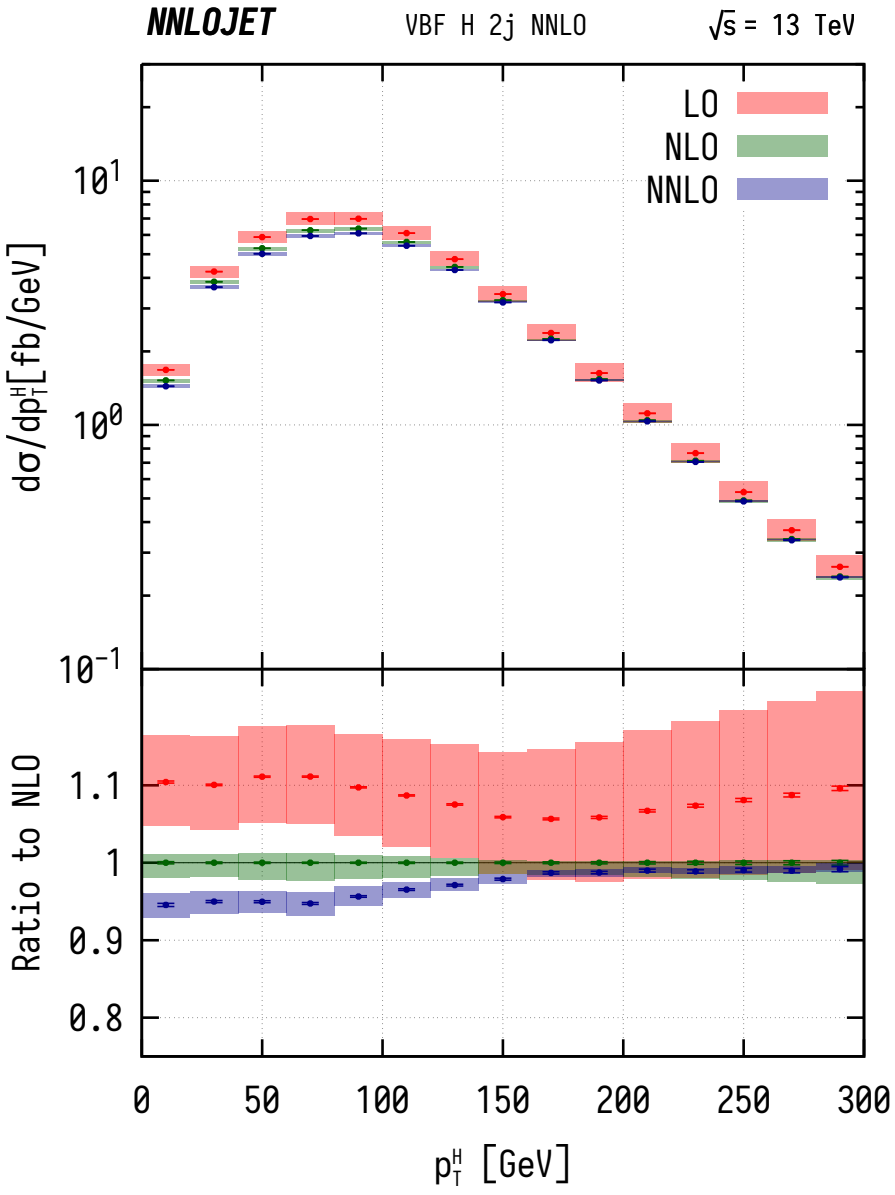

Figure 5.1: Transverse momentum distribution of VBF-2j. In red we plot the LO distribution. Both the NLO (green) and NNLO (blue) corrections reduce noticeably the scale uncertainty bands. Beyond $p_T^H \sim 150$ GeV the NNLO corrections become negligible and well within the LO and NLO uncertainty bands.

The larger impact of the NNLO corrections for the VBF-2j process can also be observed in the differential distributions. Figure 5.1 shows the transverse momentum of the Higgs boson. The NLO corrections are uniform and negative, amounting to about -10% throughout the distribution. For medium or large transverse mo-

mentum, the NNLO correction is quasi-negligible and lies within the NLO scale uncertainty band. At lower transverse momentum, where the bulk of the distribution is located, the NNLO corrections become significant at -5%, and lie outside the NLO uncertainty band.

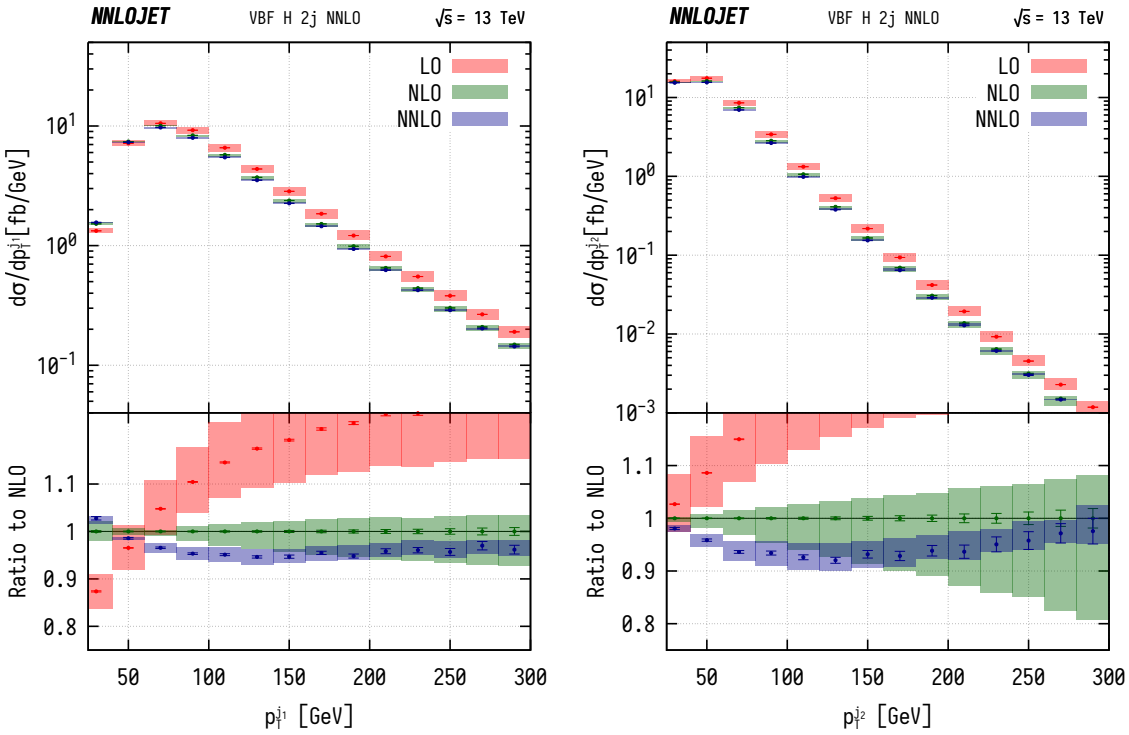

Figure 5.2: Transverse momentum distribution of leading and subleading jet for VBF-2j. Both the NLO and NNLO corrections change the shape of the observables. Note that the NLO scale uncertainty bands are much bigger than those seen in Fig. 5.1, this suggest the scale choice of Eq. (5.2) might be suboptimal for these two observables. At NNLO, however, the dependence with the scale is well reduced, which proves the convergence of the perturbative series.

The transverse momentum distributions of the leading and subleading jet (i.e. the two tagging jets for the VBF cuts) are shown in 5.2. We observe that both the NLO and NNLO corrections are not uniform; they change from positive (for the leading jet) or negligible (for the subleading jet) to negative for larger transverse momenta. We also observe that the NLO and NNLO uncertainty bands overlap in the range of the observable beyond the very low p_T^j region. The magnitude of the NNLO corrections is moderate, and never exceeds 5%, while NLO corrections can be as large as 30% and lead to a substantial modification of the shape of both distributions.

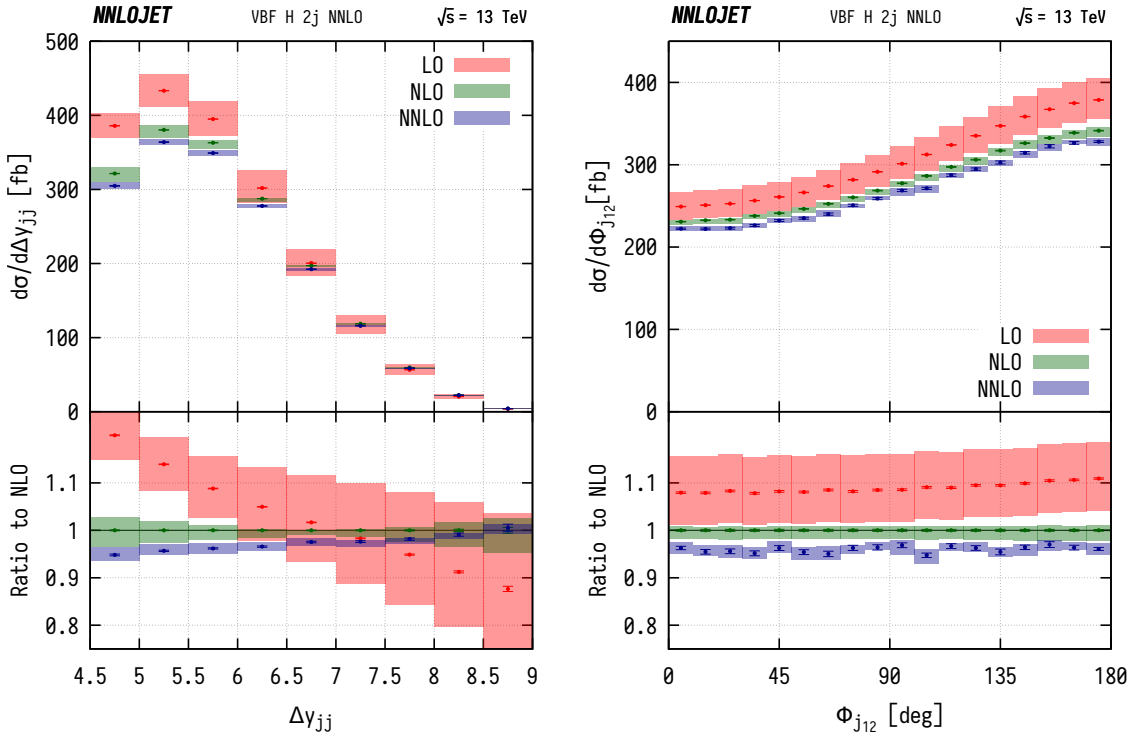

Figure 5.3: Study of the rapidity separation and angular decorrelation of the two leading jets in the VBF process. The scale uncertainties in both distributions were well under control already at NLO. The NNLO corrections further reduce the scale dependence making it almost negligible as the statistical error of the Monte Carlo integration becomes dominant.

The spatial distribution of the two tagging jets is described by their separation in rapidity Δy_{jj} and their angular decorrelation $\phi_{j_{12}}$. The VBF-2j distributions in these two variables are shown in Figure 5.3. We observe that the NLO and NNLO corrections are very uniform in $\phi_{j_{12}}$, while displaying a sizeable dependence on Δy_{jj}. For low values of this variable (which starts only at $\Delta y_{jj} = 4.5$ due to the VBF cuts (Eq. (5.3))) the corrections are negative and amount to -25% at NLO and to a further -5% at NNLO. The corrections decrease in magnitude with increasing rapidity separation and cross zero around $\Delta y_{jj} \sim 7$. At higher separations the NLO and NNLO corrections become positive, but remain rather moderate. For both spatial distributions, we observe that the NLO and NNLO uncertainty bands barely overlap. Nevertheless, the small magnitude of the NNLO corrections indicates a good perturbative convergence.

Similar observations can also be made about the invariant mass distribution of

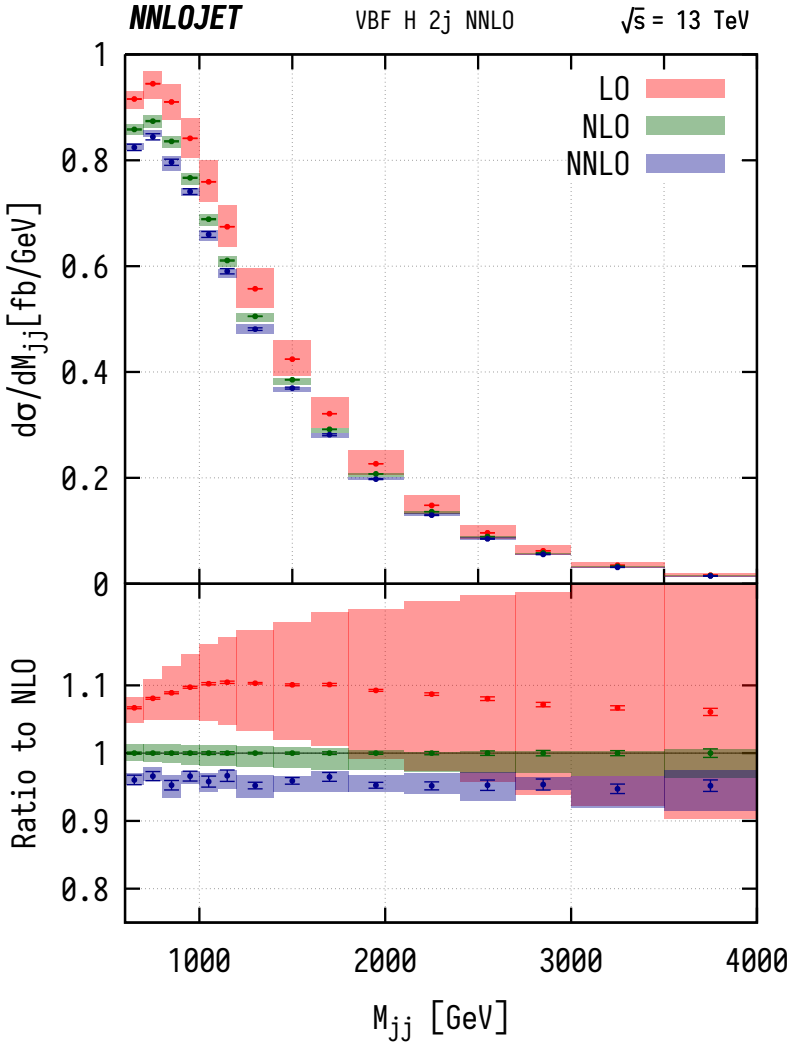

Figure 5.4: Distribution on the invariant mass of the system formed by the two tagging jets of the VBF process. Both the NLO and NNLO corrections are quite uniform across the accessible range of the observable. The scale dependence at NNLO is negligible at low and moderate values of m_{jj}, where the statistical error dominates.

the two tagging jets shown in Figure 5.4, where despite observing very small and uniform NNLO and NLO corrections, these corrections fall consistently outside the scale uncertainty bands.

5.2 NLO corrections to Higgs boson plus 3 jet production in VBF

For the Higgs plus 3 jet production (VBF-$3j$) cross section, we require one extra jet to have a transverse momentum greater than $p_{\mathrm{T}_j} > 25$ GeV and rapidity $|y_j| < 4.5$. A choice of VBF cuts is also applied to the two leading jets, namely, to their rapidity difference Δy_{jj} and their invariant mass m_{jj} to enhance the contribution from the VBF process over other Higgs boson production mechanisms. This leads to the following set of cuts on the two leading jets,

$$M_{jj} > 600 \text{ GeV}, \qquad \Delta y_{jj} = |y_{j_1} - y_{j_2}| > 3, \qquad y_{j_1} \cdot y_{j_2} < 0, \tag{5.4}$$

while the three hardest jets are required to pass the following selection cuts,

$$p_T^j > 25 \text{ GeV} \qquad\qquad |y_j| < 4.5 \tag{5.5}$$

Note that the cut on Δy_{jj} is lower than that of Section 5.1 so we need to enforce $y_{j_1} y_{j_2} < 0$ in order to find the two tagging jets in separate hemispheres. It has been chosen to allow us to compare our results with [121] over a larger range in Δy_{jj}.

The results of this calculation are shown in Fig. 5.5, where we study the rapidity separation of the two leading jets, Δy_{jj} (left frame) and the normalised rapidity distribution of the third jet (right frame),

$$z_3 = \frac{y_{j_3} - \frac{1}{2}(y_{j_1} + y_{j_2})}{y_{j_1} - y_{j_2}}. \tag{5.6}$$

In contrast to the initial findings of [121], we observe an increase of the NLO corrections for large values of Δy_{jj}. This finding has led to the identification of an error in the virtual matrix elements in [121], we are in full agreement with the revised results.*

The NNLO corrections to VBF-$2j$ shown in Section 5.1 were quite small and produced an important reduction on the scale uncertainty of the results. For VBF-

*Private communication with T. Figy.

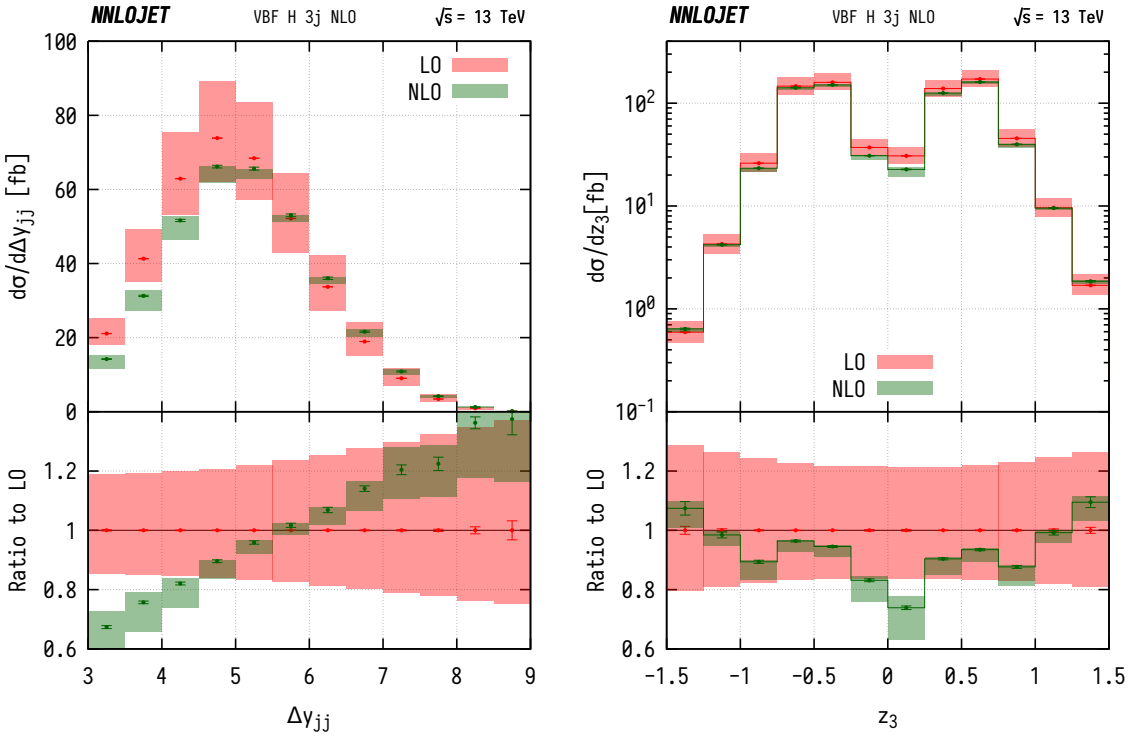

Figure 5.5: Differential distributions on Δy_{jj} and z_3, Eq. (5.6). We observe a reduction of the scale uncertainty going from LO to NLO, with a dominance of the statistical error with respect to the scale dependence for certain values of the observables. The NNLO corrections are very large, amounting to up to $\sim 30\%$ with noticeable scale uncertainty bands.

$3j$ only NLO corrections are available and these change considerably the shape of the observable with large scale uncertainties. It is thus expected that NNLO QCD corrections will make the distribution much more stable with respect to scale variations.

5.3 Jet dependence of VBF cross section

Due to the large rapidity separation imposed by the VBF cuts (Section 3.1.2) on the tagging jets, the Born cross section cannot be sensitive to the choice of jet algorithm or the parameterisation of the jet definition. Using the anti-k_T algorithm (Section 2.2.5, Eq. (2.67)) we write the distance between partons i and j as,

$$d_{ij} = \min(p_{T_i}^{-2}, p_{T_j}^{-2}) \frac{(y_i - y_j)^2 + (\phi_i - \phi_j)^2}{R^2}. \tag{5.7}$$

Partons i and j are clustered together only if $d_{ij} < \{d_{iB}, d_{jB}\}$, which can only happen when

$$R^2 > (y_i - y_j)^2 + (\phi_i - \phi_j)^2. \tag{5.8}$$

Not making any assumptions on the azimuthal distribution of the two tagging jets, at the Born level we find Eq. (5.8) is only fulfilled for values of $R > \Delta y_{jj}$, which for typical choices of VBF cuts is beyond any reasonable value of R.

Beyond NLO, where extra emissions can occur, the cross section can pick up a dependence on the definition of the jet through the jet radius. This phenomenological study is motivated by the findings of Ref. [124] where a very strong dependence of the VBF-2j results on the jet algorithm were found.

For this study we use the anti-k_T [42] algorithm with a jet radius R. We exploit the independence of the Born-type cross section with respect to the jet algorithm in order to reduce the computational times by calculating the total NNLO cross section just once with $R = 0.4$ and applying the following formula to obtain the cross section at any given R:

$$\sigma_R^{\text{VBF-2}j,\text{ NNLO}} = \sigma_{R=0.4}^{\text{VBF-2}j,\text{ NNLO}} - \sigma_{R=0.4}^{\text{VBF-3}j,\text{ NLO}} + \sigma_R^{\text{VBF-3}j,\text{ NLO}}. \tag{5.9}$$

In other words, the independence of the Born-level configuration with respect to the jet radius R allows us to ignore double singular configurations (where the Double-Real matrix element maps down onto a Born-level matrix element) greatly reducing the computational cost of the integration.

In Fig. 5.6 we show the fiducial cross section with the VBF cuts of Section 5.1 for different values of the jet radius R, which we vary between $R = 0.2$ and $R = 1.8$. We find a much softer dependence at NNLO than that of Ref. [124]. We trace this difference back to the aforementioned errors of Refs. [121] and [95] upon which [124] is based.

The dependence of the fiducial cross section with R at NNLO and NLO present similar features. At $R = 1.0$ we find the smallest k factor for the higher order corrections. We observe that as R grows the computed cross section grows as well.

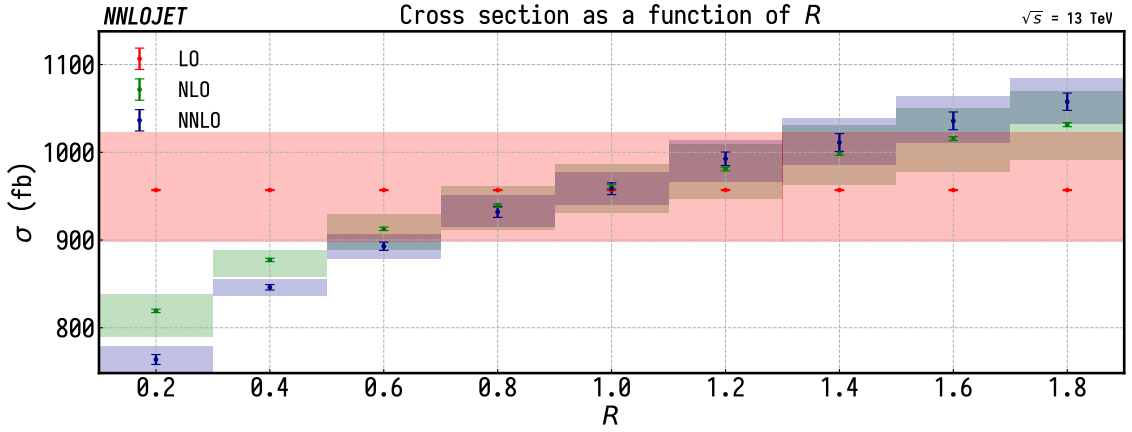

Figure 5.6: Total cross section as a function of R for LO (red), NLO (green) and NNLO (blue). Here the independence of the LO cross section with respect to the choice of R is seen explicitly. The NNLO cross section is well within the NLO scale uncertainty bands for $R > 0.4$.

This can be understood since as the cone size grows the tagging jets will tend to capture larger fractions of the total energy and, therefore, the chance of an event passing the VBF selection cuts also increases.

We study the effect of the VBF cuts in more detail in Fig. 5.7. For a fixed value of the cut on Δy_{jj} we vary the cut on m_{jj} and compute the fiducial cross section for different values jet radius R. As expected, the effect of the jet radius is increased as the requirement on m_{jj} becomes tighter.

To finalise we also study the differential behaviour of the cross section for different values of the jet radius. This is shown in Fig. 5.8 where we choose $R = \{0.4, 0.8, 1.2\}$. We find the shape of the distribution to only change for low values of the Δy_{jj} observable, with compatible results (within statistical uncertainties) for larger values of Δy_{jj}.

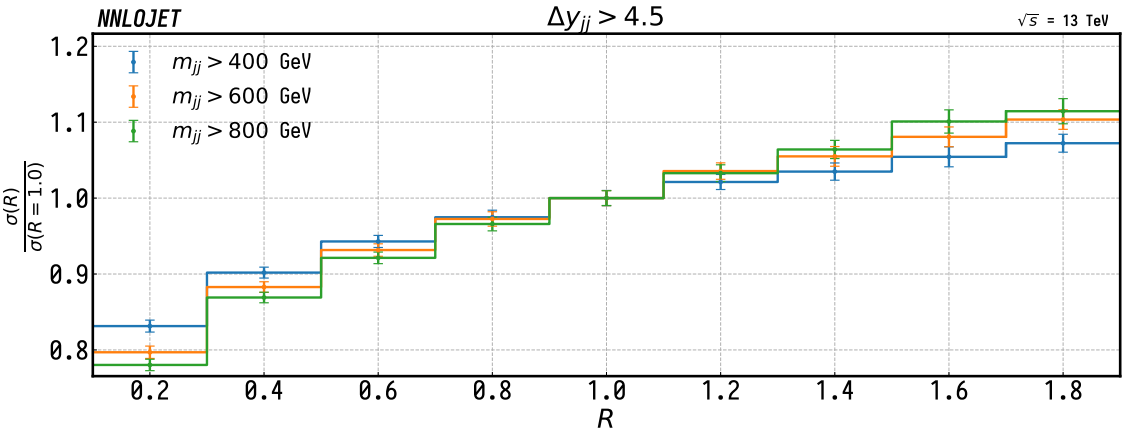

Figure 5.7: Variation of the NNLO cross section as a function of R for different values of the dijet invariant mass cut m_{jj}. We choose $R = 1.0$ to normalise the results as the effect of the higher order corrections are the smallest. In general we find the results for different values of the m_{jj} to be compatible within statistical errors. The main feature discussed in the main text can still be observed, i.e., a bigger dependence on the cross section on the jet radius R as the cut on m_{jj} becomes more restrictive.

.

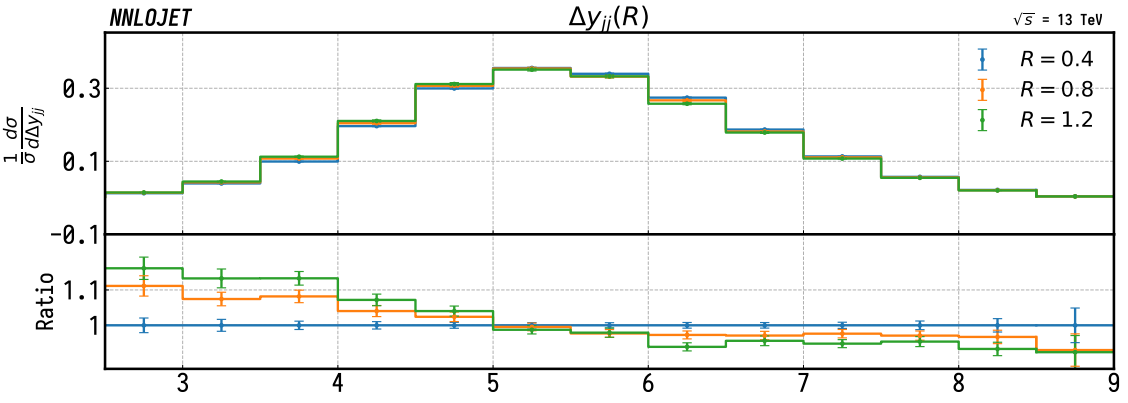

Figure 5.8: Differential distribution on the rapidity gap (Δy_{jj}) between the tagging jet for several values of the jet radius R. The computed values of the differential cross section are compatible within statistical errors beyond $\Delta y_{jj} > 5$. All other parameters are set equal to those of Section 5.1, crucially $m_{jj} > 600$ GeV and $|y_j| < 4.5$.

5.4 Phenomenology of VBF at NNLO in the HE-LHC

During run I, the LHC operated at nominal energies of $\sqrt{s} = 7$ and 8 TeV, collecting a total integrated luminosity of 29.2 fb^{-1}. In run II, of which we are in the last year now (2018), we have already exceeded the 150 fb^{-1} integrated luminosity target* and the energy has been increased to $\sqrt{s} = 13$ TeV. It has been argued these numbers, albeit impressive, are not sufficient to tackle many current issues with the Standard Model [125]. In particular, the Higgs self-coupling as well as the sub-percent study of the Higgs boson properties requires an increase in both energy and luminosity [66, 126].

There are a number of proposals for future, more energetic, hadron colliders. In this work we focus on the proposed improvements for higher energy and higher luminosity versions of the LHC [127]. The main advantage of these proposals is that they makes use of infrastructure already constructed. The High Luminosity LHC or HL-LHC [128] corresponds to an upgrade of the current hardware as well as the beam parameters. The goal is to produce 250 fb^{-1} integrated luminosity *per year*. The High Energy LHC or HE-LHC, on the other hand, is technically an in-place replacement of the current collider in the frame of the long term goal of a 100 TeV Future Circular Collider (FCC) [129] in which the LHC becomes the injector for the FCC. Crucially, an upgrade of the LHC magnets will allow the LHC to run at a center of mass energy of $\sqrt{s} = 27$ TeV. For a more technical discussion see Ref. [130].

In this section we study the prospects of the VBF Higgs boson production process in future accelerators, increasing the center of mass energy for our studies to 27 TeV.

*http://acc-stats.web.cern.ch/acc-stats/

Setup

Calculations in this section use the study appearing in the Yellow Report of the Higgs Cross Section Working Group 4 (YR4) [63] for Higgs boson production in the VBF channel at $\sqrt{s} = 13$ TeV as guideline. The choice of electroweak parameters in YR4 is,

$$\begin{aligned} m_{\mathrm{W}} &= 80.3850 \text{ GeV}, & \Gamma_{\mathrm{W}} &= 2.0850 \text{ GeV}, \\ m_{\mathrm{Z}} &= 91.1876 \text{ GeV}, & \Gamma_{\mathrm{Z}} &= 2.4952 \text{ GeV}. \end{aligned} \tag{5.10}$$

The central renormalisation and factorisation scales are set to be equal to m_{W},

$$\mu_{\mathrm{F}} = \mu_{\mathrm{R}} = m_{\mathrm{W}}. \tag{5.11}$$

The mass of the Higgs boson is set to $m_H = 125$ GeV and we have used the `PDF4LHC15_nnlo_100` [131] as provided by LHAPDF [76]. As in previous sections, the jet algorithm used is the anti-k_{T} algorithm [42] with radius parameter $R = 0.4$.

5.4.1 High Energy LHC, 27 TeV

At the HE-LHC energies of $\sqrt{s} = 27$ TeV the total inclusive cross section for the VBF mode will be increased by a factor of three with respect to the 13 TeV value shown in Table 5.1. It must be noted, however, direct comparison between the study presented here and that of Section 5.1 can not be drawn due to the very different choices for the renormalisation and factorisation scales. The choice $\mu_0 = m_{\mathrm{W}}$ has been made to be consistent with the results in YR4.

The first step toward a phenomenological study of the effects of the increase in the center of mass energy is the choice of VBF cuts as well as detector acceptance. If at $\sqrt{s} = 13$ TeV this was set to $p_T^j > 20$ GeV we increase it to a minimum of $p_T^j > 30$ GeV.

In Fig. 5.9 we show a double-differential plot of the cross section with respect to the VBF variables m_{jj} and Δy_{jj}. It is clear the bulk of the cross section occur

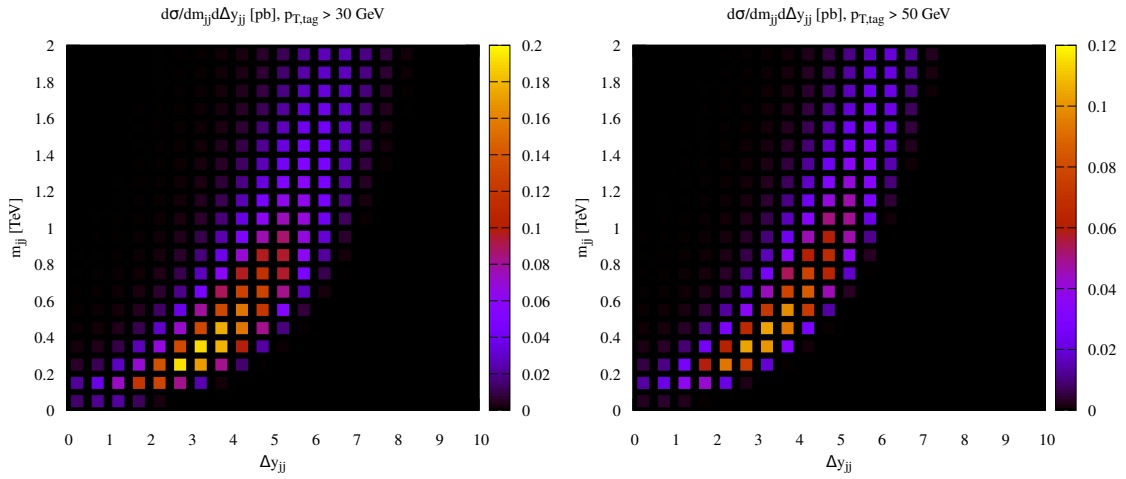

Figure 5.9: Two-dimensional plots on the rapidity gap between the two tagging jets (Δy_{jj}) and the invariant mass of the dijet system formed by those two tagging jets (m_{jj}) for two different choices of the transverse momentum cut. We observe the bulk of the cross section to be concentrated in $m_{jj} > 200$ GeV, $\Delta y_{jj} > 2.5$. These two plots have been obtained with proVBF [95] and provided by A. Karlberg.

for values of the rapidity gap of $\Delta y_{jj} > 3$ and $m_{jj} > 200$ GeV. We begin thus by defining a **minimal** set of VBF cuts with these values,

$$\Delta y_{jj} > 3, \qquad m_{jj} > 200 \text{ GeV}. \tag{5.12}$$

However, as demonstrated in Section 3.2.1, even though with these cuts we are in the region of the phase space in which the DIS approach is valid they might not be enough to completely suppress the background from competing process. To that end we define a set of **tight** VBF cuts as,

$$\Delta y_{jj} > 4.5, \qquad m_{jj} > 600 \text{ GeV}, \qquad y_1 y_2 < 0, \tag{5.13}$$

which aim to suppress background from other channels while still capturing most of the cross section.

In YR4 [63], the rapidity acceptance on each of the two tagging jets was set to be of $|y| < 5$. In Fig. 5.10 and Fig. 5.11 we show the fraction of events that are lost depending on the y-acceptance of the detector for three different choices of the cut on the transverse momentum of the tagging jets. An event is considered lost if

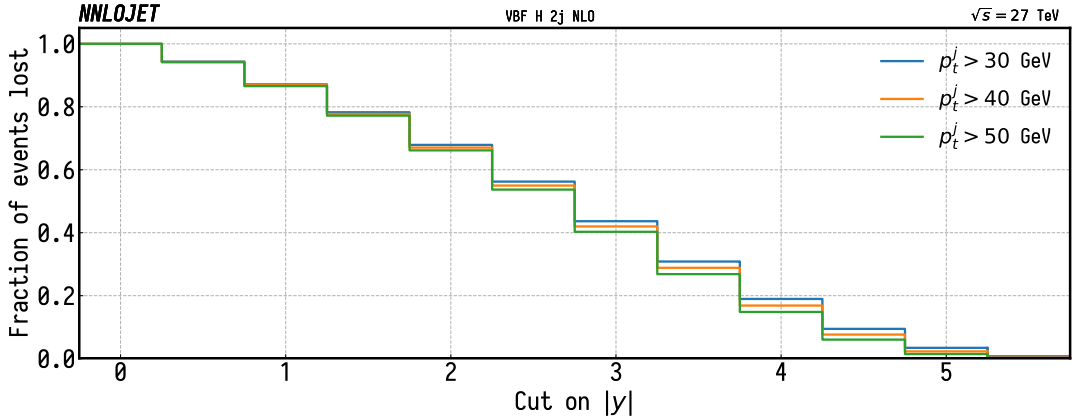

Figure 5.10: Fraction of events lost as a function of the acceptance in rapidity of the detector. Non-tagging jets can have any value of the rapidity. Only **minimal** VBF cuts are applied in this case, we observe the acceptance to be less punishing for a bigger cut on the transverse momentum.

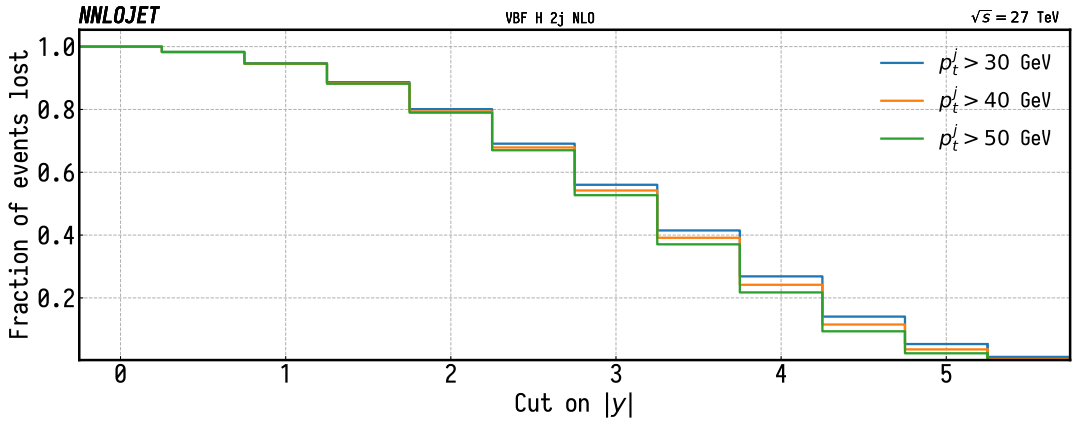

Figure 5.11: Fraction of events lost as a function of the acceptance in rapidity of the detector. Non-tagging jets can have any value of the rapidity. In contrast to Fig. 5.10, **tight** VBF cuts are applied in this case. The effect of the tighter VBF cuts is to move a bigger (relative to minimal cuts) fraction of event outside of the detector limits.

the absolute value of the rapidity of any of the two tagging jet falls outside the cut, i.e., for y-acceptance equal to 0, 100% of the events are lost. In Fig. 5.10 we impose the minimal VBF cuts of Eq. (5.12) whereas in Fig. 5.11 we impose the tighter cuts presented in Eq. (5.13). The differences between Fig. 5.10 and Fig. 5.11 are small. We find more events are lost for the smallest choice of the transverse momentum cut. This can be easily understood as reducing the cut on the transverse momentum of the jets will allow more very forward jets to pass the selection cuts. Since most events have a maximum rapidity of $|y| < 5$ we keep the YR4 choice. All events then must present two jets such that,

$$|y_j| < 5, \qquad p_T^j > 30 \text{ GeV}. \tag{5.14}$$

	σ^{NNLO}	% of inclusive
Inclusive	12443^{+123}_{-3} ± 2	100%
Minimal VBF Cuts	5044^{+50}_{-9} ± 6	41 %
Tight VBF Cuts	3054^{+35}_{-3} ± 8	25 %

Table 5.3: Total VBF-2j cross section at NNLO for a center of mass energy of $\sqrt{s} = 27$ TeV for three different choices of cuts. Inclusive imposes no cuts at all while minimal corresponds to the cuts of Eq. (5.12) and tight to the cuts of Eq. (5.13). Inclusive results obtained with proVBFH, all others with NNLOJET.

In Table 5.3 we study the effect of different choices of cuts in the total cross section. Note that although the choice of tight VBF cuts of Eq. (5.13) is more restrictive (through the cut on the transverse momentum of the jets) than those of Section 5.1, the ratio of accepted events (25% at 27 TeV vs 22% at 13 TeV) is very similar.

We begin by studying the kinematical properties of the Higgs boson, shown in Fig. 5.12. At 27 TeV we expect a wider range of the Higgs boson transverse momentum to be accessible. We find the NLO corrections to be moderate and negative, ranging between ∼10 and ∼20% relative to LO for low values of p_T^H and for most of the rapidity spectrum of the Higgs boson. At high p_T^H the NLO corrections grow considerably. The NNLO corrections are much more moderate, staying below

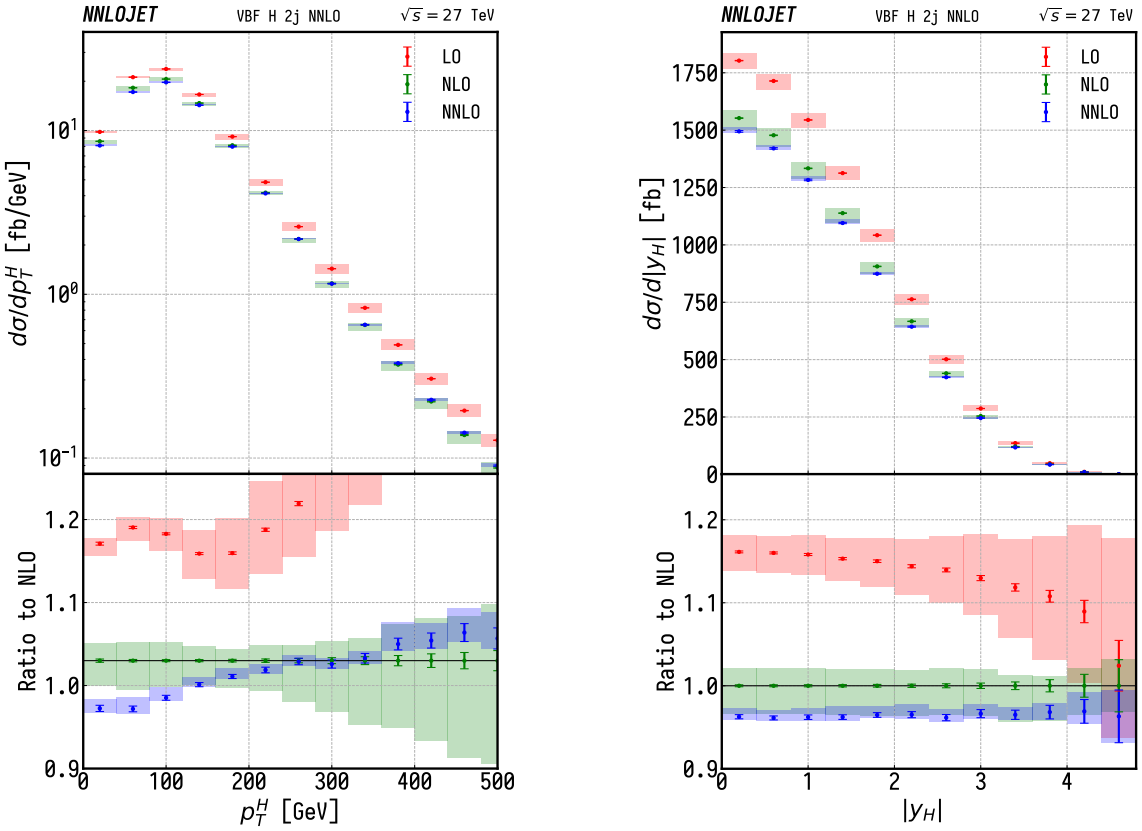

Figure 5.12: Differential distributions for the transverse momentum (left) and absolute rapidity (right) of the Higgs boson at $\sqrt{s} = 27$ TeV. Error-bars correspond exclusively to statistical errors. We find the NNLO to considerably reduce the scale uncertainties at larger values of p_T^H.

5% in magnitude relative to NLO over the entire range of the distributions, negative for low p_T^H and positive at high p_T^H. The scale uncertainties at NNLO are considerably reduced.

In Fig. 5.13 we perform the study of the transverse momentum and absolute rapidity of the two tagging jets. We find a very similar behaviour for both tagging jets. The NLO corrections are bigger in magnitude (albeit negative) for larger values of the transverse momentum. The NNLO corrections range from a moderate negative 5% to negligible at larger p_T^j, where they are compatible with 0. The distributions for the absolute rapidity of the jets tell a similar story as the Higgs boson rapidity distribution, with a roughly constant negative correction of $\sim$5% relative to NLO over the entire range of rapidity.

We conclude the study with the differential distributions related to the dijet system formed by the two tagging jets, shown in Fig. 5.14. The NLO corrections greatly change the shape of the rapidity gap Δy_{jj}, in contrast the NLO correction to the dijet invariant mass m_{jj} is a roughly constant -15%. The NNLO corrections are found to be moderate for both observables, staying at about a -5% relative to NLO for the entire range of the observables.

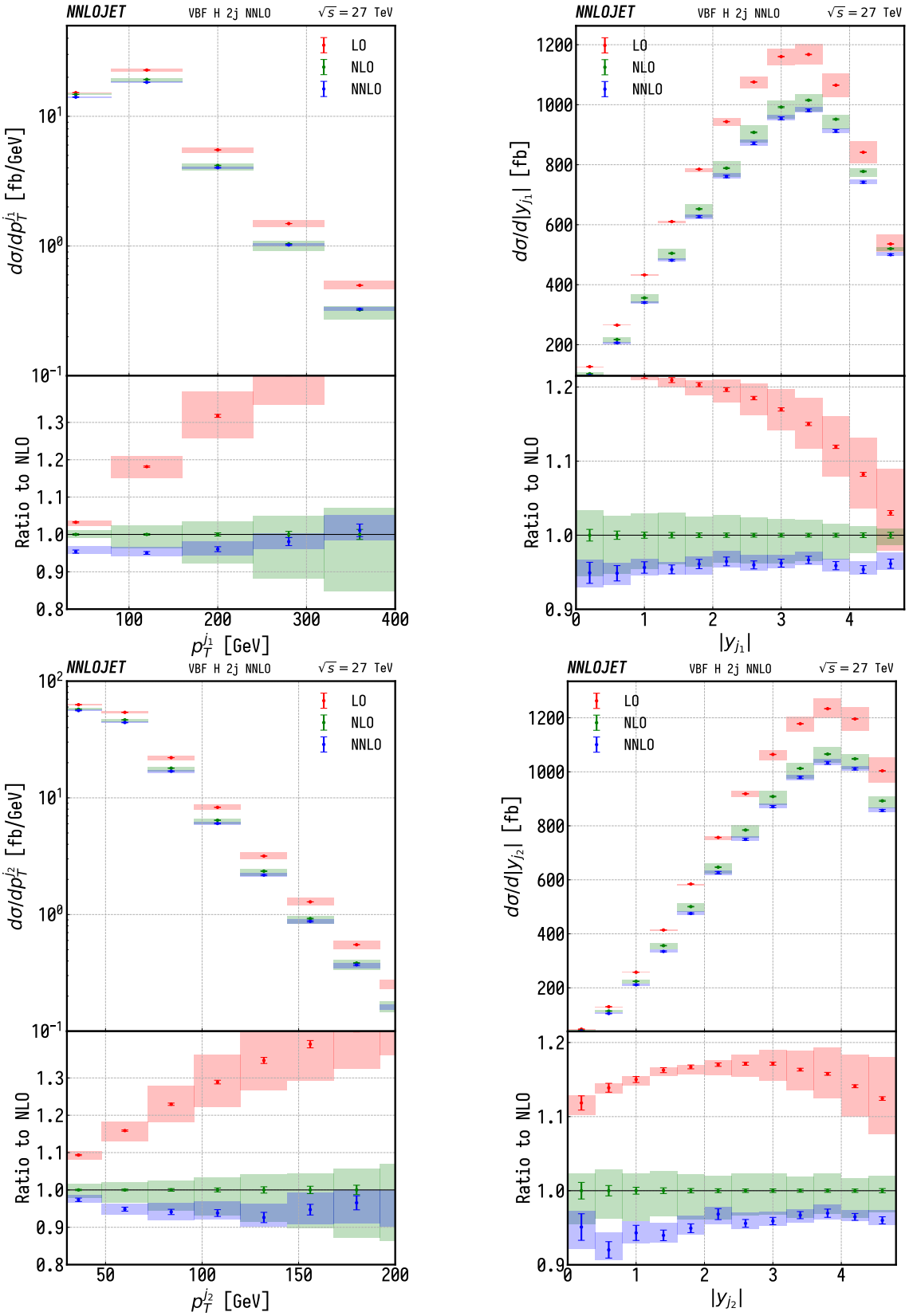

Figure 5.13: Differential distributions for the transverse momentum (left) and absolute rapidity (right) of the two tagging jets. The top row corresponds to the leading (ordered in p_T^j) jet while the bottom row corresponds to the subleading jet. NLO scale uncertainties are moderate for most the rapidity spectrum and large at high p_T^j, NNLO corrections greatly reduce scale uncertainties.

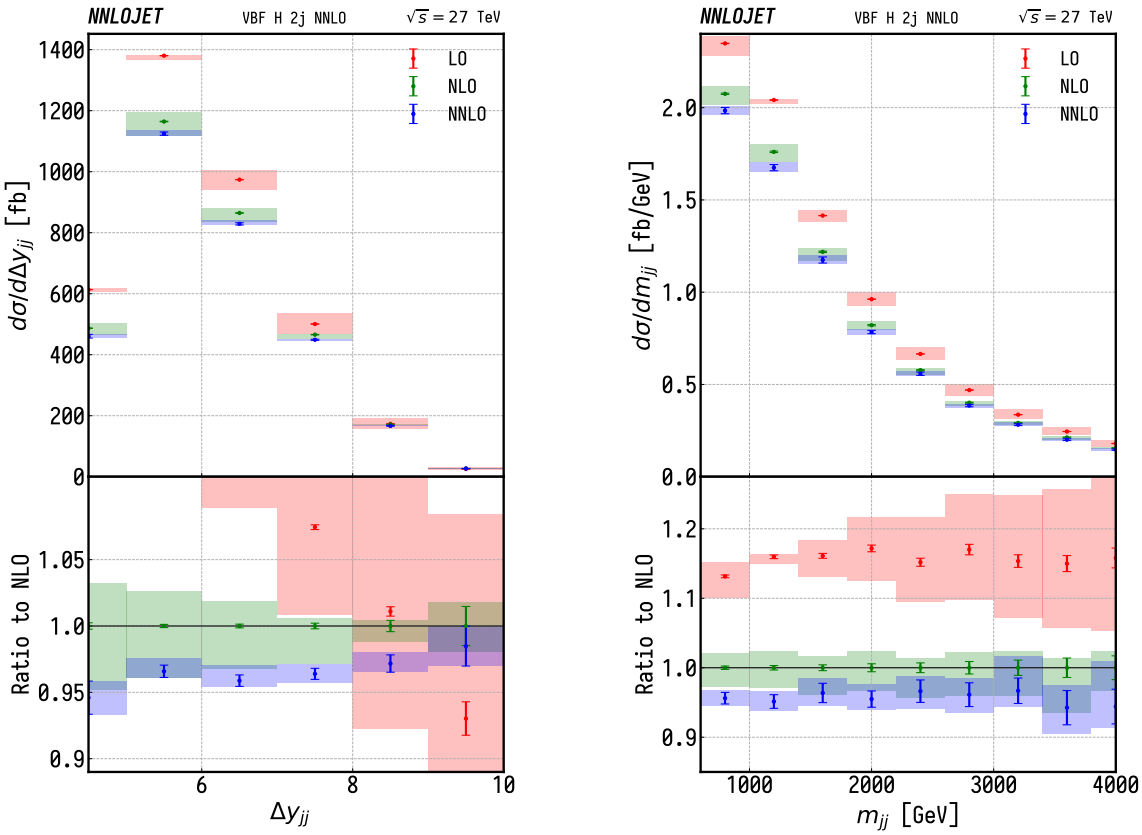

Figure 5.14: Differential distributions for the spatial distribution of the two tagging jets as well as the invariant mass of the dijet system. NLO and NNLO corrections noticeably reduce the scale uncertainties for both observables over the entire range considered.

Chapter 6

Conclusions

We have detailed the computation and implementation of the Higgs plus two jets process at NNLO via Vector Boson Fusion in the DIS approximation in NNLOjet.

As with other processes included in NNLOjet, VBF Higgs uses the antenna subtraction formalism to put infrared singularities under control.

VBF Higgs is a very complicated calculation, with 3 particles in the final state at leading order. Furthermore it is the first process in NNLOjet with more than one electroweak gauge bosons attached to the participating particles. This has led to a number of improvements and modifications to the code.

Among the work to NNLOjet realised within this thesis we can highlight the phase space generator aimed at softening the singular regions and improve convergence and the changes to the integration algorithm which allow for scalability. In Appendix D pyHepGrid is presented, a code built around NNLOjet (but easily extensible) to run applications in distributed environments.

Higgs plus two jets at NNLO and Higgs plus three jets at NLO had been computed prior to this thesis. However, these very complicated calculations proved to be flawed. Thus we claim we present the first validated calculation for both processes. This validation has been achieved by a suite of closure tests within NNLOjet as extensively described within this report as well as checks against external tools whenever possible.

We have independently implemented all relevant matrix elements for the VBF Higgs process at NNLO in the NNLOJET process library. This includes all possible combinations of amplitudes at leading order and DIS-like diagrams at higher orders. We have also built all the necessary subtraction terms using the antenna subtraction formalism.

The improvements to the NNLOJET code and the generalisation of the suite of validation tests will prove useful for future calculations using the NNLOJET framework.

Phenomenologically speaking, the importance of this process lies in its relevance for the detailed study of the newly found Higgs boson parameters. It is the second most important channel at hadron colliders such as the LHC. It will also become a crucial ingredient in future more energetic colliders (or in the very High Luminosity LHC) as demonstrated by the interests of the different experimental groups on finding the best possible selection cuts. We have presented the preliminary findings of a study done in the context of the HE/HL working group.

There are several possible extensions to this work that are being developed at the moment: the calculation of the NNLO corrections to the Higgs plus three jets process in VBF and the calculation of the differential N^3LO corrections to Higgs plus two jets. These are natural extensions to the work presented on this thesis that take advantage of the work realised in NNLOJET.

This work is a step forward on cementing the NNLO revolution that has happened in the last few years. NNLOJET aims to be the standard tool for fixed order calculations in the NNLO age. The extensive library of process, the many efficiency improvements and the strong suite of validation tests will be extremely valuable in the years (and colliders) to come.

Appendices

Appendix A

Maple input file

In this appendix we present a runcard for the maple autogeneration script `makeproc`. This script was already mentioned in Section 4.1.3 and it generates Fortran files in order to add and link a process to NNLOJET. This runcard, `VFH.map`, defines the autogeneration of the Fortran subroutines necessary to implement a process in NNLOJET. We use `monospace font` to write the lines of actual code and normal font to explain what those lines mean.

VFH.map

The first line in the runcard defines the Leading order multiplicative factor, `Ofac`. The constant `ave` stands for spin and colour average and is automatically computed by NNLOJET. The variable `amz` corresponds to $\alpha_{ew}(m_z^2)$, `nc` to the number of colours (3) and `pi` to the number π.

```
Ofac:="ave*(4d0*pi*amz)**3*nc**2/2d0";
```

The following set of lines defines the partonic content of the process. In this case it is necessary to distinguish between up and down-type quarks due to the different couplings of the Z boson. The parameters `nf, ndown` and `nup` are defined in NNLOJET as `5, 3` and `2` respectively. For instance, we only allow a number of down-type quarks equal to the number of up-type quarks for W fusion since we do

not include top quarks and must thus suppress the bottom quark as well.

```
parset:=u,ub,d,db,q,qb,Q,Qb,g:
psymset:=[g,q,qb]:
dressZ1:=q=u,qb=ub,nqqb=nup,q=d,qb=db,nqqb=ndown:
dressZ2:=Q=u,Qb=ub,nQQb=nup,Q=d,Qb=db,nQQb=ndown:
dressW1:=q=u,qb=db,nqqb=nup:
dressW2:=Q=d,Qb=ub,nQQb=nup:
dress3:=R=R,Rb=Rb,nRRb=nf,R=R,Rb=Rb,nRRb=nf:
```

Finally we define the content of the process in terms of the matrix elements and their partonic content. Each `LO, R1, ...` correspond to a different layer of the process. Each is formed by a list of lists defining each matrix element, containing:

1. The Fortran name of the function defining the matrix element.
2. The content of the matrix element in the order it should be fed to the function as positional arguments.
3. Any extra factors required for the matrix element. In this case, only colour factors.

The `makeproc` script generates a call for every possible combination of initial states attending to the argument order given in the list. In order to activate the DIS approach in NNLOJET we need the flag `keepannihil` set to `"no"` so $q\bar{q}$-initiated configurations are discarded when they correspond to colour connected states.

```
keepannihil:="no":
LO:=[
[C0g0ZFH,[qb,Q,Qb,q,ph1,ph2],1],
[C0g0WFH,[qb,Q,Qb,q,ph1,ph2],1]
]:
R1:=[
[sC1g0ZFH,[qb,g,Q,Qb,q,ph1,ph2],(nc**2-1)/nc**2],
```

```
[sC1g0WFH,[qb,g,Q,Qb,q,ph1,ph2],(nc**2-1)/nc**2]
]:
V1:=[
[C0g1ZFH,[qb,Q,Qb,q,ph1,ph2],(nc**2-1)/nc**2],
[C0g1WFH,[qb,Q,Qb,q,ph1,ph2],(nc**2-1)/nc**2]
]:
RR:=[
[sC2g0ZFH, [qb,g,g,Q,Qb,q,ph1,ph2], (nc**2-1)/nc**2],
[sC2g0WFH, [qb,g,g,Q,Qb,q,ph1,ph2], (nc**2-1)/nc**2],
[sCt2g0ZFH,[qb,gt,gt,Q,Qb,q,ph1,ph2],-(nc**2-1)/nc**4],
[sCt2g0WFH,[qb,gt,gt,Q,Qb,q,ph1,ph2],-(nc**2-1)/nc**4],
[E0g0ZFH, [qb,Q,Qb,q,R,Rb,ph1,ph2], (nc**2-1)/nc**3],
[E0g0WFH, [qb,Q,Qb,q,R,Rb,ph1,ph2], (nc**2-1)/nc**3],
[F0g0ZFH, [qb,Q,Qb,q,R,Rb,ph1,ph2], (nc**2-1)/nc**4/nf],
[F0g0WFH, [qb,Q,Qb,q,R,Rb,ph1,ph2], (nc**2-1)/nc**4/nf]
]:
RV:=[
[sC1g1ZFH, [qb,g,Q,Qb,q,ph1,ph2], (nc**2-1)/nc**2],
[sC1g1WFH, [qb,g,Q,Qb,q,ph1,ph2], (nc**2-1)/nc**2],
[sCt1g1ZFH, [qb,g,Q,Qb,q,ph1,ph2],-(nc**2-1)/nc**4],
[sCt1g1WFH, [qb,g,Q,Qb,q,ph1,ph2],-(nc**2-1)/nc**4],
[sCh1g1ZFH, [qb,g,Q,Qb,q,ph1,ph2], (nc**2-1)/nc**3*nf],
[sCh1g1WFH, [qb,g,Q,Qb,q,ph1,ph2], (nc**2-1)/nc**3*nf]
]:
VV:=[
[C0g2ZFH, [qb,Q,Qb,q,ph1,ph2], (nc**2-1)/nc**2],
[C0g2WFH, [qb,Q,Qb,q,ph1,ph2], (nc**2-1)/nc**2],
[Ct0g2ZFH, [qb,Q,Qb,q,ph1,ph2],-(nc**2-1)/nc**4],
[Ct0g2WFH, [qb,Q,Qb,q,ph1,ph2],-(nc**2-1)/nc**4],
```

```
[Ch0g2ZFH, [qb,Q,Qb,q,ph1,ph2], (nc**2-1)/nc**3*nf],
[Ch0g2WFH, [qb,Q,Qb,q,ph1,ph2], (nc**2-1)/nc**3*nf]
]:
XX:=[LO, R1, V1, RR, RV, VV]:
```

Appendix B

Relevant Antennae

In this appendix we list all antennae used in the computation of the NNLO corrections to the VBF process. The appear in the construction of the subtraction terms in Appendix C.

The first column of the table is the notation in which they are written in the Maple pseudocode, while the second column is the name in which they appear in the autogenerated Fortran files. The third column shows the notation in which the antennae are represented in this document. The last column offer some more information when it is relevant or necessary as well as point to the original publications for the antennae.

These tables have also been autogenerated with the NNLOJET autogeneration routines.

B.1 $X_3^0(i_1, i_2, i_3)$ antennae

Maple	Fortran/Form	Latex	comment
`A30FF`	`FullA30FF`	A_3^0	Eq. (5.5) of [34].
`D30FF`	`FullD30FF`	D_3^0	Eq. (6.8) of [34]. $D_3^0 = d_3^0(i_1, i_2, i_3) + d_3^0(i_1, i_3, i_2)$.
`d30FF`	`d30FF`	d_3^0	Eq. (6.13) of [34]. Only has i_2 soft limit.
`E30FF`	`FullE30FF`	E_3^0	Eq. (6.14) of [34].

Maple	Fortran/Form	Latex	comment
gA30IF	FullgA30IF	$A^0_{3,g\to q}$	Eq. (4.25) of [43]. Mixed flavour changing. $A^0_{3,g} = a^0_{3,g\to q}(i_1, \hat{i}_2, i_3) + a^0_{3,g\to q}(i_3, \hat{i}_2, i_1)$.
ga30IFgtoq	ga30IFGTOQ	$a^0_{3,g\to q}$	Only contains $i_1 \| i_2$ collinear limit. Flavour changing $g \to q$.
gd30IF	gd30IF	$d^0_{3,g}$	Eq. (4.29) of [43]. i_3 initial state i_2 soft.
qA30IF	FullqA30IF	$A^0_{3,q}$	Eq. (4.15) of [43].
qD30IF	FullqD30IF	$D^0_{3,q}$	Eq. (4.17) of [43]. $D^0_{3,q} = d^0_{3,q}(\hat{i}_1, i_2, i_3) + d^0_{3,q}(\hat{i}_1, i_3, i_2)$.
qd30IF	qd30IF	$d^0_{3,q}$	Only contains $i_1 \| i_2$ collinear limit.

Maple	Fortran/Form	Latex	comment
qgA30II	FullqgA30II	$A^0_{3,qg\to qq}$	Crossing of A^0_3. Flavour changing $g \to q$.
qqA30II	FullqqA30II	$A^0_{3,q\bar{q}}$	Crossing of A^0_3.
qqpE30II	FullqqpE30II	$E^0_{3,qq'\to qg}$	Crossing of E^0_3. Flavour changing $q' \to g$.

B.2 $X_4^0(i_1, i_2, i_3, i_4)$ antennae

Maple	Fortran/Form	Latex	comment
A40	FullA40	A^0_4	Eqs. (5.27) and (5.29) of [34].
At40	FullAt40	$\tilde{A}^0_4$	Eqs. (5.28) and (5.30) of [34].
B40	FullB40	B^0_4	Eqs. (5.37) and (5.38) of [34].
C40	FullC40	C^0_4	Eqs. (5.42) and (5.43) of [34].

B.3 $X_3^1(i_1, i_2, i_3)$ antennae

Maple	Fortran/Form	Latex	comment
`A31FF`	`FullA31FF`	A_3^1	Eqs. (5.12) and (5.13) of [34].
`Ah31FF`	`FullAh31FF`	$\hat{A}_3^1$	Eqs. (5.16) and (5.17) of [34].
`gA31IF`	`FullgA31IF`	$A_{3,g}^1$	Crossing of A_3^1. Mixed flavour changing.
`gAh31IF`	`FullgAh31IF`	$\hat{A}_{3,g}^1$	Crossing of $\hat{A}_3^1$. Mixed flavour changing.
`gAt31IF`	`FullgAt31IF`	$\tilde{A}_{3,g}^1$	Crossing of $\tilde{A}_3^1$. Mixed flavour changing.
`qA31IF`	`FullqA31IF`	$A_{3,q}^1$	Crossing of A_3^1.
`qAh31IF`	`FullqAh31IF`	$\hat{A}_{3,q}^1$	Crossing of $\hat{A}_3^1$.
`qAt31IF`	`FullqAt31IF`	$\tilde{A}_{3,q}^1$	Crossing of $\tilde{A}_3^1$.

B.4 $\mathcal{X}_3^0(i_1, i_2)$ antennae

Maple	Fortran/Form	Latex	comment
`calA30FF`	`A30FFint`	$\mathcal{A}_3^0$	Eq. (5.6) of [34].
`calD30FF`	`D30FFint`	$\mathcal{D}_3^0$	Eq. (6.9) of [34].
`calE30FF`	`E30FFint`	$\mathcal{E}_3^0$	Eq. (6.14) of [34].

Maple	Fortran/Form	Latex	comment
`calgA30IF`	`gA30IFint`	$\mathcal{A}_{3,g\to q}^0$	Eq. (4.26) of [43]. Flavour changing $g \to q$.
`calgD30gqIF`	`gD30gqIFint`	$\mathcal{D}_{3,g\to g}^0$	Eq. (4.31) of [43].
`calgD30qgIF`	`gD30qgIFint`	$\mathcal{D}_{3,g\to q}^0$	Eq. (4.30) of [43]. Flavour changing $g \to q$.
`calqA30IF`	`qA30IFint`	$\mathcal{A}_{3,q}^0$	Eq. (4.16) of [43].
`calqD30IF`	`qD30IFint`	$\mathcal{D}_{3,q}^0$	Eq. (4.20) of [43].

Maple	Fortran/Form	Latex	comment
calggD301II	ggD301IIint	$\mathcal{D}^0_{3,gg\to qg}$	Eq. (5.26) of [43] with $x_1 \leftrightarrow x_2$. Flavour changing $g \to q$ in P_1.
calggD302II	ggD302IIint	$\mathcal{D}^0_{3,gg\to gq}$	Eq. (5.26) of [43]. Flavour changing $g \to q$ in P_2.
calqgA30II	qgA30IIint	$\mathcal{A}^0_{3,qg\to qq}$	Eq. (5.23) of [43]. Flavour changing $g \to q$ in P_2.
calqqA30II	qqA30IIint	$\mathcal{A}^0_{3,qq}$	Eq. (5.24) of [43].
calqqpE30II	qqpE30IIint	$\mathcal{E}^0_{3,qq'\to qg}$	Eq. (5.28) of [43]. Flavour changing $q \to g$ in P_2.

B.5 $\mathcal{X}_3^1(i_1,i_2)$ antennae

Maple	Fortran/Form	Latex	comment
calgA31IF	gA31IFint	$\mathcal{A}^1_{3,g}$	Eq. (6.4) of [47].
calgAh31IF	gAh31IFint	$\hat{\mathcal{A}}^1_{3,g}$	Eq. (6.6) of [47].
calgAt31IF	gAt31IFint	$\tilde{\mathcal{A}}^1_{3,g}$	Eq. (6.5) of [47].
calqA31IF	qA31IFint	$\mathcal{A}^1_{3,q}$	Eq. (5.9) of [47].
calqAh31IF	qAh31IFint	$\hat{\mathcal{A}}^1_{3,q}$	Eq. (5.11) of [47].
calqAt31IF	qAt31IFint	$\tilde{\mathcal{A}}^1_{3,q}$	Eq. (5.10) of [47].

B.6 $\mathcal{X}_4^0(i_1,i_2)$ antennae

Maple	Fortran/Form	Latex	comment
calgA40IF	gA40IFint	$\mathcal{A}^0_{4,g}$	gA40. Eq. (6.2) of [47].
calgAt40IF	gAt40IFint	$\tilde{\mathcal{A}}^0_{4,g}$	gAt40. Eq. (6.3) of [47].
calqA40IF	qA40IFint	$\mathcal{A}^0_{4,q}$	qA40. Eq. (5.2) of [47].
calqAt40IF	qAt40IFint	$\tilde{\mathcal{A}}^0_{4,q}$	qAt40. Eq. (5.3) of [47].
calqB40IF	qB40IFint	$\mathcal{B}^0_{4,q}$	qB40. Eq. (5.4) of [47].
calqC40IF	qC40IFint	$\mathcal{C}^0_{4,q}$	qC40a. Eq. (5.6) of [47].
calqbC40IF	qbC40IFint	$\mathcal{C}^0_{4,\bar{q},\bar{q}q\bar{q}}$	qC40b. Eq. (5.7) of [47].
calqbbC40IF	qbbC40IFint	$\mathcal{C}^0_{4,\bar{q},q\bar{q}\bar{q}}$	qC40c. Eq. (5.8) of [47].

B.7 Mass factorisation terms, $\Gamma^n_{ab}(z)$

Maple	Fortran/Form	Latex	comment
gamma1gg	gamma1gg	$\Gamma^{(1)}_{gg}$	
gamma1ggF	gamma1ggF	$\Gamma^{(1)}_{gg,F}$	
gamma1gq	gamma1gq	$\Gamma^{(1)}_{gq}$	
gamma1qg	gamma1qg	$\Gamma^{(1)}_{qg}$	
gamma1qq	gamma1qq	$\Gamma^{(1)}_{qq}$	

Maple	Fortran/Form	Latex	comment
gamma2qQ	gamma2qQ	$\Gamma^{(2)}_{qQ}$	Eq. (A.23) of [21].
gamma2qQB	gamma2qQB	$\Gamma^{(2)}_{q\bar{Q}}$	Eq. (A.24) of [21].
gamma2qg	gamma2qg	$\Gamma^{(2)}_{qg}$	Eq. (A.26) of [21].
gamma2qgF	gamma2qgF	$\Gamma^{(2)}_{qg,F}$	
gamma2qgt	gamma2qgt	$\widetilde{\Gamma}^{(2)}_{qg}$	Eq. (A.26) of [21].
gamma2qq	gamma2qq	$\Gamma^{(2)}_{qq}$	Eq. (A.21) of [21].
gamma2qqB	gamma2qqB	$\Gamma^{(2)}_{q\bar{q}}$	Eq. (A.22) of [21].
gamma2qqBt	gamma2qqBt	$\widetilde{\Gamma}^{(2)}_{q\bar{q}q}$	Eq. (A.22) of [21].
gamma2qqF	gamma2qqF	$\Gamma^{(2)}_{qq,F}$	Eq. (A.21) of [21].
gamma2qqt	gamma2qqt	$\widetilde{\Gamma}^{(2)}_{qq}$	Eq. (A.21) of [21].
gamma2qqtt	gamma2qqtt	$\widetilde{\widetilde{\Gamma}}^{(2)}_{qq}$	Eq. (A.21) of [21].

B.8 J^1_2 antennae

Maple	Fortran/Form	Latex	comment
J21QGFF	rJ21QGFF	$J^{1,FF}_{2,QG}$	
J21QQFF	rJ21QQFF	$J^{1,FF}_{2,QQ}$	
J21hQGFF	rJ21hQGFF	$\hat{J}^{1,FF}_{2,QG}$	

Maple	Fortran/Form	Latex	comment
J21GQIF	rJ21GQIF	$J^{1,IF}_{2,GQ}$	
J21QGIF	rJ21QGIF	$J^{1,IF}_{2,QG}$	
J21QQIF	rJ21QQIF	$J^{1,IF}_{2,QQ}$	
J21QQgtoqIF	rJ21QQgtoqIF	$J^{1,IF}_{2,QQ,g\to q}$	
J21hQGIF	rJ21hQGIF	$\hat{J}^{1,IF}_{2,QG}$	

Maple	Fortran/Form	Latex	comment
J21QQII	rJ21QQII	$J^{1,II}_{2,QQ}$	
J21QGqtogII	rJ21QGqtogII	$J^{1,II}_{2,QG,qq'\to qg}$	
J21QQgtoqII2	rJ21QQgtoqII2	$J^{1,II}_{2,QQ,qg\to qq}$	

B.9 The integrated NLO J-dipoles

Final-Final Integrated Antennae		
Matrix element, M^0_{n+3}	Integrated dipole, $J^{(1)}_2$	Reduced matrix element, M^0_{n+2}
$(\cdots;i_q,j_g,k_{\bar{q}};\cdots)$	$J^{(1)}_2(I_q,K_{\bar{q}})=\mathcal{A}^0_3(s_{IK})$	$(\cdots;I_q,K_{\bar{q}};\cdots)$
$(\cdots;i_q,j_g,k_g,\cdots)$	$J^{(1)}_2(I_q,K_g)=\frac{1}{2}\mathcal{D}^0_3(s_{IK})$	$(\cdots;I_q,K_g,\cdots)$
$(\cdots;i_{q'},j_{\bar{q}};k_q,\cdots)$	$\hat{J}^{(1)}_2(I_q,K_g)=\frac{1}{2}\mathcal{E}^0_3(s_{IK})$	$(\cdots;I_q,K_g,\cdots)$
$(\cdots,i_g,j_g,k_g,\cdots)$	$J^{(1)}_2(I_g,K_g)=\frac{1}{3}\mathcal{F}^0_3(s_{IK})$	$(\cdots,I_g,K_g,\cdots)$
$(\cdots,i_g,j_{\bar{q}};k_q,\cdots)$	$\hat{J}^{(1)}_2(I_g,K_g)=\mathcal{G}^0_3(s_{IK})$	$(\cdots,I_g,K_g,\cdots)$

Table B.1: The correspondence between the real radiation matrix elements, M^0_{n+3} and the integrated NLO dipoles $J^{(1)}_2$ and reduced matrix elements, M^0_{n+2} for various particle assignments and colour structures for the final-final configuration.

Initial-Final Integrated Antennae		
Matrix element, M^0_{n+3}	Integrated dipole, $J^{(1)}_2$	Reduced matrix element, M^0_{n+2}
$(\cdots;\hat{1}_q,i_g,j_{\bar{q}};\cdots)$	$J^{(1)}_2(\hat{\bar{1}}_q,J_{\bar{q}})=\mathcal{A}^0_{3,q}(s_{\bar{1}J})-\Gamma^{(1)}_{qq}(z_1)\delta_2$	$(\cdots;\hat{\bar{1}}_q,J_{\bar{q}};\cdots)$
$(\cdots;\hat{1}_q,i_g,j_g,\cdots)$	$J^{(1)}_2(\hat{\bar{1}}_q,J_g)=\frac{1}{2}\mathcal{D}^0_{3,q}(s_{\bar{1}J})-\Gamma^{(1)}_{qq}(z_1)\delta_2$	$(\cdots;\hat{\bar{1}}_q,J_g,\cdots)$
$(\cdots;\hat{1}_q,i_{\bar{q}'};j_{q'},\cdots)$	$\hat{J}^{(1)}_2(\hat{\bar{1}}_q,J_g)=\frac{1}{2}\mathcal{E}^0_{3,q,q'\bar{q}'}(s_{\bar{1}J})$	$(\cdots;\hat{\bar{1}}_q,J_g,\cdots)$
$(\cdots;i_q,j_g,\hat{1}_g,\cdots)$	$J^{(1)}_2(J_q,\hat{\bar{1}}_g)=\mathcal{D}^0_{3,g,gq}(s_{\bar{1}J})-\frac{1}{2}\Gamma^{(1)}_{gg}(z_1)\delta_2$	$(\cdots;J_q,\hat{\bar{1}}_g,\cdots)$
$(\cdots;i_q,j_g,\hat{1}_g,\cdots)$	$\hat{J}^{(1)}_2(J_q,\hat{\bar{1}}_g)=-\frac{1}{2}\hat{\Gamma}^{(1)}_{gg}(z_1)\delta_2$	$(\cdots;J_q,\hat{\bar{1}}_g,\cdots)$
$(\cdots,\hat{1}_g,i_g,j_g,\cdots)$	$J^{(1)}_2(\hat{\bar{1}}_g,J_g)=\frac{1}{2}\mathcal{F}^0_{3,g}(s_{\bar{1}J})-\frac{1}{2}\Gamma^{(1)}_{gg}(z_1)\delta_2$	$(\cdots,\hat{\bar{1}}_g,J_g,\cdots)$
$(\cdots,\hat{1}_g,i_{\bar{q}};j_q,\cdots)$	$\hat{J}^{(1)}_2(\hat{\bar{1}}_g,J_g)=\frac{1}{2}\mathcal{G}^0_{3,g}(s_{\bar{1}J})-\frac{1}{2}\hat{\Gamma}^{(1)}_{gg}(z_1)\delta_2$	$(\cdots,\hat{\bar{1}}_g,J_g,\cdots)$
$(\cdots;i_q,\hat{1}_g,j_{\bar{q}};\cdots)$	$J^{(1)}_{2,g\to q}(\hat{\bar{1}}_q,J_{\bar{q}})=-\frac{1}{2}\mathcal{A}^0_{3,g,q\bar{q}}(s_{\bar{1}J})-S_{g\to q}\Gamma^{(1)}_{qg}(z_1)\delta_2$	$(\cdots;\hat{\bar{1}}_q,J_{\bar{q}};\cdots)$
$(\cdots;i_q,\hat{1}_g,j_g,\cdots)$	$J^{(1)}_{2,g\to q}(\hat{\bar{1}}_q,J_g)=-\mathcal{D}^0_{3,g,qg}(s_{\bar{1}J})-S_{g\to q}\Gamma^{(1)}_{qg}(z_1)\delta_2$	$(\cdots;\hat{\bar{1}}_q,J_g,\cdots)$
$(\cdots;i_{q'},\hat{1}_{q'};j_q,\cdots)$	$J^{(1)}_{2,q\to g}(J_q,\hat{\bar{1}}_g)=-\mathcal{E}^0_{3,q',qq'}(s_{\bar{1}J})-S_{q\to g}\Gamma^{(1)}_{gq}(z_1)\delta_2$	$(\cdots;J_q,\hat{\bar{1}}_g,\cdots)$
$(\cdots,i_g;\hat{1}_q,j_q,\cdots)$	$J^{(1)}_{2,q\to g}(J_g,\hat{\bar{1}}_g)=-\mathcal{G}^0_{3,q}(s_{\bar{1}J})-S_{q\to g}\Gamma^{(1)}_{gq}(z_1)\delta_2$	$(\cdots,J_g,\hat{\bar{1}}_g,\cdots)$

Table B.2: The correspondence between the real radiation matrix elements, M^0_{n+3} and the integrated NLO dipoles $J^{(1)}_2$ and reduced matrix elements, M^0_{n+2} for various particle assignments and colour structures for the initial-final configuration. For brevity $\delta(1-z_i)=\delta_i$ for $i=1,2$.

Here we write the J-dipoles in terms of the combination of integated antennae and splitting kernels. They were defined in Ref. [21].

Note that, for identity preserving dipole functions, we in principle have colour leading (N) $J^{(1)}_2$ functions and the colour sub-leading functions that depend on the

Initial-Initial Integrated Antennae		
Matrix element, M^0_{n+3}	Integrated dipole, $J^{(1)}_2$	Reduced matrix element, M^0_{n+2}
$(\cdots;\hat{1}_q,i_g,\hat{2}_{\bar{q}},\cdots)$	$J^{(1)}_2(\hat{\tilde{1}}_q,\hat{\tilde{2}}_{\bar{q}}) = \mathcal{A}^0_{3,q\bar{q}}(s_{\tilde{1}\tilde{2}}) - \Gamma^{(1)}_{qq}(z_1)\delta_2 - \Gamma^{(1)}_{qq}(z_2)\delta_1$	$(\cdots;\hat{\tilde{1}}_q,\hat{\tilde{2}}_{\bar{q}};\cdots)$
$(\cdots;\hat{1}_q,i_g,\hat{2}_g,\cdots)$	$J^{(1)}_2(\hat{\tilde{1}}_q,\hat{\tilde{2}}_g) = \mathcal{D}^0_{3,qg}(s_{\tilde{1}\tilde{2}}) - \Gamma^{(1)}_{qq}(z_1)\delta_2 - \frac{1}{2}\Gamma^{(1)}_{gg}(z_2)\delta_1$	$(\cdots;\hat{\tilde{1}}_q,\hat{\tilde{2}}_g,\cdots)$
$(\cdots;\hat{1}_q,i_g,\hat{2}_g,\cdots)$	$\hat{J}^{(1)}_2(\hat{\tilde{1}}_q,\hat{\tilde{2}}_g) = \quad - \frac{1}{2}\hat{\Gamma}^{(1)}_{gg}(z_2)\delta_1$	$(\cdots;\hat{\tilde{1}}_q,\hat{\tilde{2}}_g,\cdots)$
$(\cdots,\hat{1}_g,i_g,\hat{2}_g,\cdots)$	$J^{(1)}_2(\hat{\tilde{1}}_g,\hat{\tilde{2}}_g) = \mathcal{F}^0_{3,gg}(s_{\tilde{1}\tilde{2}}) - \frac{1}{2}\Gamma^{(1)}_{gg}(z_1)\delta_2 - \frac{1}{2}\Gamma^{(1)}_{gg}(z_2)\delta_1$	$(\cdots,\hat{\tilde{1}}_g,\hat{\tilde{2}}_g,\cdots)$
$(\cdots,\hat{1}_g,i_g,\hat{2}_g,\cdots)$	$\hat{J}^{(1)}_2(\hat{\tilde{1}}_g,\hat{\tilde{2}}_g) = \quad - \frac{1}{2}\hat{\Gamma}^{(1)}_{gg}(z_1)\delta_2 - \frac{1}{2}\hat{\Gamma}^{(1)}_{gg}(z_2)\delta_1$	$(\cdots,\hat{\tilde{1}}_g,\hat{\tilde{2}}_g,\cdots)$
$(\cdots;\hat{1}_q,\hat{2}_g,i_{\bar{q}};\cdots)$	$J^{(1)}_{2,g\to q}(\hat{\tilde{1}}_q,\hat{\tilde{2}}_{\bar{q}}) = -\mathcal{A}^0_{3,qg}(s_{\tilde{1}\tilde{2}}) - S_{g\to q}\Gamma^{(1)}_{qg}(z_2)\delta_1$	$(\cdots;\hat{\tilde{1}}_q,\hat{\tilde{2}}_{\bar{q}};\cdots)$
$(\cdots;i_q,\hat{1}_g,\hat{2}_g,\cdots)$	$J^{(1)}_{2,g\to q}(\hat{\tilde{1}}_q,\hat{\tilde{2}}_g) = -\mathcal{D}^0_{3,gg}(s_{\tilde{1}\tilde{2}}) - S_{g\to q}\Gamma^{(1)}_{qg}(z_1)\delta_2$	$(\cdots;\hat{\tilde{1}}_q,\hat{\tilde{2}}_g,\cdots)$
$(\cdots;\hat{1}_{q'},\hat{2}_{\bar{q}};i_q,\cdots)$	$J^{(1)}_{2,q\to g}(\hat{\tilde{1}}_q,\hat{\tilde{2}}_g) = -\mathcal{E}^0_{3,q'q,g}(s_{\tilde{1}\tilde{2}}) - S_{q\to g}\Gamma^{(1)}_{gq}(z_2)\delta_1$	$(\cdots;\hat{\tilde{1}}_{q'},\hat{\tilde{2}}_g,\cdots)$
$(\cdots,\hat{1}_g,\hat{2}_{\bar{q}};i_q,\cdots)$	$J^{(1)}_{2,q\to g}(\hat{\tilde{1}}_g,\hat{\tilde{2}}_g) = -\mathcal{G}^0_{3,gq}(s_{\tilde{1}\tilde{2}}) - S_{q\to g}\Gamma^{(1)}_{gq}(z_2)\delta_1$	$(\cdots,\hat{\tilde{1}}_g,\hat{\tilde{2}}_g,\cdots)$

Table B.3: The correspondence between the real radiation matrix elements, M^0_{n+3} and the integrated NLO dipoles $J^{(1)}_2$ and reduced matrix elements, M^0_{n+2} for various particle assignments and colour structures for the initial-initial configuration. For brevity $\delta(1-z_1)=\delta_1$, $\delta(1-z_2)=\delta_2$.

number of quark flavours, (N_F), notated $\hat{J}^{(1)}_2$. In the final-final case, the dipole functions only contain integrated antenna functions. In the initial-final and initial-initial spectator cases, in general, the dipole functions contain both integrated antenna functions plus tree-level mass factorisation contributions. For identity changing antennae we must take into account a spin averaging factor associated with the mass factorisation term that accommodates the fact that the number degrees of freedom in D-dimensions for a gluon differs from that of a quark. Explicitly we have,

$$S_{g\to q} = \frac{S_g}{S_q} = 1-\epsilon, \tag{B.1}$$

$$S_{q\to g} = \frac{S_q}{S_g} = \frac{1}{1-\epsilon}. \tag{B.2}$$

Appendix C

Subtraction terms

C.1 NLO: R

Let us take the first of the R subtraction terms as an example in order to define the notation and conventions used in this appendix. This is the subtraction term "`qqpsC1g0ZFHSNLO`", which regulates the limits of Fig. C.1 and is shown in Eq. (C.4).

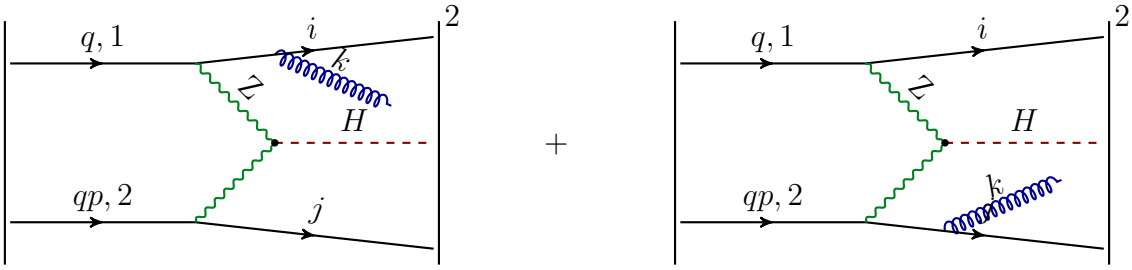

Figure C.1: Real emission matrix element squared `sC1g0ZFH` $= sC^0_{1g}$, which is a sum over the gluon being emitted from the upper and lower currents.

Let us begin with the naming convention of the subtraction term, `qqpsC1g0ZFHSNLO`. All subtraction terms refer to the matrix element they are subtracting (blue) as well as the level at which they enter (red), in this case SNLO, the S subtraction term for NLO, when the level is not written explicitly it is assumed to be a NNLO term. The prefix of the subtraction term (green) refers to the initial state, in this case q and $q' \equiv qp$. The label "ZFH" or "WFH" in the matrix element indicates whether this is a Z-fusion or a W-fusion matrix element.

The argument list, $(1, k, j, 2, i, H)$, have a direct relation with the naming convention of the particles in Fig. C.1. Particles (1,2) are always the initial partons and H the Higgs boson. The indices (i, j, k) are dummy indices and they always correspond to f.s. partons, in general for VBF we use i, j for quarks and k, l for gluons.

This subtraction term consists of only two lines, with a clear correspondence between them through the change $(1, i) \to (2, j)$,

$$\begin{aligned} &\texttt{qqpsC1g0ZFHSNLO}(\texttt{1},\texttt{k},\texttt{j},\texttt{2},\texttt{i},\texttt{H}) = \\ &\quad + A^0_{3,q}(1,k,i)\,\texttt{C0g0ZFH}(\overline{1},j,2,(\widetilde{ik}),H)\,J^{(2)}_2(\{p\}_2) \\ &\quad + A^0_{3,q}(2,k,j)\,\texttt{C0g0ZFH}(1,(\widetilde{jk}),\overline{2},i,H)\,J^{(2)}_2(\{p\}_2). \end{aligned} \tag{C.1}$$

In the first line of Eq. (C.1) the antenna $A^0_{3,q}(1, k, i)$ contains the collinear limits $1||k$, $k||i$ as well as the soft limit $k \to 0$, all limits of the left-hand side diagram of Fig. C.1. The second line in turn contains the corresponding limits for the diagram in the right.

The antenna is multiplying a reduced matrix element $\texttt{C0g0ZFH} = C^0_{0g}$ with a reduced momentum set such that partons i and k are mapped together into a single parton $\widetilde{ik}$. This mapping fulfills the conditions for the factorisation of the phase space in the limits, both in the collinear limit between i and k (notated $\widetilde{ik}$ or between k and 1 (represented as $\overline{1}$). Finally the jet selector function is as defined in Eq. (2.63), where from two final partons (j and $\widetilde{ik}$ in this case) two jets have to be found. In Fig. C.2 we present a more graphical representation of the subtraction term seen in Eq. (C.1).

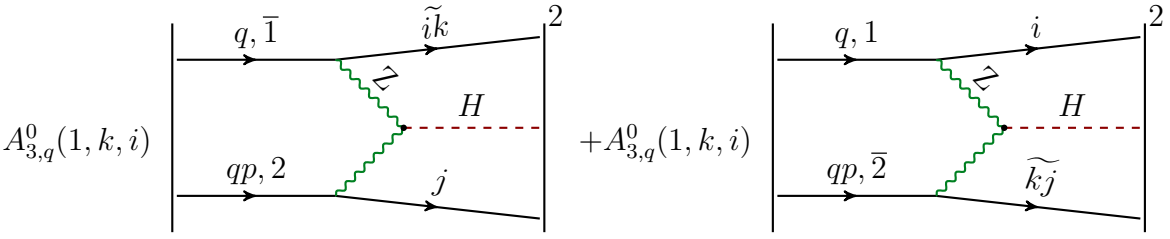

Figure C.2: Subtraction term of Eq. (C.1) where we show the reduced matrix element graphically for clarity.

Finally let us note an important difference between gluon-initiated and quark-initiated matrix elements. In Section 3.3.3, Eq. (3.25) we defined $\mathrm{s}C^0_{1g}$ as a way of simplify the notation of the subtraction terms. This simplification will now be made explicit using as an example the gluon-initiated matrix element whose subtraction term is shown in Eq. (C.5), `qgsC1g0ZFHSNLO`, which subtracts the matrix element `sC1g0ZFH`.

Let us begin with the subtraction term corresponding to a matrix element $\texttt{C1g0ZFH}(1,2,k,j,i,H)$. This is a gluon-initiated subtraction term where there are two possible singular limits: $2||k$ and $2||j$. These two limits factorise onto two different Born-level matrix element: the quark-quark initiated $\texttt{C0g0ZFH}(1,(\widetilde{jk}),\overline{2},i,H)$ and the quark-antiquark initiated $\texttt{C0g0ZFH}(1,\overline{2},(\widetilde{jk}),i,H)$:

$$\texttt{qgC1g0ZFHSNLO}(1,2,\mathtt{k},\mathtt{j},\mathtt{i},\mathtt{H}) =$$
$$-\frac{1}{2}A^0_{3,g\to q}(k,2,j)\left(\texttt{C0g0ZFH}(1,\overline{2},(\widetilde{jk}),i,H)+\texttt{C0g0ZFH}(1,(\widetilde{jk}),\overline{2},i,H)\right)J^{(2)}_2(\{p\}_2).$$

This is exactly the same subtraction term which would be needed for the matrix element $\texttt{C1g0ZFH}(1,2,j,k,i,H)$. It is then convenient to define a symmetrised version of the matrix element, $\texttt{sC1g0ZFH}(1,2,k,j,i,H)$, as

$$\texttt{sC1g0ZFH}(1,2,k,j,i,H) = \texttt{C1g0ZFH}(1,2,k,j,i,H)+\texttt{C1g0ZFH}(1,2,j,k,i,H), \quad \text{(C.2)}$$

with the coresponding subtraction term,

$$\texttt{qgsC1g0ZFHSNLO}(1,2,\mathtt{k},\mathtt{j},\mathtt{i},\mathtt{H}) =$$
$$-A^0_{3,g\to q}(k,2,j)\left(\texttt{C0g0ZFH}(1,\overline{2},(\widetilde{jk}),i,H)+\texttt{C0g0ZFH}(1,(\widetilde{jk}),\overline{2},i,H)\right)J^{(2)}_2(\{p\}_2).$$

In order to simplify the notation we can also define the LO combination,

$$\texttt{sC0g0ZFH}(1,2,j,i,H) = \texttt{C0g0ZFH}(1,2,j,i,H)+\texttt{C0g0ZFH}(1,j,2,i,H), \quad \text{(C.3)}$$

which is used in Eq. (C.5). The symmetrised matrix elements are extensively used in the construction of the subtraction terms.

qqpsC1g0ZFHSNLO(1,k,j,2,i,H)

$$\begin{aligned}
&\texttt{qqpsC1g0ZFHSNLO}(1,\texttt{k},\texttt{j},2,\texttt{i},\texttt{H}) = \\
1 \quad &+A^0_{3,q}(1,k,i)\,\texttt{C0g0ZFH}(1,j,2,(\widetilde{ik}),H)\,J^{(2)}_2(\{p\}_2) \\
2 \quad &+A^0_{3,q}(2,k,j)\,\texttt{C0g0ZFH}(1,(\widetilde{jk}),\overline{2},i,H)\,J^{(2)}_2(\{p\}_2)
\end{aligned} \tag{C.4}$$

qgsC1g0ZFHSNLO(1,2,k,j,i,H)

$$\begin{aligned}
&\texttt{qgsC1g0ZFHSNLO}(1,2,\texttt{k},\texttt{j},\texttt{i},\texttt{H}) = \\
1 \quad &-A^0_{3,g\to q}(k,2,j)\,\texttt{sC0g0ZFH}(1,\overline{2},(\widetilde{jk}),i,H)\,J^{(2)}_2(\{p\}_2)
\end{aligned} \tag{C.5}$$

qbgsC1g0ZFHSNLO(i,2,k,j,1,H)

$$\begin{aligned}
&\texttt{qbgsC1g0ZFHSNLO}(\texttt{i},2,\texttt{k},\texttt{j},1,\texttt{H}) = \\
1 \quad &-A^0_{3,g\to q}(k,2,j)\,\texttt{sC0g0ZFH}(i,\overline{2},(\widetilde{jk}),1,H)\,J^{(2)}_2(\{p\}_2)
\end{aligned} \tag{C.6}$$

qbqpsC1g0ZFHSNLO(i,k,j,2,1,H)

$$\begin{aligned}
&\texttt{qbqpsC1g0ZFHSNLO}(\texttt{i},\texttt{k},\texttt{j},2,1,\texttt{H}) = \\
1 \quad &+A^0_{3,q}(1,k,i)\,\texttt{C0g0ZFH}((\widetilde{ik}),j,2,1,H)\,J^{(2)}_2(\{p\}_2) \\
2 \quad &+A^0_{3,q}(2,k,j)\,\texttt{C0g0ZFH}(i,(\widetilde{jk}),\overline{2},1,H)\,J^{(2)}_2(\{p\}_2)
\end{aligned} \tag{C.7}$$

qqbsC1g0ZFHSNLO(1,k,i,j,2,H)

$$\begin{aligned}
&\texttt{qqbsC1g0ZFHSNLO}(1,\texttt{k},\texttt{i},\texttt{j},2,\texttt{H}) = \\
1 \quad &+A^0_{3,q\bar{q}}(1,k,2)\,\texttt{C0g0ZFH}(\overline{1},i,j,\overline{2},H)\,J^{(2)}_2(\{p\}_2) \\
2 \quad &+A^0_{3}(i,k,j)\,\texttt{C0g0ZFH}(1,(\widetilde{ik}),(\widetilde{jk}),2,H)\,J^{(2)}_2(\{p\}_2)
\end{aligned} \tag{C.8}$$

qbgsC1g0WFHSNLO(i,2,k,j,1,H)

$$\begin{aligned}
&\texttt{qbgsC1g0WFHSNLO}(\texttt{i},2,\texttt{k},\texttt{j},1,\texttt{H}) = \\
1 \quad &-A^0_{3,g\to q}(k,2,j)\,\texttt{sC0g0WFH}(i,(\widetilde{jk}),\overline{2},1,H)\,J^{(2)}_2(\{p\}_2)
\end{aligned} \tag{C.9}$$

qbqpsC1g0WFHSNLO(i,k,j,2,1,H)

$$\begin{aligned}
&\texttt{qbqpsC1g0WFHSNLO}(\texttt{i},\texttt{k},\texttt{j},2,1,\texttt{H}) = \\
1 \quad &+A^0_{3,q}(1,k,i)\,\texttt{C0g0WFH}((\widetilde{ik}),j,2,1,H)\,J^{(2)}_2(\{p\}_2) \\
2 \quad &+A^0_{3,q}(2,k,j)\,\texttt{C0g0WFH}(i,(\widetilde{jk}),\overline{2},1,H)\,J^{(2)}_2(\{p\}_2)
\end{aligned} \tag{C.10}$$

qgsC1g0WFHSNLO(1,2,k,j,i,H)

$$\begin{aligned}
&\texttt{qgsC1g0WFHSNLO}(1,2,\texttt{k},\texttt{j},\texttt{i},\texttt{H}) = \\
1 \quad &-A^0_{3,g\to q}(k,2,j)\,\texttt{sC0g0WFH}(1,\overline{2},(\widetilde{jk}),i,H)\,J^{(2)}_2(\{p\}_2)
\end{aligned} \tag{C.11}$$

qqbsC1g0WFHSNLO(1,k,i,j,2,H)

$$\begin{aligned}
&\texttt{qqbsC1g0WFHSNLO}(1,\texttt{k},\texttt{i},\texttt{j},2,\texttt{H}) = \\
1 \quad &+A^0_{3,q\bar{q}}(1,k,2)\,\texttt{C0g0WFH}(\overline{1},i,j,\overline{2},H)\,J^{(2)}_2(\{p\}_2) \\
2 \quad &+A^0_3(i,k,j)\,\texttt{C0g0WFH}(1,(\widetilde{ik}),(\widetilde{jk}),2,H)\,J^{(2)}_2(\{p\}_2)
\end{aligned} \tag{C.12}$$

qqpsC1g0WFHSNLO(1,k,j,2,i,H)

$$\begin{aligned}
&\texttt{qqpsC1g0WFHSNLO}(1,\texttt{k},\texttt{j},2,\texttt{i},\texttt{H}) = \\
1 \quad &+A^0_{3,q}(1,k,i)\,\texttt{C0g0WFH}(1,j,2,(\widetilde{ik}),H)\,J^{(2)}_2(\{p\}_2) \\
2 \quad &+A^0_{3,q}(2,k,j)\,\texttt{C0g0WFH}(1,(\widetilde{jk}),\overline{2},i,H)\,J^{(2)}_2(\{p\}_2)
\end{aligned} \tag{C.13}$$

C.2 NLO: V

In Appendix C.1 we detail a R subtraction term for a qq-initiated matrix element, `qqpsC1g0ZFHSNLO`. The integration of this subtraction term corresponds to the V subtraction term, `qqpC0g1ZFHTNLO`. This term removes the explicit poles from the virtual amplitudes shown in Fig. C.3.

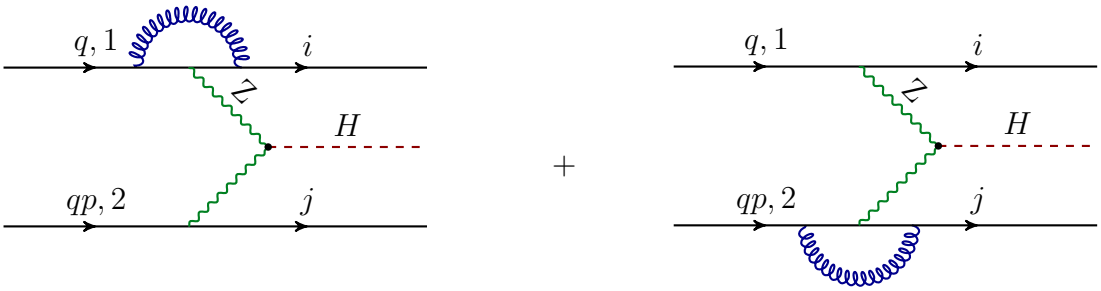

Figure C.3: Virtual amplitude corresponding to the matrix element squared `C0g1ZFH` $= C^1_{0g}$ upon interference with the tree level amplitude.

The naming convention is equal to Appendix C.1 with the only change of SNLO to TNLO to signal this is a virtual subtraction term. In Eq. (C.16) the subtraction term is written in terms of the J-dipoles defined in Appendix B.9. For clarity we write the integrated antenna and mass factorisation terms here explicitly,

$$\begin{aligned}
&\texttt{qqpC0g1ZFHTNLO}(\texttt{1},\texttt{j},\texttt{2},\texttt{i},\texttt{H}) = \\
&\quad + \left(\mathcal{A}^0_{3,q}(s_{1i}) - \Gamma^{(1)}_{qq}(z_1)\delta(1-z_2)\right)\texttt{C0g0ZFH}(\texttt{1},\texttt{j},\texttt{2},\texttt{i},\texttt{H})J^{(2)}_2(\{p\}_2) \\
&\quad + \left(\mathcal{A}^0_{3,q}(s_{2j}) - \Gamma^{(1)}_{qq}(z_2)\delta(1-z_1)\right)\texttt{C0g0ZFH}(\texttt{1},\texttt{j},\texttt{2},\texttt{i},\texttt{H})J^{(2)}_2(\{p\}_2).
\end{aligned} \tag{C.14}$$

In the first line of Eq. (C.14) we find the integrated antenna corresponding to the first line of Eq. (C.1), subtracting the poles of the left-hand diagram of Fig. C.3,

$$\mathcal{A}^0_{3,q}(s_{\bar{1}\widetilde{ik}}) = \int \mathrm{d}\Phi_X\left(p_1,p_k,p_i\right)A^0_{3,q}(1,k,i), \tag{C.15}$$

we simplify the notation in the code with $\widetilde{ik} \to i$ and $\bar{1} \to 1$ since this function depends only on $s_{\bar{1}\widetilde{ik}} \equiv s_{1i}$. The singularity in this case involves a quark in the initial state, from Eq. (2.15) it is clear the MF is just the splitting kernel for a quark initiated matrix element, $\Gamma^{(1)}_{qq}$.

qqpC0g1ZFHTNLO(1,j,2,i,H)

$$1 \qquad -\left[+ J^{1,IF}_{2,QQ}(s_{1i}) + J^{1,FI}_{2,QQ}(s_{2j}) \right] \texttt{C0g0ZFH}(1,j,2,i,H)\, J^{(2)}_2(\{p\}_2) \tag{C.16}$$

qbgC0g1ZFHTNLO(1,2,j,i,H)

$$1 \qquad -2J^{1,FI}_{2,QQ,g\to q}(s_{2j})\, \texttt{sC0g0ZFH}(i,j,2,1,H)\, J^{(2)}_2(\{p\}_2) \tag{C.17}$$

qbqpC0g1ZFHTNLO(i,j,2,1,H)

$$1 \qquad -\left[+ J^{1,IF}_{2,QQ}(s_{1i}) + J^{1,FI}_{2,QQ}(s_{2j}) \right] \texttt{C0g0ZFH}(i,j,2,1,H)\, J^{(2)}_2(\{p\}_2) \tag{C.18}$$

qgC0g1ZFHTNLO(1,2,j,i,H)

$$1 \qquad -2J^{1,FI}_{2,QQ,g\to q}(s_{2j})\, \texttt{sC0g0ZFH}(1,j,2,i,H)\, J^{(2)}_2(\{p\}_2) \tag{C.19}$$

qqbC0g1ZFHTNLO(1,j,i,2,H)

$$1 \qquad -\left[+ J^{1,II}_{2,QQ}(s_{12}) + J^{1,FF}_{2,QQ}(s_{ij}) \right] \texttt{C0g0ZFH}(1,j,i,2,H)\, J^{(2)}_2(\{p\}_2) \tag{C.20}$$

qbgC0g1WFHTNLO(1,2,j,i,H)

$$1 \qquad -2J^{1,FI}_{2,QQ,g\to q}(s_{2j})\, \texttt{sC0g0WFH}(i,j,2,1,H)\, J^{(2)}_2(\{p\}_2) \tag{C.21}$$

qbqpC0g1WFHTNLO(i,j,2,1,H)

$$1 \qquad -\left[+ J^{1,IF}_{2,QQ}(s_{1i}) + J^{1,FI}_{2,QQ}(s_{2j}) \right] \texttt{C0g0WFH}(i,j,2,1,H)\, J^{(2)}_2(\{p\}_2) \tag{C.22}$$

qgC0g1WFHTNLO(1,2,j,i,H)

$$1 \qquad -2J^{1,FI}_{2,QQ,g\to q}(s_{2j})\,\texttt{sC0g0WFH}(1,j,2,i,H)\,J^{(2)}_2(\{p\}_2) \tag{C.23}$$

qqbC0g1WFHTNLO(1,j,i,2,H)

$$1 \qquad -\Big[+J^{1,II}_{2,QQ}(s_{12})+J^{1,FF}_{2,QQ}(s_{ij})\Big]\,\texttt{C0g0WFH}(1,j,i,2,H)\,J^{(2)}_2(\{p\}_2) \tag{C.24}$$

qqpC0g1WFHTNLO(1,j,2,i,H)

$$1 \qquad -\Big[+J^{1,IF}_{2,QQ}(s_{1i})+J^{1,FI}_{2,QQ}(s_{2j})\Big]\,\texttt{C0g0WFH}(1,j,2,i,H)\,J^{(2)}_2(\{p\}_2) \tag{C.25}$$

C.3 NNLO: RR

ggsC2g0ZFHSs1(l,1,2,j,k,i,H)

$$\texttt{ggsC2g0ZFHSs1}(\texttt{l},1,2,\texttt{j},\texttt{k},\texttt{i},\texttt{H}) =$$

$$\begin{aligned}
1 \quad & -a^0_{3,g\to q}(i,1,l)\,\texttt{C1g0ZFH}((\widetilde{li}),2,j,k,\overline{1},H)\,J^{(3)}_2(\{p\}_3)\\
2 \quad & -a^0_{3,g\to q}(l,1,i)\,\texttt{C1g0ZFH}(\overline{1},2,j,k,(\widetilde{li}),H)\,J^{(3)}_2(\{p\}_3)\\
3 \quad & -a^0_{3,g\to q}(j,2,k)\,\texttt{C1g0ZFH}((\widetilde{jk}),1,i,l,\overline{2},H)\,J^{(3)}_2(\{p\}_3)\\
4 \quad & -a^0_{3,g\to q}(k,2,j)\,\texttt{C1g0ZFH}(\overline{2},1,i,l,(\widetilde{jk}),H)\,J^{(3)}_2(\{p\}_3)\\
5 \quad & -a^0_{3,g\to q}(j,2,k)\,a^0_{3,g\to q}(i,1,l)\,\texttt{C0g0ZFH}((\widetilde{li}),\overline{2},(\widetilde{jk}),\overline{1},H)\,J^{(2)}_2(\{p\}_2)\\
6 \quad & -a^0_{3,g\to q}(j,2,k)\,a^0_{3,g\to q}(l,1,i)\,\texttt{C0g0ZFH}(\overline{1},\overline{2},(\widetilde{jk}),(\widetilde{li}),H)\,J^{(2)}_2(\{p\}_2)\\
7 \quad & -a^0_{3,g\to q}(k,2,j)\,a^0_{3,g\to q}(i,1,l)\,\texttt{C0g0ZFH}((\widetilde{li}),(\widetilde{jk}),\overline{2},\overline{1},H)\,J^{(2)}_2(\{p\}_2)\\
8 \quad & -a^0_{3,g\to q}(k,2,j)\,a^0_{3,g\to q}(l,1,i)\,\texttt{C0g0ZFH}(\overline{1},(\widetilde{jk}),\overline{2},(\widetilde{li}),H)\,J^{(2)}_2(\{p\}_2)
\end{aligned} \tag{C.26}$$

qbgsC2g0ZFHS(i,2,l,j,k,1,H)

$$
\begin{aligned}
&\texttt{qbgsC2g0ZFHS}(\texttt{i},2,\texttt{l},\texttt{j},\texttt{k},1,\texttt{H}) = \\
1 \quad &+d^0_{3,g}(k,l,2)\,\texttt{sC1g0ZFH}(i,\overline{2},j,(\widetilde{kl}),1,H)\,J^{(3)}_2(\{p\}_3) \\
2 \quad &+d^0_{3,g}(j,l,2)\,\texttt{sC1g0ZFH}(i,\overline{2},k,(\widetilde{jl}),1,H)\,J^{(3)}_2(\{p\}_3) \\
3 \quad &-A^0_{3,g\to q}(k,2,j)\,\texttt{sC1g0ZFHs0}(i,l,\overline{2},(\widetilde{kj}),1,H)\,J^{(3)}_2(\{p\}_3) \\
4 \quad &+A^0_{3,q}(1,l,i)\,\texttt{sC1g0ZFH}((\widetilde{li}),2,k,j,\overline{1},H)\,J^{(3)}_2(\{p\}_3) \\
\texttt{-----} \quad &\texttt{--} \\
5 \quad &-A^0_4(k,2,l,j)\,\texttt{sC0g0ZFH}(i,(\widetilde{klj}),\overline{2},1,H)\,J^{(2)}_2(\{p\}_2) \\
6 \quad &+d^0_{3,g}(j,l,2)\,A^0_{3,g\to q}((\widetilde{lj}),\overline{2},k)\,\texttt{sC0g0ZFH}(i,\widetilde{\widetilde{k(lj)}},\overline{\overline{2}},1,H)\,J^{(2)}_2(\{p\}_2) \\
\texttt{-----} \quad &\texttt{--} \\
7 \quad &-A^0_4(k,l,2,j)\,\texttt{sC0g0ZFH}(i,(\widetilde{klj}),\overline{2},1,H)\,J^{(2)}_2(\{p\}_2) \\
8 \quad &+d^0_{3,g}(k,l,2)\,A^0_{3,g\to q}((\widetilde{lk}),\overline{2},j)\,\texttt{sC0g0ZFH}(i,\widetilde{\widetilde{j(lk)}},\overline{\overline{2}},1,H)\,J^{(2)}_2(\{p\}_2) \\
9 \quad &+A^0_{3,g\to q}(k,2,j)\,A^0_{3,q}(\overline{2},l,(\widetilde{kj}))\,\texttt{sC0g0ZFH}(i,\overline{\overline{2}},\widetilde{\widetilde{l(kj)}},1,H)\,J^{(2)}_2(\{p\}_2) \\
10 \quad &+A^0_{3,g\to q}(k,2,j)\,A^0_{3,q}(1,l,i)\,\texttt{sC0g0ZFH}((\widetilde{il}),\overline{2},(\widetilde{jk}),\overline{1},H)\,J^{(2)}_2(\{p\}_2)
\end{aligned}
\tag{C.27}
$$

qbqpsC2g0ZFHSs1(i,k,l,j,2,1,H)

$$
\begin{aligned}
&\texttt{qbqpsC2g0ZFHSs1}(\texttt{i},\texttt{k},\texttt{l},\texttt{j},2,1,\texttt{H}) = \\
1 \quad &+d^0_3(i,l,k)\,\texttt{C1g0ZFHs1}((\widetilde{il}),(\widetilde{kl}),j,2,1,H)\,J^{(3)}_2(\{p\}_3) \\
2 \quad &+d^0_{3,q}(1,k,l)\,\texttt{C1g0ZFHs1}(i,(\widetilde{kl}),j,2,\overline{1},H)\,J^{(3)}_2(\{p\}_3) \\
3 \quad &+d^0_3(j,k,l)\,\texttt{C1g0ZFHs1}(2,(\widetilde{lk}),1,i,(\widetilde{jk}),H)\,J^{(3)}_2(\{p\}_3) \\
4 \quad &+d^0_{3,q}(2,l,k)\,\texttt{C1g0ZFHs1}(\overline{2},(\widetilde{lk}),1,i,j,H)\,J^{(3)}_2(\{p\}_3) \\
5 \quad &+A^0_{3,q}(1,k,i)\,\texttt{C1g0ZFHs1}(2,l,\overline{1},(\widetilde{ik}),j,H)\,J^{(3)}_2(\{p\}_3) \\
6 \quad &+A^0_{3,q}(2,l,j)\,\texttt{C1g0ZFHs1}(i,k,(\widetilde{jl}),\overline{2},1,H)\,J^{(3)}_2(\{p\}_3) \\
\texttt{-----} \quad &\texttt{--} \\
7 \quad &+A^0_4(1,k,l,i)\,\texttt{C0g0ZFH}((\widetilde{ilk}),j,2,\overline{1},H)\,J^{(2)}_2(\{p\}_2) \\
\texttt{-----} \quad &\texttt{--} \\
8 \quad &+A^0_4(2,k,l,j)\,\texttt{C0g0ZFH}(\overline{2},1,i,(\widetilde{jlk}),H)\,J^{(2)}_2(\{p\}_2) \\
9 \quad &-d^0_3(i,l,k)\,A^0_{3,q}(1,(\widetilde{kl}),(\widetilde{il}))\,\texttt{C0g0ZFH}([(\widetilde{il}),(\widetilde{lk})],j,2,\overline{1},H)\,J^{(2)}_2(\{p\}_2) \\
10 \quad &-d^0_{3,q}(1,k,l)\,A^0_{3,q}(\overline{1},(\widetilde{kl}),i)\,\texttt{C0g0ZFH}(\widetilde{\widetilde{i(kl)}},j,2,\overline{\overline{1}},H)\,J^{(2)}_2(\{p\}_2)
\end{aligned}
$$

$$
\begin{array}{ll}
11 & -\,d_3^0(j,l,k)\,A_{3,q}^0(2,(\widetilde{kl}),(\widetilde{jl}))\,\texttt{C0g0ZFH}(\overline{2},1,i,[(\widetilde{jl}),(\widetilde{lk})],H)\,J_2^{(2)}(\{p\}_2)\\
12 & -\,d_{3,q}^0(2,k,l)\,A_{3,q}^0(\overline{2},(\widetilde{kl}),j)\,\texttt{C0g0ZFH}(\overline{\overline{2}},1,i,(\widetilde{j(\widetilde{kl})}),H)\,J_2^{(2)}(\{p\}_2)\\
13 & -\frac{1}{2}\,A_{3,q}^0(2,l,j)\,A_{3,q}^0(1,k,i)\,\texttt{C0g0ZFH}(\overline{2},\overline{1},(\widetilde{ki}),(\widetilde{jl}))\,J_2^{(2)}(\{p\}_2)\\
14 & -\frac{1}{2}\,A_{3,q}^0(2,l,j)\,A_{3,q}^0(1,k,i)\,\texttt{C0g0ZFH}((\widetilde{ik}),(\widetilde{jl}),\overline{2},\overline{1})\,J_2^{(2)}(\{p\}_2)
\end{array}
\tag{C.28}
$$

qgsC2g0ZFHS(1,2,l,j,k,i,H)

$$
\begin{array}{ll}
 & \texttt{qgsC2g0ZFHS}(\texttt{1},\texttt{2},\texttt{l},\texttt{j},\texttt{k},\texttt{i},\texttt{H}) =\\
1 & +d_{3,g}^0(k,l,2)\,\texttt{sC1g0ZFH}(1,\overline{2},j,(\widetilde{kl}),i,H)\,J_2^{(3)}(\{p\}_3)\\
2 & +d_{3,g}^0(j,l,2)\,\texttt{sC1g0ZFH}(1,\overline{2},k,(\widetilde{jl}),i,H)\,J_2^{(3)}(\{p\}_3)\\
3 & -A_{3,g\to q}^0(k,2,j)\,\texttt{sC1g0ZFHs0}(1,l,\overline{2},(\widetilde{kj}),i,H)\,J_2^{(3)}(\{p\}_3)\\
4 & +A_{3,q}^0(1,l,i)\,\texttt{sC1g0ZFH}(\overline{1},2,k,j,(\widetilde{li}),H)\,J_2^{(3)}(\{p\}_3)\\
----- & ---------------------------\\
5 & -\,A_4^0(k,2,l,j)\,\texttt{sC0g0ZFH}(1,(\widetilde{klj}),\overline{2},i,H)\,J_2^{(2)}(\{p\}_2)\\
6 & +\,d_{3,g}^0(j,l,2)\,A_{3,g\to q}^0((\widetilde{lj}),\overline{2},k)\,\texttt{sC0g0ZFH}(1,(\widetilde{k(\widetilde{lj})}),\overline{\overline{2}},i,H)\,J_2^{(2)}(\{p\}_2)\\
----- & ---------------------------\\
7 & -\,A_4^0(k,l,2,j)\,\texttt{sC0g0ZFH}(1,(\widetilde{klj}),\overline{2},i,H)\,J_2^{(2)}(\{p\}_2)\\
8 & +\,d_{3,g}^0(k,l,2)\,A_{3,g\to q}^0((\widetilde{lk}),\overline{2},j)\,\texttt{sC0g0ZFH}(1,(\widetilde{j(\widetilde{lk})}),\overline{\overline{2}},i,H)\,J_2^{(2)}(\{p\}_2)\\
9 & +\,A_{3,g\to q}^0(k,2,j)\,A_{3,q}^0(\overline{2},l,(\widetilde{kj}))\,\texttt{sC0g0ZFH}(1,\overline{\overline{2}},(\widetilde{l(\widetilde{kj})}),i,H)\,J_2^{(2)}(\{p\}_2)\\
10 & +\,A_{3,g\to q}^0(k,2,j)\,A_{3,q}^0(1,l,i)\,\texttt{sC0g0ZFH}(\overline{1},\overline{2},(\widetilde{jk}),(\widetilde{il}),H)\,J_2^{(2)}(\{p\}_2)
\end{array}
\tag{C.29}
$$

qqpsC2g0ZFHSs1(1,k,l,j,2,i,H)

$$
\begin{array}{ll}
 & \texttt{qqpsC2g0ZFHSs1}(\texttt{1},\texttt{k},\texttt{l},\texttt{j},\texttt{2},\texttt{i},\texttt{H}) =\\
1 & +d_3^0(i,l,k)\,\texttt{C1g0ZFHs1}(1,(\widetilde{kl}),j,2,(\widetilde{il}),H)\,J_2^{(3)}(\{p\}_3)\\
2 & +d_{3,q}^0(1,k,l)\,\texttt{C1g0ZFHs1}(\overline{1},(\widetilde{kl}),j,2,i,H)\,J_2^{(3)}(\{p\}_3)\\
3 & +d_3^0(j,k,l)\,\texttt{C1g0ZFHs1}(2,(\widetilde{lk}),i,1,(\widetilde{jk}),H)\,J_2^{(3)}(\{p\}_3)\\
4 & +d_{3,q}^0(2,l,k)\,\texttt{C1g0ZFHs1}(\overline{2},(\widetilde{lk}),i,1,j,H)\,J_2^{(3)}(\{p\}_3)\\
5 & +A_{3,q}^0(1,k,i)\,\texttt{C1g0ZFHs1}(2,l,(\widetilde{ik}),\overline{1},j,H)\,J_2^{(3)}(\{p\}_3)\\
6 & +A_{3,q}^0(2,l,j)\,\texttt{C1g0ZFHs1}(1,k,(\widetilde{jl}),\overline{2},i,H)\,J_2^{(3)}(\{p\}_3)
\end{array}
$$

$$
\begin{array}{ll}
----- & ---------------------------- \\
7 & +\,A_4^0(1,k,l,i)\,\texttt{C0g0ZFH}(\overline{1},j,2,(\widetilde{ilk}),H)\,J_2^{(2)}(\{p\}_2) \\
----- & ---------------------------- \\
8 & +\,A_4^0(2,k,l,j)\,\texttt{C0g0ZFH}(1,(\widetilde{jkl}),\overline{2},i,H)\,J_2^{(2)}(\{p\}_2) \\
9 & -\,d_3^0(i,l,k)\,A_{3,q}^0(1,(\widetilde{kl}),(\widetilde{il}))\,\texttt{C0g0ZFH}(\overline{1},j,2,[(\widetilde{il}),(\widetilde{lk})],H)\,J_2^{(2)}(\{p\}_2) \\
10 & -\,d_{3,q}^0(1,k,l)\,A_{3,q}^0(\overline{1},(\widetilde{kl}),i)\,\texttt{C0g0ZFH}(\overline{\overline{1}},j,2,(\widetilde{i(\widetilde{kl})}),H)\,J_2^{(2)}(\{p\}_2) \\
11 & -\,d_3^0(j,l,k)\,A_{3,q}^0(2,(\widetilde{kl}),(\widetilde{jl}))\,\texttt{C0g0ZFH}(1,[(\widetilde{jl}),(\widetilde{lk})],\overline{2},i,H)\,J_2^{(2)}(\{p\}_2) \\
12 & -\,d_{3,q}^0(2,k,l)\,A_{3,q}^0(\overline{2},(\widetilde{kl}),j)\,\texttt{C0g0ZFH}(1,(\widetilde{j(\widetilde{kl})}),\overline{\overline{2}},i,H)\,J_2^{(2)}(\{p\}_2) \\
13 & -\frac{1}{2}\,A_{3,q}^0(2,l,j)\,A_{3,q}^0(1,k,i)\,\texttt{C0g0ZFH}(\overline{1},(\widetilde{jl}),\overline{2},(\widetilde{ik}))\,J_2^{(2)}(\{p\}_2) \\
14 & -\frac{1}{2}\,A_{3,q}^0(2,l,j)\,A_{3,q}^0(1,k,i)\,\texttt{C0g0ZFH}(\overline{1},(\widetilde{jl}),\overline{2},(\widetilde{ik}))\,J_2^{(2)}(\{p\}_2)
\end{array}
\tag{C.30}
$$

qbgsCt2g0ZFHS(i,2,l,j,k,1,H)

$$
\begin{array}{ll}
 & \texttt{qbgsCt2g0ZFHS}(\texttt{i},2,\texttt{l},\texttt{j},\texttt{k},1,\texttt{H}) = \\
1 & +A_{3,q}^0(1,l,i)\,\texttt{sC1g0ZFH}((\widetilde{il}),2,k,j,\overline{1},H)\,J_2^{(3)}(\{p\}_3) \\
2 & +A_3^0(j,l,k)\,\texttt{sC1g0ZFH}(i,2,(\widetilde{jl}),(\widetilde{kl}),1,H)\,J_2^{(3)}(\{p\}_3) \\
3 & -A_{3,g\to q}^0(j,2,k)\,\texttt{sC1g0ZFHs0}(i,l,\overline{2},(\widetilde{kj}),1,H)\,J_2^{(3)}(\{p\}_3) \\
----- & ---------------------------- \\
4 & -\,\tilde{A}_4^0(j,l,2,k)\,\texttt{sC0g0ZFH}(i,(\widetilde{jlk}),\overline{2},1,H)\,J_2^{(2)}(\{p\}_2) \\
5 & +\,A_3^0(k,l,j)\,A_{3,g\to q}^0((\widetilde{kl}),2,(\widetilde{jl}))\,\texttt{sC0g0ZFH}(i,[(\widetilde{kl}),(\widetilde{jl})],\overline{2},1,H)\,J_2^{(2)}(\{p\}_2) \\
6 & +\,A_{3,g\to q}^0(j,2,k)\,A_{3,q}^0(\overline{2},l,(\widetilde{jk}))\,\texttt{sC0g0ZFH}(i,\overline{\overline{2}},(\widetilde{l(\widetilde{jk})}),1,H)\,J_2^{(2)}(\{p\}_2) \\
7 & +\,A_{3,g\to q}^0(j,2,k)\,A_{3,q}^0(1,l,i)\,\texttt{sC0g0ZFH}((\widetilde{il}),(\widetilde{jk}),\overline{2},\overline{1},H)\,J_2^{(2)}(\{p\}_2)
\end{array}
\tag{C.31}
$$

qbqpsCt2g0ZFHS(i,k,l,j,2,1,H)

$$
\begin{array}{ll}
 & \texttt{qbqpsCt2g0ZFHS}(\texttt{i},\texttt{k},\texttt{l},\texttt{j},2,1,\texttt{H}) = \\
1 & +A_{3,q}^0(1,l,i)\,\texttt{C1g0ZFHs1}((\widetilde{il}),k,j,2,\overline{1},H)\,J_2^{(3)}(\{p\}_3) \\
2 & +A_{3,q}^0(1,k,i)\,\texttt{C1g0ZFHs1}((\widetilde{ik}),l,j,2,\overline{1},H)\,J_2^{(3)}(\{p\}_3) \\
3 & +A_{3,q}^0(2,l,j)\,\texttt{C1g0ZFHs1}(\overline{2},k,1,i,(\widetilde{jl}),H)\,J_2^{(3)}(\{p\}_3) \\
4 & +A_{3,q}^0(2,k,j)\,\texttt{C1g0ZFHs1}(\overline{2},l,1,i,(\widetilde{jk}),H)\,J_2^{(3)}(\{p\}_3)
\end{array}
$$

$$
\begin{array}{ll}
----- & --------------------------\\
5 & +\tilde{A}_4^0(1,k,l,i)\,\texttt{C0g0ZFH}((\widetilde{ilk}),j,2,\overline{1},H)\,J_2^{(2)}(\{p\}_2)\\
----- & --------------------------\\
6 & +\tilde{A}_4^0(2,k,l,j)\,\texttt{C0g0ZFH}(i,(\widetilde{jkl}),\overline{2},1,H)\,J_2^{(2)}(\{p\}_2)\\
7 & -A_{3,q}^0(1,l,i)\,A_{3,q}^0(\overline{1},k,(\widetilde{li}))\,\texttt{C0g0ZFH}((\widetilde{k(\widetilde{li})}),j,2,\overline{\overline{1}},H)\,J_2^{(2)}(\{p\}_2)\\
8 & -A_{3,q}^0(1,k,i)\,A_{3,q}^0(\overline{1},l,(\widetilde{ki}))\,\texttt{C0g0ZFH}((\widetilde{l(\widetilde{ki})}),j,2,\overline{\overline{1}},H)\,J_2^{(2)}(\{p\}_2)\\
9 & -A_{3,q}^0(2,l,j)\,A_{3,q}^0(\overline{2},k,(\widetilde{lj}))\,\texttt{C0g0ZFH}(i,(\widetilde{k(\widetilde{lj})}),\overline{\overline{2}},1,H)\,J_2^{(2)}(\{p\}_2)\\
10 & -A_{3,q}^0(2,k,j)\,A_{3,q}^0(\overline{2},l,(\widetilde{kj}))\,\texttt{C0g0ZFH}(i,(\widetilde{l(\widetilde{kj})}),\overline{\overline{2}},1,H)\,J_2^{(2)}(\{p\}_2)\\
11 & +A_{3,q}^0(1,l,i)\,\texttt{C1g0ZFHs1}(2,k,\overline{1},(\widetilde{il}),j,H)\,J_2^{(3)}(\{p\}_3)\\
12 & +A_{3,q}^0(1,k,i)\,\texttt{C1g0ZFHs1}(2,l,\overline{1},(\widetilde{ik}),j,H)\,J_2^{(3)}(\{p\}_3)\\
13 & +A_{3,q}^0(2,l,j)\,\texttt{C1g0ZFHs1}(i,k,(\widetilde{jl}),\overline{2},1,H)\,J_2^{(3)}(\{p\}_3)\\
14 & +A_{3,q}^0(2,k,j)\,\texttt{C1g0ZFHs1}(i,l,(\widetilde{jk}),\overline{2},1,H)\,J_2^{(3)}(\{p\}_3)\\
15 & -A_{3,q}^0(2,k,j)\,A_{3,q}^0(1,l,i)\,\texttt{C0g0ZFH}((\widetilde{il}),(\widetilde{jk}),\overline{2},\overline{1},H)\,J_2^{(2)}(\{p\}_2)\\
16 & -A_{3,q}^0(2,l,j)\,A_{3,q}^0(1,k,i)\,\texttt{C0g0ZFH}((\widetilde{ik}),(\widetilde{jl}),\overline{2},\overline{1},H)\,J_2^{(2)}(\{p\}_2)
\end{array}
\tag{C.32}
$$

qgsCt2g0ZFHS(1,2,l,j,k,i,H)

$$
\begin{array}{ll}
 & \texttt{qgsCt2g0ZFHS}(\texttt{1},\texttt{2},\texttt{l},\texttt{j},\texttt{k},\texttt{i},\texttt{H}) =\\
1 & +A_{3,q}^0(1,l,i)\,\texttt{sC1g0ZFH}(\overline{1},2,k,j,(\widetilde{il}),H)\,J_2^{(3)}(\{p\}_3)\\
2 & +A_3^0(j,l,k)\,\texttt{sC1g0ZFH}(1,2,(\widetilde{jl}),(\widetilde{kl}),i,H)\,J_2^{(3)}(\{p\}_3)\\
3 & -A_{3,g\to q}^0(j,2,k)\,\texttt{sC1g0ZFHs0}(1,l,\overline{2},(\widetilde{kj}),i,H)\,J_2^{(3)}(\{p\}_3)\\
----- & --------------------------\\
4 & -\tilde{A}_4^0(j,l,2,k)\,\texttt{sC0g0ZFH}(1,(\widetilde{jlk}),\overline{2},i,H)\,J_2^{(2)}(\{p\}_2)\\
5 & +A_3^0(k,l,j)\,A_{3,g\to q}^0((\widetilde{kl}),2,(\widetilde{jl}))\,\texttt{sC0g0ZFH}(1,[(\widetilde{kl}),(\widetilde{jl})],\overline{2},i,H)\,J_2^{(2)}(\{p\}_2)\\
6 & +A_{3,g\to q}^0(j,2,k)\,A_{3,q}^0(\overline{2},l,(\widetilde{jk}))\,\texttt{sC0g0ZFH}(1,\overline{\overline{2}},(\widetilde{l(\widetilde{jk})}),i,H)\,J_2^{(2)}(\{p\}_2)\\
7 & +A_{3,g\to q}^0(j,2,k)\,A_{3,q}^0(1,l,i)\,\texttt{sC0g0ZFH}(\overline{1},(\widetilde{jk}),\overline{2},(\widetilde{il}),H)\,J_2^{(2)}(\{p\}_2)
\end{array}
\tag{C.33}
$$

qqpsCt2g0ZFHS(1,k,l,j,2,i,H)

$$\texttt{qqpsCt2g0ZFHS}(\texttt{1},\texttt{k},\texttt{l},\texttt{j},\texttt{2},\texttt{i},\texttt{H}) =$$

$$
\begin{array}{ll}
1 & +A_{3,q}^0(1,l,i)\,\texttt{C1g0ZFHs1}(\overline{1},k,j,2,(\widetilde{il}),H)\,J_2^{(3)}(\{p\}_3) \\
2 & +A_{3,q}^0(1,k,i)\,\texttt{C1g0ZFHs1}(\overline{1},l,j,2,(\widetilde{ik}),H)\,J_2^{(3)}(\{p\}_3) \\
3 & +A_{3,q}^0(2,l,j)\,\texttt{C1g0ZFHs1}(\overline{2},k,i,1,(\widetilde{jl}),H)\,J_2^{(3)}(\{p\}_3) \\
4 & +A_{3,q}^0(2,k,j)\,\texttt{C1g0ZFHs1}(\overline{2},l,i,1,(\widetilde{jk}),H)\,J_2^{(3)}(\{p\}_3) \\
----- & ---------------------------- \\
5 & +\tilde{A}_4^0(1,k,l,i)\,\texttt{C0g0ZFH}(\overline{1},j,2,(\widetilde{ilk}),H)\,J_2^{(2)}(\{p\}_2) \\
----- & ---------------------------- \\
6 & +\tilde{A}_4^0(2,k,l,j)\,\texttt{C0g0ZFH}(1,(\widetilde{jkl}),\overline{2},i,H)\,J_2^{(2)}(\{p\}_2) \\
7 & -A_{3,q}^0(1,l,i)\,A_{3,q}^0(\overline{1},k,(\widetilde{li}))\,\texttt{C0g0ZFH}(\overline{\overline{1}},j,2,(\widetilde{k(\widetilde{li})}),H)\,J_2^{(2)}(\{p\}_2) \\
8 & -A_{3,q}^0(1,k,i)\,A_{3,q}^0(\overline{1},l,(\widetilde{ki}))\,\texttt{C0g0ZFH}(\overline{\overline{1}},j,2,(\widetilde{l(\widetilde{ki})}),H)\,J_2^{(2)}(\{p\}_2) \\
9 & -A_{3,q}^0(2,l,j)\,A_{3,q}^0(\overline{2},k,(\widetilde{lj}))\,\texttt{C0g0ZFH}(1,(\widetilde{k(\widetilde{lj})}),\overline{\overline{2}},i,H)\,J_2^{(2)}(\{p\}_2) \\
10 & -A_{3,q}^0(2,k,j)\,A_{3,q}^0(\overline{2},l,(\widetilde{kj}))\,\texttt{C0g0ZFH}(1,(\widetilde{l(\widetilde{kj})}),\overline{\overline{2}},i,H)\,J_2^{(2)}(\{p\}_2) \\
11 & +A_{3,q}^0(1,l,i)\,\texttt{C1g0ZFHs1}(2,k,(\widetilde{il}),\overline{1},j,H)\,J_2^{(3)}(\{p\}_3) \\
12 & +A_{3,q}^0(1,k,i)\,\texttt{C1g0ZFHs1}(2,l,(\widetilde{ik}),\overline{1},j,H)\,J_2^{(3)}(\{p\}_3) \\
13 & +A_{3,q}^0(2,l,j)\,\texttt{C1g0ZFHs1}(1,k,(\widetilde{jl}),\overline{2},i,H)\,J_2^{(3)}(\{p\}_3) \\
14 & +A_{3,q}^0(2,k,j)\,\texttt{C1g0ZFHs1}(1,l,(\widetilde{jk}),\overline{2},i,H)\,J_2^{(3)}(\{p\}_3) \\
15 & -A_{3,q}^0(2,k,j)\,A_{3,q}^0(1,l,i)\,\texttt{C0g0ZFH}(\overline{1},(\widetilde{jk}),\overline{2},(\widetilde{il}),H)\,J_2^{(2)}(\{p\}_2) \\
16 & -A_{3,q}^0(2,l,j)\,A_{3,q}^0(1,k,i)\,\texttt{C0g0ZFH}(\overline{1},(\widetilde{jl}),\overline{2},(\widetilde{ik}),H)\,J_2^{(2)}(\{p\}_2)
\end{array}
\tag{C.34}
$$

qbqpE0g0ZFHSs1(i,j,2,1,k,l,H)

$$
\begin{array}{ll}
 & \texttt{qbqpE0g0ZFHSs1}(\texttt{i},\texttt{j},2,1,\texttt{k},\texttt{l},\texttt{H}) = \\
1 & +E_3^0(i,l,k)\,\texttt{C1g0ZFHs1}((\widetilde{il}),(\widetilde{lk}),j,2,1,H)\,J_2^{(3)}(\{p\}_3) \\
2 & +E_3^0(j,l,k)\,\texttt{C1g0ZFHs1}(2,(\widetilde{lk}),1,i,(\widetilde{jl}),H)\,J_2^{(3)}(\{p\}_3) \\
----- & ---------------------------- \\
3 & +B_4^0(1,k,l,i)\,\texttt{C0g0ZFH}((\widetilde{ilk}),j,2,\overline{1},H)\,J_2^{(2)}(\{p\}_2) \\
4 & -E_3^0(i,l,k)\,A_{3,q}^0(1,(\widetilde{kl}),(\widetilde{il}))\,\texttt{C0g0ZFH}([(\widetilde{il}),(\widetilde{kl})],j,2,\overline{1},H)\,J_2^{(2)}(\{p\}_2) \\
----- & ---------------------------- \\
5 & +B_4^0(2,k,l,j)\,\texttt{C0g0ZFH}(i,(\widetilde{jlk}),\overline{2},1,H)\,J_2^{(2)}(\{p\}_2) \\
6 & -E_3^0(j,l,k)\,A_{3,q}^0(2,(\widetilde{kl}),(\widetilde{jl}))\,\texttt{C0g0ZFH}(i,[(\widetilde{jl}),(\widetilde{kl})],\overline{2},1,H)\,J_2^{(2)}(\{p\}_2)
\end{array}
$$

(C.35)

qbqpF0g0ZFHS(i,j,2,1,l,k,H)

$$\texttt{qbqpF0g0ZFHS}(\texttt{i},\texttt{j},2,1,\texttt{l},\texttt{k},\texttt{H}) =$$

	$-$
1	$-\,C_4^0(i,k,l,1)\,\texttt{C0g0ZFH}((\widetilde{ikl}),j,2,\overline{1},H)\,J_2^{(3)}(\{p\}_2)$
	$-$
2	$-\,C_4^0(1,l,k,i)\,\texttt{C0g0ZFH}((\widetilde{ikl}),j,2,\overline{1},H)\,J_2^{(3)}(\{p\}_2)$
	$-$
3	$-\,C_4^0(k,i,1,l)\,\texttt{C0g0ZFH}((\widetilde{ikl}),j,2,\overline{1},H)\,J_2^{(3)}(\{p\}_2)$
	$-$
4	$-\,C_4^0(2,k,l,j)\,\texttt{C0g0ZFH}(i,(\widetilde{jkl}),\overline{2},1,H)\,J_2^{(3)}(\{p\}_2)$
	$-$
5	$-\,C_4^0(j,l,k,2)\,\texttt{C0g0ZFH}(i,(\widetilde{jkl}),\overline{2},1,H)\,J_2^{(3)}(\{p\}_2)$
	$-$
6	$-\,C_4^0(l,j,2,k)\,\texttt{C0g0ZFH}(i,(\widetilde{jkl}),\overline{2},1,H)\,J_2^{(3)}(\{p\}_2)$
	$-$
7	$-\,C_4^0(l,1,i,k)\,\texttt{C0g0ZFH}(\overline{1},j,2,(\widetilde{ikl}),H)\,J_2^{(3)}(\{p\}_2)$
	$-$
8	$-\,C_4^0(k,2,j,l)\,\texttt{C0g0ZFH}(i,\overline{2},(\widetilde{jkl}),1,H)\,J_2^{(3)}(\{p\}_2)$

(C.36)

qbRE0g0ZFHS(i,l,k,1,j,2,H)

$$\texttt{qbRE0g0ZFHS}(\texttt{i},\texttt{l},\texttt{k},1,\texttt{j},2,\texttt{H}) =$$

1	$-E_{3,qq'\to qg}^0(1,2,j)\,\texttt{C1g0ZFH}(i,\overline{2},l,k,\overline{1},H)\,J_2^{(3)}(\{p\}_3)$
	$-$
2	$+\,B_4^0(1,2,j,k)\,\texttt{C0g0ZFH}(i,l,\overline{2},\overline{1},H)\,J_2^{(2)}(\{p\}_2)$
	$-$
3	$+\,B_4^0(1,2,j,l)\,\texttt{C0g0ZFH}(i,\overline{2},k,\overline{1},H)\,J_2^{(2)}(\{p\}_2)$
4	$-\,E_{3,qq'\to qg}^0(1,2,j)\,A_{3,qg\to qq}^0(\overline{1},\overline{2},k)\,\texttt{C0g0ZFH}(i,l,\overline{\overline{2}},\overline{\overline{1}},H)\,J_2^{(2)}(\{p\}_2)$

$$5 \quad -E^0_{3,qq'\to qg}(1,2,j)\,A^0_{3,qg\to qq}(\overline{1},\overline{2},l)\,\texttt{C0g0ZFH}(i,\overline{\overline{2}},k,\overline{\overline{1}},H)\,J^{(2)}_2(\{p\}_2)$$

(C.37)

qqpE0g0ZFHSs1(1,j,2,i,k,l,H)

$$\texttt{qqpE0g0ZFHSs1}(1,\texttt{j},2,\texttt{i},\texttt{k},\texttt{l},\texttt{H}) =$$

$$1 \quad +E^0_3(i,l,k)\,\texttt{C1g0ZFHs1}(1,(\widetilde{lk}),j,2,(\widetilde{il}),H)\,J^{(3)}_2(\{p\}_3)$$

$$2 \quad +E^0_3(j,l,k)\,\texttt{C1g0ZFHs1}(2,(\widetilde{lk}),i,1,(\widetilde{jl}),H)\,J^{(3)}_2(\{p\}_3)$$

$$---\quad ----------$$

$$3 \quad +B^0_4(1,k,l,i)\,\texttt{C0g0ZFH}(\overline{1},j,2,(\widetilde{ilk}),H)\,J^{(2)}_2(\{p\}_2)$$

$$4 \quad -E^0_3(i,l,k)\,A^0_{3,q}(1,(\widetilde{kl}),(\widetilde{il}))\,\texttt{C0g0ZFH}(\overline{1},j,2,[(\widetilde{il}),(\widetilde{kl})],H)\,J^{(2)}_2(\{p\}_2)$$

$$---\quad ----------$$

$$5 \quad +B^0_4(2,k,l,j)\,\texttt{C0g0ZFH}(1,(\widetilde{jlk}),\overline{2},i,H)\,J^{(2)}_2(\{p\}_2)$$

$$6 \quad -E^0_3(j,l,k)\,A^0_{3,q}(2,(\widetilde{kl}),(\widetilde{jl}))\,\texttt{C0g0ZFH}(1,[(\widetilde{jl}),(\widetilde{kl})],\overline{2},i,H)\,J^{(2)}_2(\{p\}_2)$$

(C.38)

qqpF0g0ZFHS(1,j,2,i,l,k,H)

$$\texttt{qqpF0g0ZFHS}(1,\texttt{j},2,\texttt{i},\texttt{l},\texttt{k},\texttt{H}) =$$

$$---\quad ----------$$

$$1 \quad -C^0_4(1,k,l,i)\,\texttt{C0g0ZFH}(\overline{1},j,2,(\widetilde{ikl}),H)\,J^{(3)}_2(\{p\}_2)$$

$$---\quad ----------$$

$$2 \quad -C^0_4(i,l,k,1)\,\texttt{C0g0ZFH}(\overline{1},j,2,(\widetilde{ikl}),H)\,J^{(3)}_2(\{p\}_2)$$

$$---\quad ----------$$

$$3 \quad -C^0_4(l,i,1,k)\,\texttt{C0g0ZFH}(\overline{1},j,2,(\widetilde{ikl}),H)\,J^{(3)}_2(\{p\}_2)$$

$$---\quad ----------$$

$$4 \quad -C^0_4(2,k,l,j)\,\texttt{C0g0ZFH}(1,(\widetilde{jkl}),\overline{2},i,H)\,J^{(3)}_2(\{p\}_2)$$

$$---\quad ----------$$

$$5 \quad -C^0_4(j,l,k,2)\,\texttt{C0g0ZFH}(1,(\widetilde{jkl}),\overline{2},i,H)\,J^{(3)}_2(\{p\}_2)$$

$$---\quad ----------$$

$$6 \quad -C^0_4(l,j,2,k)\,\texttt{C0g0ZFH}(1,(\widetilde{jkl}),\overline{2},i,H)\,J^{(3)}_2(\{p\}_2)$$

$$---\quad ----------$$

$$
\begin{array}{ll}
7 & -C_4^0(k,1,i,l)\,\texttt{C0g0ZFH}((\widetilde{ikl}),j,2,\overline{1},H)\,J_2^{(3)}(\{p\}_2) \\
\text{- - - - -} & \text{- -} \\
8 & -C_4^0(k,2,j,l)\,\texttt{C0g0ZFH}(1,\overline{2},(\widetilde{jkl}),i,H)\,J_2^{(3)}(\{p\}_2)
\end{array}
\tag{C.39}
$$

qRE0g0ZFHS(1,l,k,i,j,2,H)

$$
\begin{array}{ll}
 & \texttt{qRE0g0ZFHS}(1,\texttt{l},\texttt{k},\texttt{i},\texttt{j},2,\texttt{H}) = \\
1 & -E_{3,qq'\to qg}^0(1,2,j)\,\texttt{C1g0ZFH}(\overline{1},\overline{2},l,k,i,H)\,J_2^{(3)}(\{p\}_3) \\
\text{- - - - -} & \text{- -} \\
2 & +B_4^0(1,2,j,k)\,\texttt{C0g0ZFH}(\overline{1},l,\overline{2},i,H)\,J_2^{(2)}(\{p\}_2) \\
\text{- - - - -} & \text{- -} \\
3 & +B_4^0(1,2,j,l)\,\texttt{C0g0ZFH}(\overline{1},\overline{2},k,i,H)\,J_2^{(2)}(\{p\}_2) \\
4 & -E_{3,qq'\to qg}^0(1,2,j)\,A_{3,qg\to qq}^0(\overline{1},\overline{2},k)\,\texttt{C0g0ZFH}(\overline{\overline{1}},l,\overline{\overline{2}},i,H)\,J_2^{(2)}(\{p\}_2) \\
5 & -E_{3,qq'\to qg}^0(1,2,j)\,A_{3,qg\to qq}^0(\overline{1},\overline{2},l)\,\texttt{C0g0ZFH}(\overline{\overline{1}},\overline{\overline{2}},k,i,H)\,J_2^{(2)}(\{p\}_2)
\end{array}
\tag{C.40}
$$

ggsC2g0WFHSs1(l,1,2,j,k,i,H)

$$
\begin{array}{ll}
 & \texttt{ggsC2g0WFHSs1}(\texttt{l},1,2,\texttt{j},\texttt{k},\texttt{i},\texttt{H}) = \\
1 & -a_{3,g\to q}^0(i,1,l)\,\texttt{C1g0WFH}((\widetilde{li}),2,j,k,\overline{1},H)\,J_2^{(3)}(\{p\}_3) \\
2 & -a_{3,g\to q}^0(l,1,i)\,\texttt{C1g0WFH}(\overline{1},2,j,k,(\widetilde{li}),H)\,J_2^{(3)}(\{p\}_3) \\
3 & -a_{3,g\to q}^0(j,2,k)\,\texttt{C1g0WFH}((\widetilde{jk}),1,i,l,\overline{2},H)\,J_2^{(3)}(\{p\}_3) \\
4 & -a_{3,g\to q}^0(k,2,j)\,\texttt{C1g0WFH}(\overline{2},1,i,l,(\widetilde{jk}),H)\,J_2^{(3)}(\{p\}_3) \\
5 & -a_{3,g\to q}^0(j,2,k)\,a_{3,g\to q}^0(i,1,l)\,\texttt{C0g0WFH}((\widetilde{li}),\overline{2},(\widetilde{jk}),\overline{1},H)\,J_2^{(2)}(\{p\}_2) \\
6 & -a_{3,g\to q}^0(j,2,k)\,a_{3,g\to q}^0(l,1,i)\,\texttt{C0g0WFH}(\overline{1},\overline{2},(\widetilde{jk}),(\widetilde{li}),H)\,J_2^{(2)}(\{p\}_2) \\
7 & -a_{3,g\to q}^0(k,2,j)\,a_{3,g\to q}^0(i,1,l)\,\texttt{C0g0WFH}((\widetilde{li}),(\widetilde{jk}),\overline{2},\overline{1},H)\,J_2^{(2)}(\{p\}_2) \\
8 & -a_{3,g\to q}^0(k,2,j)\,a_{3,g\to q}^0(l,1,i)\,\texttt{C0g0WFH}(\overline{1},(\widetilde{jk}),\overline{2},(\widetilde{li}),H)\,J_2^{(2)}(\{p\}_2)
\end{array}
\tag{C.41}
$$

qbgsC2g0WFHS(i,2,l,j,k,1,H)

$$
\texttt{qbgsC2g0WFHS}(\texttt{i},2,\texttt{l},\texttt{j},\texttt{k},1,\texttt{H}) =
$$

$$
\begin{aligned}
1 \quad & +d^0_{3,g}(k,l,2)\,\texttt{sC1g0WFH}(i,\overline{2},j,(\widetilde{kl}),1,H)\,J^{(3)}_2(\{p\}_3)\\
2 \quad & +d^0_{3,g}(j,l,2)\,\texttt{sC1g0WFH}(i,\overline{2},k,(\widetilde{jl}),1,H)\,J^{(3)}_2(\{p\}_3)\\
3 \quad & -A^0_{3,g\to q}(k,2,j)\,\texttt{sC1g0WFHs0}(i,l,\overline{2},(\widetilde{kj}),1,H)\,J^{(3)}_2(\{p\}_3)\\
4 \quad & +A^0_{3,q}(1,l,i)\,\texttt{sC1g0WFH}((\widetilde{li}),2,k,j,\overline{1},H)\,J^{(3)}_2(\{p\}_3)\\
\text{-----} \quad & \text{----------}\\
5 \quad & -A^0_4(k,2,l,j)\,\texttt{sC0g0WFH}(i,(\widetilde{klj}),\overline{2},1,H)\,J^{(2)}_2(\{p\}_2)\\
6 \quad & +d^0_{3,g}(j,l,2)\,A^0_{3,g\to q}((\widetilde{lj}),\overline{2},k)\,\texttt{sC0g0WFH}(i,\widetilde{\widetilde{k(\widetilde{lj})}},\overline{\overline{2}},1,H)\,J^{(2)}_2(\{p\}_2)\\
\text{-----} \quad & \text{----------}\\
7 \quad & -A^0_4(k,l,2,j)\,\texttt{sC0g0WFH}(i,(\widetilde{klj}),\overline{2},1,H)\,J^{(2)}_2(\{p\}_2)\\
8 \quad & +d^0_{3,g}(k,l,2)\,A^0_{3,g\to q}((\widetilde{lk}),\overline{2},j)\,\texttt{sC0g0WFH}(i,\widetilde{\widetilde{j(\widetilde{lk})}},\overline{\overline{2}},1,H)\,J^{(2)}_2(\{p\}_2)\\
9 \quad & +A^0_{3,g\to q}(k,2,j)\,A^0_{3,q}(\overline{2},l,(\widetilde{kj}))\,\texttt{sC0g0WFH}(i,\overline{\overline{2}},\widetilde{\widetilde{l(\widetilde{kj})}},1,H)\,J^{(2)}_2(\{p\}_2)\\
10 \quad & +A^0_{3,g\to q}(k,2,j)\,A^0_{3,q}(1,l,i)\,\texttt{sC0g0WFH}((\widetilde{il}),\overline{2},(\widetilde{jk}),\overline{1},H)\,J^{(2)}_2(\{p\}_2)
\end{aligned}
\tag{C.42}
$$

qbqpsC2g0WFHSs1(i,k,l,j,2,1,H)

$$
\begin{aligned}
&\texttt{qbqpsC2g0WFHSs1}(\texttt{i},\texttt{k},\texttt{l},\texttt{j},2,1,\texttt{H}) =\\
1 \quad & +d^0_3(i,l,k)\,\texttt{C1g0WFHs1}((\widetilde{il}),(\widetilde{kl}),j,2,1,H)\,J^{(3)}_2(\{p\}_3)\\
2 \quad & +d^0_{3,q}(1,k,l)\,\texttt{C1g0WFHs1}(i,(\widetilde{kl}),j,2,\overline{1},H)\,J^{(3)}_2(\{p\}_3)\\
3 \quad & +d^0_3(j,k,l)\,\texttt{C1g0WFHs1}(2,(\widetilde{lk}),1,i,(\widetilde{jk}),H)\,J^{(3)}_2(\{p\}_3)\\
4 \quad & +d^0_{3,q}(2,l,k)\,\texttt{C1g0WFHs1}(\overline{2},(\widetilde{lk}),1,i,j,H)\,J^{(3)}_2(\{p\}_3)\\
5 \quad & +A^0_{3,q}(1,k,i)\,\texttt{C1g0WFHs1}(2,l,\overline{1},(\widetilde{ik}),j,H)\,J^{(3)}_2(\{p\}_3)\\
6 \quad & +A^0_{3,q}(2,l,j)\,\texttt{C1g0WFHs1}(i,k,(\widetilde{jl}),\overline{2},1,H)\,J^{(3)}_2(\{p\}_3)\\
\text{-----} \quad & \text{----------}\\
7 \quad & +A^0_4(1,k,l,i)\,\texttt{C0g0WFH}((\widetilde{ilk}),j,2,\overline{1},H)\,J^{(2)}_2(\{p\}_2)\\
\text{-----} \quad & \text{----------}\\
8 \quad & +A^0_4(2,k,l,j)\,\texttt{C0g0WFH}(\overline{2},1,i,(\widetilde{jlk}),H)\,J^{(2)}_2(\{p\}_2)\\
9 \quad & -d^0_3(i,l,k)\,A^0_{3,q}(1,(\widetilde{kl}),(\widetilde{il}))\,\texttt{C0g0WFH}([(\widetilde{il}),(\widetilde{lk})],j,2,\overline{1},H)\,J^{(2)}_2(\{p\}_2)\\
10 \quad & -d^0_{3,q}(1,k,l)\,A^0_{3,q}(\overline{1},(\widetilde{kl}),i)\,\texttt{C0g0WFH}((\widetilde{i(\widetilde{kl})}),j,2,\overline{\overline{1}},H)\,J^{(2)}_2(\{p\}_2)\\
11 \quad & -d^0_3(j,l,k)\,A^0_{3,q}(2,(\widetilde{kl}),(\widetilde{jl}))\,\texttt{C0g0WFH}(\overline{2},1,i,[(\widetilde{jl}),(\widetilde{lk})],H)\,J^{(2)}_2(\{p\}_2)\\
12 \quad & -d^0_{3,q}(2,k,l)\,A^0_{3,q}(\overline{2},(\widetilde{kl}),j)\,\texttt{C0g0WFH}(\overline{\overline{2}},1,i,\widetilde{j(\widetilde{kl})},H)\,J^{(2)}_2(\{p\}_2)
\end{aligned}
$$

$$
\begin{aligned}
13 \quad & -\frac{1}{2}\, A^0_{3,q}(2,l,j)\, A^0_{3,q}(1,k,i)\, \texttt{C0g0WFH}(\overline{2},\overline{1},(\widetilde{ki}),(\widetilde{jl}))\, J^{(2)}_2(\{p\}_2) \\
14 \quad & -\frac{1}{2}\, A^0_{3,q}(2,l,j)\, A^0_{3,q}(1,k,i)\, \texttt{C0g0WFH}((\widetilde{ik}),(\widetilde{jl}),\overline{2},\overline{1})\, J^{(2)}_2(\{p\}_2)
\end{aligned}
\tag{C.43}
$$

qgsC2g0WFHS(1,2,l,j,k,i,H)

$$
\begin{aligned}
&\texttt{qgsC2g0WFHS}(1,2,\texttt{l},\texttt{j},\texttt{k},\texttt{i},\texttt{H}) = \\
1 \quad & +d^0_{3,g}(k,l,2)\, \texttt{sC1g0WFH}(1,\overline{2},j,(\widetilde{kl}),i,H)\, J^{(3)}_2(\{p\}_3) \\
2 \quad & +d^0_{3,g}(j,l,2)\, \texttt{sC1g0WFH}(1,\overline{2},k,(\widetilde{jl}),i,H)\, J^{(3)}_2(\{p\}_3) \\
3 \quad & -A^0_{3,g\to q}(k,2,j)\, \texttt{sC1g0WFHs0}(1,l,\overline{2},(\widetilde{kj}),i,H)\, J^{(3)}_2(\{p\}_3) \\
4 \quad & +A^0_{3,q}(1,l,i)\, \texttt{sC1g0WFH}(\overline{1},2,k,j,(\widetilde{li}),H)\, J^{(3)}_2(\{p\}_3) \\
\text{-----} \quad & \text{--} \\
5 \quad & -A^0_4(k,2,l,j)\, \texttt{sC0g0WFH}(1,(\widetilde{klj}),\overline{2},i,H)\, J^{(2)}_2(\{p\}_2) \\
6 \quad & +d^0_{3,g}(j,l,2)\, A^0_{3,g\to q}((\widetilde{lj}),\overline{2},k)\, \texttt{sC0g0WFH}(1,\widetilde{\widetilde{k(\widetilde{lj})}},\overline{\overline{2}},i,H)\, J^{(2)}_2(\{p\}_2) \\
\text{-----} \quad & \text{--} \\
7 \quad & -A^0_4(k,l,2,j)\, \texttt{sC0g0WFH}(1,(\widetilde{klj}),\overline{2},i,H)\, J^{(2)}_2(\{p\}_2) \\
8 \quad & +d^0_{3,g}(k,l,2)\, A^0_{3,g\to q}((\widetilde{lk}),\overline{2},j)\, \texttt{sC0g0WFH}(1,\widetilde{\widetilde{j(\widetilde{lk})}},\overline{\overline{2}},i,H)\, J^{(2)}_2(\{p\}_2) \\
9 \quad & +A^0_{3,g\to q}(k,2,j)\, A^0_{3,q}(\overline{2},l,(\widetilde{kj}))\, \texttt{sC0g0WFH}(1,\overline{\overline{2}},\widetilde{\widetilde{l(\widetilde{kj})}},i,H)\, J^{(2)}_2(\{p\}_2) \\
10 \quad & +A^0_{3,g\to q}(k,2,j)\, A^0_{3,q}(1,l,i)\, \texttt{sC0g0WFH}(\overline{1},\overline{2},(\widetilde{jk}),(\widetilde{il}),H)\, J^{(2)}_2(\{p\}_2)
\end{aligned}
\tag{C.44}
$$

qqpsC2g0WFHSs1(1,k,l,j,2,i,H)

$$
\begin{aligned}
&\texttt{qqpsC2g0WFHSs1}(1,\texttt{k},\texttt{l},\texttt{j},2,\texttt{i},\texttt{H}) = \\
1 \quad & +d^0_3(i,l,k)\, \texttt{C1g0WFHs1}(1,(\widetilde{kl}),j,2,(\widetilde{il}),H)\, J^{(3)}_2(\{p\}_3) \\
2 \quad & +d^0_{3,q}(1,k,l)\, \texttt{C1g0WFHs1}(\overline{1},(\widetilde{kl}),j,2,i,H)\, J^{(3)}_2(\{p\}_3) \\
3 \quad & +d^0_3(j,k,l)\, \texttt{C1g0WFHs1}(2,(\widetilde{lk}),i,1,(\widetilde{jk}),H)\, J^{(3)}_2(\{p\}_3) \\
4 \quad & +d^0_{3,q}(2,l,k)\, \texttt{C1g0WFHs1}(\overline{2},(\widetilde{lk}),i,1,j,H)\, J^{(3)}_2(\{p\}_3) \\
5 \quad & +A^0_{3,q}(1,k,i)\, \texttt{C1g0WFHs1}(2,l,(\widetilde{ik}),\overline{1},j,H)\, J^{(3)}_2(\{p\}_3) \\
6 \quad & +A^0_{3,q}(2,l,j)\, \texttt{C1g0WFHs1}(1,k,(\widetilde{jl}),\overline{2},i,H)\, J^{(3)}_2(\{p\}_3) \\
\text{-----} \quad & \text{--} \\
7 \quad & +A^0_4(1,k,l,i)\, \texttt{C0g0WFH}(\overline{1},j,2,(\widetilde{ilk}),H)\, J^{(2)}_2(\{p\}_2)
\end{aligned}
$$

$$
\begin{array}{ll}
\text{-----} & \text{---------------------------} \\
8 & + A_4^0(2,k,l,j)\,\texttt{C0g0WFH}(1,(\widetilde{jkl}),\overline{2},i,H)\,J_2^{(2)}(\{p\}_2) \\
9 & - d_3^0(i,l,k)\,A_{3,q}^0(1,(\widetilde{kl}),(\widetilde{il}))\,\texttt{C0g0WFH}(\overline{1},j,2,[(\widetilde{il}),(\widetilde{lk})],H)\,J_2^{(2)}(\{p\}_2) \\
10 & - d_{3,q}^0(1,k,l)\,A_{3,q}^0(\overline{1},(\widetilde{kl}),i)\,\texttt{C0g0WFH}(\overline{\overline{1}},j,2,(\widetilde{i(\widetilde{kl})}),H)\,J_2^{(2)}(\{p\}_2) \\
11 & - d_3^0(j,l,k)\,A_{3,q}^0(2,(\widetilde{kl}),(\widetilde{jl}))\,\texttt{C0g0WFH}(1,[(\widetilde{jl}),(\widetilde{lk})],\overline{2},i,H)\,J_2^{(2)}(\{p\}_2) \\
12 & - d_{3,q}^0(2,k,l)\,A_{3,q}^0(\overline{2},(\widetilde{kl}),j)\,\texttt{C0g0WFH}(1,(\widetilde{j(\widetilde{kl})}),\overline{\overline{2}},i,H)\,J_2^{(2)}(\{p\}_2) \\
13 & -\frac{1}{2}\,A_{3,q}^0(2,l,j)\,A_{3,q}^0(1,k,i)\,\texttt{C0g0WFH}(\overline{1},(\widetilde{jl}),\overline{2},(\widetilde{ik}))\,J_2^{(2)}(\{p\}_2) \\
14 & -\frac{1}{2}\,A_{3,q}^0(2,l,j)\,A_{3,q}^0(1,k,i)\,\texttt{C0g0WFH}(\overline{1},(\widetilde{jl}),\overline{2},(\widetilde{ik}))\,J_2^{(2)}(\{p\}_2)
\end{array}
\tag{C.45}
$$

qqpsCt2g0WFHS(1,k,l,j,2,i,H)

$$
\begin{array}{ll}
 & \texttt{qqpsCt2g0WFHS}(\texttt{1},\texttt{k},\texttt{l},\texttt{j},\texttt{2},\texttt{i},\texttt{H}) = \\
1 & +A_{3,q}^0(1,l,i)\,\texttt{C1g0WFHs1}(\overline{1},k,j,2,(\widetilde{il}),H)\,J_2^{(3)}(\{p\}_3) \\
2 & +A_{3,q}^0(1,k,i)\,\texttt{C1g0WFHs1}(\overline{1},l,j,2,(\widetilde{ik}),H)\,J_2^{(3)}(\{p\}_3) \\
3 & +A_{3,q}^0(2,l,j)\,\texttt{C1g0WFHs1}(\overline{2},k,i,1,(\widetilde{jl}),H)\,J_2^{(3)}(\{p\}_3) \\
4 & +A_{3,q}^0(2,k,j)\,\texttt{C1g0WFHs1}(\overline{2},l,i,1,(\widetilde{jk}),H)\,J_2^{(3)}(\{p\}_3) \\
\text{-----} & \text{---------------------------} \\
5 & + \tilde{A}_4^0(1,k,l,i)\,\texttt{C0g0WFH}(\overline{1},j,2,(\widetilde{ilk}),H)\,J_2^{(2)}(\{p\}_2) \\
\text{-----} & \text{---------------------------} \\
6 & + \tilde{A}_4^0(2,k,l,j)\,\texttt{C0g0WFH}(1,(\widetilde{jkl}),\overline{2},i,H)\,J_2^{(2)}(\{p\}_2) \\
7 & - A_{3,q}^0(1,l,i)\,A_{3,q}^0(\overline{1},k,(\widetilde{li}))\,\texttt{C0g0WFH}(\overline{\overline{1}},j,2,(\widetilde{k(\widetilde{li})}),H)\,J_2^{(2)}(\{p\}_2) \\
8 & - A_{3,q}^0(1,k,i)\,A_{3,q}^0(\overline{1},l,(\widetilde{ki}))\,\texttt{C0g0WFH}(\overline{\overline{1}},j,2,(\widetilde{l(\widetilde{ki})}),H)\,J_2^{(2)}(\{p\}_2) \\
9 & - A_{3,q}^0(2,l,j)\,A_{3,q}^0(\overline{2},k,(\widetilde{lj}))\,\texttt{C0g0WFH}(1,(\widetilde{k(\widetilde{lj})}),\overline{\overline{2}},i,H)\,J_2^{(2)}(\{p\}_2) \\
10 & - A_{3,q}^0(2,k,j)\,A_{3,q}^0(\overline{2},l,(\widetilde{kj}))\,\texttt{C0g0WFH}(1,(\widetilde{l(\widetilde{kj})}),\overline{\overline{2}},i,H)\,J_2^{(2)}(\{p\}_2) \\
11 & +A_{3,q}^0(1,l,i)\,\texttt{C1g0WFHs1}(2,k,(\widetilde{il}),\overline{1},j,H)\,J_2^{(3)}(\{p\}_3) \\
12 & +A_{3,q}^0(1,k,i)\,\texttt{C1g0WFHs1}(2,l,(\widetilde{ik}),\overline{1},j,H)\,J_2^{(3)}(\{p\}_3) \\
13 & +A_{3,q}^0(2,l,j)\,\texttt{C1g0WFHs1}(1,k,(\widetilde{jl}),\overline{2},i,H)\,J_2^{(3)}(\{p\}_3) \\
14 & +A_{3,q}^0(2,k,j)\,\texttt{C1g0WFHs1}(1,l,(\widetilde{jk}),\overline{2},i,H)\,J_2^{(3)}(\{p\}_3) \\
15 & - A_{3,q}^0(2,k,j)\,A_{3,q}^0(1,l,i)\,\texttt{C0g0WFH}(\overline{1},(\widetilde{jk}),\overline{2},(\widetilde{il}),H)\,J_2^{(2)}(\{p\}_2) \\
16 & - A_{3,q}^0(2,l,j)\,A_{3,q}^0(1,k,i)\,\texttt{C0g0WFH}(\overline{1},(\widetilde{jl}),\overline{2},(\widetilde{ik}),H)\,J_2^{(2)}(\{p\}_2)
\end{array}
$$

(C.46)

qbqpE0g0WFHSs1(i,j,2,1,k,l,H)

$$\texttt{qbqpE0g0WFHSs1}(\texttt{i},\texttt{j},2,1,\texttt{k},\texttt{l},\texttt{H}) =$$

1 $+E_3^0(i,l,k)\,\texttt{C1g0WFHs1}((\widetilde{il}),(\widetilde{lk}),j,2,1,H)\,J_2^{(3)}(\{p\}_3)$

2 $+E_3^0(j,l,k)\,\texttt{C1g0WFHs1}(2,(\widetilde{lk}),1,i,(\widetilde{jl}),H)\,J_2^{(3)}(\{p\}_3)$

– –

3 $+\,B_4^0(1,k,l,i)\,\texttt{C0g0WFH}((\widetilde{ilk}),j,2,\overline{1},H)\,J_2^{(2)}(\{p\}_2)$

4 $-\,E_3^0(i,l,k)\,A_{3,q}^0(1,(\widetilde{kl}),(\widetilde{il}))\,\texttt{C0g0WFH}([(\widetilde{il}),(\widetilde{kl})],j,2,\overline{1},H)\,J_2^{(2)}(\{p\}_2)$

– –

5 $+\,B_4^0(2,k,l,j)\,\texttt{C0g0WFH}(i,(\widetilde{jlk}),\overline{2},1,H)\,J_2^{(2)}(\{p\}_2)$

6 $-\,E_3^0(j,l,k)\,A_{3,q}^0(2,(\widetilde{kl}),(\widetilde{jl}))\,\texttt{C0g0WFH}(i,[(\widetilde{jl}),(\widetilde{kl})],\overline{2},1,H)\,J_2^{(2)}(\{p\}_2)$

(C.47)

qbRE0g0WFHS(i,l,k,1,j,2,H)

$$\texttt{qbRE0g0WFHS}(\texttt{i},\texttt{l},\texttt{k},1,\texttt{j},2,\texttt{H}) =$$

1 $-E_{3,qq'\to qg}^0(1,2,j)\,\texttt{C1g0WFH}(i,\overline{2},l,k,\overline{1},H)\,J_2^{(3)}(\{p\}_3)$

– –

2 $+\,B_4^0(1,2,j,k)\,\texttt{C0g0WFH}(i,l,\overline{2},\overline{1},H)\,J_2^{(2)}(\{p\}_2)$

– –

3 $+\,B_4^0(1,2,j,l)\,\texttt{C0g0WFH}(i,\overline{2},k,\overline{1},H)\,J_2^{(2)}(\{p\}_2)$

4 $-\,E_{3,qq'\to qg}^0(1,2,j)\,A_{3,qg\to qq}^0(\overline{1},\overline{2},k)\,\texttt{C0g0WFH}(i,l,\overline{\overline{2}},\overline{\overline{1}},H)\,J_2^{(2)}(\{p\}_2)$

5 $-\,E_{3,qq'\to qg}^0(1,2,j)\,A_{3,qg\to qq}^0(\overline{1},\overline{2},l)\,\texttt{C0g0WFH}(i,\overline{\overline{2}},k,\overline{\overline{1}},H)\,J_2^{(2)}(\{p\}_2)$

(C.48)

qqpE0g0WFHSs1(1,j,2,i,k,l,H)

$$\texttt{qqpE0g0WFHSs1}(1,\texttt{j},2,\texttt{i},\texttt{k},\texttt{l},\texttt{H}) =$$

1 $+E_3^0(i,l,k)\,\texttt{C1g0WFHs1}(1,(\widetilde{lk}),j,2,(\widetilde{il}),H)\,J_2^{(3)}(\{p\}_3)$

2 $+E_3^0(j,l,k)\,\texttt{C1g0WFHs1}(2,(\widetilde{lk}),i,1,(\widetilde{jl}),H)\,J_2^{(3)}(\{p\}_3)$

– –

$$
\begin{array}{ll}
3 & + B_4^0(1,k,l,i)\,\texttt{C0g0WFH}(\overline{1},j,2,(\widetilde{ilk}),H)\,J_2^{(2)}(\{p\}_2) \\
4 & - E_3^0(i,l,k)\,A_{3,q}^0(1,(\widetilde{kl}),(\widetilde{il}))\,\texttt{C0g0WFH}(\overline{1},j,2,[(\widetilde{il}),(\widetilde{kl})],H)\,J_2^{(2)}(\{p\}_2) \\
- - - - - & - \\
5 & + B_4^0(2,k,l,j)\,\texttt{C0g0WFH}(1,(\widetilde{jlk}),\overline{2},i,H)\,J_2^{(2)}(\{p\}_2) \\
6 & - E_3^0(j,l,k)\,A_{3,q}^0(2,(\widetilde{kl}),(\widetilde{jl}))\,\texttt{C0g0WFH}(1,[(\widetilde{jl}),(\widetilde{kl})],\overline{2},i,H)\,J_2^{(2)}(\{p\}_2)
\end{array}
\tag{C.49}
$$

qqpF0g0WFHS(1,j,2,i,l,k,H)

$$
\begin{array}{ll}
 & \texttt{qqpF0g0WFHS}(1,\texttt{j},2,\texttt{i},\texttt{l},\texttt{k},\texttt{H}) = \\
- - - - - & - \\
1 & - C_4^0(1,k,l,i)\,\texttt{C0g0WFH}(\overline{1},j,2,(\widetilde{ikl}),H)\,J_2^{(3)}(\{p\}_2) \\
- - - - - & - \\
2 & - C_4^0(i,l,k,1)\,\texttt{C0g0WFH}(\overline{1},j,2,(\widetilde{ikl}),H)\,J_2^{(3)}(\{p\}_2) \\
- - - - - & - \\
3 & - C_4^0(l,i,1,k)\,\texttt{C0g0WFH}(\overline{1},j,2,(\widetilde{ikl}),H)\,J_2^{(3)}(\{p\}_2) \\
- - - - - & - \\
4 & - C_4^0(2,k,l,j)\,\texttt{C0g0WFH}(1,(\widetilde{jkl}),\overline{2},i,H)\,J_2^{(3)}(\{p\}_2) \\
- - - - - & - \\
5 & - C_4^0(j,l,k,2)\,\texttt{C0g0WFH}(1,(\widetilde{jkl}),\overline{2},i,H)\,J_2^{(3)}(\{p\}_2) \\
- - - - - & - \\
6 & - C_4^0(l,j,2,k)\,\texttt{C0g0WFH}(1,(\widetilde{jkl}),\overline{2},i,H)\,J_2^{(3)}(\{p\}_2) \\
- - - - - & - \\
7 & - C_4^0(k,1,i,l)\,\texttt{C0g0WFH}((\widetilde{ikl}),j,2,\overline{1},H)\,J_2^{(3)}(\{p\}_2) \\
- - - - - & - \\
8 & - C_4^0(k,2,j,l)\,\texttt{C0g0WFH}(1,\overline{2},(\widetilde{jkl}),i,H)\,J_2^{(3)}(\{p\}_2)
\end{array}
\tag{C.50}
$$

qRE0g0WFHS(1,l,k,i,j,2,H)

$$
\begin{array}{ll}
 & \texttt{qRE0g0WFHS}(1,\texttt{l},\texttt{k},\texttt{i},\texttt{j},2,\texttt{H}) = \\
1 & - E_{3,qq'\to qg}^0(1,2,j)\,\texttt{C1g0WFH}(\overline{1},\overline{2},l,k,i,H)\,J_2^{(3)}(\{p\}_3)
\end{array}
$$

$-\,-\,-\,-\,-$ $\quad$ $-\,-$

2 $\quad + B_4^0(1,2,j,k)\,\texttt{C0g0WFH}(\overline{1},l,\overline{2},i,H)\,J_2^{(2)}(\{p\}_2)$

$-\,-\,-\,-\,-$ $\quad$ $-\,-$

3 $\quad + B_4^0(1,2,j,l)\,\texttt{C0g0WFH}(\overline{1},\overline{2},k,i,H)\,J_2^{(2)}(\{p\}_2)$

4 $\quad - E^0_{3,qq'\to qg}(1,2,j)\,A^0_{3,qg\to qq}(\overline{1},\overline{2},k)\,\texttt{C0g0WFH}(\overline{\overline{1}},l,\overline{\overline{2}},i,H)\,J_2^{(2)}(\{p\}_2)$

5 $\quad - E^0_{3,qq'\to qg}(1,2,j)\,A^0_{3,qg\to qq}(\overline{1},\overline{2},l)\,\texttt{C0g0WFH}(\overline{\overline{1}},\overline{\overline{2}},k,i,H)\,J_2^{(2)}(\{p\}_2)$

(C.51)

C.4 NNLO: RV

ggsC1g1ZFHT(1,2,j,k,i,H)

1 $\quad -J^{1,IF}_{2,QQ,g\to q}(s_{1i})\,\texttt{C1g0ZFH}(i,2,j,k,1,H)\,J_2^{(3)}(\{p\}_3)$

2 $\quad -J^{1,IF}_{2,QQ,g\to q}(s_{1i})\,a^0_{3,g\to q}(k,2,j)\,\texttt{C0g0ZFH}(i,\overline{2},(\widetilde{jk}),1,H)\,J_2^{(2)}(\{p\}_2)$

3 $\quad -J^{1,IF}_{2,QQ,g\to q}(s_{1i})\,a^0_{3,g\to q}(j,2,k)\,\texttt{C0g0ZFH}(i,(\widetilde{jk}),\overline{2},1,H)\,J_2^{(2)}(\{p\}_2)$

4 $\quad -J^{1,IF}_{2,QQ,g\to q}(s_{1i})\,\texttt{C1g0ZFH}(1,2,j,k,i,H)\,J_2^{(3)}(\{p\}_3)$

5 $\quad -J^{1,IF}_{2,QQ,g\to q}(s_{1i})\,a^0_{3,g\to q}(k,2,j)\,\texttt{C0g0ZFH}(1,\overline{2},(\widetilde{jk}),i,H)\,J_2^{(2)}(\{p\}_2)$

6 $\quad -J^{1,IF}_{2,QQ,g\to q}(s_{1i})\,a^0_{3,g\to q}(j,2,k)\,\texttt{C0g0ZFH}(1,(\widetilde{jk}),\overline{2},i,H)\,J_2^{(2)}(\{p\}_2)$

7 $\quad -J^{1,FI}_{2,QQ,g\to q}(s_{2j})\,\texttt{C1g0ZFH}(j,1,i,k,2,H)\,J_2^{(3)}(\{p\}_3)$

8 $\quad -J^{1,IF}_{2,QQ,g\to q}(s_{2j})\,a^0_{3,g\to q}(k,1,i)\,\texttt{C0g0ZFH}(\overline{1},2,j,(\widetilde{ik}),H)\,J_2^{(2)}(\{p\}_2)$

9 $\quad -J^{1,IF}_{2,QQ,g\to q}(s_{2j})\,a^0_{3,g\to q}(i,1,k)\,\texttt{C0g0ZFH}((\widetilde{ik}),2,j,\overline{1},H)\,J_2^{(2)}(\{p\}_2)$

10 $\quad -J^{1,FI}_{2,QQ,g\to q}(s_{2j})\,\texttt{C1g0ZFH}(2,1,i,k,j,H)\,J_2^{(3)}(\{p\}_3)$

11 $\quad -J^{1,IF}_{2,QQ,g\to q}(s_{2j})\,a^0_{3,g\to q}(k,1,i)\,\texttt{C0g0ZFH}(\overline{1},j,2,(\widetilde{ik}),j,H)\,J_2^{(2)}(\{p\}_2)$

12 $\quad -J^{1,IF}_{2,QQ,g\to q}(s_{2j})\,a^0_{3,g\to q}(i,1,k)\,\texttt{C0g0ZFH}((\widetilde{ik}),j,2,\overline{1},j,H)\,J_2^{(2)}(\{p\}_2)$

(C.52)

qbgsC1g1ZFHTs1(i,2,j,k,1,H)

1 $\quad -J^{1,FI}_{2,QG}(s_{2k})\,\texttt{sC1g0ZFH}(i,2,j,k,1,H)\,J_2^{(3)}(\{p\}_3)$

2 $\quad -J^{1,FI}_{2,QG}(s_{2j})\,\texttt{sC1g0ZFH}(i,2,j,k,1,H)\,J_2^{(3)}(\{p\}_3)$

$$
\begin{aligned}
3 \quad & -J^{1,IF}_{2,QQ}(s_{1i})\,\texttt{sC1g0ZFH}(i,2,j,k,1,H)\,J^{(3)}_2(\{p\}_3) \\
4 \quad & -A^0_{3,g\to q}(k,2,j)\,\Bigg[\texttt{sC0g1ZFH}(i,(\widetilde{kj}),\overline{2},1,H)\,\delta(1-x_1)\,\delta(1-x_2) \\
& +\Bigg(+J^{1,FI}_{2,QQ}(s_{\overline{2}(\widetilde{jk})})+J^{1,IF}_{2,QQ}(s_{1i})\Bigg)\,\texttt{sC0g0ZFH}(i,(\widetilde{kj}),\overline{2},1,H)\Bigg]\,J^{(2)}_2(\{p\}_2) \\
5 \quad & -\Bigg[A^1_{3,g}(k,2,j)\,\delta(1-x_1)\,\delta(1-x_2) \\
& +\Bigg(+J^{1,FI}_{2,QG}(s_{2k})+J^{1,FI}_{2,QG}(s_{2j})-J^{1,FI}_{2,QQ}(s_{\overline{2}(\widetilde{jk})})\Bigg)\,A^0_{3,g\to q}(k,2,j)\Bigg]\,\texttt{sC0g0ZFH}(i,\overline{2},(\widetilde{jk}),1,H)\,J^{(2)}_2(\{p\}_2) \\
6 \quad & -2J^{1,FI}_{2,QQ,g\to q}(s_{2k})\,\texttt{sC1g0ZFHs0}(i,j,2,k,1,H)\,J^{(3)}_2(\{p\}_3) \\
7 \quad & +2J^{1,FI}_{2,QQ,g\to q}(s_{2k})\,A^0_{3,q}(2,j,k)\,\texttt{sC0g0ZFH}(i,(\widetilde{jk}),\overline{2},1,H)\,J^{(2)}_2(\{p\}_2) \\
8 \quad & +2J^{1,FI}_{2,QQ,g\to q}(s_{2k})\,A^0_{3,q}(1,j,i)\,\texttt{sC0g0ZFH}((\widetilde{ij}),k,2,\overline{1},H)\,J^{(2)}_2(\{p\}_2)
\end{aligned}
\tag{C.53}
$$

qbqpsC1g1ZFHT(i,k,j,2,1,H)

$$
\begin{aligned}
1 \quad & -J^{1,FF}_{2,QG}(s_{ik})\,\texttt{C1g0ZFHs1}(i,k,j,2,1,H)\,J^{(3)}_2(\{p\}_3) \\
2 \quad & -J^{1,IF}_{2,QG}(s_{1k})\,\texttt{C1g0ZFHs1}(i,k,j,2,1,H)\,J^{(3)}_2(\{p\}_3) \\
3 \quad & -J^{1,FF}_{2,QG}(s_{jk})\,\texttt{C1g0ZFHs1}(2,k,1,i,j,H)\,J^{(3)}_2(\{p\}_3) \\
4 \quad & -J^{1,FI}_{2,GQ}(s_{2k})\,\texttt{C1g0ZFHs1}(2,k,1,i,j,H)\,J^{(3)}_2(\{p\}_3) \\
5 \quad & -J^{1,IF}_{2,QQ}(s_{1i})\,\texttt{C1g0ZFHs1}(2,k,1,i,j,H)\,J^{(3)}_2(\{p\}_3) \\
6 \quad & -J^{1,FI}_{2,QQ}(s_{2j})\,\texttt{C1g0ZFHs1}(i,k,j,2,1,H)\,J^{(3)}_2(\{p\}_3) \\
7 \quad & +A^0_{3,q}(1,k,i)\,\Bigg[\texttt{C0g1ZFH}((\widetilde{ik}),j,2,\overline{1},H)\,\delta(1-x_1)\,\delta(1-x_2) \\
& +\Bigg(+J^{1,IF}_{2,QQ}(s_{\overline{1}(\widetilde{ik})})+J^{1,FI}_{2,QQ}(s_{2j})\Bigg)\,\texttt{C0g0ZFH}((\widetilde{ik}),j,2,\overline{1},H)\Bigg]\,J^{(2)}_2(\{p\}_2) \\
8 \quad & +A^0_{3,q}(2,k,j)\,\Bigg[\texttt{C0g1ZFH}(i,(\widetilde{jk}),\overline{2},1,H)\,\delta(1-x_1)\,\delta(1-x_2) \\
& +\Bigg(+J^{1,FI}_{2,QQ}(s_{\overline{2}(\widetilde{jk})})+J^{1,IF}_{2,QQ}(s_{1i})\Bigg)\,\texttt{C0g0ZFH}(i,(\widetilde{jk}),\overline{2},1,H)\Bigg]\,J^{(2)}_2(\{p\}_2) \\
9 \quad & +\Bigg[A^1_{3,q}(1,k,i)\,\delta(1-x_1)\,\delta(1-x_2) \\
& +\Bigg(+J^{1,FF}_{2,QG}(s_{ik})+J^{1,IF}_{2,QG}(s_{1k})-J^{1,IF}_{2,QQ}(s_{\overline{1}(\widetilde{ik})})\Bigg)\,A^0_{3,q}(1,k,i)\Bigg]\,\texttt{C0g0ZFH}((\widetilde{ik}),j,2,\overline{1},H)\,J^{(2)}_2(\{p\}_2) \\
10 \quad & +\Bigg[A^1_{3,q}(2,k,j)\,\delta(1-x_1)\,\delta(1-x_2) \\
& +\Bigg(+J^{1,FF}_{2,QG}(s_{jk})+J^{1,FI}_{2,GQ}(s_{2k})-J^{1,FI}_{2,QQ}(s_{\overline{2}(\widetilde{jk})})\Bigg)\,A^0_{3,q}(2,k,j)\Bigg]\,\texttt{C0g0ZFH}(i,(\widetilde{jk}),\overline{2},1,H)\,J^{(2)}_2(\{p\}_2)
\end{aligned}
\tag{C.54}
$$

qbRsC1g1ZFHT(1,2,i,j,k,H)

$$
\begin{aligned}
1 \quad & -J^{1,II}_{2,QG,qq'\to qg}(s_{12})\,\texttt{C1g0ZFH}(i,2,j,k,1,H)\,J^{(3)}_2(\{p\}_3)\\
2 \quad & -J^{1,II}_{2,QG,qq'\to qg}(s_{12})\,A^0_{3,qg\to qq}(1,2,k)\,\texttt{C0g0ZFH}(i,j,\overline{2},\overline{1},H)\,J^{(2)}_2(\{p\}_2)\\
3 \quad & -J^{1,II}_{2,QG,qq'\to qg}(s_{12})\,A^0_{3,qg\to qq}(1,2,j)\,\texttt{C0g0ZFH}(i,\overline{2},k,\overline{1},H)\,J^{(2)}_2(\{p\}_2)
\end{aligned}
\tag{C.55}
$$

qgsC1g1ZFHTs1(1,2,j,k,i,H)

$$
\begin{aligned}
1 \quad & -J^{1,FI}_{2,QG}(s_{2k})\,\texttt{sC1g0ZFH}(1,2,j,k,i,H)\,J^{(3)}_2(\{p\}_3)\\
2 \quad & -J^{1,FI}_{2,QG}(s_{2j})\,\texttt{sC1g0ZFH}(1,2,j,k,i,H)\,J^{(3)}_2(\{p\}_3)\\
3 \quad & -J^{1,IF}_{2,QQ}(s_{1i})\,\texttt{sC1g0ZFH}(1,2,j,k,i,H)\,J^{(3)}_2(\{p\}_3)\\
4 \quad & -A^0_{3,g\to q}(k,2,j)\,\Bigg[\texttt{sC0g1ZFH}(1,(\widetilde{kj}),\overline{2},i,H)\,\delta(1-x_1)\,\delta(1-x_2)\\
& +\Bigg(+J^{1,FI}_{2,QQ}(s_{\overline{2}(\widetilde{jk})})+J^{1,IF}_{2,QQ}(s_{1i})\Bigg)\,\texttt{sC0g0ZFH}(1,(\widetilde{kj}),\overline{2},i,H)\Bigg]\,J^{(2)}_2(\{p\}_2)\\
5 \quad & -\Bigg[A^1_{3,g}(k,2,j)\,\delta(1-x_1)\,\delta(1-x_2)\\
& +\Bigg(+J^{1,FI}_{2,QG}(s_{2k})+J^{1,FI}_{2,QG}(s_{2j})-J^{1,FI}_{2,QQ}(s_{\overline{2}(\widetilde{jk})})\Bigg)\,A^0_{3,g\to q}(k,2,j)\Bigg]\,\texttt{sC0g0ZFH}(1,\overline{2},(\widetilde{jk}),i,H)\,J^{(2)}_2(\{p\}_2)\\
6 \quad & -2J^{1,FI}_{2,QQ,g\to q}(s_{2k})\,\texttt{sC1g0ZFHs0}(1,j,2,k,i,H)\,J^{(3)}_2(\{p\}_3)\\
7 \quad & +2J^{1,FI}_{2,QQ,g\to q}(s_{2k})\,A^0_{3,q}(2,j,k)\,\texttt{sC0g0ZFH}(1,(\widetilde{jk}),\overline{2},i,H)\,J^{(2)}_2(\{p\}_2)\\
8 \quad & +2J^{1,FI}_{2,QQ,g\to q}(s_{2k})\,A^0_{3,q}(1,j,i)\,\texttt{sC0g0ZFH}(\overline{1},k,2,(\widetilde{ij}),H)\,J^{(2)}_2(\{p\}_2)
\end{aligned}
\tag{C.56}
$$

qqpsC1g1ZFHT(1,k,j,2,i,H)

$$
\begin{aligned}
1 \quad & -J^{1,FF}_{2,QG}(s_{ik})\,\texttt{C1g0ZFHs1}(1,k,j,2,i,H)\,J^{(3)}_2(\{p\}_3)\\
2 \quad & -J^{1,IF}_{2,QG}(s_{1k})\,\texttt{C1g0ZFHs1}(1,k,j,2,i,H)\,J^{(3)}_2(\{p\}_3)\\
3 \quad & -J^{1,FF}_{2,QG}(s_{jk})\,\texttt{C1g0ZFHs1}(2,k,i,1,j,H)\,J^{(3)}_2(\{p\}_3)\\
4 \quad & -J^{1,FI}_{2,GQ}(s_{2k})\,\texttt{C1g0ZFHs1}(2,k,i,1,j,H)\,J^{(3)}_2(\{p\}_3)\\
5 \quad & -J^{1,IF}_{2,QQ}(s_{1i})\,\texttt{C1g0ZFHs1}(2,k,i,1,j,H)\,J^{(3)}_2(\{p\}_3)\\
6 \quad & -J^{1,FI}_{2,QQ}(s_{2j})\,\texttt{C1g0ZFHs1}(1,k,j,2,i,H)\,J^{(3)}_2(\{p\}_3)\\
7 \quad & +A^0_{3,q}(1,k,i)\,\Bigg[\texttt{C0g1ZFH}(\overline{1},j,2,(\widetilde{ik}),H)\,\delta(1-x_1)\,\delta(1-x_2)\\
& +\Bigg(+J^{1,IF}_{2,QQ}(s_{\overline{1}(\widetilde{ik})})+J^{1,FI}_{2,QQ}(s_{2j})\Bigg)\,\texttt{C0g0ZFH}(\overline{1},j,2,(\widetilde{ik}),H)\Bigg]\,J^{(2)}_2(\{p\}_2)
\end{aligned}
$$

$$
\begin{aligned}
8 \quad & + A^0_{3,q}(2,k,j) \Bigg[\texttt{C0g1ZFH}(1,(\widetilde{jk}),\overline{2},i,H)\,\delta(1-x_1)\,\delta(1-x_2) \\
& + \Bigg(+ J^{1,FI}_{2,QQ}(s_{\overline{2}(\widetilde{jk})}) + J^{1,IF}_{2,QQ}(s_{1i}) \Bigg) \texttt{C0g0ZFH}(1,(\widetilde{jk}),\overline{2},i,H) \Bigg] J^{(2)}_2(\{p\}_2) \\
9 \quad & + \Bigg[A^1_{3,q}(1,k,i)\,\delta(1-x_1)\,\delta(1-x_2) \\
& + \Bigg(+ J^{1,FF}_{2,QG}(s_{ik}) + J^{1,IF}_{2,QG}(s_{1k}) - J^{1,IF}_{2,QQ}(s_{\overline{1}(\widetilde{ik})}) \Bigg) A^0_{3,q}(1,k,i) \Bigg] \texttt{C0g0ZFH}(\overline{1},j,2,(\widetilde{ik}),H)\, J^{(2)}_2(\{p\}_2) \\
10 \quad & + \Bigg[A^1_{3,q}(2,k,j)\,\delta(1-x_1)\,\delta(1-x_2) \\
& + \Bigg(+ J^{1,FF}_{2,QG}(s_{jk}) + J^{1,FI}_{2,GQ}(s_{2k}) - J^{1,FI}_{2,QQ}(s_{\overline{2}(\widetilde{jk})}) \Bigg) A^0_{3,q}(2,k,j) \Bigg] \texttt{C0g0ZFH}(1,(\widetilde{jk}),\overline{2},i,H)\, J^{(2)}_2(\{p\}_2)
\end{aligned}
\tag{C.57}
$$

qRsC1g1ZFHT(1,2,i,j,k,H)

$$
\begin{aligned}
1 \quad & - J^{1,II}_{2,QG,qq'\to qg}(s_{12})\, \texttt{C1g0ZFH}(1,2,j,k,i,H)\, J^{(3)}_2(\{p\}_3) \\
2 \quad & - J^{1,II}_{2,QG,qq'\to qg}(s_{12})\, A^0_{3,qg\to qq}(1,2,k)\, \texttt{C0g0ZFH}(\overline{1},j,\overline{2},i,H)\, J^{(2)}_2(\{p\}_2) \\
3 \quad & - J^{1,II}_{2,QG,qq'\to qg}(s_{12})\, A^0_{3,qg\to qq}(1,2,j)\, \texttt{C0g0ZFH}(\overline{1},\overline{2},k,i,H)\, J^{(2)}_2(\{p\}_2)
\end{aligned}
\tag{C.58}
$$

qbgsCt1g1ZFHT(i,2,j,k,1,H)

$$
\begin{aligned}
1 \quad & - J^{1,IF}_{2,QQ}(s_{1i})\, \texttt{sC1g0ZFH}(i,2,j,k,1,H)\, J^{(3)}_2(\{p\}_3) \\
2 \quad & - J^{1,FF}_{2,QQ}(s_{jk})\, \texttt{sC1g0ZFH}(i,2,j,k,1,H)\, J^{(3)}_2(\{p\}_3) \\
3 \quad & - A^0_{3,g\to q}(j,2,k) \Bigg[\texttt{sC0g1ZFH}(i,(\widetilde{jk}),\overline{2},1,H)\,\delta(1-x_1)\,\delta(1-x_2) \\
& + \Bigg(+ J^{1,FI}_{2,QQ}(s_{\overline{2}(\widetilde{jk})}) + J^{1,IF}_{2,QQ}(s_{1i}) \Bigg) \texttt{sC0g0ZFH}(i,(\widetilde{kj}),\overline{2},1,H) \Bigg] J^{(2)}_2(\{p\}_2) \\
4 \quad & - \Bigg[\tilde{A}^1_{3,g}(j,2,k)\,\delta(1-x_1)\,\delta(1-x_2) \\
& + \Bigg(+ J^{1,FF}_{2,QQ}(s_{jk}) - J^{1,IF}_{2,QQ}(s_{\overline{2}(\widetilde{jk})}) \Bigg) A^0_{3,g\to q}(j,2,k) \Bigg] \texttt{sC0g0ZFH}(i,(\widetilde{jk}),\overline{2},1,H)\, J^{(2)}_2(\{p\}_2) \\
5 \quad & - 2J^{1,FI}_{2,QQ,g\to q}(s_{k2})\, \texttt{sC1g0ZFHs0}(i,j,2,k,1,H)\, J^{(3)}_2(\{p\}_3) \\
6 \quad & + 2J^{1,FI}_{2,QQ,g\to q}(s_{2k})\, A^0_{3,q}(2,j,k)\, \texttt{sC0g0ZFH}(i,(\widetilde{jk}),\overline{2},1,H)\, J^{(2)}_2(\{p\}_2) \\
7 \quad & + 2J^{1,FI}_{2,QQ,g\to q}(s_{2k})\, A^0_{3,q}(1,j,i)\, \texttt{sC0g0ZFH}((\widetilde{ij}),k,2,\overline{1},H)\, J^{(2)}_2(\{p\}_2)
\end{aligned}
\tag{C.59}
$$

qbqpsCt1g1ZFHTs1(i,k,j,2,1,H)

$$
1 \quad - J^{1,IF}_{2,QQ}(s_{1i})\, \texttt{C1g0ZFH}(i,k,j,2,1,H)\, J^{(3)}_2(\{p\}_3)
$$

$$
\begin{aligned}
2 \quad & -J^{1,FI}_{2,QQ}(s_{2j})\,\texttt{C1g0ZFH}(i,k,j,2,1,H)\,J^{(3)}_2(\{p\}_3) \\
3 \quad & +A^0_{3,q}(1,k,i)\Bigg[\texttt{C0g1ZFH}((\widetilde{ik}),j,2,\overline{1},H)\,\delta(1-x_1)\,\delta(1-x_2) \\
& +\Bigg(+J^{1,IF}_{2,QQ}(s_{\overline{1}(\widetilde{ik})})+J^{1,FI}_{2,QQ}(s_{2j})\Bigg)\,\texttt{C0g0ZFH}((\widetilde{ik}),j,2,\overline{1},H)\Bigg]\,J^{(2)}_2(\{p\}_2) \\
4 \quad & +A^0_{3,q}(2,k,j)\Bigg[\texttt{C0g1ZFH}(i,(\widetilde{jk}),\overline{2},1,H)\,\delta(1-x_1)\,\delta(1-x_2) \\
& +\Bigg(+J^{1,FI}_{2,QQ}(s_{\overline{2}(\widetilde{jk})})+J^{1,IF}_{2,QQ}(s_{1i})\Bigg)\,\texttt{C0g0ZFH}(i,(\widetilde{jk}),\overline{2},1,H)\Bigg]\,J^{(2)}_2(\{p\}_2) \\
5 \quad & +\Bigg[\tilde{A}^1_{3,q}(1,k,i)\,\delta(1-x_1)\,\delta(1-x_2) \\
& +\Bigg(+J^{1,IF}_{2,QQ}(s_{1i})-J^{1,IF}_{2,QQ}(s_{\overline{1}(\widetilde{ik})})\Bigg)\,A^0_{3,q}(1,k,i)\Bigg]\,\texttt{C0g0ZFH}((\widetilde{ik}),j,2,\overline{1},H)\,J^{(2)}_2(\{p\}_2) \\
6 \quad & +\Bigg[\tilde{A}^1_{3,q}(2,k,j)\,\delta(1-x_1)\,\delta(1-x_2) \\
& +\Bigg(+J^{1,FI}_{2,QQ}(s_{2j})-J^{1,FI}_{2,QQ}(s_{\overline{2}(\widetilde{jk})})\Bigg)\,A^0_{3,q}(2,k,j)\Bigg]\,\texttt{C0g0ZFH}(i,(\widetilde{jk}),\overline{2},1,H)\,J^{(2)}_2(\{p\}_2)
\end{aligned}
\tag{C.60}
$$

qgsCt1g1ZFHT(1,2,j,k,i,H)

$$
\begin{aligned}
1 \quad & -J^{1,IF}_{2,QQ}(s_{1i})\,\texttt{sC1g0ZFH}(1,2,j,k,i,H)\,J^{(3)}_2(\{p\}_3) \\
2 \quad & -J^{1,FF}_{2,QQ}(s_{jk})\,\texttt{sC1g0ZFH}(1,2,j,k,i,H)\,J^{(3)}_2(\{p\}_3) \\
3 \quad & -A^0_{3,g\to q}(j,2,k)\Bigg[\texttt{sC0g1ZFH}(1,(\widetilde{jk}),\overline{2},i,H)\,\delta(1-x_1)\,\delta(1-x_2) \\
& +\Bigg(+J^{1,FI}_{2,QQ}(s_{\overline{2}(\widetilde{jk})})+J^{1,IF}_{2,QQ}(s_{1i})\Bigg)\,\texttt{sC0g0ZFH}(1,(\widetilde{kj}),\overline{2},i,H)\Bigg]\,J^{(2)}_2(\{p\}_2) \\
4 \quad & -\Bigg[\tilde{A}^1_{3,g}(j,2,k)\,\delta(1-x_1)\,\delta(1-x_2) \\
& +\Bigg(+J^{1,FF}_{2,QQ}(s_{jk})-J^{1,IF}_{2,QQ}(s_{\overline{2}(\widetilde{jk})})\Bigg)\,A^0_{3,g\to q}(j,2,k)\Bigg]\,\texttt{sC0g0ZFH}(1,(\widetilde{jk}),\overline{2},i,H)\,J^{(2)}_2(\{p\}_2) \\
5 \quad & -2J^{1,FI}_{2,QQ,g\to q}(s_{k2})\,\texttt{sC1g0ZFHs0}(1,j,2,k,i,H)\,J^{(3)}_2(\{p\}_3) \\
6 \quad & +2J^{1,FI}_{2,QQ,g\to q}(s_{2k})\,A^0_{3,q}(2,j,k)\,\texttt{sC0g0ZFH}(1,(\widetilde{jk}),\overline{2},i,H)\,J^{(2)}_2(\{p\}_2) \\
7 \quad & +2J^{1,FI}_{2,QQ,g\to q}(s_{2k})\,A^0_{3,q}(1,j,i)\,\texttt{sC0g0ZFH}(\overline{1},k,2,(\widetilde{ij}),H)\,J^{(2)}_2(\{p\}_2)
\end{aligned}
\tag{C.61}
$$

qqpsCt1g1ZFHT(1,k,j,2,i,H)

$$
\begin{aligned}
1 \quad & -J^{1,IF}_{2,QQ}(s_{1i})\,\texttt{C1g0ZFH}(1,k,j,2,i,H)\,J^{(3)}_2(\{p\}_3) \\
2 \quad & -J^{1,FI}_{2,QQ}(s_{2j})\,\texttt{C1g0ZFH}(1,k,j,2,i,H)\,J^{(3)}_2(\{p\}_3) \\
3 \quad & +A^0_{3,q}(1,k,i)\Bigg[\texttt{C0g1ZFH}(\overline{1},j,2,(\widetilde{ik}),H)\,\delta(1-x_1)\,\delta(1-x_2)
\end{aligned}
$$

$$
\begin{aligned}
&\quad + \Big(+ J^{1,IF}_{2,QQ}(s_{\overline{1}(i\widetilde{k})}) + J^{1,FI}_{2,QQ}(s_{2j}) \Big)\, \texttt{C0g0ZFH}(\overline{1}, j, 2, (\widetilde{ik}), H) \Big]\, J_2^{(2)}(\{p\}_2) \\
4 \quad &+ A^0_{3,q}(2,k,j) \Big[\texttt{C0g1ZFH}(1, (\widetilde{jk}), \overline{2}, i, H)\, \delta(1-x_1)\, \delta(1-x_2) \\
&\quad + \Big(+ J^{1,FI}_{2,QQ}(s_{\overline{2}(\widetilde{jk})}) + J^{1,IF}_{2,QQ}(s_{1i}) \Big)\, \texttt{C0g0ZFH}(1, (\widetilde{jk}), \overline{2}, i, H) \Big]\, J_2^{(2)}(\{p\}_2) \\
5 \quad &+ \Big[\tilde{A}^1_{3,q}(1,k,i)\, \delta(1-x_1)\, \delta(1-x_2) \\
&\quad + \Big(+ J^{1,IF}_{2,QQ}(s_{1i}) - J^{1,IF}_{2,QQ}(s_{\overline{1}(i\widetilde{k})}) \Big)\, A^0_{3,q}(1,k,i) \Big]\, \texttt{C0g0ZFH}(\overline{1}, j, 2, (\widetilde{ik}), H)\, J_2^{(2)}(\{p\}_2) \\
6 \quad &+ \Big[\tilde{A}^1_{3,q}(2,k,j)\, \delta(1-x_1)\, \delta(1-x_2) \\
&\quad + \Big(+ J^{1,FI}_{2,QQ}(s_{2j}) - J^{1,FI}_{2,QQ}(s_{\overline{2}(\widetilde{jk})}) \Big)\, A^0_{3,q}(2,k,j) \Big]\, \texttt{C0g0ZFH}(1, (\widetilde{jk}), \overline{2}, i, H)\, J_2^{(2)}(\{p\}_2)
\end{aligned}
\tag{C.62}
$$

qbgsCh1g1ZFHT(i,2,j,k,1,H)

$$
\begin{aligned}
1 \quad &-2\hat{J}^{1,FI}_{2,QG}(s_{2j})\, \texttt{sC1g0ZFH}(i,2,j,k,1,H)\, J_2^{(3)}(\{p\}_3) \\
2 \quad &- \Big[\hat{A}^1_{3,g}(j,2,k)\, \delta(1-x_1)\, \delta(1-x_2) + 2\hat{J}^{1,FI}_{2,QG}(s_{2j})\, A^0_{3,g\to q}(j,2,k) \Big]\, \texttt{sC0g0ZFH}(i, (\widetilde{jk}), \overline{2}, 1, H)\, J_2^{(2)}(\{p\}_2)
\end{aligned}
\tag{C.63}
$$

qbqpsCh1g1ZFHT(i,k,j,2,1,H)

$$
\begin{aligned}
1 \quad &-2\hat{J}^{1,FF}_{2,QG}(s_{ik})\, \texttt{C1g0ZFHs1}(i,k,j,2,1,H)\, J_2^{(3)}(\{p\}_3) \\
2 \quad &-2\hat{J}^{1,FF}_{2,QG}(s_{jk})\, \texttt{C1g0ZFHs1}(2,k,1,i,j,H)\, J_2^{(3)}(\{p\}_3) \\
3 \quad &+ \Big[\hat{A}^1_{3,q}(1,k,i)\, \delta(1-x_1)\, \delta(1-x_2) + 2\hat{J}^{1,FF}_{2,QG}(s_{ik})\, A^0_{3,q}(1,k,i) \Big]\, \texttt{C0g0ZFH}((\widetilde{ik}), j, 2, \overline{1}, H)\, J_2^{(2)}(\{p\}_2) \\
4 \quad &+ \Big[\hat{A}^1_{3,q}(2,k,j)\, \delta(1-x_1)\, \delta(1-x_2) + 2\hat{J}^{1,FF}_{2,QG}(s_{jk})\, A^0_{3,q}(2,k,j) \Big]\, \texttt{C0g0ZFH}(i, (\widetilde{jk}), \overline{2}, 1, H)\, J_2^{(2)}(\{p\}_2)
\end{aligned}
\tag{C.64}
$$

qgsCh1g1ZFHT(1,2,j,k,i,H)

$$
\begin{aligned}
1 \quad &-2\hat{J}^{1,FI}_{2,QG}(s_{2j})\, \texttt{sC1g0ZFH}(1,2,j,k,i,H)\, J_2^{(3)}(\{p\}_3) \\
2 \quad &- \Big[\hat{A}^1_{3,g}(j,2,k)\, \delta(1-x_1)\, \delta(1-x_2) + 2\hat{J}^{1,FI}_{2,QG}(s_{2j})\, A^0_{3,g\to q}(j,2,k) \Big]\, \texttt{sC0g0ZFH}(1, (\widetilde{jk}), \overline{2}, i, H)\, J_2^{(2)}(\{p\}_2)
\end{aligned}
\tag{C.65}
$$

qqpsCh1g1ZFHT(1,k,j,2,i,H)

$$
1 \quad -2\hat{J}^{1,FF}_{2,QG}(s_{ik})\, \texttt{C1g0ZFHs1}(1,k,j,2,i,H)\, J_2^{(3)}(\{p\}_3)
$$

$$
\begin{aligned}
2 \quad & -2\hat{J}^{1,FF}_{2,QG}(s_{jk})\,\texttt{C1gOZFHs1}(2,k,i,1,j,H)\,J^{(3)}_2(\{p\}_3) \\
3 \quad & +\Big[\,\hat{A}^1_{3,q}(1,k,i)\,\delta(1-x_1)\,\delta(1-x_2)+2\hat{J}^{1,FF}_{2,QG}(s_{ik})\,A^0_{3,q}(1,k,i)\Big]\,\texttt{COgOZFH}(\overline{1},j,2,(\widetilde{ik}),H)\,J^{(2)}_2(\{p\}_2) \\
4 \quad & +\Big[\,\hat{A}^1_{3,q}(2,k,j)\,\delta(1-x_1)\,\delta(1-x_2)+2\hat{J}^{1,FF}_{2,QG}(s_{jk})\,A^0_{3,q}(2,k,j)\Big]\,\texttt{COgOZFH}(1,(\widetilde{jk}),\overline{2},i,H)\,J^{(2)}_2(\{p\}_2)
\end{aligned}
\tag{C.66}
$$

ggsC1g1WFHT(1,2,j,k,i,H)

$$
\begin{aligned}
1 \quad & -J^{1,IF}_{2,QQ,g\to q}(s_{1i})\,\texttt{C1gOWFH}(i,2,j,k,1,H)\,J^{(3)}_2(\{p\}_3) \\
2 \quad & -J^{1,IF}_{2,QQ,g\to q}(s_{1i})\,a^0_{3,g\to q}(k,2,j)\,\texttt{COgOWFH}(i,\overline{2},(\widetilde{jk}),1,H)\,J^{(2)}_2(\{p\}_2) \\
3 \quad & -J^{1,IF}_{2,QQ,g\to q}(s_{1i})\,a^0_{3,g\to q}(j,2,k)\,\texttt{COgOWFH}(i,(\widetilde{jk}),\overline{2},1,H)\,J^{(2)}_2(\{p\}_2) \\
4 \quad & -J^{1,IF}_{2,QQ,g\to q}(s_{1i})\,\texttt{C1gOWFH}(1,2,j,k,i,H)\,J^{(3)}_2(\{p\}_3) \\
5 \quad & -J^{1,IF}_{2,QQ,g\to q}(s_{1i})\,a^0_{3,g\to q}(k,2,j)\,\texttt{COgOWFH}(1,\overline{2},(\widetilde{jk}),i,H)\,J^{(2)}_2(\{p\}_2) \\
6 \quad & -J^{1,IF}_{2,QQ,g\to q}(s_{1i})\,a^0_{3,g\to q}(j,2,k)\,\texttt{COgOWFH}(1,(\widetilde{jk}),\overline{2},i,H)\,J^{(2)}_2(\{p\}_2) \\
7 \quad & -J^{1,FI}_{2,QQ,g\to q}(s_{2j})\,\texttt{C1gOWFH}(j,1,i,k,2,H)\,J^{(3)}_2(\{p\}_3) \\
8 \quad & -J^{1,IF}_{2,QQ,g\to q}(s_{2j})\,a^0_{3,g\to q}(k,1,i)\,\texttt{COgOWFH}(\overline{1},2,j,(\widetilde{ik}),H)\,J^{(2)}_2(\{p\}_2) \\
9 \quad & -J^{1,IF}_{2,QQ,g\to q}(s_{2j})\,a^0_{3,g\to q}(i,1,k)\,\texttt{COgOWFH}((\widetilde{ik}),2,j,\overline{1},H)\,J^{(2)}_2(\{p\}_2) \\
10 \quad & -J^{1,FI}_{2,QQ,g\to q}(s_{2j})\,\texttt{C1gOWFH}(2,1,i,k,j,H)\,J^{(3)}_2(\{p\}_3) \\
11 \quad & -J^{1,IF}_{2,QQ,g\to q}(s_{2j})\,a^0_{3,g\to q}(k,1,i)\,\texttt{COgOWFH}(\overline{1},j,2,(\widetilde{ik}),j,H)\,J^{(2)}_2(\{p\}_2) \\
12 \quad & -J^{1,IF}_{2,QQ,g\to q}(s_{2j})\,a^0_{3,g\to q}(i,1,k)\,\texttt{COgOWFH}((\widetilde{ik}),j,2,\overline{1},j,H)\,J^{(2)}_2(\{p\}_2)
\end{aligned}
\tag{C.67}
$$

qbgsC1g1WFHTs1(i,2,j,k,1,H)

$$
\begin{aligned}
1 \quad & -J^{1,FI}_{2,QG}(s_{2k})\,\texttt{sC1gOWFH}(i,2,j,k,1,H)\,J^{(3)}_2(\{p\}_3) \\
2 \quad & -J^{1,FI}_{2,QG}(s_{2j})\,\texttt{sC1gOWFH}(i,2,j,k,1,H)\,J^{(3)}_2(\{p\}_3) \\
3 \quad & -J^{1,IF}_{2,QQ}(s_{1i})\,\texttt{sC1gOWFH}(i,2,j,k,1,H)\,J^{(3)}_2(\{p\}_3) \\
4 \quad & -A^0_{3,g\to q}(k,2,j)\,\Big[\,\texttt{sCOg1WFH}(i,(\widetilde{kj}),\overline{2},1,H)\,\delta(1-x_1)\,\delta(1-x_2) \\
& +\Big(+J^{1,FI}_{2,QQ}(s_{\overline{2}(\widetilde{jk})})+J^{1,IF}_{2,QQ}(s_{1i})\Big)\,\texttt{sCOgOWFH}(i,(\widetilde{kj}),\overline{2},1,H)\Big]\,J^{(2)}_2(\{p\}_2) \\
5 \quad & -\Big[\,A^1_{3,g}(k,2,j)\,\delta(1-x_1)\,\delta(1-x_2) \\
& +\Big(+J^{1,FI}_{2,QG}(s_{2k})+J^{1,FI}_{2,QG}(s_{2j})-J^{1,FI}_{2,QQ}(s_{\overline{2}(\widetilde{jk})})\Big)\,A^0_{3,g\to q}(k,2,j)\Big]\,\texttt{sCOgOWFH}(i,\overline{2},(\widetilde{jk}),1,H)\,J^{(2)}_2(\{p\}_2) \\
6 \quad & -2J^{1,FI}_{2,QQ,g\to q}(s_{2k})\,\texttt{sC1gOWFHs0}(i,j,2,k,1,H)\,J^{(3)}_2(\{p\}_3)
\end{aligned}
$$

$$
\begin{aligned}
7 \quad & +2J^{1,FI}_{2,QQ,g\to q}(s_{2k})\, A^0_{3,q}(2,j,k)\, \texttt{sC0g0WFH}(i,(\widetilde{jk}),\overline{2},1,H)\, J^{(2)}_2(\{p\}_2) \\
8 \quad & +2J^{1,FI}_{2,QQ,g\to q}(s_{2k})\, A^0_{3,q}(1,j,i)\, \texttt{sC0g0WFH}((\widetilde{ij}),k,2,\overline{1},H)\, J^{(2)}_2(\{p\}_2)
\end{aligned}
\tag{C.68}
$$

qbqpsC1g1WFHT(i,k,j,2,1,H)

$$
\begin{aligned}
1 \quad & -J^{1,FF}_{2,QG}(s_{ik})\, \texttt{C1g0WFHs1}(i,k,j,2,1,H)\, J^{(3)}_2(\{p\}_3) \\
2 \quad & -J^{1,IF}_{2,QG}(s_{1k})\, \texttt{C1g0WFHs1}(i,k,j,2,1,H)\, J^{(3)}_2(\{p\}_3) \\
3 \quad & -J^{1,FF}_{2,QG}(s_{jk})\, \texttt{C1g0WFHs1}(2,k,1,i,j,H)\, J^{(3)}_2(\{p\}_3) \\
4 \quad & -J^{1,FI}_{2,GQ}(s_{2k})\, \texttt{C1g0WFHs1}(2,k,1,i,j,H)\, J^{(3)}_2(\{p\}_3) \\
5 \quad & -J^{1,IF}_{2,QQ}(s_{1i})\, \texttt{C1g0WFHs1}(2,k,1,i,j,H)\, J^{(3)}_2(\{p\}_3) \\
6 \quad & -J^{1,FI}_{2,QQ}(s_{2j})\, \texttt{C1g0WFHs1}(i,k,j,2,1,H)\, J^{(3)}_2(\{p\}_3) \\
7 \quad & +A^0_{3,q}(1,k,i)\Bigg[\texttt{C0g1WFH}((\widetilde{ik}),j,2,\overline{1},H)\,\delta(1-x_1)\,\delta(1-x_2) \\
& +\Bigg(+J^{1,IF}_{2,QQ}(s_{\overline{1}(\widetilde{ik})})+J^{1,FI}_{2,QQ}(s_{2j})\Bigg)\texttt{C0g0WFH}((\widetilde{ik}),j,2,\overline{1},H)\Bigg]\,J^{(2)}_2(\{p\}_2) \\
8 \quad & +A^0_{3,q}(2,k,j)\Bigg[\texttt{C0g1WFH}(i,(\widetilde{jk}),\overline{2},1,H)\,\delta(1-x_1)\,\delta(1-x_2) \\
& +\Bigg(+J^{1,FI}_{2,QQ}(s_{\overline{2}(\widetilde{jk})})+J^{1,IF}_{2,QQ}(s_{1i})\Bigg)\texttt{C0g0WFH}(i,(\widetilde{jk}),\overline{2},1,H)\Bigg]\,J^{(2)}_2(\{p\}_2) \\
9 \quad & +\Bigg[A^1_{3,q}(1,k,i)\,\delta(1-x_1)\,\delta(1-x_2) \\
& +\Bigg(+J^{1,FF}_{2,QG}(s_{ik})+J^{1,IF}_{2,QG}(s_{1k})-J^{1,IF}_{2,QQ}(s_{\overline{1}(\widetilde{ik})})\Bigg)A^0_{3,q}(1,k,i)\Bigg]\,\texttt{C0g0WFH}((\widetilde{ik}),j,2,\overline{1},H)\,J^{(2)}_2(\{p\}_2) \\
10 \quad & +\Bigg[A^1_{3,q}(2,k,j)\,\delta(1-x_1)\,\delta(1-x_2) \\
& +\Bigg(+J^{1,FF}_{2,QG}(s_{jk})+J^{1,FI}_{2,GQ}(s_{2k})-J^{1,FI}_{2,QQ}(s_{\overline{2}(\widetilde{jk})})\Bigg)A^0_{3,q}(2,k,j)\Bigg]\,\texttt{C0g0WFH}(i,(\widetilde{jk}),\overline{2},1,H)\,J^{(2)}_2(\{p\}_2)
\end{aligned}
\tag{C.69}
$$

qgsC1g1WFHTs1(1,2,j,k,i,H)

$$
\begin{aligned}
1 \quad & -J^{1,FI}_{2,QG}(s_{2k})\, \texttt{sC1g0WFH}(1,2,j,k,i,H)\, J^{(3)}_2(\{p\}_3) \\
2 \quad & -J^{1,FI}_{2,QG}(s_{2j})\, \texttt{sC1g0WFH}(1,2,j,k,i,H)\, J^{(3)}_2(\{p\}_3) \\
3 \quad & -J^{1,IF}_{2,QQ}(s_{1i})\, \texttt{sC1g0WFH}(1,2,j,k,i,H)\, J^{(3)}_2(\{p\}_3) \\
4 \quad & -A^0_{3,g\to q}(k,2,j)\Bigg[\texttt{sC0g1WFH}(1,(\widetilde{kj}),\overline{2},i,H)\,\delta(1-x_1)\,\delta(1-x_2) \\
& +\Bigg(+J^{1,FI}_{2,QQ}(s_{\overline{2}(\widetilde{jk})})+J^{1,IF}_{2,QQ}(s_{1i})\Bigg)\texttt{sC0g0WFH}(1,(\widetilde{kj}),\overline{2},i,H)\Bigg]\,J^{(2)}_2(\{p\}_2) \\
5 \quad & -\Bigg[A^1_{3,g}(k,2,j)\,\delta(1-x_1)\,\delta(1-x_2)
\end{aligned}
$$

$$
\begin{aligned}
&\quad +\Big(+ J^{1,FI}_{2,QG}(s_{2k}) + J^{1,FI}_{2,QG}(s_{2j}) - J^{1,FI}_{2,QQ}(s_{\overline{2}(\widetilde{jk})}) \Big)\, A^0_{3,g\to q}(k,2,j) \Big]\, \texttt{sCOgOWFH}(1,\overline{2},(\widetilde{jk}),i,H)\, J^{(2)}_2(\{p\}_2) \\
6 &\quad -2J^{1,FI}_{2,QQ,g\to q}(s_{2k})\, \texttt{sC1gOWFHsO}(1,j,2,k,i,H)\, J^{(3)}_2(\{p\}_3) \\
7 &\quad +2J^{1,FI}_{2,QQ,g\to q}(s_{2k})\, A^0_{3,q}(2,j,k)\, \texttt{sCOgOWFH}(1,(\widetilde{jk}),\overline{2},i,H)\, J^{(2)}_2(\{p\}_2) \\
8 &\quad +2J^{1,FI}_{2,QQ,g\to q}(s_{2k})\, A^0_{3,q}(1,j,i)\, \texttt{sCOgOWFH}(\overline{1},k,2,(\widetilde{ij}),H)\, J^{(2)}_2(\{p\}_2)
\end{aligned}
\tag{C.70}
$$

qqpsC1g1WFHT(1,k,j,2,i,H)

$$
\begin{aligned}
1 &\quad -J^{1,FF}_{2,QG}(s_{ik})\, \texttt{C1gOWFHs1}(1,k,j,2,i,H)\, J^{(3)}_2(\{p\}_3) \\
2 &\quad -J^{1,IF}_{2,QG}(s_{1k})\, \texttt{C1gOWFHs1}(1,k,j,2,i,H)\, J^{(3)}_2(\{p\}_3) \\
3 &\quad -J^{1,FF}_{2,QG}(s_{jk})\, \texttt{C1gOWFHs1}(2,k,i,1,j,H)\, J^{(3)}_2(\{p\}_3) \\
4 &\quad -J^{1,FI}_{2,GQ}(s_{2k})\, \texttt{C1gOWFHs1}(2,k,i,1,j,H)\, J^{(3)}_2(\{p\}_3) \\
5 &\quad -J^{1,IF}_{2,QQ}(s_{1i})\, \texttt{C1gOWFHs1}(2,k,i,1,j,H)\, J^{(3)}_2(\{p\}_3) \\
6 &\quad -J^{1,FI}_{2,QQ}(s_{2j})\, \texttt{C1gOWFHs1}(1,k,j,2,i,H)\, J^{(3)}_2(\{p\}_3) \\
7 &\quad + A^0_{3,q}(1,k,i) \Big[\texttt{COg1WFH}(\overline{1},j,2,(\widetilde{ik}),H)\, \delta(1-x_1)\, \delta(1-x_2) \\
&\quad + \Big(+ J^{1,IF}_{2,QQ}(s_{\overline{1}(\widetilde{ik})}) + J^{1,FI}_{2,QQ}(s_{2j}) \Big)\, \texttt{COgOWFH}(\overline{1},j,2,(\widetilde{ik}),H) \Big]\, J^{(2)}_2(\{p\}_2) \\
8 &\quad + A^0_{3,q}(2,k,j) \Big[\texttt{COg1WFH}(1,(\widetilde{jk}),\overline{2},i,H)\, \delta(1-x_1)\, \delta(1-x_2) \\
&\quad + \Big(+ J^{1,FI}_{2,QQ}(s_{\overline{2}(\widetilde{jk})}) + J^{1,IF}_{2,QQ}(s_{1i}) \Big)\, \texttt{COgOWFH}(1,(\widetilde{jk}),\overline{2},i,H) \Big]\, J^{(2)}_2(\{p\}_2) \\
9 &\quad + \Big[A^1_{3,q}(1,k,i)\, \delta(1-x_1)\, \delta(1-x_2) \\
&\quad + \Big(+ J^{1,FF}_{2,QG}(s_{ik}) + J^{1,IF}_{2,QG}(s_{1k}) - J^{1,IF}_{2,QQ}(s_{\overline{1}(\widetilde{ik})}) \Big)\, A^0_{3,q}(1,k,i) \Big]\, \texttt{COgOWFH}(\overline{1},j,2,(\widetilde{ik}),H)\, J^{(2)}_2(\{p\}_2) \\
10 &\quad + \Big[A^1_{3,q}(2,k,j)\, \delta(1-x_1)\, \delta(1-x_2) \\
&\quad + \Big(+ J^{1,FF}_{2,QG}(s_{jk}) + J^{1,FI}_{2,GQ}(s_{2k}) - J^{1,FI}_{2,QQ}(s_{\overline{2}(\widetilde{jk})}) \Big)\, A^0_{3,q}(2,k,j) \Big]\, \texttt{COgOWFH}(1,(\widetilde{jk}),\overline{2},i,H)\, J^{(2)}_2(\{p\}_2)
\end{aligned}
\tag{C.71}
$$

qbgsCt1g1WFHT(i,2,j,k,1,H)

$$
\begin{aligned}
1 &\quad -J^{1,IF}_{2,QQ}(s_{1i})\, \texttt{sC1gOWFH}(i,2,j,k,1,H)\, J^{(3)}_2(\{p\}_3) \\
2 &\quad -J^{1,FF}_{2,QQ}(s_{jk})\, \texttt{sC1gOWFH}(i,2,j,k,1,H)\, J^{(3)}_2(\{p\}_3) \\
3 &\quad - A^0_{3,g\to q}(j,2,k) \Big[\texttt{sCOg1WFH}(i,(\widetilde{jk}),\overline{2},1,H)\, \delta(1-x_1)\, \delta(1-x_2) \\
&\quad + \Big(+ J^{1,FI}_{2,QQ}(s_{\overline{2}(\widetilde{jk})}) + J^{1,IF}_{2,QQ}(s_{1i}) \Big)\, \texttt{sCOgOWFH}(i,(\widetilde{kj}),\overline{2},1,H) \Big]\, J^{(2)}_2(\{p\}_2)
\end{aligned}
$$

$$
\begin{aligned}
4 \quad & -\Bigg[\tilde{A}^1_{3,g}(j,2,k)\,\delta(1-x_1)\,\delta(1-x_2) \\
& +\Bigg(+J^{1,FF}_{2,QQ}(s_{jk}) - J^{1,IF}_{2,QQ}(s_{\overline{2}(\widetilde{jk})}) \Bigg) A^0_{3,g\to q}(j,2,k) \Bigg] \texttt{sC0g0WFH}(i,(\widetilde{jk}),\overline{2},1,H)\, J^{(2)}_2(\{p\}_2) \\
5 \quad & -2J^{1,FI}_{2,QQ,g\to q}(s_{k2})\,\texttt{sC1g0WFHs0}(i,j,2,k,1,H)\, J^{(3)}_2(\{p\}_3) \\
6 \quad & +2J^{1,FI}_{2,QQ,g\to q}(s_{2k})\, A^0_{3,q}(2,j,k)\,\texttt{sC0g0WFH}(i,(\widetilde{jk}),\overline{2},1,H)\, J^{(2)}_2(\{p\}_2) \\
7 \quad & +2J^{1,FI}_{2,QQ,g\to q}(s_{2k})\, A^0_{3,q}(1,j,i)\,\texttt{sC0g0WFH}((\widetilde{ij}),k,2,\overline{1},H)\, J^{(2)}_2(\{p\}_2)
\end{aligned}
\tag{C.72}
$$

qbqpsCt1g1WFHTs1(i,k,j,2,1,H)

$$
\begin{aligned}
1 \quad & -J^{1,IF}_{2,QQ}(s_{1i})\,\texttt{C1g0WFH}(i,k,j,2,1,H)\, J^{(3)}_2(\{p\}_3) \\
2 \quad & -J^{1,FI}_{2,QQ}(s_{2j})\,\texttt{C1g0WFH}(i,k,j,2,1,H)\, J^{(3)}_2(\{p\}_3) \\
3 \quad & +A^0_{3,q}(1,k,i) \Bigg[\texttt{C0g1WFH}((\widetilde{ik}),j,2,\overline{1},H)\,\delta(1-x_1)\,\delta(1-x_2) \\
& +\Bigg(+J^{1,IF}_{2,QQ}(s_{\overline{1}(\widetilde{ik})}) + J^{1,FI}_{2,QQ}(s_{2j}) \Bigg) \texttt{C0g0WFH}((\widetilde{ik}),j,2,\overline{1},H) \Bigg] J^{(2)}_2(\{p\}_2) \\
4 \quad & +A^0_{3,q}(2,k,j) \Bigg[\texttt{C0g1WFH}(i,(\widetilde{jk}),\overline{2},1,H)\,\delta(1-x_1)\,\delta(1-x_2) \\
& +\Bigg(+J^{1,FI}_{2,QQ}(s_{\overline{2}(\widetilde{jk})}) + J^{1,IF}_{2,QQ}(s_{1i}) \Bigg) \texttt{C0g0WFH}(i,(\widetilde{jk}),\overline{2},1,H) \Bigg] J^{(2)}_2(\{p\}_2) \\
5 \quad & +\Bigg[\tilde{A}^1_{3,q}(1,k,i)\,\delta(1-x_1)\,\delta(1-x_2) \\
& +\Bigg(+J^{1,IF}_{2,QQ}(s_{1i}) - J^{1,IF}_{2,QQ}(s_{\overline{1}(\widetilde{ik})}) \Bigg) A^0_{3,q}(1,k,i) \Bigg] \texttt{C0g0WFH}((\widetilde{ik}),j,2,\overline{1},H)\, J^{(2)}_2(\{p\}_2) \\
6 \quad & +\Bigg[\tilde{A}^1_{3,q}(2,k,j)\,\delta(1-x_1)\,\delta(1-x_2) \\
& +\Bigg(+J^{1,FI}_{2,QQ}(s_{2j}) - J^{1,FI}_{2,QQ}(s_{\overline{2}(\widetilde{jk})}) \Bigg) A^0_{3,q}(2,k,j) \Bigg] \texttt{C0g0WFH}(i,(\widetilde{jk}),\overline{2},1,H)\, J^{(2)}_2(\{p\}_2)
\end{aligned}
\tag{C.73}
$$

qgsCt1g1WFHT(1,2,j,k,i,H)

$$
\begin{aligned}
1 \quad & -J^{1,IF}_{2,QQ}(s_{1i})\,\texttt{sC1g0WFH}(1,2,j,k,i,H)\, J^{(3)}_2(\{p\}_3) \\
2 \quad & -J^{1,FF}_{2,QQ}(s_{jk})\,\texttt{sC1g0WFH}(1,2,j,k,i,H)\, J^{(3)}_2(\{p\}_3) \\
3 \quad & -A^0_{3,g\to q}(j,2,k) \Bigg[\texttt{sC0g1WFH}(1,(\widetilde{jk}),\overline{2},i,H)\,\delta(1-x_1)\,\delta(1-x_2) \\
& +\Bigg(+J^{1,FI}_{2,QQ}(s_{\overline{2}(\widetilde{jk})}) + J^{1,IF}_{2,QQ}(s_{1i}) \Bigg) \texttt{sC0g0WFH}(1,(\widetilde{kj}),\overline{2},i,H) \Bigg] J^{(2)}_2(\{p\}_2) \\
4 \quad & -\Bigg[\tilde{A}^1_{3,g}(j,2,k)\,\delta(1-x_1)\,\delta(1-x_2) \\
& +\Bigg(+J^{1,FF}_{2,QQ}(s_{jk}) - J^{1,IF}_{2,QQ}(s_{\overline{2}(\widetilde{jk})}) \Bigg) A^0_{3,g\to q}(j,2,k) \Bigg] \texttt{sC0g0WFH}(1,(\widetilde{jk}),\overline{2},i,H)\, J^{(2)}_2(\{p\}_2)
\end{aligned}
$$

$$
\begin{aligned}
5 \quad & -2J^{1,FI}_{2,QQ,g\to q}(s_{k2})\,\texttt{sC1g0WFHs0}(1,j,2,k,i,H)\,J^{(3)}_2(\{p\}_3)\\
6 \quad & +2J^{1,FI}_{2,QQ,g\to q}(s_{2k})\,A^0_{3,q}(2,j,k)\,\texttt{sC0g0WFH}(1,(\widetilde{jk}),\overline{2},i,H)\,J^{(2)}_2(\{p\}_2)\\
7 \quad & +2J^{1,FI}_{2,QQ,g\to q}(s_{2k})\,A^0_{3,q}(1,j,i)\,\texttt{sC0g0WFH}(\overline{1},k,2,(\widetilde{ij}),H)\,J^{(2)}_2(\{p\}_2)
\end{aligned}
\tag{C.74}
$$

qqpsCt1g1WFHT(1,k,j,2,i,H)

$$
\begin{aligned}
1 \quad & -J^{1,IF}_{2,QQ}(s_{1i})\,\texttt{C1g0WFH}(1,k,j,2,i,H)\,J^{(3)}_2(\{p\}_3)\\
2 \quad & -J^{1,FI}_{2,QQ}(s_{2j})\,\texttt{C1g0WFH}(1,k,j,2,i,H)\,J^{(3)}_2(\{p\}_3)\\
3 \quad & +A^0_{3,q}(1,k,i)\Big[\texttt{C0g1WFH}(\overline{1},j,2,(\widetilde{ik}),H)\,\delta(1-x_1)\,\delta(1-x_2)\\
& \quad +\Big(+J^{1,IF}_{2,QQ}(s_{\overline{1}(\widetilde{ik})})+J^{1,FI}_{2,QQ}(s_{2j})\Big)\,\texttt{C0g0WFH}(\overline{1},j,2,(\widetilde{ik}),H)\Big]\,J^{(2)}_2(\{p\}_2)\\
4 \quad & +A^0_{3,q}(2,k,j)\Big[\texttt{C0g1WFH}(1,(\widetilde{jk}),\overline{2},i,H)\,\delta(1-x_1)\,\delta(1-x_2)\\
& \quad +\Big(+J^{1,FI}_{2,QQ}(s_{\overline{2}(\widetilde{jk})})+J^{1,IF}_{2,QQ}(s_{1i})\Big)\,\texttt{C0g0WFH}(1,(\widetilde{jk}),\overline{2},i,H)\Big]\,J^{(2)}_2(\{p\}_2)\\
5 \quad & +\Big[\tilde{A}^1_{3,q}(1,k,i)\,\delta(1-x_1)\,\delta(1-x_2)\\
& \quad +\Big(+J^{1,IF}_{2,QQ}(s_{1i})-J^{1,IF}_{2,QQ}(s_{\overline{1}(\widetilde{ik})})\Big)\,A^0_{3,q}(1,k,i)\Big]\,\texttt{C0g0WFH}(\overline{1},j,2,(\widetilde{ik}),H)\,J^{(2)}_2(\{p\}_2)\\
6 \quad & +\Big[\tilde{A}^1_{3,q}(2,k,j)\,\delta(1-x_1)\,\delta(1-x_2)\\
& \quad +\Big(+J^{1,FI}_{2,QQ}(s_{2j})-J^{1,FI}_{2,QQ}(s_{\overline{2}(\widetilde{jk})})\Big)\,A^0_{3,q}(2,k,j)\Big]\,\texttt{C0g0WFH}(1,(\widetilde{jk}),\overline{2},i,H)\,J^{(2)}_2(\{p\}_2)
\end{aligned}
\tag{C.75}
$$

qbqpsCh1g1WFHT(i,k,j,2,1,H)

$$
\begin{aligned}
1 \quad & -2\hat{J}^{1,FF}_{2,QG}(s_{ik})\,\texttt{C1g0WFHs1}(i,k,j,2,1,H)\,J^{(3)}_2(\{p\}_3)\\
2 \quad & -2\hat{J}^{1,FF}_{2,QG}(s_{jk})\,\texttt{C1g0WFHs1}(2,k,1,i,j,H)\,J^{(3)}_2(\{p\}_3)\\
3 \quad & +\Big[\hat{A}^1_{3,q}(1,k,i)\,\delta(1-x_1)\,\delta(1-x_2)+2\hat{J}^{1,FF}_{2,QG}(s_{ik})\,A^0_{3,q}(1,k,i)\Big]\,\texttt{C0g0WFH}((\widetilde{ik}),j,2,\overline{1},H)\,J^{(2)}_2(\{p\}_2)\\
4 \quad & +\Big[\hat{A}^1_{3,q}(2,k,j)\,\delta(1-x_1)\,\delta(1-x_2)+2\hat{J}^{1,FF}_{2,QG}(s_{jk})\,A^0_{3,q}(2,k,j)\Big]\,\texttt{C0g0WFH}(i,(\widetilde{jk}),\overline{2},1,H)\,J^{(2)}_2(\{p\}_2)
\end{aligned}
\tag{C.76}
$$

qqpsCh1g1WFHT(1,k,j,2,i,H)

$$
\begin{aligned}
1 \quad & -2\hat{J}^{1,FF}_{2,QG}(s_{ik})\,\texttt{C1g0WFHs1}(1,k,j,2,i,H)\,J^{(3)}_2(\{p\}_3)\\
2 \quad & -2\hat{J}^{1,FF}_{2,QG}(s_{jk})\,\texttt{C1g0WFHs1}(2,k,i,1,j,H)\,J^{(3)}_2(\{p\}_3)
\end{aligned}
$$

$$
\begin{aligned}
3 \quad &+\Big[\,\hat{A}^1_{3,q}(1,k,i)\,\delta(1-x_1)\,\delta(1-x_2)+2\hat{J}^{1,FF}_{2,QG}(s_{ik})\,A^0_{3,q}(1,k,i)\Big]\,\texttt{C0g0WFH}(\overline{1},j,2,(\widetilde{ik}),H)\,J^{(2)}_2(\{p\}_2)\\
4 \quad &+\Big[\,\hat{A}^1_{3,q}(2,k,j)\,\delta(1-x_1)\,\delta(1-x_2)+2\hat{J}^{1,FF}_{2,QG}(s_{jk})\,A^0_{3,q}(2,k,j)\Big]\,\texttt{C0g0WFH}(1,(\widetilde{jk}),\overline{2},i,H)\,J^{(2)}_2(\{p\}_2)
\end{aligned}
\tag{C.77}
$$

C.5 NNLO: VV

ggC0g2ZFHU

$$
\begin{aligned}
&\texttt{ggC0g2ZFHU}(1,2,3,4,\texttt{H}) =\\
1 \quad &+\Big[-\frac{1}{2}S_{g\to q}\,\Gamma^{(1)}_{qg}(z_1)\otimes\mathcal{A}^0_{3,g\to q}(s_{23})-\frac{1}{4}\,\mathcal{A}^0_{3,g\to q}(s_{23})\otimes\mathcal{A}^0_{3,g\to q}(s_{14})-S^2_{g\to q}\,\Gamma^{(1)}_{qg}(z_1)\otimes\Gamma^{(1)}_{qg}(z_2)\\
&\quad-\frac{1}{2}S_{g\to q}\,\Gamma^{(1)}_{qg}(z_2)\otimes\mathcal{A}^0_{3,g\to q}(s_{14})\Big]\,\texttt{C0g0ZFH}(1,3,2,4,H)\\
2 \quad &+\Big[-\frac{1}{2}S_{g\to q}\,\Gamma^{(1)}_{qg}(z_1)\otimes\mathcal{A}^0_{3,g\to q}(s_{23})-\frac{1}{4}\,\mathcal{A}^0_{3,g\to q}(s_{23})\otimes\mathcal{A}^0_{3,g\to q}(s_{14})-S^2_{g\to q}\,\Gamma^{(1)}_{qg}(z_1)\otimes\Gamma^{(1)}_{qg}(z_2)\\
&\quad-\frac{1}{2}S_{g\to q}\,\Gamma^{(1)}_{qg}(z_2)\otimes\mathcal{A}^0_{3,g\to q}(s_{14})\Big]\,\texttt{C0g0ZFH}(1,2,3,4,H)\\
3 \quad &+\Big[-\frac{1}{2}S_{g\to q}\,\Gamma^{(1)}_{qg}(z_1)\otimes\mathcal{A}^0_{3,g\to q}(s_{23})-\frac{1}{4}\,\mathcal{A}^0_{3,g\to q}(s_{23})\otimes\mathcal{A}^0_{3,g\to q}(s_{14})-S^2_{g\to q}\,\Gamma^{(1)}_{qg}(z_1)\otimes\Gamma^{(1)}_{qg}(z_2)\\
&\quad-\frac{1}{2}S_{g\to q}\,\Gamma^{(1)}_{qg}(z_2)\otimes\mathcal{A}^0_{3,g\to q}(s_{14})\Big]\,\texttt{C0g0ZFH}(4,2,3,1,H)\\
4 \quad &+\Big[-\frac{1}{2}S_{g\to q}\,\Gamma^{(1)}_{qg}(z_1)\otimes\mathcal{A}^0_{3,g\to q}(s_{23})-\frac{1}{4}\,\mathcal{A}^0_{3,g\to q}(s_{23})\otimes\mathcal{A}^0_{3,g\to q}(s_{14})-S^2_{g\to q}\,\Gamma^{(1)}_{qg}(z_1)\otimes\Gamma^{(1)}_{qg}(z_2)\\
&\quad-\frac{1}{2}S_{g\to q}\,\Gamma^{(1)}_{qg}(z_2)\otimes\mathcal{A}^0_{3,g\to q}(s_{14})\Big]\,\texttt{C0g0ZFH}(4,3,2,1,H)
\end{aligned}
\tag{C.78}
$$

qbgC0g2ZFHU

$$
\begin{aligned}
&\texttt{qbgC0g2ZFHU}(1,2,3,4,\texttt{H}) =\\
1 \quad &+\Big[+\mathcal{A}^0_{3,g\to q}(s_{23})+2S_{g\to q}\,\Gamma^{(1)}_{qg}(z_2)\Big]\,\Big(-\frac{b_0}{\epsilon}\texttt{sC0g0ZFH}(4,3,2,1,H)+\texttt{sC0g1ZFH}(4,3,2,1,H)\Big)\\
2 \quad &+\Big[+\mathcal{A}^0_{3,g\to q}(s_{23})\otimes\mathcal{A}^0_{3,q}(s_{14})+2S_{g\to q}\,\Gamma^{(1)}_{qg}(z_2)\otimes\mathcal{A}^0_{3,q}(s_{14})-2S_{g\to q}\,\Gamma^{(1)}_{qg}(z_2)\otimes\Gamma^{(1)}_{qq}(z_1)\\
&\quad+\mathcal{A}^0_{3,g\to q}(s_{23})\otimes\mathcal{A}^0_{3,q}(s_{23})+2S_{g\to q}\,\Gamma^{(1)}_{qg}(z_2)\otimes\mathcal{A}^0_{3,q}(s_{23})-2S_{g\to q}\,\Gamma^{(1)}_{qg}(z_2)\otimes\Gamma^{(1)}_{qq}(z_2)\\
&\quad\Big]\,\texttt{sC0g0ZFH}(4,3,2,1,H)\\
3 \quad &+\Big[-\Gamma^{(1)}_{qq}(z_1)\otimes\mathcal{A}^0_{3,g\to q}(s_{23})-2S_{g\to q}\,\Gamma^{(1)}_{qg}(z_2)\otimes\Gamma^{(1)}_{qq}(z_1)-\Gamma^{(1)}_{gg}(z_2)\otimes\mathcal{A}^0_{3,g\to q}(s_{23})
\end{aligned}
$$

$$
\begin{aligned}
& - 2S_{g\to q}\,\Gamma^{(1)}_{gg}(z_2)\otimes\Gamma^{(1)}_{qg}(z_2)\Big]\texttt{sC0g0ZFH}(4,3,2,1,H)\\
4\quad & +\Big[+S_{g\to q}\,\Gamma^{(1)}_{gg}(z_2)\otimes\Gamma^{(1)}_{qg}(z_2)+2S_{g\to q}\,\Gamma^{(1)}_{qg}(z_2)\otimes\Gamma^{(1)}_{qq}(z_1)+S_{g\to q}\,\Gamma^{(1)}_{qg}(z_2)\otimes\Gamma^{(1)}_{qq}(z_2)\\
& \Big]\texttt{sC0g0ZFH}(4,3,2,1,H)\\
5\quad & +\Big[+\frac{b_0}{\epsilon}\left(\frac{s_{23}}{\mu_R^2}\right)^{-\epsilon}\mathcal{A}^0_{3,g\to q}(s_{23})+2S_{g\to q}\,\Gamma^{(2)}_{qg}(z_2)-\mathcal{A}^0_{3,g\to q}(s_{23})\otimes\mathcal{A}^0_{3,q}(s_{23})\\
& +2\,\mathcal{A}^0_{4,g}(s_{23})+\mathcal{A}^1_{3,g}(s_{23})\Big]\texttt{sC0g0ZFH}(4,3,2,1,H)
\end{aligned}
\tag{C.79}
$$

qbqpC0g2ZFHU

$$
\begin{aligned}
&\texttt{qbqpC0g2ZFHU}(4,3,2,1,\texttt{H})=\\
1\quad & +\Big[-\mathcal{A}^0_{3,q}(s_{14})-\mathcal{A}^0_{3,q}(s_{23})+\Gamma^{(1)}_{qq}(z_1)\\
& +\Gamma^{(1)}_{qq}(z_2)\Big]\left(-\frac{b_0}{\epsilon}\texttt{C0g0ZFH}(4,3,2,1,H)+\texttt{C0g1ZFH}(4,3,2,1,H)\right)\\
2\quad & +\Big[-\mathcal{A}^0_{3,q}(s_{14})\otimes\mathcal{A}^0_{3,q}(s_{14})-2\,\mathcal{A}^0_{3,q}(s_{14})\otimes\mathcal{A}^0_{3,q}(s_{23})-\mathcal{A}^0_{3,q}(s_{23})\otimes\mathcal{A}^0_{3,q}(s_{23})\Big]\texttt{C0g0ZFH}(4,3,2,1,H)\\
3\quad & +\Big[+\mathcal{A}^0_{3,q}(s_{23})\mathcal{A}^0_{3,q}(s_{14})\Big]\texttt{C0g0ZFH}(4,3,2,1,H)\\
4\quad & +\Big[+\Gamma^{(1)}_{qq}(z_1)\otimes\mathcal{A}^0_{3,q}(s_{14})+\Gamma^{(1)}_{qq}(z_1)\otimes\mathcal{A}^0_{3,q}(s_{23})+\Gamma^{(1)}_{qq}(z_2)\otimes\mathcal{A}^0_{3,q}(s_{14})\\
& +\Gamma^{(1)}_{qq}(z_2)\otimes\mathcal{A}^0_{3,q}(s_{23})\Big]\texttt{C0g0ZFH}(4,3,2,1,H)\\
5\quad & +\Big[-\Gamma^{(1)}_{qq}(z_1)\otimes\Gamma^{(1)}_{qq}(z_1)-2\,\Gamma^{(1)}_{qq}(z_1)\otimes\Gamma^{(1)}_{qq}(z_2)-\Gamma^{(1)}_{qq}(z_2)\otimes\Gamma^{(1)}_{qq}(z_2)\Big]\texttt{C0g0ZFH}(4,3,2,1,H)\\
6\quad & +\Big[+\frac{1}{2}\,\Gamma^{(1)}_{qq}(z_1)\otimes\Gamma^{(1)}_{qq}(z_1)+\Gamma^{(1)}_{qq}(z_1)\otimes\Gamma^{(1)}_{qq}(z_2)+\frac{1}{2}\,\Gamma^{(1)}_{qq}(z_2)\otimes\Gamma^{(1)}_{qq}(z_2)\Big]\texttt{C0g0ZFH}(4,3,2,1,H)\\
7\quad & +\Big[-\mathcal{A}^1_{3,q}(s_{14})-\mathcal{A}^1_{3,q}(s_{23})\Big]\texttt{C0g0ZFH}(4,3,2,1,H)\\
8\quad & +\Big[+\mathcal{A}^0_{3,q}(s_{14})\otimes\mathcal{A}^0_{3,q}(s_{14})+\mathcal{A}^0_{3,q}(s_{23})\otimes\mathcal{A}^0_{3,q}(s_{23})\Big]\texttt{C0g0ZFH}(4,3,2,1,H)\\
9\quad & +\Big[-\mathcal{A}^0_{4,q}(s_{14})-\mathcal{A}^0_{4,q}(s_{23})\Big]\texttt{C0g0ZFH}(4,3,2,1,H)\\
10\quad & +\Big[+\Gamma^{(2)}_{qq}(z_1)+\Gamma^{(2)}_{qq}(z_2)\Big]\texttt{C0g0ZFH}(4,3,2,1,H)\\
11\quad & +\Big[-\frac{b_0}{\epsilon}\left(\frac{s_{14}}{\mu_R^2}\right)^{-\epsilon}\mathcal{A}^0_{3,q}(s_{14})-\frac{b_0}{\epsilon}\left(\frac{s_{23}}{\mu_R^2}\right)^{-\epsilon}\mathcal{A}^0_{3,q}(s_{23})\Big]\texttt{C0g0ZFH}(4,3,2,1,H)
\end{aligned}
\tag{C.80}
$$

qbRC0g2ZFHU

$$
\texttt{qbRC0g2ZFHU}(1,2,3,4,\texttt{H})=
$$

$$
\begin{aligned}
1 \quad & + \Big[- S_{q\to g}\,\Gamma^{(1)}_{gq}(z_2) \otimes \mathcal{A}^0_{3,qg\to qq}(s_{12}) - \Gamma^{(1)}_{gq}(z_2) \otimes \Gamma^{(1)}_{qg}(z_2) \Big] \texttt{C0g0ZFH}(4,3,2,1,H) \\
2 \quad & + \Big[+ \frac{1}{2}\,\Gamma^{(1)}_{gq}(z_2)\Gamma^{(1)}_{qg}(z_2) \Big] \texttt{C0g0ZFH}(4,3,2,1,H) \\
3 \quad & + \Big[- S_{q\to g}\,\Gamma^{(1)}_{gq}(z_2) \otimes \mathcal{A}^0_{3,qg\to qq}(s_{12}) - \Gamma^{(1)}_{gq}(z_2) \otimes \Gamma^{(1)}_{qg}(z_2) \Big] \texttt{C0g0ZFH}(4,2,3,1,H) \\
4 \quad & + \Big[+ \frac{1}{2}\,\Gamma^{(1)}_{gq}(z_2)\Gamma^{(1)}_{qg}(z_2) \Big] \texttt{C0g0ZFH}(4,2,3,1,H) \\
5 \quad & + \Big[- \mathcal{B}^0_{4,qq'}(s_{12}) + \Gamma^{(2)}_{q\bar{Q}}(z_2) \Big] \texttt{C0g0ZFH}(4,2,3,1,H) \\
6 \quad & + \Big[- \mathcal{B}^0_{4,qq'}(s_{12}) + \Gamma^{(2)}_{q\bar{Q}}(z_2) \Big] \texttt{C0g0ZFH}(4,3,2,1,H)
\end{aligned}
\tag{C.81}
$$

qgC0g2ZFHU

$$
\begin{aligned}
&\texttt{qgC0g2ZFHU}(1,2,3,4,\texttt{H}) = \\
1 \quad & + \Big[+ \mathcal{A}^0_{3,g\to q}(s_{23}) + 2S_{g\to q}\,\Gamma^{(1)}_{qg}(z_2) \Big] \left(-\frac{b_0}{\epsilon} \texttt{sC0g0ZFH}(1,3,2,4,H) + \texttt{sC0g1ZFH}(1,3,2,4,H) \right) \\
2 \quad & + \Big[+ \mathcal{A}^0_{3,g\to q}(s_{23}) \otimes \mathcal{A}^0_{3,q}(s_{14}) + 2S_{g\to q}\,\Gamma^{(1)}_{qg}(z_2) \otimes \mathcal{A}^0_{3,q}(s_{14}) - 2S_{g\to q}\,\Gamma^{(1)}_{qg}(z_2) \otimes \Gamma^{(1)}_{qq}(z_1) \\
& \quad + \mathcal{A}^0_{3,g\to q}(s_{23}) \otimes \mathcal{A}^0_{3,q}(s_{23}) + 2S_{g\to q}\,\Gamma^{(1)}_{qg}(z_2) \otimes \mathcal{A}^0_{3,q}(s_{23}) - 2S_{g\to q}\,\Gamma^{(1)}_{qg}(z_2) \otimes \Gamma^{(1)}_{qq}(z_2) \\
& \quad \Big] \texttt{sC0g0ZFH}(1,3,2,4,H) \\
3 \quad & + \Big[- \Gamma^{(1)}_{qq}(z_1) \otimes \mathcal{A}^0_{3,g\to q}(s_{23}) - 2S_{g\to q}\,\Gamma^{(1)}_{qg}(z_2) \otimes \Gamma^{(1)}_{qq}(z_1) - \Gamma^{(1)}_{gg}(z_2) \otimes \mathcal{A}^0_{3,g\to q}(s_{23}) \\
& \quad - 2S_{g\to q}\,\Gamma^{(1)}_{gg}(z_2) \otimes \Gamma^{(1)}_{qg}(z_2) \Big] \texttt{sC0g0ZFH}(1,3,2,4,H) \\
4 \quad & + \Big[+ S_{g\to q}\,\Gamma^{(1)}_{gg}(z_2) \otimes \Gamma^{(1)}_{qg}(z_2) + 2S_{g\to q}\,\Gamma^{(1)}_{qg}(z_2) \otimes \Gamma^{(1)}_{qq}(z_1) + S_{g\to q}\,\Gamma^{(1)}_{qg}(z_2) \otimes \Gamma^{(1)}_{qq}(z_2) \\
& \quad \Big] \texttt{sC0g0ZFH}(1,3,2,4,H) \\
5 \quad & + \Big[+ \frac{b_0}{\epsilon} \left(\frac{s_{23}}{\mu_R^2} \right)^{-\epsilon} \mathcal{A}^0_{3,g\to q}(s_{23}) + 2S_{g\to q}\,\Gamma^{(2)}_{qg}(z_2) - \mathcal{A}^0_{3,g\to q}(s_{23}) \otimes \mathcal{A}^0_{3,q}(s_{23}) \\
& \quad + 2\,\mathcal{A}^0_{4,g}(s_{23}) + \mathcal{A}^1_{3,g}(s_{23}) \Big] \texttt{sC0g0ZFH}(1,3,2,4,H)
\end{aligned}
\tag{C.82}
$$

qqpC0g2ZFHU

$$
\begin{aligned}
&\texttt{qqpC0g2ZFHU}(1,3,2,4,\texttt{H}) = \\
1 \quad & + \Big[- \mathcal{A}^0_{3,q}(s_{14}) - \mathcal{A}^0_{3,q}(s_{23}) + \Gamma^{(1)}_{qq}(z_1) \\
& \quad + \Gamma^{(1)}_{qq}(z_2) \Big] \left(-\frac{b_0}{\epsilon} \texttt{C0g0ZFH}(1,3,2,4,H) + \texttt{C0g1ZFH}(1,3,2,4,H) \right)
\end{aligned}
$$

$$
\begin{aligned}
2 \quad & + \Big[- \mathcal{A}^0_{3,q}(s_{14}) \otimes \mathcal{A}^0_{3,q}(s_{14}) - 2\,\mathcal{A}^0_{3,q}(s_{14}) \otimes \mathcal{A}^0_{3,q}(s_{23}) - \mathcal{A}^0_{3,q}(s_{23}) \otimes \mathcal{A}^0_{3,q}(s_{23}) \Big] \texttt{C0g0ZFH}(1,3,2,4,H) \\
3 \quad & + \Big[+ \mathcal{A}^0_{3,q}(s_{23}) \mathcal{A}^0_{3,q}(s_{14}) \Big] \texttt{C0g0ZFH}(1,3,2,4,H) \\
4 \quad & + \Big[+ \Gamma^{(1)}_{qq}(z_1) \otimes \mathcal{A}^0_{3,q}(s_{14}) + \Gamma^{(1)}_{qq}(z_1) \otimes \mathcal{A}^0_{3,q}(s_{23}) + \Gamma^{(1)}_{qq}(z_2) \otimes \mathcal{A}^0_{3,q}(s_{14}) \\
& \quad + \Gamma^{(1)}_{qq}(z_2) \otimes \mathcal{A}^0_{3,q}(s_{23}) \Big] \texttt{C0g0ZFH}(1,3,2,4,H) \\
5 \quad & + \Big[- \Gamma^{(1)}_{qq}(z_1) \otimes \Gamma^{(1)}_{qq}(z_1) - 2\,\Gamma^{(1)}_{qq}(z_1) \otimes \Gamma^{(1)}_{qq}(z_2) - \Gamma^{(1)}_{qq}(z_2) \otimes \Gamma^{(1)}_{qq}(z_2) \Big] \texttt{C0g0ZFH}(1,3,2,4,H) \\
6 \quad & + \Big[+ \frac{1}{2}\,\Gamma^{(1)}_{qq}(z_1) \otimes \Gamma^{(1)}_{qq}(z_1) + \Gamma^{(1)}_{qq}(z_1) \otimes \Gamma^{(1)}_{qq}(z_2) + \frac{1}{2}\,\Gamma^{(1)}_{qq}(z_2) \otimes \Gamma^{(1)}_{qq}(z_2) \Big] \texttt{C0g0ZFH}(1,3,2,4,H) \\
7 \quad & + \Big[- \mathcal{A}^1_{3,q}(s_{14}) - \mathcal{A}^1_{3,q}(s_{23}) \Big] \texttt{C0g0ZFH}(1,3,2,4,H) \\
8 \quad & + \Big[+ \mathcal{A}^0_{3,q}(s_{14}) \otimes \mathcal{A}^0_{3,q}(s_{14}) + \mathcal{A}^0_{3,q}(s_{23}) \otimes \mathcal{A}^0_{3,q}(s_{23}) \Big] \texttt{C0g0ZFH}(1,3,2,4,H) \\
9 \quad & + \Big[- \mathcal{A}^0_{4,q}(s_{14}) - \mathcal{A}^0_{4,q}(s_{23}) \Big] \texttt{C0g0ZFH}(1,3,2,4,H) \\
10 \quad & + \Big[+ \Gamma^{(2)}_{qq}(z_1) + \Gamma^{(2)}_{qq}(z_2) \Big] \texttt{C0g0ZFH}(1,3,2,4,H) \\
11 \quad & + \Big[- \frac{b_0}{\epsilon} \left(\frac{s_{14}}{\mu_R^2} \right)^{-\epsilon} \mathcal{A}^0_{3,q}(s_{14}) - \frac{b_0}{\epsilon} \left(\frac{s_{23}}{\mu_R^2} \right)^{-\epsilon} \mathcal{A}^0_{3,q}(s_{23}) \Big] \texttt{C0g0ZFH}(1,3,2,4,H)
\end{aligned}
\tag{C.83}
$$

qRC0g2ZFHU

$$
\begin{aligned}
& \texttt{qRC0g2ZFHU}(1,2,3,4,\texttt{H}) = \\
1 \quad & + \Big[- S_{q\to g}\,\Gamma^{(1)}_{gq}(z_2) \otimes \mathcal{A}^0_{3,qg\to qq}(s_{12}) - \Gamma^{(1)}_{gq}(z_2) \otimes \Gamma^{(1)}_{qg}(z_2) \Big] \texttt{C0g0ZFH}(1,3,2,4,H) \\
2 \quad & + \Big[+ \frac{1}{2}\,\Gamma^{(1)}_{gq}(z_2) \Gamma^{(1)}_{qg}(z_2) \Big] \texttt{C0g0ZFH}(1,3,2,4,H) \\
3 \quad & + \Big[- S_{q\to g}\,\Gamma^{(1)}_{gq}(z_2) \otimes \mathcal{A}^0_{3,qg\to qq}(s_{12}) - \Gamma^{(1)}_{gq}(z_2) \otimes \Gamma^{(1)}_{qg}(z_2) \Big] \texttt{C0g0ZFH}(1,2,3,4,H) \\
4 \quad & + \Big[+ \frac{1}{2}\,\Gamma^{(1)}_{gq}(z_2) \Gamma^{(1)}_{qg}(z_2) \Big] \texttt{C0g0ZFH}(1,2,3,4,H) \\
5 \quad & + \Big[- \mathcal{B}^0_{4,qq'}(s_{12}) + \Gamma^{(2)}_{q\bar{Q}}(z_2) \Big] \texttt{C0g0ZFH}(1,2,3,4,H) \\
6 \quad & + \Big[- \mathcal{B}^0_{4,qq'}(s_{12}) + \Gamma^{(2)}_{qQ}(z_2) \Big] \texttt{C0g0ZFH}(1,3,2,4,H)
\end{aligned}
\tag{C.84}
$$

qbgCt0g2ZFHU

$$
\begin{aligned}
& \texttt{qbgCt0g2ZFHU}(1,2,3,4,\texttt{H}) = \\
1 \quad & + \Big[+ \mathcal{A}^0_{3,g\to q}(s_{23}) + 2 S_{g\to q}\,\Gamma^{(1)}_{qg}(z_2) \Big] \texttt{sC0g1ZFH}(4,3,2,1,H)
\end{aligned}
$$

$$
\begin{aligned}
2 \quad &+\Big[+ \mathcal{A}^0_{3,g\to q}(s_{23}) \otimes \mathcal{A}^0_{3,q}(s_{14}) + 2S_{g\to q}\,\Gamma^{(1)}_{qg}(z_2) \otimes \mathcal{A}^0_{3,q}(s_{14}) - 2S_{g\to q}\,\Gamma^{(1)}_{qg}(z_2) \otimes \Gamma^{(1)}_{qq}(z_1) \\
&\quad + \mathcal{A}^0_{3,g\to q}(s_{23}) \otimes \mathcal{A}^0_{3,q}(s_{23}) + 2S_{g\to q}\,\Gamma^{(1)}_{qg}(z_2) \otimes \mathcal{A}^0_{3,q}(s_{23}) - 2S_{g\to q}\,\Gamma^{(1)}_{qg}(z_2) \otimes \Gamma^{(1)}_{qq}(z_2) \\
&\quad \Big]\texttt{sC0g0ZFH}(4,3,2,1,H) \\
3 \quad &+\Big[- \Gamma^{(1)}_{qq}(z_1) \otimes \mathcal{A}^0_{3,g\to q}(s_{23}) - 2S_{g\to q}\,\Gamma^{(1)}_{qg}(z_2) \otimes \Gamma^{(1)}_{qq}(z_1) \Big]\texttt{sC0g0ZFH}(4,3,2,1,H) \\
4 \quad &+\Big[+ 2S_{g\to q}\,\Gamma^{(1)}_{qg}(z_2) \otimes \Gamma^{(1)}_{qq}(z_1) + S_{g\to q}\,\Gamma^{(1)}_{qg}(z_2) \otimes \Gamma^{(1)}_{qq}(z_2) \\
&\quad \Big]\texttt{sC0g0ZFH}(4,3,2,1,H) \\
5 \quad &+\Big[+ \tilde{\mathcal{A}}^0_{4,g}(s_{23}) - 2S_{g\to q}\,\widetilde{\Gamma}^{(2)}_{qg}(z_2) + \tilde{\mathcal{A}}^1_{3,g}(s_{23}) \\
&\quad - \mathcal{A}^0_{3,g\to q}(s_{23}) \otimes \mathcal{A}^0_{3,q}(s_{23}) \Big]\texttt{sC0g0ZFH}(4,3,2,1,H)
\end{aligned}
\tag{C.85}
$$

qbqpCt0g2ZFHU

$$
\begin{aligned}
&\texttt{qbqpCt0g2ZFHU}(4,3,2,1,\texttt{H}) = \\
1 \quad &+\Big[- \mathcal{A}^0_{3,q}(s_{14}) + \Gamma^{(1)}_{qq}(z_1) - \mathcal{A}^0_{3,q}(s_{23}) \\
&\quad + \Gamma^{(1)}_{qq}(z_2) \Big]\texttt{C0g1ZFH}(4,3,2,1,H) \\
2 \quad &+\Big[+ \Gamma^{(1)}_{qq}(z_1) \otimes \mathcal{A}^0_{3,q}(s_{14}) + \Gamma^{(1)}_{qq}(z_1) \otimes \mathcal{A}^0_{3,q}(s_{23}) + \Gamma^{(1)}_{qq}(z_2) \otimes \mathcal{A}^0_{3,q}(s_{14}) \\
&\quad + \Gamma^{(1)}_{qq}(z_2) \otimes \mathcal{A}^0_{3,q}(s_{23}) \Big]\texttt{C0g0ZFH}(4,3,2,1,H) \\
3 \quad &+\Big[- \frac{1}{2}\,\mathcal{A}^0_{3,q}(s_{14}) \otimes \mathcal{A}^0_{3,q}(s_{14}) - \mathcal{A}^0_{3,q}(s_{23}) \otimes \mathcal{A}^0_{3,q}(s_{14}) - \frac{1}{2}\,\mathcal{A}^0_{3,q}(s_{23}) \otimes \mathcal{A}^0_{3,q}(s_{23}) \Big]\texttt{C0g0ZFH}(4,3,2,1,H) \\
4 \quad &+\Big[- \frac{1}{2}\,\Gamma^{(1)}_{qq}(z_1) \otimes \Gamma^{(1)}_{qq}(z_1) - \Gamma^{(1)}_{qq}(z_1) \otimes \Gamma^{(1)}_{qq}(z_2) - \frac{1}{2}\,\Gamma^{(1)}_{qq}(z_2) \otimes \Gamma^{(1)}_{qq}(z_2) \Big]\texttt{C0g0ZFH}(4,3,2,1,H) \\
5 \quad &+\Big[- \frac{1}{2}\,\tilde{\mathcal{A}}^0_{4,q}(s_{14}) - 2\,\mathcal{C}^0_{4,q}(s_{14}) - \mathcal{C}^0_{4,\bar{q},\bar{q}q\bar{q}}(s_{14}) \\
&\quad - \tilde{\mathcal{A}}^1_{3,q}(s_{14}) + \frac{1}{2}\,\mathcal{A}^0_{3,q}(s_{14}) \otimes \mathcal{A}^0_{3,q}(s_{14}) - \widetilde{\widetilde{\Gamma}}^{(2)}_{qq}(z_1) \Big]\texttt{C0g0ZFH}(4,3,2,1,H) \\
6 \quad &+\Big[- \frac{1}{2}\,\tilde{\mathcal{A}}^0_{4,q}(s_{23}) - 2\,\mathcal{C}^0_{4,q}(s_{23}) - \mathcal{C}^0_{4,\bar{q},\bar{q}q\bar{q}}(s_{23}) \\
&\quad - \tilde{\mathcal{A}}^1_{3,q}(s_{23}) + \frac{1}{2}\,\mathcal{A}^0_{3,q}(s_{23}) \otimes \mathcal{A}^0_{3,q}(s_{23}) - \widetilde{\widetilde{\Gamma}}^{(2)}_{qq}(z_2) \Big]\texttt{C0g0ZFH}(4,3,2,1,H) \\
7 \quad &+\Big[- \mathcal{C}^0_{4,\bar{q},q\bar{q}\bar{q}}(s_{14}) - \Gamma^{(2)}_{q\bar{q}}t(z_1) \Big]\texttt{C0g0ZFH}(1,3,2,4,H) \\
8 \quad &+\Big[- \mathcal{C}^0_{4,\bar{q},q\bar{q}\bar{q}}(s_{23}) - \Gamma^{(2)}_{q\bar{q}}t(z_2) \Big]\texttt{C0g0ZFH}(4,2,3,1,H)
\end{aligned}
\tag{C.86}
$$

qgCt0g2ZFHU

$$
\begin{aligned}
&\texttt{qgCt0g2ZFHU}(1,2,3,4,\texttt{H}) = \\
1 \quad &+\Big[+ \mathcal{A}^0_{3,g\to q}(s_{23}) + 2S_{g\to q}\,\Gamma^{(1)}_{qg}(z_2)\Big]\texttt{sC0g1ZFH}(1,3,2,4,H) \\
2 \quad &+\Big[+ \mathcal{A}^0_{3,g\to q}(s_{23})\otimes\mathcal{A}^0_{3,q}(s_{14}) + 2S_{g\to q}\,\Gamma^{(1)}_{qg}(z_2)\otimes\mathcal{A}^0_{3,q}(s_{14}) - 2S_{g\to q}\,\Gamma^{(1)}_{qg}(z_2)\otimes\Gamma^{(1)}_{qq}(z_1) \\
&\quad + \mathcal{A}^0_{3,g\to q}(s_{23})\otimes\mathcal{A}^0_{3,q}(s_{23}) + 2S_{g\to q}\,\Gamma^{(1)}_{qg}(z_2)\otimes\mathcal{A}^0_{3,q}(s_{23}) - 2S_{g\to q}\,\Gamma^{(1)}_{qg}(z_2)\otimes\Gamma^{(1)}_{qq}(z_2) \\
&\quad \Big]\texttt{sC0g0ZFH}(1,3,2,4,H) \\
3 \quad &+\Big[- \Gamma^{(1)}_{qq}(z_1)\otimes\mathcal{A}^0_{3,g\to q}(s_{23}) - 2S_{g\to q}\,\Gamma^{(1)}_{qg}(z_2)\otimes\Gamma^{(1)}_{qq}(z_1)\Big]\texttt{sC0g0ZFH}(1,3,2,4,H) \\
4 \quad &+\Big[+ 2S_{g\to q}\,\Gamma^{(1)}_{qg}(z_2)\otimes\Gamma^{(1)}_{qq}(z_1) + S_{g\to q}\,\Gamma^{(1)}_{qg}(z_2)\otimes\Gamma^{(1)}_{qq}(z_2)\Big]\texttt{sC0g0ZFH}(1,3,2,4,H) \\
5 \quad &+\Big[+ \tilde{\mathcal{A}}^0_{4,g}(s_{23}) - 2S_{g\to q}\,\widetilde{\Gamma}^{(2)}_{qg}(z_2) + \tilde{\mathcal{A}}^1_{3,g}(s_{23}) \\
&\quad - \mathcal{A}^0_{3,g\to q}(s_{23})\otimes\mathcal{A}^0_{3,q}(s_{23})\Big]\texttt{sC0g0ZFH}(1,3,2,4,H)
\end{aligned}
\tag{C.87}
$$

qqpCt0g2ZFHU

$$
\begin{aligned}
&\texttt{qqpCt0g2ZFHU}(1,3,2,4,\texttt{H}) = \\
1 \quad &+\Big[- \mathcal{A}^0_{3,q}(s_{14}) + \Gamma^{(1)}_{qq}(z_1) - \mathcal{A}^0_{3,q}(s_{23}) \\
&\quad + \Gamma^{(1)}_{qq}(z_2)\Big]\texttt{C0g1ZFH}(1,3,2,4,H) \\
2 \quad &+\Big[+ \Gamma^{(1)}_{qq}(z_1)\otimes\mathcal{A}^0_{3,q}(s_{14}) + \Gamma^{(1)}_{qq}(z_1)\otimes\mathcal{A}^0_{3,q}(s_{23}) + \Gamma^{(1)}_{qq}(z_2)\otimes\mathcal{A}^0_{3,q}(s_{14}) \\
&\quad + \Gamma^{(1)}_{qq}(z_2)\otimes\mathcal{A}^0_{3,q}(s_{23})\Big]\texttt{C0g0ZFH}(1,3,2,4,H) \\
3 \quad &+\Big[- \frac{1}{2}\,\mathcal{A}^0_{3,q}(s_{14})\otimes\mathcal{A}^0_{3,q}(s_{14}) - \mathcal{A}^0_{3,q}(s_{23})\otimes\mathcal{A}^0_{3,q}(s_{14}) - \frac{1}{2}\,\mathcal{A}^0_{3,q}(s_{23})\otimes\mathcal{A}^0_{3,q}(s_{23})\Big]\texttt{C0g0ZFH}(1,3,2,4,H) \\
4 \quad &+\Big[- \frac{1}{2}\,\Gamma^{(1)}_{qq}(z_1)\otimes\Gamma^{(1)}_{qq}(z_1) - \Gamma^{(1)}_{qq}(z_1)\otimes\Gamma^{(1)}_{qq}(z_2) - \frac{1}{2}\,\Gamma^{(1)}_{qq}(z_2)\otimes\Gamma^{(1)}_{qq}(z_2)\Big]\texttt{C0g0ZFH}(1,3,2,4,H) \\
5 \quad &+\Big[- \frac{1}{2}\,\tilde{\mathcal{A}}^0_{4,q}(s_{14}) - 2\,\mathcal{C}^0_{4,q}(s_{14}) - \mathcal{C}^0_{4,\bar{q},\bar{q}q\bar{q}}(s_{14}) \\
&\quad - \tilde{\mathcal{A}}^1_{3,q}(s_{14}) + \frac{1}{2}\,\mathcal{A}^0_{3,q}(s_{14})\otimes\mathcal{A}^0_{3,q}(s_{14}) - \widetilde{\widetilde{\Gamma}}^{(2)}_{qq}(z_1)\Big]\texttt{C0g0ZFH}(1,3,2,4,H) \\
6 \quad &+\Big[- \frac{1}{2}\,\tilde{\mathcal{A}}^0_{4,q}(s_{23}) - 2\,\mathcal{C}^0_{4,q}(s_{23}) - \mathcal{C}^0_{4,\bar{q},\bar{q}q\bar{q}}(s_{23}) \\
&\quad - \tilde{\mathcal{A}}^1_{3,q}(s_{23}) + \frac{1}{2}\,\mathcal{A}^0_{3,q}(s_{23})\otimes\mathcal{A}^0_{3,q}(s_{23}) - \widetilde{\widetilde{\Gamma}}^{(2)}_{qq}(z_2)\Big]\texttt{C0g0ZFH}(1,3,2,4,H) \\
7 \quad &+\Big[- \mathcal{C}^0_{4,\bar{q},q\bar{q}\bar{q}}(s_{14}) - \Gamma^{(2)}_{q\bar{q}}t(z_1)\Big]\texttt{C0g0ZFH}(4,3,2,1,H)
\end{aligned}
$$

$$8 \quad +\Big[-\mathcal{C}^0_{4,\bar{q},q\bar{q}\bar{q}}(s_{23}) - \Gamma^{(2)}_{q\bar{q}} t(z_2)\Big]\texttt{C0g0ZFH}(1,2,3,4,H) \tag{C.88}$$

qbgCh0g2ZFHU

$$\begin{aligned}
&\texttt{qbgCh0g2ZFHU}(\texttt{1},\texttt{2},\texttt{3},\texttt{4},\texttt{H}) = \\
1 \quad &+\Big[-2\frac{b_F}{\epsilon} S_{g\to q}\,\Gamma^{(1)}_{qg}(z_2) - \frac{b_F}{\epsilon}\,\mathcal{A}^0_{3,g\to q}(s_{23})\Big]\texttt{sC0g0ZFH}(4,3,2,1,H) \\
2 \quad &+\Big[-\Gamma^{(1)}_{gg,F}(z_2)\otimes\mathcal{A}^0_{3,g\to q}(s_{23}) - S_{g\to q}\,\Gamma^{(1)}_{gg,F}(z_2)\otimes\Gamma^{(1)}_{qg}(z_2)\Big]\texttt{sC0g0ZFH}(4,3,2,1,H) \\
3 \quad &+\Big[+\frac{b_F}{\epsilon}\left(\frac{s_{23}}{\mu_R^2}\right)^{-\epsilon}\mathcal{A}^0_{3,g\to q}(s_{23}) + 2S_{g\to q}\,\Gamma^{(2)}_{qg,F}(z_2) + \hat{\mathcal{A}}^1_{3,g}(s_{23})\Big]\texttt{sC0g0ZFH}(4,3,2,1,H)
\end{aligned} \tag{C.89}$$

qbqpCh0g2ZFHU

$$\begin{aligned}
&\texttt{qbqpCh0g2ZFHU}(\texttt{4},\texttt{3},\texttt{2},\texttt{1},\texttt{H}) = \\
1 \quad &+\Big[+\frac{b_F}{\epsilon}\,\mathcal{A}^0_{3,q}(s_{14}) - \frac{b_F}{\epsilon}\,\Gamma^{(1)}_{qq}(z_1) + \frac{b_F}{\epsilon}\,\mathcal{A}^0_{3,q}(s_{23}) \\
&\quad - \frac{b_F}{\epsilon}\,\Gamma^{(1)}_{qq}(z_2)\Big]\texttt{C0g0ZFH}(4,3,2,1,H) \\
2 \quad &+\Big[-\mathcal{B}^0_{4,q}(s_{14}) - \mathcal{B}^0_{4,q}(s_{23}) + \Gamma^{(2)}_{qq,F}(z_1) \\
&\quad + \Gamma^{(2)}_{qq,F}(z_2)\Big]\texttt{C0g0ZFH}(4,3,2,1,H) \\
3 \quad &+\Big[-\frac{b_F}{\epsilon}\,\mathcal{A}^0_{3,q}(s_{14})\left(\frac{s_{14}}{\mu_R^2}\right)^{-\epsilon} - \frac{b_F}{\epsilon}\,\mathcal{A}^0_{3,q}(s_{23})\left(\frac{s_{23}}{\mu_R^2}\right)^{-\epsilon} - \hat{\mathcal{A}}^1_{3,q}(s_{14}) \\
&\quad - \hat{\mathcal{A}}^1_{3,q}(s_{23})\Big]\texttt{C0g0ZFH}(4,3,2,1,H)
\end{aligned} \tag{C.90}$$

qgCh0g2ZFHU

$$\begin{aligned}
&\texttt{qgCh0g2ZFHU}(\texttt{1},\texttt{2},\texttt{3},\texttt{4},\texttt{H}) = \\
1 \quad &+\Big[-2\frac{b_F}{\epsilon} S_{g\to q}\,\Gamma^{(1)}_{qg}(z_2) - \frac{b_F}{\epsilon}\,\mathcal{A}^0_{3,g\to q}(s_{23})\Big]\texttt{sC0g0ZFH}(1,3,2,4,H) \\
2 \quad &+\Big[-\Gamma^{(1)}_{gg,F}(z_2)\otimes\mathcal{A}^0_{3,g\to q}(s_{23}) - S_{g\to q}\,\Gamma^{(1)}_{gg,F}(z_2)\otimes\Gamma^{(1)}_{qg}(z_2)\Big]\texttt{sC0g0ZFH}(1,3,2,4,H) \\
3 \quad &+\Big[+\frac{b_F}{\epsilon}\left(\frac{s_{23}}{\mu_R^2}\right)^{-\epsilon}\mathcal{A}^0_{3,g\to q}(s_{23}) + 2S_{g\to q}\,\Gamma^{(2)}_{qg,F}(z_2) + \hat{\mathcal{A}}^1_{3,g}(s_{23})\Big]\texttt{sC0g0ZFH}(1,3,2,4,H)
\end{aligned} \tag{C.91}$$

qqpCh0g2ZFHU

$$
\begin{aligned}
&\texttt{qqpCh0g2ZFHU}(1,3,2,4,\texttt{H}) = \\
1 \quad &+\Bigg[+ \frac{b_F}{\epsilon}\,\mathcal{A}^0_{3,q}(s_{14}) - \frac{b_F}{\epsilon}\,\Gamma^{(1)}_{qq}(z_1) + \frac{b_F}{\epsilon}\,\mathcal{A}^0_{3,q}(s_{23}) \\
&\quad - \frac{b_F}{\epsilon}\,\Gamma^{(1)}_{qq}(z_2)\Bigg]\texttt{C0g0ZFH}(1,3,2,4,H) \\
2 \quad &+\Bigg[- \mathcal{B}^0_{4,q}(s_{14}) - \mathcal{B}^0_{4,q}(s_{23}) + \Gamma^{(2)}_{qq,F}(z_1) \\
&\quad + \Gamma^{(2)}_{qq,F}(z_2)\Bigg]\texttt{C0g0ZFH}(1,3,2,4,H) \\
3 \quad &+\Bigg[- \frac{b_F}{\epsilon}\,\mathcal{A}^0_{3,q}(s_{14})\left(\frac{s_{14}}{\mu_R^2}\right)^{-\epsilon} - \frac{b_F}{\epsilon}\,\mathcal{A}^0_{3,q}(s_{23})\left(\frac{s_{23}}{\mu_R^2}\right)^{-\epsilon} - \hat{\mathcal{A}}^1_{3,q}(s_{14}) \\
&\quad - \hat{\mathcal{A}}^1_{3,q}(s_{23})\Bigg]\texttt{C0g0ZFH}(1,3,2,4,H)
\end{aligned}
\tag{C.92}
$$

ggC0g2WFHU

$$
\begin{aligned}
&\texttt{ggC0g2WFHU}(1,2,3,4,\texttt{H}) = \\
1 \quad &+\Bigg[- \frac{1}{2}S_{g\to q}\,\Gamma^{(1)}_{qg}(z_1)\otimes\mathcal{A}^0_{3,g\to q}(s_{23}) - \frac{1}{4}\,\mathcal{A}^0_{3,g\to q}(s_{23})\otimes\mathcal{A}^0_{3,g\to q}(s_{14}) - S^2_{g\to q}\,\Gamma^{(1)}_{qg}(z_1)\otimes\Gamma^{(1)}_{qg}(z_2) \\
&\quad - \frac{1}{2}S_{g\to q}\,\Gamma^{(1)}_{qg}(z_2)\otimes\mathcal{A}^0_{3,g\to q}(s_{14})\Bigg]\texttt{C0g0WFH}(1,3,2,4,H) \\
2 \quad &+\Bigg[- \frac{1}{2}S_{g\to q}\,\Gamma^{(1)}_{qg}(z_1)\otimes\mathcal{A}^0_{3,g\to q}(s_{23}) - \frac{1}{4}\,\mathcal{A}^0_{3,g\to q}(s_{23})\otimes\mathcal{A}^0_{3,g\to q}(s_{14}) - S^2_{g\to q}\,\Gamma^{(1)}_{qg}(z_1)\otimes\Gamma^{(1)}_{qg}(z_2) \\
&\quad - \frac{1}{2}S_{g\to q}\,\Gamma^{(1)}_{qg}(z_2)\otimes\mathcal{A}^0_{3,g\to q}(s_{14})\Bigg]\texttt{C0g0WFH}(1,2,3,4,H) \\
3 \quad &+\Bigg[- \frac{1}{2}S_{g\to q}\,\Gamma^{(1)}_{qg}(z_1)\otimes\mathcal{A}^0_{3,g\to q}(s_{23}) - \frac{1}{4}\,\mathcal{A}^0_{3,g\to q}(s_{23})\otimes\mathcal{A}^0_{3,g\to q}(s_{14}) - S^2_{g\to q}\,\Gamma^{(1)}_{qg}(z_1)\otimes\Gamma^{(1)}_{qg}(z_2) \\
&\quad - \frac{1}{2}S_{g\to q}\,\Gamma^{(1)}_{qg}(z_2)\otimes\mathcal{A}^0_{3,g\to q}(s_{14})\Bigg]\texttt{C0g0WFH}(4,2,3,1,H) \\
4 \quad &+\Bigg[- \frac{1}{2}S_{g\to q}\,\Gamma^{(1)}_{qg}(z_1)\otimes\mathcal{A}^0_{3,g\to q}(s_{23}) - \frac{1}{4}\,\mathcal{A}^0_{3,g\to q}(s_{23})\otimes\mathcal{A}^0_{3,g\to q}(s_{14}) - S^2_{g\to q}\,\Gamma^{(1)}_{qg}(z_1)\otimes\Gamma^{(1)}_{qg}(z_2) \\
&\quad - \frac{1}{2}S_{g\to q}\,\Gamma^{(1)}_{qg}(z_2)\otimes\mathcal{A}^0_{3,g\to q}(s_{14})\Bigg]\texttt{C0g0WFH}(4,3,2,1,H)
\end{aligned}
\tag{C.93}
$$

qbgC0g2WFHU

$$
\begin{aligned}
&\texttt{qbgC0g2WFHU}(1,2,3,4,\texttt{H}) = \\
1 \quad &+\Bigg[+ \mathcal{A}^0_{3,g\to q}(s_{23}) + 2S_{g\to q}\,\Gamma^{(1)}_{qg}(z_2)\Bigg]\left(-\frac{b_0}{\epsilon}\texttt{sC0g0WFH}(4,3,2,1,H) + \texttt{sC0g1WFH}(4,3,2,1,H)\right) \\
2 \quad &+\Bigg[+ \mathcal{A}^0_{3,g\to q}(s_{23})\otimes\mathcal{A}^0_{3,q}(s_{14}) + 2S_{g\to q}\,\Gamma^{(1)}_{qg}(z_2)\otimes\mathcal{A}^0_{3,q}(s_{14}) - 2S_{g\to q}\,\Gamma^{(1)}_{qg}(z_2)\otimes\Gamma^{(1)}_{qq}(z_1)
\end{aligned}
$$

$$
\begin{aligned}
&\quad + \mathcal{A}^0_{3,g\to q}(s_{23}) \otimes \mathcal{A}^0_{3,q}(s_{23}) + 2S_{g\to q}\,\Gamma^{(1)}_{qg}(z_2) \otimes \mathcal{A}^0_{3,q}(s_{23}) - 2S_{g\to q}\,\Gamma^{(1)}_{qg}(z_2) \otimes \Gamma^{(1)}_{qq}(z_2) \\
&\quad \Big]\,\texttt{sC0g0WFH}(4,3,2,1,H) \\
3 \quad &+\Big[- \Gamma^{(1)}_{qq}(z_1) \otimes \mathcal{A}^0_{3,g\to q}(s_{23}) - 2S_{g\to q}\,\Gamma^{(1)}_{qg}(z_2) \otimes \Gamma^{(1)}_{qq}(z_1) - \Gamma^{(1)}_{gg}(z_2) \otimes \mathcal{A}^0_{3,g\to q}(s_{23}) \\
&\quad - 2S_{g\to q}\,\Gamma^{(1)}_{gg}(z_2) \otimes \Gamma^{(1)}_{qg}(z_2) \Big]\,\texttt{sC0g0WFH}(4,3,2,1,H) \\
4 \quad &+\Big[+ 2S_{g\to q}\,\Gamma^{(1)}_{qg}(z_2) \otimes \Gamma^{(1)}_{qq}(z_1) + S_{g\to q}\,\Gamma^{(1)}_{qg}(z_2) \otimes \Gamma^{(1)}_{qq}(z_2) + S_{g\to q}\,\Gamma^{(1)}_{gg}(z_2) \otimes \Gamma^{(1)}_{qg}(z_2) \\
&\quad \Big]\,\texttt{sC0g0WFH}(4,3,2,1,H) \\
5 \quad &+\Big[+ \frac{b_0}{\epsilon}\left(\frac{s_{23}}{\mu_R^2}\right)^{-\epsilon} \mathcal{A}^0_{3,g\to q}(s_{23}) - \mathcal{A}^0_{3,g\to q}(s_{23}) \otimes \mathcal{A}^0_{3,q}(s_{23}) + 2S_{g\to q}\,\Gamma^{(2)}_{qg}(z_2) \\
&\quad + 2\,\mathcal{A}^0_{4,g}(s_{23}) + \mathcal{A}^1_{3,g}(s_{23}) \Big]\,\texttt{sC0g0WFH}(4,3,2,1,H)
\end{aligned}
\tag{C.94}
$$

qbqpC0g2WFHU

$$
\begin{aligned}
&\texttt{qbqpC0g2WFHU}(4,3,2,1,\texttt{H}) = \\
1 \quad &+\Big[- \mathcal{A}^0_{3,q}(s_{14}) + \Gamma^{(1)}_{qq}(z_1) - \mathcal{A}^0_{3,q}(s_{23}) \\
&\quad + \Gamma^{(1)}_{qq}(z_2) \Big] \left(-\frac{b_0}{\epsilon}\texttt{C0g0WFH}(4,3,2,1,H) + \texttt{C0g1WFH}(4,3,2,1,H) \right) \\
2 \quad &+\Big[- \mathcal{A}^0_{3,q}(s_{14}) \otimes \mathcal{A}^0_{3,q}(s_{14}) - 2\,\mathcal{A}^0_{3,q}(s_{14}) \otimes \mathcal{A}^0_{3,q}(s_{23}) - \mathcal{A}^0_{3,q}(s_{23}) \otimes \mathcal{A}^0_{3,q}(s_{23}) \Big]\,\texttt{C0g0WFH}(4,3,2,1,H) \\
3 \quad &+\Big[+ \mathcal{A}^0_{3,q}(s_{23})\mathcal{A}^0_{3,q}(s_{14}) \Big]\,\texttt{C0g0WFH}(4,3,2,1,H) \\
4 \quad &+\Big[+ \Gamma^{(1)}_{qq}(z_1) \otimes \mathcal{A}^0_{3,q}(s_{14}) + \Gamma^{(1)}_{qq}(z_1) \otimes \mathcal{A}^0_{3,q}(s_{23}) + \Gamma^{(1)}_{qq}(z_2) \otimes \mathcal{A}^0_{3,q}(s_{14}) \\
&\quad + \Gamma^{(1)}_{qq}(z_2) \otimes \mathcal{A}^0_{3,q}(s_{23}) \Big]\,\texttt{C0g0WFH}(4,3,2,1,H) \\
5 \quad &+\Big[- \Gamma^{(1)}_{qq}(z_1) \otimes \Gamma^{(1)}_{qq}(z_1) - 2\,\Gamma^{(1)}_{qq}(z_1) \otimes \Gamma^{(1)}_{qq}(z_2) - \Gamma^{(1)}_{qq}(z_2) \otimes \Gamma^{(1)}_{qq}(z_2) \Big]\,\texttt{C0g0WFH}(4,3,2,1,H) \\
6 \quad &+\Big[+ \frac{1}{2}\,\Gamma^{(1)}_{qq}(z_1) \otimes \Gamma^{(1)}_{qq}(z_1) + \Gamma^{(1)}_{qq}(z_1) \otimes \Gamma^{(1)}_{qq}(z_2) + \frac{1}{2}\,\Gamma^{(1)}_{qq}(z_2) \otimes \Gamma^{(1)}_{qq}(z_2) \Big]\,\texttt{C0g0WFH}(4,3,2,1,H) \\
7 \quad &+\Big[- \mathcal{A}^1_{3,q}(s_{14}) - \mathcal{A}^1_{3,q}(s_{23}) \Big]\,\texttt{C0g0WFH}(4,3,2,1,H) \\
8 \quad &+\Big[+ \mathcal{A}^0_{3,q}(s_{14}) \otimes \mathcal{A}^0_{3,q}(s_{14}) + \mathcal{A}^0_{3,q}(s_{23}) \otimes \mathcal{A}^0_{3,q}(s_{23}) \Big]\,\texttt{C0g0WFH}(4,3,2,1,H) \\
9 \quad &+\Big[- \mathcal{A}^0_{4,q}(s_{14}) - \mathcal{A}^0_{4,q}(s_{23}) \Big]\,\texttt{C0g0WFH}(4,3,2,1,H) \\
10 \quad &+\Big[+ \Gamma^{(2)}_{qq}(z_1) + \Gamma^{(2)}_{qq}(z_2) \Big]\,\texttt{C0g0WFH}(4,3,2,1,H) \\
11 \quad &+\Big[- \frac{b_0}{\epsilon}\,\mathcal{A}^0_{3,q}(s_{14})\left(\frac{s_{14}}{\mu_R^2}\right)^{-\epsilon} - \frac{b_0}{\epsilon}\,\mathcal{A}^0_{3,q}(s_{23})\left(\frac{s_{23}}{\mu_R^2}\right)^{-\epsilon} \Big]\,\texttt{C0g0WFH}(4,3,2,1,H)
\end{aligned}
\tag{C.95}
$$

qbRC0g2WFHU

$$
\begin{aligned}
&\texttt{qbRC0g2WFHU}(1,2,3,4,\texttt{H}) = \\
1 \quad &+\Big[- S_{q\to g}\,\Gamma^{(1)}_{gq}(z_2)\otimes\mathcal{A}^0_{3,qg\to qq}(s_{12}) - \Gamma^{(1)}_{gq}(z_2)\otimes\Gamma^{(1)}_{qg}(z_2)\Big]\texttt{C0g0WFH}(4,3,2,1,H) \\
2 \quad &+\Big[+ \frac{1}{2}\,\Gamma^{(1)}_{gq}(z_2)\Gamma^{(1)}_{qg}(z_2)\Big]\texttt{C0g0WFH}(4,3,2,1,H) \\
3 \quad &+\Big[- S_{q\to g}\,\Gamma^{(1)}_{gq}(z_2)\otimes\mathcal{A}^0_{3,qg\to qq}(s_{12}) - \Gamma^{(1)}_{gq}(z_2)\otimes\Gamma^{(1)}_{qg}(z_2)\Big]\texttt{C0g0WFH}(4,2,3,1,H) \\
4 \quad &+\Big[+ \frac{1}{2}\,\Gamma^{(1)}_{gq}(z_2)\Gamma^{(1)}_{qg}(z_2)\Big]\texttt{C0g0WFH}(4,2,3,1,H) \\
5 \quad &+\Big[- \mathcal{B}^0_{4,qq'}(s_{12}) + \Gamma^{(2)}_{q\bar{Q}}(z_2)\Big]\texttt{C0g0WFH}(4,2,3,1,H) \\
6 \quad &+\Big[- \mathcal{B}^0_{4,qq'}(s_{12}) + \Gamma^{(2)}_{qQ}(z_2)\Big]\texttt{C0g0WFH}(4,3,2,1,H)
\end{aligned}
\tag{C.96}
$$

qgC0g2WFHU

$$
\begin{aligned}
&\texttt{qgC0g2WFHU}(1,2,3,4,\texttt{H}) = \\
1 \quad &+\Big[+ \mathcal{A}^0_{3,g\to q}(s_{23}) + 2S_{g\to q}\,\Gamma^{(1)}_{qg}(z_2)\Big]\left(-\frac{b_0}{\epsilon}\texttt{sC0g0WFH}(1,3,2,4,H) + \texttt{sC0g1WFH}(1,3,2,4,H)\right) \\
2 \quad &+\Big[+ \mathcal{A}^0_{3,g\to q}(s_{23})\otimes\mathcal{A}^0_{3,q}(s_{14}) + 2S_{g\to q}\,\Gamma^{(1)}_{qg}(z_2)\otimes\mathcal{A}^0_{3,q}(s_{14}) - 2S_{g\to q}\,\Gamma^{(1)}_{qg}(z_2)\otimes\Gamma^{(1)}_{qq}(z_1) \\
&\quad + \mathcal{A}^0_{3,g\to q}(s_{23})\otimes\mathcal{A}^0_{3,q}(s_{23}) + 2S_{g\to q}\,\Gamma^{(1)}_{qg}(z_2)\otimes\mathcal{A}^0_{3,q}(s_{23}) - 2S_{g\to q}\,\Gamma^{(1)}_{qg}(z_2)\otimes\Gamma^{(1)}_{qq}(z_2) \\
&\quad \Big]\texttt{sC0g0WFH}(1,3,2,4,H) \\
3 \quad &+\Big[- \Gamma^{(1)}_{qq}(z_1)\otimes\mathcal{A}^0_{3,g\to q}(s_{23}) - 2S_{g\to q}\,\Gamma^{(1)}_{qg}(z_2)\otimes\Gamma^{(1)}_{qq}(z_1) - \Gamma^{(1)}_{gg}(z_2)\otimes\mathcal{A}^0_{3,g\to q}(s_{23}) \\
&\quad - 2S_{g\to q}\,\Gamma^{(1)}_{gg}(z_2)\otimes\Gamma^{(1)}_{qg}(z_2)\Big]\texttt{sC0g0WFH}(1,3,2,4,H) \\
4 \quad &+\Big[+ 2S_{g\to q}\,\Gamma^{(1)}_{qg}(z_2)\otimes\Gamma^{(1)}_{qq}(z_1) + S_{g\to q}\,\Gamma^{(1)}_{qg}(z_2)\otimes\Gamma^{(1)}_{qq}(z_2) + S_{g\to q}\,\Gamma^{(1)}_{gg}(z_2)\otimes\Gamma^{(1)}_{qg}(z_2) \\
&\quad \Big]\texttt{sC0g0WFH}(1,3,2,4,H) \\
5 \quad &+\Big[+ \frac{b_0}{\epsilon}\left(\frac{s_{23}}{\mu_R^2}\right)^{-\epsilon}\mathcal{A}^0_{3,g\to q}(s_{23}) - \mathcal{A}^0_{3,g\to q}(s_{23})\otimes\mathcal{A}^0_{3,q}(s_{23}) + 2S_{g\to q}\,\Gamma^{(2)}_{qg}(z_2) \\
&\quad + 2\,\mathcal{A}^0_{4,g}(s_{23}) + \mathcal{A}^1_{3,g}(s_{23})\Big]\texttt{sC0g0WFH}(1,3,2,4,H)
\end{aligned}
\tag{C.97}
$$

qqpC0g2WFHU

$$
\texttt{qqpC0g2WFHU}(1,3,2,4,\texttt{H}) =
$$

$$
\begin{aligned}
1 \quad & + \Big[- \mathcal{A}^0_{3,q}(s_{14}) + \Gamma^{(1)}_{qq}(z_1) - \mathcal{A}^0_{3,q}(s_{23}) \\
& \quad + \Gamma^{(1)}_{qq}(z_2) \Big] \left(-\frac{b_0}{\epsilon} \texttt{C0g0WFH}(1,3,2,4,H) + \texttt{C0g1WFH}(1,3,2,4,H) \right) \\
2 \quad & + \Big[- \mathcal{A}^0_{3,q}(s_{14}) \otimes \mathcal{A}^0_{3,q}(s_{14}) - 2\,\mathcal{A}^0_{3,q}(s_{14}) \otimes \mathcal{A}^0_{3,q}(s_{23}) - \mathcal{A}^0_{3,q}(s_{23}) \otimes \mathcal{A}^0_{3,q}(s_{23}) \Big] \texttt{C0g0WFH}(1,3,2,4,H) \\
3 \quad & + \Big[+ \mathcal{A}^0_{3,q}(s_{23}) \mathcal{A}^0_{3,q}(s_{14}) \Big] \texttt{C0g0WFH}(1,3,2,4,H) \\
4 \quad & + \Big[+ \Gamma^{(1)}_{qq}(z_1) \otimes \mathcal{A}^0_{3,q}(s_{14}) + \Gamma^{(1)}_{qq}(z_1) \otimes \mathcal{A}^0_{3,q}(s_{23}) + \Gamma^{(1)}_{qq}(z_2) \otimes \mathcal{A}^0_{3,q}(s_{14}) \\
& \quad + \Gamma^{(1)}_{qq}(z_2) \otimes \mathcal{A}^0_{3,q}(s_{23}) \Big] \texttt{C0g0WFH}(1,3,2,4,H) \\
5 \quad & + \Big[- \Gamma^{(1)}_{qq}(z_1) \otimes \Gamma^{(1)}_{qq}(z_1) - 2\,\Gamma^{(1)}_{qq}(z_1) \otimes \Gamma^{(1)}_{qq}(z_2) - \Gamma^{(1)}_{qq}(z_2) \otimes \Gamma^{(1)}_{qq}(z_2) \Big] \texttt{C0g0WFH}(1,3,2,4,H) \\
6 \quad & + \Big[+ \frac{1}{2}\,\Gamma^{(1)}_{qq}(z_1) \otimes \Gamma^{(1)}_{qq}(z_1) + \Gamma^{(1)}_{qq}(z_1) \otimes \Gamma^{(1)}_{qq}(z_2) + \frac{1}{2}\,\Gamma^{(1)}_{qq}(z_2) \otimes \Gamma^{(1)}_{qq}(z_2) \Big] \texttt{C0g0WFH}(1,3,2,4,H) \\
7 \quad & + \Big[- \mathcal{A}^1_{3,q}(s_{14}) - \mathcal{A}^1_{3,q}(s_{23}) \Big] \texttt{C0g0WFH}(1,3,2,4,H) \\
8 \quad & + \Big[+ \mathcal{A}^0_{3,q}(s_{14}) \otimes \mathcal{A}^0_{3,q}(s_{14}) + \mathcal{A}^0_{3,q}(s_{23}) \otimes \mathcal{A}^0_{3,q}(s_{23}) \Big] \texttt{C0g0WFH}(1,3,2,4,H) \\
9 \quad & + \Big[- \mathcal{A}^0_{4,q}(s_{14}) - \mathcal{A}^0_{4,q}(s_{23}) \Big] \texttt{C0g0WFH}(1,3,2,4,H) \\
10 \quad & + \Big[+ \Gamma^{(2)}_{qq}(z_1) + \Gamma^{(2)}_{qq}(z_2) \Big] \texttt{C0g0WFH}(1,3,2,4,H) \\
11 \quad & + \Big[- \frac{b_0}{\epsilon}\,\mathcal{A}^0_{3,q}(s_{14}) \left(\frac{s_{14}}{\mu_R^2} \right)^{-\epsilon} - \frac{b_0}{\epsilon}\,\mathcal{A}^0_{3,q}(s_{23}) \left(\frac{s_{23}}{\mu_R^2} \right)^{-\epsilon} \Big] \texttt{C0g0WFH}(1,3,2,4,H)
\end{aligned}
\tag{C.98}
$$

qRC0g2WFHU

$$
\begin{aligned}
& \texttt{qRC0g2WFHU}(1,2,3,4,\texttt{H}) = \\
1 \quad & + \Big[- S_{q\to g}\,\Gamma^{(1)}_{gq}(z_2) \otimes \mathcal{A}^0_{3,qg\to qq}(s_{12}) - \Gamma^{(1)}_{gq}(z_2) \otimes \Gamma^{(1)}_{qg}(z_2) \Big] \texttt{C0g0WFH}(1,3,2,4,H) \\
2 \quad & + \Big[+ \frac{1}{2}\,\Gamma^{(1)}_{gq}(z_2) \Gamma^{(1)}_{qg}(z_2) \Big] \texttt{C0g0WFH}(1,3,2,4,H) \\
3 \quad & + \Big[- S_{q\to g}\,\Gamma^{(1)}_{gq}(z_2) \otimes \mathcal{A}^0_{3,qg\to qq}(s_{12}) - \Gamma^{(1)}_{gq}(z_2) \otimes \Gamma^{(1)}_{qg}(z_2) \Big] \texttt{C0g0WFH}(1,2,3,4,H) \\
4 \quad & + \Big[+ \frac{1}{2}\,\Gamma^{(1)}_{gq}(z_2) \Gamma^{(1)}_{qg}(z_2) \Big] \texttt{C0g0WFH}(1,2,3,4,H) \\
5 \quad & + \Big[- \mathcal{B}^0_{4,qq'}(s_{12}) + \Gamma^{(2)}_{q\bar{Q}}(z_2) \Big] \texttt{C0g0WFH}(1,2,3,4,H) \\
6 \quad & + \Big[- \mathcal{B}^0_{4,qq'}(s_{12}) + \Gamma^{(2)}_{qQ}(z_2) \Big] \texttt{C0g0WFH}(1,3,2,4,H)
\end{aligned}
\tag{C.99}
$$

qbgCt0g2WFHU

$$
\begin{aligned}
&\texttt{qbgCt0g2WFHU}(1,2,3,4,\texttt{H}) = \\
1 \quad &+\Big[+ \mathcal{A}^0_{3,g\to q}(s_{23}) + 2S_{g\to q}\,\Gamma^{(1)}_{qg}(z_2)\Big]\texttt{sC0g1WFH}(4,3,2,1,H) \\
2 \quad &+\Big[+ \mathcal{A}^0_{3,g\to q}(s_{23})\otimes\mathcal{A}^0_{3,q}(s_{14}) + 2S_{g\to q}\,\Gamma^{(1)}_{qg}(z_2)\otimes\mathcal{A}^0_{3,q}(s_{14}) - 2S_{g\to q}\,\Gamma^{(1)}_{qg}(z_2)\otimes\Gamma^{(1)}_{qq}(z_1) \\
&\quad + \mathcal{A}^0_{3,g\to q}(s_{23})\otimes\mathcal{A}^0_{3,q}(s_{23}) + 2S_{g\to q}\,\Gamma^{(1)}_{qg}(z_2)\otimes\mathcal{A}^0_{3,q}(s_{23}) - 2S_{g\to q}\,\Gamma^{(1)}_{qg}(z_2)\otimes\Gamma^{(1)}_{qq}(z_2) \\
&\quad \Big]\texttt{sC0g0WFH}(4,3,2,1,H) \\
3 \quad &+\Big[- \Gamma^{(1)}_{qq}(z_1)\otimes\mathcal{A}^0_{3,g\to q}(s_{23}) - 2S_{g\to q}\,\Gamma^{(1)}_{qg}(z_2)\otimes\Gamma^{(1)}_{qq}(z_1)\Big]\texttt{sC0g0WFH}(4,3,2,1,H) \\
4 \quad &+\Big[+ 2S_{g\to q}\,\Gamma^{(1)}_{qg}(z_2)\otimes\Gamma^{(1)}_{qq}(z_1) + S_{g\to q}\,\Gamma^{(1)}_{qg}(z_2)\otimes\Gamma^{(1)}_{qq}(z_2) \\
&\quad \Big]\texttt{sC0g0WFH}(4,3,2,1,H) \\
5 \quad &+\Big[+ \tilde{\mathcal{A}}^0_{4,g}(s_{23}) - 2S_{g\to q}\,\widetilde{\Gamma}^{(2)}_{qg}(z_2) + \tilde{\mathcal{A}}^1_{3,g}(s_{23}) \\
&\quad - \mathcal{A}^0_{3,g\to q}(s_{23})\otimes\mathcal{A}^0_{3,q}(s_{23})\Big]\texttt{sC0g0WFH}(4,3,2,1,H)
\end{aligned}
\tag{C.100}
$$

qbqpCt0g2WFHU

$$
\begin{aligned}
&\texttt{qbqpCt0g2WFHU}(4,3,2,1,\texttt{H}) = \\
1 \quad &+\Big[- \mathcal{A}^0_{3,q}(s_{14}) + \Gamma^{(1)}_{qq}(z_1) - \mathcal{A}^0_{3,q}(s_{23}) \\
&\quad + \Gamma^{(1)}_{qq}(z_2)\Big]\texttt{C0g1WFH}(4,3,2,1,H) \\
2 \quad &+\Big[+ \Gamma^{(1)}_{qq}(z_1)\otimes\mathcal{A}^0_{3,q}(s_{14}) + \Gamma^{(1)}_{qq}(z_1)\otimes\mathcal{A}^0_{3,q}(s_{23}) + \Gamma^{(1)}_{qq}(z_2)\otimes\mathcal{A}^0_{3,q}(s_{14}) \\
&\quad + \Gamma^{(1)}_{qq}(z_2)\otimes\mathcal{A}^0_{3,q}(s_{23})\Big]\texttt{C0g0WFH}(4,3,2,1,H) \\
3 \quad &+\Big[- \frac{1}{2}\,\mathcal{A}^0_{3,q}(s_{14})\otimes\mathcal{A}^0_{3,q}(s_{14}) - \mathcal{A}^0_{3,q}(s_{23})\otimes\mathcal{A}^0_{3,q}(s_{14}) - \frac{1}{2}\,\mathcal{A}^0_{3,q}(s_{23})\otimes\mathcal{A}^0_{3,q}(s_{23})\Big]\texttt{C0g0WFH}(4,3,2,1,H) \\
4 \quad &+\Big[- \frac{1}{2}\,\Gamma^{(1)}_{qq}(z_1)\otimes\Gamma^{(1)}_{qq}(z_1) - \Gamma^{(1)}_{qq}(z_1)\otimes\Gamma^{(1)}_{qq}(z_2) - \frac{1}{2}\,\Gamma^{(1)}_{qq}(z_2)\otimes\Gamma^{(1)}_{qq}(z_2)\Big]\texttt{C0g0WFH}(4,3,2,1,H) \\
5 \quad &+\Big[- \frac{1}{2}\,\tilde{\mathcal{A}}^0_{4,q}(s_{14}) - 2\,\mathcal{C}^0_{4,q}(s_{14}) - \mathcal{C}^0_{4,\bar{q},\bar{q}q\bar{q}}(s_{14}) \\
&\quad - \tilde{\mathcal{A}}^1_{3,q}(s_{14}) + \frac{1}{2}\,\mathcal{A}^0_{3,q}(s_{14})\otimes\mathcal{A}^0_{3,q}(s_{14}) - \widetilde{\widetilde{\Gamma}}^{(2)}_{qq}(z_1)\Big]\texttt{C0g0WFH}(4,3,2,1,H) \\
6 \quad &+\Big[- \frac{1}{2}\,\tilde{\mathcal{A}}^0_{4,q}(s_{23}) - 2\,\mathcal{C}^0_{4,q}(s_{23}) - \mathcal{C}^0_{4,\bar{q},\bar{q}q\bar{q}}(s_{23}) \\
&\quad - \tilde{\mathcal{A}}^1_{3,q}(s_{23}) + \frac{1}{2}\,\mathcal{A}^0_{3,q}(s_{23})\otimes\mathcal{A}^0_{3,q}(s_{23}) - \widetilde{\widetilde{\Gamma}}^{(2)}_{qq}(z_2)\Big]\texttt{C0g0WFH}(4,3,2,1,H)
\end{aligned}
$$

$$
\begin{aligned}
7 \quad &+\Big[-\mathcal{C}^0_{4,\bar{q},q\bar{q}\bar{q}}(s_{14}) - \Gamma^{(2)}_{q\bar{q}} t(z_1)\Big]\texttt{C0g0WFH}(1,3,2,4,H)\\
8 \quad &+\Big[-\mathcal{C}^0_{4,\bar{q},q\bar{q}\bar{q}}(s_{23}) - \Gamma^{(2)}_{q\bar{q}} t(z_2)\Big]\texttt{C0g0WFH}(4,2,3,1,H)
\end{aligned}
\tag{C.101}
$$

qgCt0g2WFHU

$$
\begin{aligned}
&\texttt{qgCt0g2WFHU}(1,2,3,4,\texttt{H}) =\\
1 \quad &+\Big[+\mathcal{A}^0_{3,g\to q}(s_{23}) + 2S_{g\to q}\,\Gamma^{(1)}_{qg}(z_2)\Big]\texttt{sC0g1WFH}(1,3,2,4,H)\\
2 \quad &+\Big[+\mathcal{A}^0_{3,g\to q}(s_{23})\otimes\mathcal{A}^0_{3,q}(s_{14}) + 2S_{g\to q}\,\Gamma^{(1)}_{qg}(z_2)\otimes\mathcal{A}^0_{3,q}(s_{14}) - 2S_{g\to q}\,\Gamma^{(1)}_{qg}(z_2)\otimes\Gamma^{(1)}_{qq}(z_1)\\
&\quad +\mathcal{A}^0_{3,g\to q}(s_{23})\otimes\mathcal{A}^0_{3,q}(s_{23}) + 2S_{g\to q}\,\Gamma^{(1)}_{qg}(z_2)\otimes\mathcal{A}^0_{3,q}(s_{23}) - 2S_{g\to q}\,\Gamma^{(1)}_{qg}(z_2)\otimes\Gamma^{(1)}_{qq}(z_2)\\
&\quad \Big]\texttt{sC0g0WFH}(1,3,2,4,H)\\
3 \quad &+\Big[-\Gamma^{(1)}_{qq}(z_1)\otimes\mathcal{A}^0_{3,g\to q}(s_{23}) - 2S_{g\to q}\,\Gamma^{(1)}_{qg}(z_2)\otimes\Gamma^{(1)}_{qq}(z_1)\Big]\texttt{sC0g0WFH}(1,3,2,4,H)\\
4 \quad &+\Big[+2S_{g\to q}\,\Gamma^{(1)}_{qg}(z_2)\otimes\Gamma^{(1)}_{qq}(z_1) + S_{g\to q}\,\Gamma^{(1)}_{qg}(z_2)\otimes\Gamma^{(1)}_{qq}(z_2)\\
&\quad \Big]\texttt{sC0g0WFH}(1,3,2,4,H)\\
5 \quad &+\Big[+\tilde{\mathcal{A}}^0_{4,g}(s_{23}) - 2S_{g\to q}\,\widetilde{\Gamma}^{(2)}_{qg}(z_2) + \tilde{\mathcal{A}}^1_{3,g}(s_{23})\\
&\quad -\mathcal{A}^0_{3,g\to q}(s_{23})\otimes\mathcal{A}^0_{3,q}(s_{23})\Big]\texttt{sC0g0WFH}(1,3,2,4,H)
\end{aligned}
\tag{C.102}
$$

qqpCt0g2WFHU

$$
\begin{aligned}
&\texttt{qqpCt0g2WFHU}(1,3,2,4,\texttt{H}) =\\
1 \quad &+\Big[-\mathcal{A}^0_{3,q}(s_{14}) + \Gamma^{(1)}_{qq}(z_1) - \mathcal{A}^0_{3,q}(s_{23})\\
&\quad +\Gamma^{(1)}_{qq}(z_2)\Big]\texttt{C0g1WFH}(1,3,2,4,H)\\
2 \quad &+\Big[+\Gamma^{(1)}_{qq}(z_1)\otimes\mathcal{A}^0_{3,q}(s_{14}) + \Gamma^{(1)}_{qq}(z_1)\otimes\mathcal{A}^0_{3,q}(s_{23}) + \Gamma^{(1)}_{qq}(z_2)\otimes\mathcal{A}^0_{3,q}(s_{14})\\
&\quad +\Gamma^{(1)}_{qq}(z_2)\otimes\mathcal{A}^0_{3,q}(s_{23})\Big]\texttt{C0g0WFH}(1,3,2,4,H)\\
3 \quad &+\Big[-\frac{1}{2}\,\mathcal{A}^0_{3,q}(s_{14})\otimes\mathcal{A}^0_{3,q}(s_{14}) - \mathcal{A}^0_{3,q}(s_{23})\otimes\mathcal{A}^0_{3,q}(s_{14}) - \frac{1}{2}\,\mathcal{A}^0_{3,q}(s_{23})\otimes\mathcal{A}^0_{3,q}(s_{23})\Big]\texttt{C0g0WFH}(1,3,2,4,H)\\
4 \quad &+\Big[-\frac{1}{2}\,\Gamma^{(1)}_{qq}(z_1)\otimes\Gamma^{(1)}_{qq}(z_1) - \Gamma^{(1)}_{qq}(z_1)\otimes\Gamma^{(1)}_{qq}(z_2) - \frac{1}{2}\,\Gamma^{(1)}_{qq}(z_2)\otimes\Gamma^{(1)}_{qq}(z_2)\Big]\texttt{C0g0WFH}(1,3,2,4,H)\\
5 \quad &+\Big[-\frac{1}{2}\,\tilde{\mathcal{A}}^0_{4,q}(s_{14}) - 2\,\mathcal{C}^0_{4,q}(s_{14}) - \mathcal{C}^0_{4,\bar{q},\bar{q}q\bar{q}}(s_{14})
\end{aligned}
$$

$$
\begin{aligned}
&\quad - \tilde{\mathcal{A}}^1_{3,q}(s_{14}) + \frac{1}{2}\,\mathcal{A}^0_{3,q}(s_{14}) \otimes \mathcal{A}^0_{3,q}(s_{14}) - \widetilde{\widetilde{\Gamma}}^{(2)}_{qq}(z_1)\Big]\texttt{C0g0WFH}(1,3,2,4,H)\\
6 \qquad &+\Big[- \frac{1}{2}\,\tilde{\mathcal{A}}^0_{4,q}(s_{23}) - 2\,\mathcal{C}^0_{4,q}(s_{23}) - \mathcal{C}^0_{4,\bar{q},\bar{q}q\bar{q}}(s_{23})\\
&\quad - \tilde{\mathcal{A}}^1_{3,q}(s_{23}) + \frac{1}{2}\,\mathcal{A}^0_{3,q}(s_{23}) \otimes \mathcal{A}^0_{3,q}(s_{23}) - \widetilde{\widetilde{\Gamma}}^{(2)}_{qq}(z_2)\Big]\texttt{C0g0WFH}(1,3,2,4,H)\\
7 \qquad &+\Big[- \mathcal{C}^0_{4,\bar{q},q\bar{q}\bar{q}}(s_{14}) - \Gamma^{(2)}_{q\bar{q}}t(z_1)\Big]\texttt{C0g0WFH}(4,3,2,1,H)\\
8 \qquad &+\Big[- \mathcal{C}^0_{4,\bar{q},q\bar{q}\bar{q}}(s_{23}) - \Gamma^{(2)}_{q\bar{q}}t(z_2)\Big]\texttt{C0g0WFH}(1,2,3,4,H)
\end{aligned}
\tag{C.103}
$$

qbgCh0g2WFHU

$$
\begin{aligned}
&\texttt{qbgCh0g2WFHU}(1,2,3,4,\texttt{H}) =\\
1 \qquad &+\Big[- \frac{b_F}{\epsilon}\,\mathcal{A}^0_{3,g\to q}(s_{23}) - 2\frac{b_F}{\epsilon}S_{g\to q}\,\Gamma^{(1)}_{qg}(z_2)\Big]\texttt{sC0g0WFH}(4,3,2,1,H)\\
2 \qquad &+\Big[- \Gamma^{(1)}_{gg,F}(z_2) \otimes \mathcal{A}^0_{3,g\to q}(s_{23}) - S_{g\to q}\,\Gamma^{(1)}_{gg,F}(z_2) \otimes \Gamma^{(1)}_{qg}(z_2)\Big]\texttt{sC0g0WFH}(4,3,2,1,H)\\
3 \qquad &+\Big[+ \frac{b_F}{\epsilon}\left(\frac{s_{23}}{\mu_R^2}\right)^{-\epsilon}\mathcal{A}^0_{3,g\to q}(s_{23}) + 2S_{g\to q}\,\Gamma^{(2)}_{qg,F}(z_2) + \hat{\mathcal{A}}^1_{3,g}(s_{23})\Big]\texttt{sC0g0WFH}(4,3,2,1,H)
\end{aligned}
\tag{C.104}
$$

qbqpCh0g2WFHU

$$
\begin{aligned}
&\texttt{qbqpCh0g2WFHU}(4,3,2,1,\texttt{H}) =\\
1 \qquad &+\Big[+ \frac{b_F}{\epsilon}\,\mathcal{A}^0_{3,q}(s_{14}) - \frac{b_F}{\epsilon}\,\Gamma^{(1)}_{qq}(z_1) + \frac{b_F}{\epsilon}\,\mathcal{A}^0_{3,q}(s_{23})\\
&\quad - \frac{b_F}{\epsilon}\,\Gamma^{(1)}_{qq}(z_2)\Big]\texttt{C0g0WFH}(4,3,2,1,H)\\
2 \qquad &+\Big[- \mathcal{B}^0_{4,q}(s_{14}) - \mathcal{B}^0_{4,q}(s_{23}) + \Gamma^{(2)}_{qq,F}(z_1)\\
&\quad + \Gamma^{(2)}_{qq,F}(z_2)\Big]\texttt{C0g0WFH}(4,3,2,1,H)\\
3 \qquad &+\Big[- \frac{b_F}{\epsilon}\left(\frac{s_{14}}{\mu_R^2}\right)^{-\epsilon}\mathcal{A}^0_{3,q}(s_{14}) - \frac{b_F}{\epsilon}\left(\frac{s_{23}}{\mu_R^2}\right)^{-\epsilon}\mathcal{A}^0_{3,q}(s_{23}) - \hat{\mathcal{A}}^1_{3,q}(s_{14})\\
&\quad - \hat{\mathcal{A}}^1_{3,q}(s_{23})\Big]\texttt{C0g0WFH}(4,3,2,1,H)
\end{aligned}
\tag{C.105}
$$

qgCh0g2WFHU

$$
\begin{aligned}
&\texttt{qgCh0g2WFHU}(1,2,3,4,\texttt{H}) =\\
1 \qquad &+\Big[- \frac{b_F}{\epsilon}\,\mathcal{A}^0_{3,g\to q}(s_{23}) - 2\frac{b_F}{\epsilon}S_{g\to q}\,\Gamma^{(1)}_{qg}(z_2)\Big]\texttt{sC0g0WFH}(1,3,2,4,H)
\end{aligned}
$$

$$
\begin{aligned}
2 \quad &+\Big[-\Gamma^{(1)}_{gg,F}(z_2) \otimes \mathcal{A}^0_{3,g\to q}(s_{23}) - S_{g\to q}\,\Gamma^{(1)}_{gg,F}(z_2) \otimes \Gamma^{(1)}_{qg}(z_2) \Big] \texttt{sC0g0WFH}(1,3,2,4,H) \\
3 \quad &+\Big[+\frac{b_F}{\epsilon}\left(\frac{s_{23}}{\mu_R^2}\right)^{-\epsilon} \mathcal{A}^0_{3,g\to q}(s_{23}) + 2S_{g\to q}\,\Gamma^{(2)}_{qg,F}(z_2) + \hat{\mathcal{A}}^1_{3,g}(s_{23}) \Big] \texttt{sC0g0WFH}(1,3,2,4,H)
\end{aligned}
\tag{C.106}
$$

qqpCh0g2WFHU

$$
\begin{aligned}
&\texttt{qqpCh0g2WFHU}(1,3,2,4,\texttt{H}) = \\
1 \quad &+\Big[+\frac{b_F}{\epsilon}\,\mathcal{A}^0_{3,q}(s_{14}) - \frac{b_F}{\epsilon}\,\Gamma^{(1)}_{qq}(z_1) + \frac{b_F}{\epsilon}\,\mathcal{A}^0_{3,q}(s_{23}) \\
&\quad -\frac{b_F}{\epsilon}\,\Gamma^{(1)}_{qq}(z_2) \Big] \texttt{C0g0WFH}(1,3,2,4,H) \\
2 \quad &+\Big[-\mathcal{B}^0_{4,q}(s_{14}) - \mathcal{B}^0_{4,q}(s_{23}) + \Gamma^{(2)}_{qq,F}(z_1) \\
&\quad +\Gamma^{(2)}_{qq,F}(z_2) \Big] \texttt{C0g0WFH}(1,3,2,4,H) \\
3 \quad &+\Big[-\frac{b_F}{\epsilon}\left(\frac{s_{14}}{\mu_R^2}\right)^{-\epsilon} \mathcal{A}^0_{3,q}(s_{14}) - \frac{b_F}{\epsilon}\left(\frac{s_{23}}{\mu_R^2}\right)^{-\epsilon} \mathcal{A}^0_{3,q}(s_{23}) - \hat{\mathcal{A}}^1_{3,q}(s_{14}) \\
&\quad -\hat{\mathcal{A}}^1_{3,q}(s_{23}) \Big] \texttt{C0g0WFH}(1,3,2,4,H)
\end{aligned}
\tag{C.107}
$$

Appendix D

pyHepGrid

by Juan Cruz-Martinez and Duncan Walker, OC325.

Note: the most recent public version of pyhepgrid alongside with its documentation can be found in `https://www.ippp.dur.ac.uk/~jmartinez/pyhepgrid.html`

The growing complexity of calculations and simulations in many areas of science has been accompanied by advances in the computational world which have helped their development. One particularly relevant advance has been Grid Computing and distributed systems.

The basic requirement for a task to be distributable is for it to be paralleliseable: that different subtasks can be carried over as independent "jobs". Monte Carlo methods, ubiquitous in Particle Physics, are a good example of a paralleliseable task as events can be computed independently from each other. Grid computing allows one to increase the resources available by distributing a given task into many different jobs to be computed by different "workers". Roughly speaking, multicore CPUs, commonplace today, are a small-scale Grid Computing system.

Several grid computing solutions exist which are available to the phenomenologist, each with their own particularities but they all share the same goal: to distribute a task among independent workers.

Since all these available systems work in a very similar manner, it would be desirable to construct an external user interface in order to unify interactions with

each of these systems without requiring "backend"-specific user knowledge. This interface must be general enough so changes in those "backend" system don't break the user interface and, at the same time, it must be extensible from the user perspective in order to make flexible for any given task.. With this guiding principles in mind we wrote pyHepGrid, a python 3.4 code which unifies all backends.

Implemented tools

At the moment of writing, the only tools implemented in pyHepGrid are those available to Durham phenomenologists. In particular, we implemented ARC [132], DIRAC [114] together with the LCG File Catalogue developed by CERN*, and a generic interface for Slurm [133] with subinterfaces for the different systems available from Durham.

General functioning. Initialisation, run and management

The functioning of pyHepGrid can be divided in three main modes: initialisation, run and management. All necessary information in order to submit a program to a distributed system is configured in an `ini`-type file.

During the **initialisation** process, pyHepGrid ensures all components required to run the executable are available in the target system. If a remote filesystem is to be used, it will tar up the necessary files and copy them to the appropriate location. After that, the configuration parameters at the time of initialisation is saved in the database and the "job" is marked as initialised.

Let us take as an example a typical NNLOJET production run in the GridPP systems. The requirements for a NNLOJET production run are the LHAPDF library as well as the Vegas grid file. The initialisation procedure will ensure the LHAPDF library is available in the LFC system and will tar up the NNLOJET executable as well as other NNLOJET-specific files in order to copy them to the LFC as well.

The **run** procedure is more simple, where an initialised job is selected and sub-

*http://lcgdm.web.cern.ch/lfc

mitted to the target system. The **run** and **initialisation** modes are separated with the following points in mind:

a) Often it is necessary to submit several times the same job. Following the example of NNLOJET, we might find that after a given number of event we still have not reached the target precision, so we want to be able to submit new jobs with more events without initialising the job again.

b) A powerful advantage of an unified interface for all backends is to be able to distribute jobs among different distributed systems.

After the job is submitted an entry is generate in the run table of the database. Several entries in the run table can point to the same entry in the initialisation table.

Finally, the **management** mode present the user with an unified interface which allows complete control of the jobs running in any distributing system: printing standard output or error, retrieving results, cancelling or rescheduling jobs, etc.

Bibliography

[1] J. Cruz-Martinez, T. Gehrmann, E. W. N. Glover, and A. Huss. "Second-order QCD effects in Higgs boson production through vector boson fusion". In: (2018). arXiv: 1802.02445 [hep-ph].

[2] M. E. Peskin and D. V. Schroeder. *An Introduction to quantum field theory*. Reading, USA: Addison-Wesley, 1995. ISBN: 9780201503975. URL: http://www.slac.stanford.edu/~mpeskin/QFT.html.

[3] P. W. Higgs. "Broken Symmetries and the Masses of Gauge Bosons". In: *Phys. Rev. Lett.* 13 (1964). [,160(1964)], pp. 508–509. DOI: 10.1103/PhysRevLett.13.508.

[4] P. W. Higgs. "Spontaneous Symmetry Breakdown without Massless Bosons". In: *Phys. Rev.* 145 (1966), pp. 1156–1163. DOI: 10.1103/PhysRev.145.1156.

[5] F. Englert and R. Brout. "Broken Symmetry and the Mass of Gauge Vector Mesons". In: *Phys. Rev. Lett.* 13 (1964). [,157(1964)], pp. 321–323. DOI: 10.1103/PhysRevLett.13.321.

[6] Y. Nambu. "Axial vector current conservation in weak interactions". In: *Phys. Rev. Lett.* 4 (1960). [,107(1960)], pp. 380–382. DOI: 10.1103/PhysRevLett.4.380; Y. Nambu and G. Jona-Lasinio. "Dynamical Model of Elementary Particles Based on an Analogy with Superconductivity. 1." In: *Phys. Rev.* 122 (1961). [,127(1961)], pp. 345–358. DOI: 10.1103/PhysRev.122.345; J. Goldstone. "Field Theories with Superconductor Solutions". In: *Nuovo Cim.* 19 (1961), pp. 154–164. DOI: 10.1007/BF02812722; J. Goldstone, A. Salam,

and S. Weinberg. "Broken Symmetries". In: *Phys. Rev.* 127 (1962), pp. 965–970. DOI: 10.1103/PhysRev.127.965.

[7] R. P. Feynman. "Space - time approach to quantum electrodynamics". In: *Phys. Rev.* 76 (1949). [,99(1949)], pp. 769–789. DOI: 10.1103/PhysRev.76.769.

[8] L. J. Dixon. "Calculating scattering amplitudes efficiently". In: *QCD and beyond. Proceedings, Theoretical Advanced Study Institute in Elementary Particle Physics, TASI-95, Boulder, USA, June 4-30, 1995*. 1996, pp. 539–584. arXiv: hep-ph/9601359 [hep-ph]. URL: http://www-public.slac.stanford.edu/sciDoc/docMeta.aspx?slacPubNumber=SLAC-PUB-7106; L. J. Dixon. "A brief introduction to modern amplitude methods". In: *Proceedings, 2012 European School of High-Energy Physics (ESHEP 2012): La Pommeraye, Anjou, France, June 06-19, 2012*. 2014, pp. 31–67. DOI: 10.5170/CERN-2014-008.31. arXiv: 1310.5353 [hep-ph]. URL: https://inspirehep.net/record/1261436/files/arXiv:1310.5353.pdf.

[9] J. Campbell, J. Huston, and F. Krauss. *The black book of quantum chromodynamics: a primer for the LHC era*. Oxford: Oxford University Press, 2018. URL: https://cds.cern.ch/record/2286381.

[10] G. 't Hooft and M. J. G. Veltman. "Regularization and Renormalization of Gauge Fields". In: *Nucl. Phys.* B44 (1972), pp. 189–213. DOI: 10.1016/0550-3213(72)90279-9.

[11] R. K. Ellis, W. J. Stirling, and B. R. Webber. *QCD and collider physics*. Cambridge University Press, 1996, pp. 1–435.

[12] P. A. Baikov, K. G. Chetyrkin, and J. H. Kühn. "Five-Loop Running of the QCD coupling constant". In: *Phys. Rev. Lett.* 118.8 (2017), p. 082002. DOI: 10.1103/PhysRevLett.118.082002. arXiv: 1606.08659 [hep-ph].

[13] J. R. Andersen et al. "Handbook of LHC Higgs Cross Sections: 3. Higgs Properties". In: (2013). Ed. by S. Heinemeyer, C. Mariotti, G. Passarino, and R. Tanaka. DOI: 10.5170/CERN-2013-004. arXiv: 1307.1347 [hep-ph].

[14] T. A. collaboration. "Combined measurements of Higgs boson production and decay using up to 80 fb^{-1} of proton–proton collision data at $\sqrt{s} = 13$ TeV collected with the ATLAS experiment". In: (2018).

[15] G. Aad et al. "Combined Measurement of the Higgs Boson Mass in *pp* Collisions at $\sqrt{s} = 7$ and 8 TeV with the ATLAS and CMS Experiments". In: *Phys. Rev. Lett.* 114 (2015), p. 191803. DOI: 10.1103/PhysRevLett.114.191803. arXiv: 1503.07589 [hep-ex].

[16] C. Patrignani et al. "Review of Particle Physics". In: *Chin. Phys.* C40.10 (2016), p. 100001. DOI: 10.1088/1674-1137/40/10/100001.

[17] J. Ellis, M. K. Gaillard, and D. V. Nanopoulos. "A Historical Profile of the Higgs Boson". In: *The standard theory of particle physics: Essays to celebrate CERN's 60th anniversary*. Ed. by L. Maiani and L. Rolandi. 2016, pp. 255–274. DOI: 10.1142/9789814733519_0014. arXiv: 1504.07217 [hep-ph]. URL: http://inspirehep.net/record/1364889/files/arXiv:1504.07217.pdf.

[18] *Combined Standard Model Higgs boson searches with up to 2.3 inverse femtobarns of pp collision data at sqrt(s)=7 TeV at the LHC*. Tech. rep. CMS-PAS-HIG-11-023. Geneva: CERN, 2011. URL: https://cds.cern.ch/record/1399607; *Combined Standard Model Higgs boson searches with up to 2.3 fb-1 of pp collisions at sqrts=7 TeV at the LHC*. Tech. rep. ATLAS-CONF-2011-157. Geneva: CERN, Nov. 2011. URL: https://cds.cern.ch/record/1399599.

[19] G. Bernardi and M. Herndon. "Standard model Higgs boson searches through the 125 GeV boson discovery". In: *Rev. Mod. Phys.* 86.2 (2014), p. 479. DOI: 10.1103/RevModPhys.86.479. arXiv: 1210.0021 [hep-ex].

[20] A. Gehrmann-De Ridder, E. W. N. Glover, and J. Pires. "Real-Virtual corrections for gluon scattering at NNLO". In: *JHEP* 02 (2012), p. 141. DOI: 10.1007/JHEP02(2012)141. arXiv: 1112.3613 [hep-ph].

[21] J. Currie, E. W. N. Glover, and S. Wells. "Infrared Structure at NNLO Using Antenna Subtraction". In: *JHEP* 04 (2013), p. 066. DOI: 10.1007/JHEP04(2013)066. arXiv: 1301.4693 [hep-ph].

[22] V. N. Gribov and L. N. Lipatov. "Deep inelastic e p scattering in perturbation theory". In: *Sov. J. Nucl. Phys.* 15 (1972). [Yad. Fiz.15,781(1972)], pp. 438–450; Y. L. Dokshitzer. "Calculation of the Structure Functions for Deep Inelastic Scattering and e+ e- Annihilation by Perturbation Theory in Quantum Chromodynamics." In: *Sov. Phys. JETP* 46 (1977). [Zh. Eksp. Teor. Fiz.73,1216(1977)], pp. 641–653; G. Altarelli and G. Parisi. "Asymptotic Freedom in Parton Language". In: *Nucl. Phys.* B126 (1977), pp. 298–318. DOI: 10.1016/0550-3213(77)90384-4.

[23] F. Bloch and A. Nordsieck. "Note on the Radiation Field of the electron". In: *Phys. Rev.* 52 (1937), pp. 54–59. DOI: 10.1103/PhysRev.52.54.

[24] T. Kinoshita. "Mass Singularities of Feynman Amplitudes". In: *Journal of Mathematical Physics* 3.4 (1962), pp. 650–677. DOI: 10.1063/1.1724268. eprint: https://doi.org/10.1063/1.1724268. URL: https://doi.org/10.1063/1.1724268.

[25] T. D. Lee and M. Nauenberg. "Degenerate Systems and Mass Singularities". In: *Phys. Rev.* 133 (6B Mar. 1964), B1549–B1562. DOI: 10.1103/PhysRev.133.B1549. URL: https://link.aps.org/doi/10.1103/PhysRev.133.B1549.

[26] M. Mangano, S. Parke, and Z. Xu. "Duality and multi-gluon scattering". In: *Nuclear Physics B* 298.4 (1988), pp. 653–672. ISSN: 0550-3213. DOI: https://doi.org/10.1016/0550-3213(88)90001-6. URL: http://www.sciencedirect.com/science/article/pii/0550321388900016.

[27] S. Catani. "The Singular behavior of QCD amplitudes at two loop order". In: *Phys. Lett.* B427 (1998), pp. 161–171. DOI: 10.1016/S0370-2693(98)00332-3. arXiv: hep-ph/9802439 [hep-ph].

[28] S. Catani and M. H. Seymour. "A General algorithm for calculating jet cross-sections in NLO QCD". In: *Nucl. Phys.* B485 (1997). [Erratum: Nucl. Phys.B510,503(1998)], pp. 291–419. DOI: 10.1016/S0550-3213(96)00589-5,10.1016/S0550-3213(98)81022-5. arXiv: hep-ph/9605323 [hep-ph].

[29] R. K. Ellis, G. Marchesini, and B. R. Webber. "Soft Radiation in Parton Parton Scattering". In: *Nucl. Phys.* B286 (1987). [Erratum: Nucl. Phys.B294,1180(1987)], p. 643. DOI: 10.1016/0550-3213(87)90456-1,10.1016/0550-3213(87)90628-6.

[30] E. W. Nigel Glover and J. Pires. "Antenna subtraction for gluon scattering at NNLO". In: *JHEP* 06 (2010), p. 096. DOI: 10.1007/JHEP06(2010)096. arXiv: 1003.2824 [hep-ph].

[31] J. M. Campbell and E. W. N. Glover. "Double unresolved approximations to multiparton scattering amplitudes". In: *Nucl. Phys.* B527 (1998), pp. 264–288. DOI: 10.1016/S0550-3213(98)00295-8. arXiv: hep-ph/9710255 [hep-ph].

[32] S. Catani and M. Grazzini. "Collinear factorization and splitting functions for next-to-next-to-leading order QCD calculations". In: *Phys. Lett.* B446 (1999), pp. 143–152. DOI: 10.1016/S0370-2693(98)01513-5. arXiv: hep-ph/9810389 [hep-ph].

[33] Z. Bern, V. Del Duca, W. B. Kilgore, and C. R. Schmidt. "The infrared behavior of one loop QCD amplitudes at next-to-next-to leading order". In: *Phys. Rev.* D60 (1999), p. 116001. DOI: 10.1103/PhysRevD.60.116001. arXiv: hep-ph/9903516 [hep-ph].

[34] A. Gehrmann-De Ridder, T. Gehrmann, and E. W. N. Glover. "Antenna subtraction at NNLO". In: *JHEP* 09 (2005), p. 056. DOI: 10.1088/1126-6708/2005/09/056. arXiv: hep-ph/0505111 [hep-ph].

[35] S. Catani and M. Grazzini. "An NNLO subtraction formalism in hadron collisions and its application to Higgs boson production at the LHC". In: *Phys. Rev. Lett.* 98 (2007), p. 222002. DOI: 10.1103/PhysRevLett.98.222002. arXiv: hep-ph/0703012 [hep-ph].

[36] M. Czakon. "The NNLO subtraction scheme STRIPPER: Implementation and application". In: *PoS* RADCOR2015 (2016), p. 004.

[37] A. Kardos et al. "CoLoRFulNNLO for LHC processes". In: *14th DESY Workshop on Elementary Particle Physics: Loops and Legs in Quantum Field Theory 2018 (LL2018) St Goar, Germany, April 29-May 4, 2018*. 2018. arXiv: 1807.04976 [hep-ph].

[38] G. Altarelli. "Collider Physics within the Standard Model: a Primer". In: (2013). arXiv: 1303.2842 [hep-ph].

[39] J. E. Huth et al. "Toward a standardization of jet definitions". In: *1990 DPF Summer Study on High-energy Physics: Research Directions for the Decade (Snowmass 90) Snowmass, Colorado, June 25-July 13, 1990*. 1990, pp. 0134–136. URL: http://lss.fnal.gov/cgi-bin/find_paper.pl?conf-90-249.

[40] S. D. Ellis and D. E. Soper. "Successive combination jet algorithm for hadron collisions". In: *Phys. Rev.* D48 (1993), pp. 3160–3166. DOI: 10.1103/PhysRevD.48.3160. arXiv: hep-ph/9305266 [hep-ph]; S. Catani, Y. L. Dokshitzer, M. H. Seymour, and B. R. Webber. "Longitudinally invariant K_t clustering algorithms for hadron hadron collisions". In: *Nucl. Phys.* B406 (1993), pp. 187–224. DOI: 10.1016/0550-3213(93)90166-M.

[41] Y. L. Dokshitzer, G. D. Leder, S. Moretti, and B. R. Webber. "Better jet clustering algorithms". In: *JHEP* 08 (1997), p. 001. DOI: 10.1088/1126-6708/1997/08/001. arXiv: hep-ph/9707323 [hep-ph]; M. Wobisch and

T. Wengler. "Hadronization corrections to jet cross-sections in deep inelastic scattering". In: *Monte Carlo generators for HERA physics. Proceedings, Workshop, Hamburg, Germany, 1998-1999*. 1998, pp. 270–279. arXiv: hep-ph/9907280 [hep-ph]. URL: https://inspirehep.net/record/484872/files/arXiv:hep-ph_9907280.pdf.

[42] M. Cacciari, G. P. Salam, and G. Soyez. "The Anti-k(t) jet clustering algorithm". In: *JHEP* 04 (2008), p. 063. DOI: 10.1088/1126-6708/2008/04/063. arXiv: 0802.1189 [hep-ph].

[43] D. A. Kosower. "Antenna factorization of gauge theory amplitudes". In: *Phys. Rev.* D57 (1998), pp. 5410–5416. DOI: 10.1103/PhysRevD.57.5410. arXiv: hep-ph/9710213 [hep-ph]; D. A. Kosower. "Antenna factorization in strongly ordered limits". In: *Phys. Rev.* D71 (2005), p. 045016. DOI: 10.1103/PhysRevD.71.045016. arXiv: hep-ph/0311272 [hep-ph]; A. Daleo, T. Gehrmann, and D. Maitre. "Antenna subtraction with hadronic initial states". In: *JHEP* 04 (2007), p. 016. DOI: 10.1088/1126-6708/2007/04/016. arXiv: hep-ph/0612257 [hep-ph].

[44] J. R. Currie. "Antenna Subtraction for NNLO Calculations at the LHC". PhD thesis. Durham U. (main), 2012. URL: http://etheses.dur.ac.uk/4942/.

[45] A. Gehrmann-De Ridder, T. Gehrmann, and E. W. N. Glover. "Gluon-gluon antenna functions from Higgs boson decay". In: *Phys. Lett.* B612 (2005), pp. 49–60. DOI: 10.1016/j.physletb.2005.03.003. arXiv: hep-ph/0502110 [hep-ph].

[46] A. Gehrmann-De Ridder, T. Gehrmann, and E. W. N. Glover. "Quark-gluon antenna functions from neutralino decay". In: *Phys. Lett.* B612 (2005), pp. 36–48. DOI: 10.1016/j.physletb.2005.02.039. arXiv: hep-ph/0501291 [hep-ph].

[47] A. Daleo, A. Gehrmann-De Ridder, T. Gehrmann, and G. Luisoni. "Antenna subtraction at NNLO with hadronic initial states: initial-final configurations". In: *JHEP* 01 (2010), p. 118. DOI: 10.1007/JHEP01(2010)118. arXiv: 0912.0374 [hep-ph].

[48] R. Boughezal, A. Gehrmann-De Ridder, and M. Ritzmann. "Antenna subtraction at NNLO with hadronic initial states: double real radiation for initial-initial configurations with two quark flavours". In: *JHEP* 02 (2011), p. 098. DOI: 10.1007/JHEP02(2011)098. arXiv: 1011.6631 [hep-ph].

[49] T. Gehrmann and P. F. Monni. "Antenna subtraction at NNLO with hadronic initial states: real-virtual initial-initial configurations". In: *JHEP* 12 (2011), p. 049. DOI: 10.1007/JHEP12(2011)049. arXiv: 1107.4037 [hep-ph].

[50] A. Gehrmann-De Ridder, T. Gehrmann, and M. Ritzmann. "Antenna subtraction at NNLO with hadronic initial states: double real initial-initial configurations". In: *JHEP* 10 (2012), p. 047. DOI: 10.1007/JHEP10(2012)047. arXiv: 1207.5779 [hep-ph].

[51] X. Chen et al. "NNLO QCD corrections to Higgs boson production at large transverse momentum". In: *JHEP* 10 (2016), p. 066. DOI: 10.1007/JHEP10(2016)066. arXiv: 1607.08817 [hep-ph].

[52] V. D. Barger, R. J. N. Phillips, and D. Zeppenfeld. "Mini - jet veto: A Tool for the heavy Higgs search at the LHC". In: *Phys. Lett.* B346 (1995), pp. 106–114. DOI: 10.1016/0370-2693(95)00008-9. arXiv: hep-ph/9412276 [hep-ph].

[53] D. L. Rainwater, D. Zeppenfeld, and K. Hagiwara. "Searching for $H \to \tau^+\tau^-$ in weak boson fusion at the CERN LHC". In: *Phys. Rev.* D59 (1998), p. 014037. DOI: 10.1103/PhysRevD.59.014037. arXiv: hep-ph/9808468 [hep-ph].

[54] M. Rauch. "Vector-Boson Fusion and Vector-Boson Scattering". In: (2016). arXiv: 1610.08420 [hep-ph].

[55] T. Plehn, D. L. Rainwater, and D. Zeppenfeld. "A Method for identifying $H \to \tau^+\tau^- \to e^\pm\mu^\mp p_T$ at the CERN LHC". In: *Phys. Rev.* D61 (2000), p. 093005. DOI: 10.1103/PhysRevD.61.093005. arXiv: hep-ph/9911385 [hep-ph].

[56] G. Aad et al. "Evidence for the Higgs-boson Yukawa coupling to tau leptons with the ATLAS detector". In: *JHEP* 04 (2015), p. 117. DOI: 10.1007/JHEP04(2015)117. arXiv: 1501.04943 [hep-ex].

[57] S. Chatrchyan et al. "Evidence for the 125 GeV Higgs boson decaying to a pair of τ leptons". In: *JHEP* 05 (2014), p. 104. DOI: 10.1007/JHEP05(2014)104. arXiv: 1401.5041 [hep-ex].

[58] O. J. P. Eboli and D. Zeppenfeld. "Observing an invisible Higgs boson". In: *Phys. Lett.* B495 (2000), pp. 147–154. DOI: 10.1016/S0370-2693(00)01213-2. arXiv: hep-ph/0009158 [hep-ph].

[59] G. Aad et al. "Search for invisible decays of a Higgs boson using vector-boson fusion in pp collisions at $\sqrt{s} = 8$ TeV with the ATLAS detector". In: *JHEP* 01 (2016), p. 172. DOI: 10.1007/JHEP01(2016)172. arXiv: 1508.07869 [hep-ex].

[60] V. Khachatryan et al. "Searches for invisible decays of the Higgs boson in pp collisions at $\sqrt{s} = 7$, 8, and 13 TeV". In: *JHEP* 02 (2017), p. 135. DOI: 10.1007/JHEP02(2017)135. arXiv: 1610.09218 [hep-ex].

[61] T. Plehn, D. L. Rainwater, and D. Zeppenfeld. "Determining the structure of Higgs couplings at the LHC". In: *Phys. Rev. Lett.* 88 (20), p. 051801. DOI: 10.1103/PhysRevLett.88.051801. arXiv: hep-ph/0105325 [hep-ph].

[62] J. R. Andersen, K. Arnold, and D. Zeppenfeld. "Azimuthal Angle Correlations for Higgs Boson plus Multi-Jet Events". In: *JHEP* 06 (2010), p. 091. DOI: 10.1007/JHEP06(2010)091. arXiv: 1001.3822 [hep-ph].

[63] D. de Florian et al. "Handbook of LHC Higgs Cross Sections: 4. Deciphering the Nature of the Higgs Sector". In: (2016). DOI: 10.23731/CYRM-2017-002. arXiv: 1610.07922 [hep-ph].

[64] M. J. Dolan, C. Englert, N. Greiner, and M. Spannowsky. "Further on up the road: $hhjj$ production at the LHC". In: *Phys. Rev. Lett.* 112 (2014), p. 101802. DOI: 10.1103/PhysRevLett.112.101802. arXiv: 1310.1084 [hep-ph].

[65] A. J. Barr et al. "Higgs Self-Coupling Measurements at a 100 TeV Hadron Collider". In: *JHEP* 02 (2015), p. 016. DOI: 10.1007/JHEP02(2015)016. arXiv: 1412.7154 [hep-ph].

[66] A. S. Belyaev, P. B. Schaefers, and M. C. Thomas. "Precise test of Higgs properties via triple Higgs production in VBF at future colliders". In: (2018). arXiv: 1801.10157 [hep-ph].

[67] T. Han, G. Valencia, and S. Willenbrock. "Structure function approach to vector boson scattering in p p collisions". In: *Phys. Rev. Lett.* 69 (1992), pp. 3274–3277. DOI: 10.1103/PhysRevLett.69.3274. arXiv: hep-ph/9206246 [hep-ph].

[68] P. Bolzoni, F. Maltoni, S.-O. Moch, and M. Zaro. "Higgs production via vector-boson fusion at NNLO in QCD". In: *Phys. Rev. Lett.* 105 (2010), p. 011801. DOI: 10.1103/PhysRevLett.105.011801. arXiv: 1003.4451 [hep-ph].

[69] P. Bolzoni, F. Maltoni, S.-O. Moch, and M. Zaro. "Vector boson fusion at NNLO in QCD: SM Higgs and beyond". In: *Phys. Rev.* D85 (2012), p. 035002. DOI: 10.1103/PhysRevD.85.035002. arXiv: 1109.3717 [hep-ph].

[70] F. A. Dreyer and A. Karlberg. "Vector-Boson Fusion Higgs Production at Three Loops in QCD". In: *Phys. Rev. Lett.* 117.7 (2016), p. 072001. DOI: 10.1103/PhysRevLett.117.072001. arXiv: 1606.00840 [hep-ph].

[71] M. Ciccolini, A. Denner, and S. Dittmaier. "Electroweak and QCD corrections to Higgs production via vector-boson fusion at the LHC". In: *Phys. Rev.* D77 (2008), p. 013002. DOI: 10.1103/PhysRevD.77.013002. arXiv: 0710.4749 [hep-ph].

[72] F. Campanario, T. M. Figy, S. Plätzer, and M. Sjödahl. "Electroweak Higgs Boson Plus Three Jet Production at Next-to-Leading-Order QCD". In: *Phys. Rev. Lett.* 111.21 (2013), p. 211802. DOI: 10.1103/PhysRevLett.111.211802. arXiv: 1308.2932 [hep-ph].

[73] J. R. Andersen, T. Binoth, G. Heinrich, and J. M. Smillie. "Loop induced interference effects in Higgs Boson plus two jet production at the LHC". In: *JHEP* 02 (2008), p. 057. DOI: 10.1088/1126-6708/2008/02/057. arXiv: 0709.3513 [hep-ph].

[74] X. Chen, T. Gehrmann, E. W. N. Glover, and M. Jaquier. "Precise QCD predictions for the production of Higgs + jet final states". In: *Phys. Lett.* B740 (2015), pp. 147–150. DOI: 10.1016/j.physletb.2014.11.021. arXiv: 1408.5325 [hep-ph].

[75] R. D. Ball et al. "Parton distributions for the LHC Run II". In: *JHEP* 04 (2015), p. 040. DOI: 10.1007/JHEP04(2015)040. arXiv: 1410.8849 [hep-ph].

[76] A. Buckley et al. "LHAPDF6: parton density access in the LHC precision era". In: *Eur. Phys. J.* C75 (2015), p. 132. DOI: 10.1140/epjc/s10052-015-3318-8. arXiv: 1412.7420 [hep-ph].

[77] S. P. Jones, M. Kerner, and G. Luisoni. "Next-to-Leading-Order QCD Corrections to Higgs Boson Plus Jet Production with Full Top-Quark Mass Dependence". In: *Phys. Rev. Lett.* 120.16 (2018), p. 162001. DOI: 10.1103/PhysRevLett.120.162001. arXiv: 1802.00349 [hep-ph].

[78] T. Gehrmann et al. "Calculation of the quark and gluon form factors to three loops in QCD". In: *JHEP* 06 (2010), p. 094. DOI: 10.1007/JHEP06(2010)094. arXiv: 1004.3653 [hep-ph].

[79] L. W. Garland et al. "Two loop QCD helicity amplitudes for e+ e- —¿ three jets". In: *Nucl. Phys.* B642 (2002), pp. 227–262. DOI: 10.1016/S0550-3213(02)00627-2. arXiv: hep-ph/0206067 [hep-ph].

[80] T. Gehrmann et al. "Jet cross sections and transverse momentum distributions with NNLOJET". In: *13th International Symposium on Radiative Corrections: Application of Quantum Field Theory to Phenomenology (RADCOR 2017) St. Gilgen, Austria, September 24-29, 2017*. 2018. arXiv: 1801.06415 [hep-ph]. URL: https://inspirehep.net/record/1649093/files/arXiv:1801.06415.pdf.

[81] X. Chen et al. "Precise QCD Description of the Higgs Boson Transverse Momentum Spectrum". In: (2018). arXiv: 1805.00736 [hep-ph].

[82] W. Bizoń et al. "Fiducial distributions in Higgs and Drell-Yan production at N^{3}LL+NNLO". In: (2018). arXiv: 1805.05916 [hep-ph].

[83] L. Cieri et al. "Higgs boson production at the LHC using the q_T subtraction formalism at N^{3}LO QCD". In: (2018). arXiv: 1807.11501 [hep-ph].

[84] A. Gehrmann-De Ridder et al. "Precise QCD predictions for the production of a Z boson in association with a hadronic jet". In: *Phys. Rev. Lett.* 117.2 (2016), p. 022001. DOI: 10.1103/PhysRevLett.117.022001. arXiv: 1507.02850 [hep-ph].

[85] A. Gehrmann-De Ridder et al. "The NNLO QCD corrections to Z boson production at large transverse momentum". In: *JHEP* 07 (2016), p. 133. DOI: 10.1007/JHEP07(2016)133. arXiv: 1605.04295 [hep-ph].

[86] A. Gehrmann-De Ridder et al. "NNLO QCD corrections for Drell-Yan p_T^Z and ϕ^* observables at the LHC". In: *JHEP* 11 (2016), p. 094. DOI: 10.1007/JHEP11(2016)094. arXiv: 1610.01843 [hep-ph].

[87] R. Gauld et al. "Precise predictions for the angular coefficients in Z-boson production at the LHC". In: *JHEP* 11 (2017), p. 003. DOI: 10.1007/JHEP11(2017)003. arXiv: 1708.00008 [hep-ph].

[88] A. Gehrmann-De Ridder et al. "NNLO QCD corrections to the transverse momentum distribution of weak gauge bosons". In: (2017). arXiv: 1712.07543 [hep-ph].

[89] J. Currie, E. W. N. Glover, and J. Pires. "Next-to-Next-to Leading Order QCD Predictions for Single Jet Inclusive Production at the LHC". In: *Phys. Rev. Lett.* 118.7 (2017), p. 072002. DOI: 10.1103/PhysRevLett.118.072002. arXiv: 1611.01460 [hep-ph].

[90] J. Currie et al. "Precise predictions for dijet production at the LHC". In: *Phys. Rev. Lett.* 119.15 (2017), p. 152001. DOI: 10.1103/PhysRevLett.119.152001. arXiv: 1705.10271 [hep-ph].

[91] J. Currie, T. Gehrmann, and J. Niehues. "Precise QCD predictions for the production of dijet final states in deep inelastic scattering". In: *Phys. Rev. Lett.* 117.4 (2016), p. 042001. DOI: 10.1103/PhysRevLett.117.042001. arXiv: 1606.03991 [hep-ph].

[92] J. Currie, T. Gehrmann, A. Huss, and J. Niehues. "NNLO QCD corrections to jet production in deep inelastic scattering". In: *JHEP* 07 (2017), p. 018. DOI: 10.1007/JHEP07(2017)018. arXiv: 1703.05977 [hep-ph].

[93] J. Niehues and D. M. Walker. "NNLO QCD Corrections to Jet Production in Charged Current Deep Inelastic Scattering". In: (2018). arXiv: 1807.02529 [hep-ph].

[94] T. Gehrmann et al. "NNLO QCD corrections to event orientation in e^+e^- annihilation". In: *Phys. Lett.* B775 (2017), pp. 185–189. DOI: 10.1016/j.physletb.2017.10.069. arXiv: 1709.01097 [hep-ph].

[95] M. Cacciari et al. "Fully Differential Vector-Boson-Fusion Higgs Production at Next-to-Next-to-Leading Order". In: *Phys. Rev. Lett.* 115.8 (2015), p. 082002. DOI: 10.1103/PhysRevLett.115.082002. arXiv: 1506.02660 [hep-ph].

[96] J. Currie et al. "N^{3}LO corrections to jet production in deep inelastic scattering using the Projection-to-Born method". In: *JHEP* 05 (2018), p. 209. DOI: 10.1007/JHEP05(2018)209. arXiv: 1803.09973 [hep-ph].

[97] G. P. Lepage. "A New Algorithm for Adaptive Multidimensional Integration". In: *J. Comput. Phys.* 27 (1978), p. 192. DOI: 10.1016/0021-9991(78)90004-9.

[98] G. P. Lepage. "Vegas: An adaptive multidimensional integration program". In: (1980).

[99] IEC. *ISO/IEC 1539-1 (1997-12): Information technology — Programming languages — Fortran — Part 1: Base language*. IEC, 1997, p. 346.

[100] R. M. Stallman and G. DeveloperCommunity. *GNU Compiler Collection (GCC)*. URL: https://gcc.gnu.org/.

[101] Intel. *Intel(R) Fortran Compiler*.

[102] L. Dagum and R. Menon. "OpenMP: an industry standard API for shared-memory programming". In: *IEEE Computational Science and Engineering* 5.1 (Jan. 1998), pp. 46–55. ISSN: 1070-9924. DOI: 10.1109/99.660313.

[103] M. Cacciari, G. P. Salam, and G. Soyez. "FastJet User Manual". In: *Eur. Phys. J.* C72 (2012), p. 1896. DOI: 10.1140/epjc/s10052-012-1896-2. arXiv: 1111.6097 [hep-ph].

[104] T. Carli et al. "A posteriori inclusion of parton density functions in NLO QCD final-state calculations at hadron colliders: the APPLGRID project". In: *The European Physical Journal C* 66.3 (Apr. 2010), pp. 503–524. ISSN: 1434-6052. DOI: 10.1140/epjc/s10052-010-1255-0. URL: https://doi.org/10.1140/epjc/s10052-010-1255-0.

[105] J. A. M. Vermaseren. "New features of FORM". In: (2000). arXiv: math-ph/0010025 [math-ph].

[106] W. M. I. Maplesoft. *Maple 2016*. Waterloo, Ontario.

[107] W. Kahan. "Pracniques: Further Remarks on Reducing Truncation Errors". In: *Commun. ACM* 8.1 (Jan. 1965), pp. 40–. ISSN: 0001-0782. DOI: 10.1145/363707.363723. URL: http://doi.acm.org/10.1145/363707.363723.

[108] T. A. Morgan. "Precision Z Boson Phenomenology at the LHC". PhD thesis. Durham U. (main), 2016. URL: http://etheses.dur.ac.uk/11773/.

[109] F. Cascioli, P. Maierhofer, and S. Pozzorini. "Scattering Amplitudes with Open Loops". In: *Phys. Rev. Lett.* 108 (2012), p. 111601. DOI: 10.1103/PhysRevLett.108.111601. arXiv: 1111.5206 [hep-ph].

[110] W. H. Press, S. A. Teukolsky, W. T. Vetterling, and B. P. Flannery. *Numerical Recipes in FORTRAN; The Art of Scientific Computing*. 2nd. New York, NY, USA: Cambridge University Press, 1993. ISBN: 0521437164.

[111] T. Hahn. "CUBA: A Library for multidimensional numerical integration". In: *Comput. Phys. Commun.* 168 (2005), pp. 78–95. DOI: 10.1016/j.cpc.2005.01.010. arXiv: hep-ph/0404043 [hep-ph].

[112] G. Marsaglia, B. Narasimhan, and A. Zaman. "A random number generator for PC's". In: *Computer Physics Communications* 60.3 (1990), pp. 345–349. ISSN: 0010-4655. DOI: https://doi.org/10.1016/0010-4655(90)90033-W. URL: http://www.sciencedirect.com/science/article/pii/001046559090033W.

[113] F. James. "A Review of Pseudorandom Number Generators". In: *Comput. Phys. Commun.* 60 (1990), pp. 329–344. DOI: 10.1016/0010-4655(90)90032-V.

[114] D. Bauer et al. "The GridPP DIRAC project - DIRAC for non-LHC communities". In: *Journal of Physics: Conference Series* 664.6 (2015), p. 062036. URL: http://stacks.iop.org/1742-6596/664/i=6/a=062036.

[115] J. M. Campbell, R. K. Ellis, and W. T. Giele. "A Multi-Threaded Version of MCFM". In: *Eur. Phys. J.* C75.6 (2015), p. 246. DOI: 10.1140/epjc/s10052-015-3461-2. arXiv: 1503.06182 [physics.comp-ph].

[116] R. Kleiss, W. Stirling, and S. Ellis. "A new Monte Carlo treatment of multiparticle phase space at high energies". In: *Computer Physics Communications* 40.2 (1986), pp. 359–373. ISSN: 0010-4655. DOI: https://doi.org/10.1016/0010-4655(86)90119-0. URL: http://www.sciencedirect.com/science/article/pii/0010465586901190.

[117] E. Byckling and K. Kajantie. *Particle kinematics*. A Wiley-Interscience publication. Wiley, 1973. ISBN: 9780471128854. URL: https://books.google.co.uk/books?id%20=%20jrofAQAAMAAJ.

[118] P. Nyborg, H. S. Song, W. Kernan, and R. H. Good. "Phase-Space Considerations for Four-Particle Final States". In: *Phys. Rev.* 140 (1965), B914–B920. DOI: 10.1103/PhysRev.140.B914.

[119] J. Alwall et al. "The automated computation of tree-level and next-to-leading order differential cross sections, and their matching to parton shower simulations". In: *JHEP* 07 (2014), p. 079. DOI: 10.1007/JHEP07(2014)079. arXiv: 1405.0301 [hep-ph].

[120] T. Figy, C. Oleari, and D. Zeppenfeld. "Next-to-leading order jet distributions for Higgs boson production via weak boson fusion". In: *Phys. Rev.* D68 (2003), p. 073005. DOI: 10.1103/PhysRevD.68.073005. arXiv: hep-ph/0306109 [hep-ph].

[121] T. Figy, V. Hankele, and D. Zeppenfeld. "Next-to-leading order QCD corrections to Higgs plus three jet production in vector-boson fusion". In: *JHEP* 02 (2008), p. 076. DOI: 10.1088/1126-6708/2008/02/076. arXiv: 0710.5621 [hep-ph].

[122] M. Cacciari et al. "Erratum: Fully Differential Vector-Boson-Fusion Higgs Production at Next-to-Next-to-Leading Order [Phys. Rev. Lett. 115, 082002 (2015)]". In: *Phys. Rev. Lett.* 120 (13 Mar. 2018), p. 139901. DOI: 10.1103/PhysRevLett.120.139901. URL: https://link.aps.org/doi/10.1103/PhysRevLett.120.139901.

[123] G. P. Salam and J. Rojo. "A Higher Order Perturbative Parton Evolution Toolkit (HOPPET)". In: *Comput. Phys. Commun.* 180 (2009), pp. 120–156. DOI: 10.1016/j.cpc.2008.08.010. arXiv: 0804.3755 [hep-ph].

[124] M. Rauch and D. Zeppenfeld. "Jet clustering dependence of Higgs boson production in vector-boson fusion". In: *Phys. Rev.* D95.11 (2017), p. 114015. DOI: 10.1103/PhysRevD.95.114015. arXiv: 1703.05676 [hep-ph].

[125] N. Arkani-Hamed, T. Han, M. Mangano, and L.-T. Wang. "Physics opportunities of a 100 TeV proton–proton collider". In: *Phys. Rept.* 652 (2016), pp. 1–49. DOI: 10.1016/j.physrep.2016.07.004. arXiv: 1511.06495 [hep-ph].

[126] W. Kilian et al. "Multi-Higgs Production and Unitarity in Vector-Boson Fusion at Future Hadron Colliders". In: (2018). arXiv: 1808.05534 [hep-ph].

[127] E. Todesco, M. Lamont, and L. Rossi. "High luminosity LHC and high energy LHC". In: *Proceedings, CMS Workshop: Perspectives on Physics and on CMS at Very High Luminosity, HL-LHC: Alushta, Crimea, Ukraine, May 28–31, 2012*. 2013, pp. 15–28. URL: http://inspirehep.net/record/1269582/files/p15.pdf.

[128] L. Rossi and O. Brüning. "Introduction to the HL-LHC Project". In: *Adv. Ser. Direct. High Energy Phys.* 24 (2015), pp. 1–17. DOI: 10.1142/9789814675475_0001.

[129] M. Benedikt and F. Zimmermann. "Towards future circular colliders". In: *Journal of the Korean Physical Society* 69.6 (Sept. 2016), pp. 893–902. ISSN:

1976-8524. DOI: 10.3938/jkps.69.893. URL: https://doi.org/10.3938/jkps.69.893.

[130] F. Zimmermann. "HE-LHC Overview, Parameters and Challenges". In: *ICFA Beam Dyn. Newslett.* 72 (2017), pp. 138–141.

[131] J. Butterworth et al. "PDF4LHC recommendations for LHC Run II". In: *J. Phys.* G43 (2016), p. 023001. DOI: 10.1088/0954-3899/43/2/023001. arXiv: 1510.03865 [hep-ph].

[132] M. Ellert et al. "Advanced Resource Connector middleware for lightweight computational Grids". In: *Future Generation Computer Systems* 23.2 (2007), pp. 219–240. ISSN: 0167-739X. DOI: https://doi.org/10.1016/j.future.2006.05.008. URL: http://www.sciencedirect.com/science/article/pii/S0167739X06001178.

[133] A. B. Yoo, M. A. Jette, and M. Grondona. "SLURM: Simple Linux Utility for Resource Management". In: *Job Scheduling Strategies for Parallel Processing.* Berlin, Heidelberg: Springer Berlin Heidelberg, 2003, pp. 44–60. ISBN: 978-3-540-39727-4.